AD_____

Award Number: DAMD17-98-1-8627

TITLE: Mitochondrial Mechanisms of Neuronal Injury

PRINCIPAL INVESTIGATOR: Ian J. Reynolds, Ph.D.

CONTRACTING ORGANIZATION: University of Pittsburgh
Pittsburgh, Pennsylvania 15261

REPORT DATE: November 2003

TYPE OF REPORT: Final

PREPARED FOR: U.S. Army Medical Research and Materiel Command
Fort Detrick, Maryland 21702-5012

DISTRIBUTION STATEMENT: Approved for Public Release;
Distribution Unlimited

REPORT DOCUMENTATION PAGE

Form Approved
OMB No. 074-0188

1. AGENCY USE ONLY (Leave blank)	2. REPORT DATE	3. REPORT TYPE AND DATES COVERED
	November 2003	Final (1 Sep 1998 - 31 Oct 2003)

4. TITLE AND SUBTITLE
Mitochondrial Mechanisms of Neuronal Injury

5. FUNDING NUMBERS
DAMD17-98-1-8627

6. AUTHOR(S)
Ian J. Reynolds, Ph.D.

7. PERFORMING ORGANIZATION NAME(S) AND ADDRESS(ES)
University of Pittsburgh
Pittsburgh, Pennsylvania 15260

E-Mail: iannmda@pop.pitt.edu

8. PERFORMING ORGANIZATION REPORT NUMBER

9. SPONSORING / MONITORING AGENCY NAME(S) AND ADDRESS(ES)
U.S. Army Medical Research and Materiel Command
Fort Detrick, Maryland 21702-5012

10. SPONSORING / MONITORING AGENCY REPORT NUMBER

11. SUPPLEMENTARY NOTES
Original contains color plates: All DTIC reproductions will be in black and white.

12a. DISTRIBUTION / AVAILABILITY STATEMENT
Approved for Public Release; Distribution Unlimited

12b. DISTRIBUTION CODE

13. ABSTRACT (Maximum 200 Words)

This project is focused on understanding the mechanisms of neuronal injury in acute and chronic neurodegenerative diseases. In particular, we are interested in the role that mitochondria play in both the maintenance of neuronal viability and in the execution of neurons following injurious stimuli. Our prior studies have shown that mitochondria are an essential target for calcium overload in excitotoxic neuronal injury. We have developed a model of neuronal injury in an organotypic slice preparation that should provide insight into mitochondrial events in dopaminergic neurons. We hope that this will allow the study of mitochondrial physiology in neurons that are selectively vulnerable in Parkinson's disease. In addition, we are investigating the properties of mitochondrial trafficking in neurons, which, together with an in situ study of mitochondrial DNA replication, will start to provide an unprecedented insight into mitochondrial biogenesis, movement and turnover. We believe that an understanding of the long-term properties of mitochondria in neurons will provide information that is critical to the full appreciation of the mechanisms of neuronal injury in chronic neurodegenerative disease.

14. SUBJECT TERMS
Neurotoxin, mitochondria, neurodegeneration, excitotoxicity, apoptosis, stroke, Parkinson's disease

15. NUMBER OF PAGES
132

16. PRICE CODE

17. SECURITY CLASSIFICATION OF REPORT	18. SECURITY CLASSIFICATION OF THIS PAGE	19. SECURITY CLASSIFICATION OF ABSTRACT	20. LIMITATION OF ABSTRACT
Unclassified	Unclassified	Unclassified	Unlimited

Table of Contents

Introduction.

This project is focused on understanding the mechanisms of neuronal injury in acute and chronic neurodegenerative diseases. In particular, we are interested in the role that mitochondria play in both the maintenance of neuronal viability and in the execution of neurons following injurious stimuli. Our prior studies have shown that mitochondria are an essential target for calcium overload in excitotoxic neuronal injury. In the experiments summarized here we have pursued the study of mitochondria in neurons in additional ways. We are developing a model of neuronal injury in an organotypic slice preparation that should provide insights into mitochondrial events in dopaminergic neurons. We hope that this will allow the study of mitochondrial physiology in neurons that are selectively vulnerable in Parkinson's disease. In addition, we have started to investigate the properties of mitochondrial trafficking in neurons, which, together with an in situ study of mitochondrial DNA replication, will start to provide an unprecedented insight into mitochondrial biogenesis, movement and turnover. In combination with our previous studies on the impact of neuronal injury on mitochondrial function, we believe that an understanding of the long-term properties of mitochondria in neurons will provide information that is critical to the full appreciation of the mechanisms of neuronal injury in chronic neurodegenerative disease.

Body.

This project was originally funded from 9/98 until 8/01, during which time Dr Teresa Hastings was a co-investigator. In 2001 the project was continued with two supplements. One supplement was intended to allow us to develop an organotypic slice preparation that contains substantia nigra, striatum and cortex in order to use this preparation to study mitochondrial function in fully innervated dopaminergic neurons. The second supplement was provided as a part of a consortium arrangement (the consortium was directed by Dr Gary Fiskum at the University of Maryland). The project is designed to start studies of mitochondrial trafficking in neurons, and to investigate the site of mtDNA synthesis, both in primary cultures in neurons. The first supplement lasted for one year, and the second for two years. Progress on each section of the various projects is documented below.

Progress on original project.

1) Microscope set-up. This project started with the construction of an effective in vitro fluorescence imaging system. This was accomplished in the first year of the project and provided the technical capabilities for most of the research publications that have resulted from this project.

2) Glutamate Injury Model. Our first goals were to understand the mechanisms of neuronal injury caused by glutamate. We developed novel methods to estimate the magnitude of mitochondrial calcium loads associated with injury and established that the magnitude of the mitochondrial calcium load was closely associated with neuronal injury (Brocard et al. 2001). Our previous studies showed that mitochondrial depolarization

was a key factor in neuronal injury caused by glutamate. Further investigation of mitochondrial membrane potential in our neurons showed the unexpected phenomenon of spontaneous changes in the membrane potential signal. We were able to establish that this phenomenon is linked to changes in ATP synthesis because of the modulation by oligomycin (Buckman and Reynolds 2001). We have further developed the approach to studying spontaneous changes in mitochondrial membrane potential in a project that was developed and funded independently of these initial findings (now supported by R21 NS41299, (Vergun et al. 2003b)). We have investigated the impact of drugs that alter mitochondrial calcium handling and were rather surprised to find that increased calcium retention did not increase neuronal injury (Scanlon et al. 2000), indicating that there is still much to learn about the relationship between mitochondrial calcium loading and neuronal injury. Most recently, we investigated the relationship between glycolysis, oxidative phosphorylation and mitochondrial calcium loading. These studies showed that cell metabolism in cultured neurons is supported equally by the two ATP generating mechanisms, which is rather different from he situation *in vivo* (Vergun et al. 2003a). These studies also generated a methods paper describing the use of Mitotracker dyes for studying mitochondria in neurons and astrocytes (Buckman et al. 2001).

3) Mechanism of "Death Factor" release. The final major goal of the initial project was to study the relationship between mitochondria and the mechanisms of injury associated with the release of apoptogens. In this part of the project we investigated the properties of mitochondria in the circumstances where permeability transition might occur, oxidant production by mitochondria, and some targets of the oxidants. These studies provided the first evidence that brain mitochondria show a profoundly different response to injury compared to liver mitochondria, in that the swelling associated with permeability transition is much smaller in brain compared to liver (Berman et al. 2000). We also experimented with tamoxifen, which is a putative transition inhibitor. We found that while tamoxifen changed the glutamate-induced mitochondrial depolarization, this was not associated with neuroprotection (Hoyt et al. 2000), which has generated the suspicion that transition may not be a key event in glutamate mediated injury to neurons. We have provided an important characterization of the mechanisms of oxidant production by brain mitochondria (Votyakova and Reynolds 2001), which revealed that mitochondrial membrane potential is a key regulator of oxidant production. We also showed that dopamine was an important regulator of mitochondrial function, probably as a consequence of dopamine oxidation (Berman and Hastings 1999). Finally, we showed that a potential target of oxidants in neurons is the intracellular release of zinc. This released zinc is subsequently neurotoxic, and may be an important, under appreciated mechanism responsible for neuronal injury in many neurodegenerative disease states (Aizenman et al. 2000).

Progress on supplement 1: Organotypic slices.

We have spent considerable time on the development of the organotypic slice culture, and the development of methods to quantitatively assess injury. We have established the culture preparation successfully (Figure 1). We assessed the use of dihydroxytryptamine(DHT) as a live-cell marker for the dopaminergic neurons.

However, we subsequently discarded this approach because it became clear that DHT was toxic by itself. We evaluated the effects of several dopaminergic neurotoxins, including 6-hydroxydopamine (6OHDA), MPP+ and rotenone. Surprisingly, these toxins had relatively little effect alone, other than a minor rearrangement of the tyrosine hydroxylase staining. However addition of the toxins together with NMDA resulted in a profound injury to dopaminergic neurons that was fully reversed by the addition of MK801 (Figure 2). We used a blinded measurement approach to determine the selectivity of injury by measuring the mean nuclear diameter of dopaminergic and non-dopaminergic neurons in the substantia nigra. These measurements showed substantial selectivity of the two toxin approach for killing dopaminergic neurons (Figure 3). We are currently preparing these findings for publication.

We feel we have essentially met the goal of the original one-year supplement. We have effectively established the organotypic slice culture model and also determined the parameters necessary for killing the dopaminergic neurons selectively. We plan to continue this approach by studying the fate of the mitochondria in the dopaminergic neurons. To do this, we plan to introduce mitochondrially targeted fluorescent proteins into the preparation using lentiviral vectors that will express mt-eYFP under the control of a tyrosine hydroxylase promoter. This will allow us to assess when and where mitochondrial trafficking is altered as the dopaminergic neurons are injured. An application to support these studies is currently pending at the Michael J. Fox Foundation.

Progress on supplement 2: Mitochondrial trafficking.

The second supplement was focused on the examination of the biogenesis and trafficking of mitochondria. We previously reported success with an in situ method for examining mtDNA replication in the primary neuronal cultures using bromodeoxyuridine immunohistochemistry (Figure 4). Using this approach we have been investigating the impact of toxins on the replication of mtDNA, and also looking for evidence for turnover. Perhaps surprisingly, very few of the approaches so far have shown effects on the rate of mtDNA replication. Glutamate has no effect when examined after 3hr, and the antiviral drug dideoxycytidine also was without effect. However, we very recently found that rotenone apparently decreased mtDNA synthesis at concentrations below those causing frank toxicity to neurons. This suggests that the rate of mtDNA replication may, indeed be a factor in neuronal injury. Our immediate goals are to try to determine where the replication occurs. As documented below, we now have several approaches whereby we can decrease the amount of mitochondrial movement. This will allow us to stop movement while replication occurs, so the sites at which we find newly synthesized mtDNA will presumably be the site where the synthesis occurs. This will allow us to test the hypothesis that mtDNA replication can occur distant from the nucleus in neurons in culture.

The other goal was to examine mitochondrial movement. To do this, we used mitochondrially targeted enhanced yellow fluorescent protein (mt-eYFP). A variety of transfection methods have been used, and these result in the expression of the protein in a

small fraction of neurons which can then be monitored to quantitate movement. A number of important findings have resulted from these studies. We recently published a study showing that glutamate causes inhibition of mitochondrial movement and also a profound remodeling of mitochondrial morphology (Rintoul et al. 2003). We think there are several mechanisms associated with the glutamate effect. Firstly, several different drugs that impair mitochondrial ATP synthesis inhibit movement, so we think that ATP supply is critical to support movement. Secondly, glutamate clearly disrupts the cytoskeleton in a calcium-dependent way. This is also likely to contribute to movement inhibition, but might also account for the shape change. The former conclusion lead to another study. We hypothesized that nitric oxide should also regulate movement if used at concentrations sufficient to inhibit complex IV, an effect that is well established in the literature at this time. Studies using the NO donor PAPA nonoate established the validity of this hypothesis, and we are currently preparing a manuscript on this topic. We also established that zinc inhibits mitochondrial movement by a mechanism that probably does not involve the gross inhibition of mitochondrial function. Interestingly, this effect of zinc is inhibited by wortmannin, a phosphatidyl inositol 3 kinase inhibitor, which has provided insights into possible intracellular signaling mechanisms that might regulate mitochondrial movement. We are currently investigating these mechanisms.

The studies on mitochondrial trafficking are continuing and are the basis for a new R01 application to the National Institutes of Health that was submitted in the fall of 2003.

Figure 1

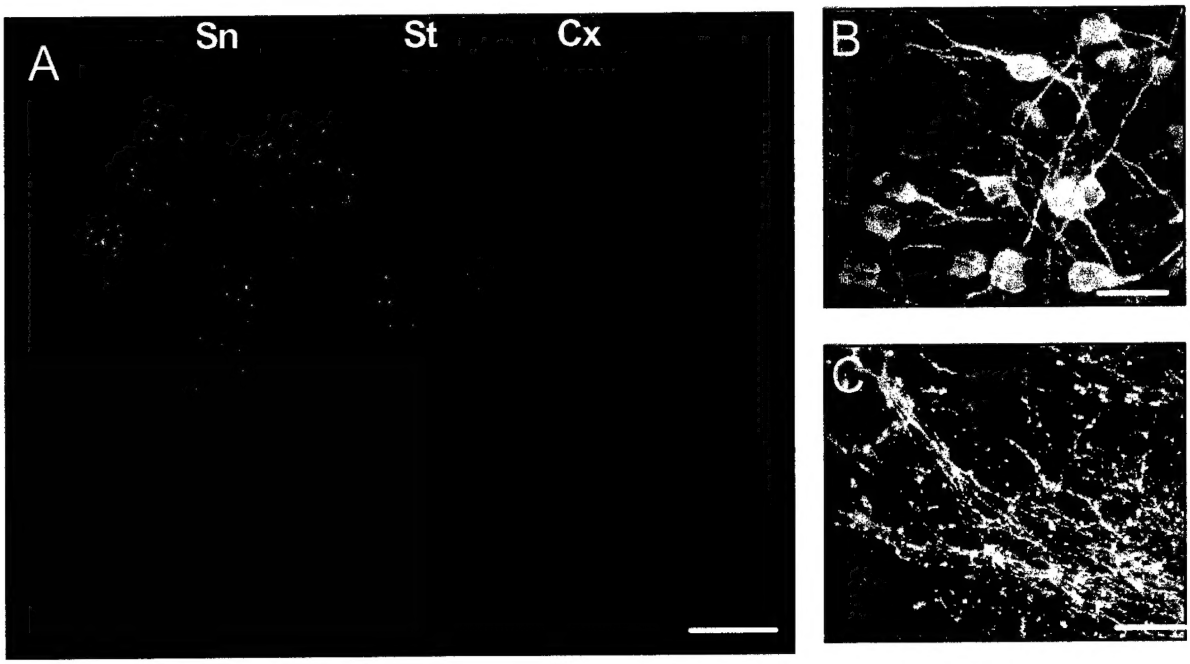

Examples of TH staining in a healthy slice. Panel A is a low-power montage of the entire slice, with the SN on the left, the striatum at center top, and the cortex at the right. B shows healthy cell bodies, while the panel C shows TH-stained fibers in the striatum.

Figure 2

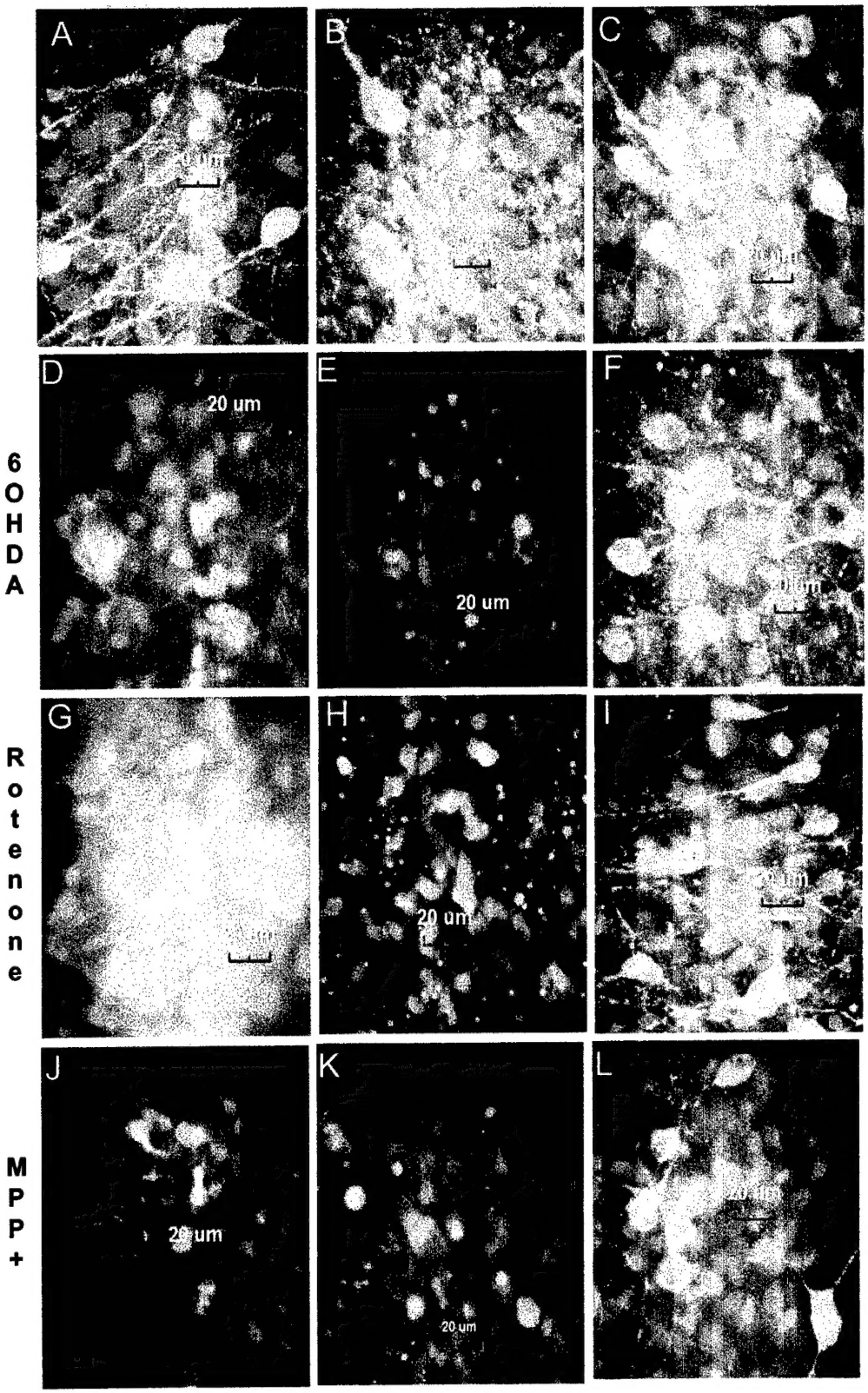

Effects of neurotoxins on the slice culture. TH staining is green while Hoechst staining is in red. In each case the toxin alone shows little injury, while the toxin in combination with NMDA produces profound DA injury that is reversed by MK801.

Figure 3

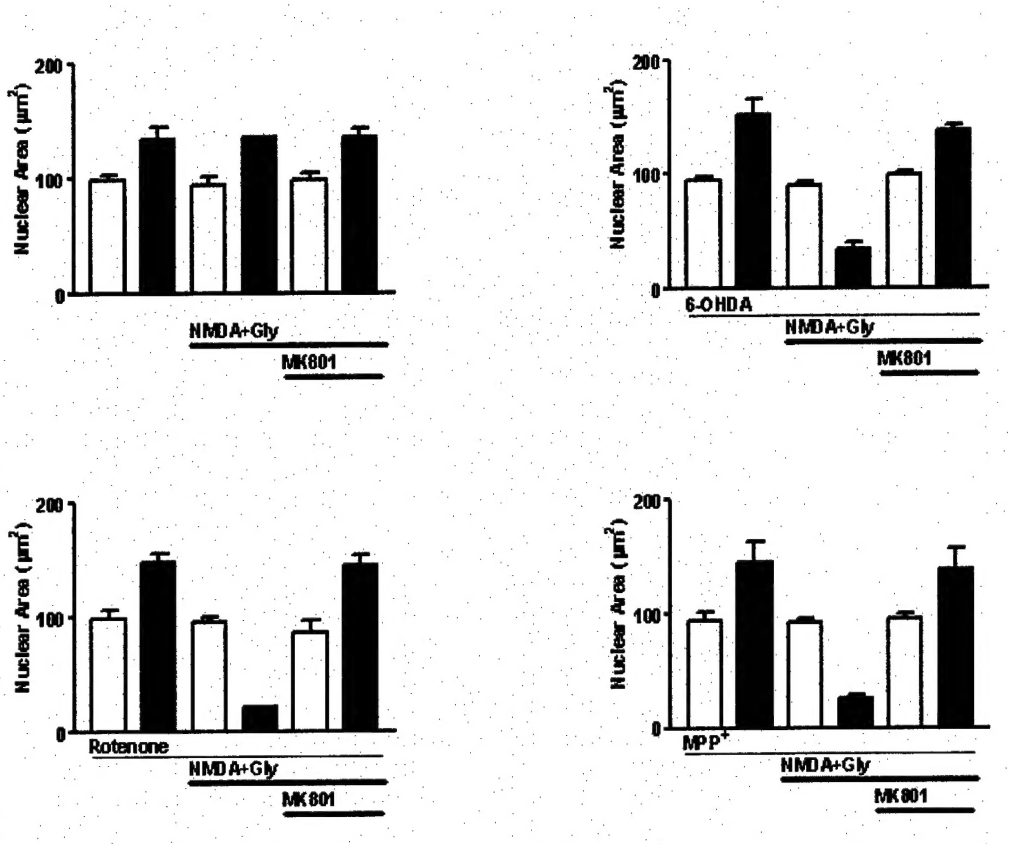

Effects of injury on the size of neuronal nuclei. The filled bars show the size of the nucleus in the TH positive cells, while the open bars are non-TH nuclei in the substantial nigra portion of the slice. The data show that injury (indicated by nuclear shrinkage) only occurs when NMDA is present together with a dopaminergic neurotoxin, and that this injury is selective for TH positive cells.

Figure 4.

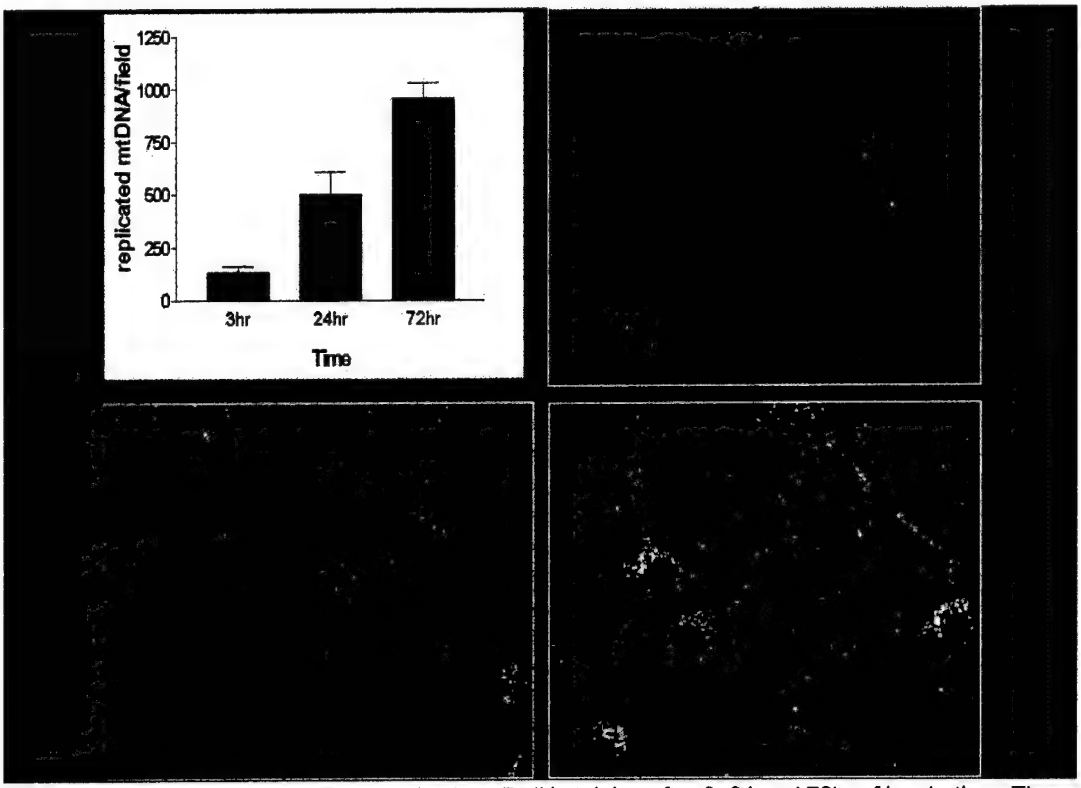

BrdU immunohistochemistry. The panels show BrdU staining after 3, 24 and 72hr of incubation. The graph shows mean values for BrdU dots at the same time points. The cultures are also stained with Hoechst 33342 to reveal neuronal nuclei.

Key Research Accomplishments.

During this project we have:

1) Developed methods for estimating mitochondrial calcium loads following excitotoxic neuronal injury.

2) Provided the first description of spontaneous mitochondrial depolarizations in intact neurons.

3) Developed methods for the use of Mitotracker dyes in neural cultures.

4) Described mechanisms for generation of oxidants by mitochondria.

5) Characterized properties of permeability transition in liver and brain mitochondria.

6) Demonstrated toxic effects of dopamine on brain mitochondria.

7) Demonstrated effects of tamoxifen on neuron mitochondria

8) Discovered oxidant induced intracellular zinc mobilization in neurons.

9) Provided first example of toxin-induced inhibition of mitochondrial movement.

10) Established an in vitro slice model useful for studies of Parkinson's Disease.

Reportable Outcomes.

The following peer reviewed papers were cited in the progress report. All are included in the appendix.

Aizenman E., Stout A. K., Hartnett K. A., Dineley K. E., McLaughlin B. A., and Reynolds I. J. (2000) Induction of neuronal apoptosis by thiol oxidation: putative role of intracellular zinc release. *J Neurochem* **75,** 1878-1888.

Berman S. B. and Hastings T. G. (1999) Dopamine oxidation alters mitochondrial respiration and induces permeability transitionin brain mitochondria: implications for Parkinson's disease. *J Neurochem* **73,** 1127-1137.

Berman S. B., Watkins S. C., and Hastings T. G. (2000) Quantitative biochemical and ultrastructural comparison of mitochondrial permeability transition in isolated brain and liver mitochondria: evidence for relative insensitivity of brain mitochondria. *Exp Neurol* **164,** 415-425.

Brocard J. B., Tassetto M., and Reynolds I. J. (2001) Quantitative evaluation of mitochondrial calcium content following glutamate receptor stimulation in rat cortical neurones. *J Physiol (Lond)* **531,** 793-805.

Buckman J. F., Hernandez H., Kress G. J., Votyakova T. V., Pal S., and Reynolds I. J. (2001) MitoTracker labeling in primary neuronal and astrocytic cultures: influence of mitochondrial membrane potential and oxidants. *J Neurosci Meth* **104,** 165-176.

Buckman J. F. and Reynolds I. J. (2001) Spontaneous changes in mitochondrial membrane potential in cultured neurons. *J Neurosci* **21,** 5054-5065.

Hoyt K. R., McLaughlin B. A., Higgins D. S., and Reynolds I. J. (2000) Inhibition of glutamate-induced mitochondrial depolarization by tamoxifen in cultured neurons. *J Pharmacol Exp Ther* **293,** 480-486.

Rintoul G. L., Filiano A. J., Brocard J. B., Kress G. J., and Reynolds I. J. (2003) Glutamate decreases mitochondrial size and movement in primary forebrain neurons. *J Neurosci* **23,** 7881-7888.

Scanlon J. M., Brocard J. B., Stout A. K., and Reynolds I. J. (2000) Pharmacological investigation of mitochondrial Ca^{2+} transport in central neurons: studies with CGP 37157, an inhibitor of the mitochondrial Na^{+}-Ca^{2+} exchanger. *Cell Calcium* **28,** 317-328.

Vergun O., Han Y. Y., and Reynolds I. J. (2003a) Glucose deprivation produces a prolonged increase in sensitivity to glutamate in cultured rat cortical neurons. *Exp Neurol* **183,** 682-694.

Vergun O., Votyakova T. V., and Reynolds I. J. (2003b) Spontaneous changes in mitochondrial membrane potential in single isolated brain mitochondria. *Biophysical Journal* **85,** 3358-3366.

Votyakova T. V. and Reynolds I. J. (2001) $\Delta\psi$m-dependent and independent production of reactive oxygen species by brain mitochondria. *J Neurochem* **79,** 266-277.

In addition to these papers we have published 16 abstracts reflecting presentations at the Society for Neuroscience, American Society for Neurochemistry and Biophysical Society annual meetings.

We have additionally been awarded one grant and have applied for two other grants based on the outcome of this project:

Awarded:

NIH grant R21 NS41299, Mitochondrial function in neurodegeneration.

Pending:

NIH grant R01 (number not yet assigned) The life history of mitochondria in neurons.

Michael J. Fox Foundation Fast Track Award, Mitochondrial trafficking in dopaminergic neuron injury.

Conclusions.

This project has been based on the investigation of the role of mitochondria in various models of neuronal injury. All of the conclusions of the studies we have performed over the last five years are consistent with an important role of mitochondria in neuronal injury. Needless to say, there were many surprises encountered as we pursued our original research plan that have resulted in new insights into the normal function of mitochondria as well as their dysfunction as cells are assaulted by toxins.

It remains clear that the interaction between mitochondria and calcium is a critical determinant of the impact of toxins on neurons. Excitotoxic injury imposes a severe calcium load that results in mitochondrial dysfunction. This suggests a clear principle that modifying mitochondrial calcium loading could be a valuable new approach to neuroprotection. These studies also show that mitochondria are both the source and the target of oxidants in relation to neurodegeneration. Modifying the generation of oxidants or increasing the ability of neurons to handle oxidant exposure represent a potential therapeutic target that has been recognized by many. Our studies offer some possible specific targets of the oxidants, such as the targets of dopamine (which are still being investigated but may include creatine kinase) and also the previously unrecognized release of zinc. Again, interfering with these effects that are secondary to oxidant production could represent valuable approaches for future studies.

One of the most exciting findings of our recent experiments has been the observation that the trafficking of mitochondria is a highly regulated phenomenon. This has generated the broad hypothesis that an important mechanism for neurotoxins may be the prevention of the appropriate delivery and/or retrieval of mitochondria from cellular targets. This is a novel concept that we are busy exploring at the moment. However, we have already established the general principles that trafficking can be interrupted by ATP depletion, cytoskeletal disruption and also specific intracellular signaling pathways. This will be an important topic for future studies that will go well beyond our initial efforts in this area.

Finally, we hope to be able to combine the studies of mitochondrial trafficking into a novel in vitro Parkinson's disease model. We have been able to establish the organotypic slice culture system and have now completed initial studies that demonstrate the utility of the model for investigating dopaminergic injury mechanisms. By combining our latest techniques for studying mitochondrial trafficking we are positioned to perform some unique experiments that will, for the first time, reveal specific information about trafficking of mitochondria to identified presynaptic nerve terminals and the impact of injury on that process.

By combining studies on isolated mitochondria, dissociated neuronal cultures and anatomically authentic slice cultures, we have been able to assemble some unique insights into the various properties of mitochondrial function that are vulnerable to injury. These studies have already started to yield information about potential

therapeutic targets and we anticipate further insights in the future that may provide the opportunity to treat diseases that are currently resistant to therapeutic intervention.

Journal of Neurochemistry
Lippincott Williams & Wilkins, Inc., Philadelphia

Induction of Neuronal Apoptosis by Thiol Oxidation: Putative Role of Intracellular Zinc Release

Elias Aizenman, *Amy K. Stout, Karen A. Hartnett, *Kirk E. Dineley, BethAnn McLaughlin, and *Ian J. Reynolds

*Departments of Neurobiology and *Pharmacology, University of Pittsburgh School of Medicine, Pittsburgh, Pennsylvania, U.S.A.*

Abstract: The membrane-permeant oxidizing agent 2,2′-dithiodipyridine (DTDP) can induce Zn^{2+} release from metalloproteins in cell-free systems. Here, we report that brief exposure to DTDP triggers apoptotic cell death in cultured neurons, detected by the presence of both DNA laddering and asymmetric chromatin formation. Neuronal death was blocked by increased extracellular potassium levels, by tetraethylammonium, and by the broad-spectrum cysteine protease inhibitor butoxy-carbonyl-aspartate-fluoromethylketone. *N,N,N′,N′*-Tetrakis-(2-pyridylmethyl)ethylenediamine (TPEN) and other cell-permeant metal chelators also effectively blocked DTDP-induced toxicity in neurons. Cell death, however, was not abolished by the NMDA receptor blocker MK-801, by the intracellular calcium release antagonist dantrolene, or by high concentrations of ryanodine. DTDP generated increases in fluorescence signals in cultured neurons loaded with the zinc-selective dye Newport Green. The fluorescence signals following DTDP treatment also increased in fura-2- and magfura-2-loaded neurons. These responses were completely reversed by TPEN, consistent with a DTDP-mediated increase in intracellular free Zn^{2+} concentrations. Our studies suggest that under conditions of oxidative stress, Zn^{2+} released from intracellular stores may contribute to the initiation of neuronal apoptosis. **Key Words:** Oxidation—Apoptosis—Zinc—Cerebral cortex—Tissue culture.
J. Neurochem. **75,** 1878–1888 (2000).

Zinc has been reported to be toxic to neurons in vitro and in vivo (Choi et al., 1988; Cuajungco and Lees, 1998*a*; Weiss et al., 1993; Koh and Choi, 1994; Manev et al., 1997; Sheline et al., 2000). Heretofore, Zn^{2+}-mediated cell death has been shown to be dependent on influx of the cation into cells because injury could be blocked by cell-impermeant metal chelators (Koh et al., 1996) and by antagonists of voltage- or glutamate-gated ion channels that are permeable to Ca^{2+} (Weiss et al., 1993; Koh and Choi, 1994; Sensi et al., 1997). Zn^{2+} influx has been suggested to contribute to the neuronal damage associated with ischemia and epilepsy as Zn^{2+} is present in synaptic vesicles (Frederickson, 1989), can be released from neurons on depolarization (Assaf and Chung, 1984; Howell et al., 1984; Aniksztejn et al., 1987; Vogt et al., 2000), and translocates from presynaptic sites into postsynaptic neurons (Sloviter, 1985; Koh et al., 1996; Frederickson et al., 1988; Lee et al., 2000).

Rather than existing as a free ion in the cytoplasm, most neuronal Zn^{2+} is packaged either in synaptic vesicles or is tightly complexed to proteins such as metallothionein (MT) and Zn^{2+} finger-containing transcription factors (Frederickson, 1989; Berg, 1990). In the present study we tested the hypothesis that these intracellular stores represent a potential source for Zn^{2+}-mediated neurotoxicity in neurons. As Zn^{2+} can be released from MT in cell-free systems by oxidizing agents that can catalyze disulfide exchange, such as 2,2′-dithiodipyridine (DTDP) (Jiang et al., 1998; Maret and Vallee, 1998), we examined whether a limited exposure of neurons in culture to DTDP resulted in neuronal injury. We also investigated whether the release of Zn^{2+} from intracellular stores following DTDP treatment could be measured with fluorescent probes.

MATERIALS AND METHODS

Cell culture and toxicity assays

Cortical cultures were prepared from embryonic day 16 Sprague–Dawley rats as previously described (Hartnett et al., 1997). In brief, cortices were dissociated and plated onto poly-

Received May 25, 2000; revised manuscript received July 4, 2000; accepted July 5, 2000.

Address correspondence and reprint requests to Dr. E. Aizenman at Department of Neurobiology, University of Pittsburgh School of Medicine, E1456 BST, Pittsburgh, PA 15261, U.S.A. E-mail: redox@pitt.edu

The present address of Dr. A. K. Stout is MitoKor, 11494 Sorrento Valley Road, San Diego, CA 92121, U.S.A.

The present address of Ms. K. A. Hartnett is Beckim Industries, 3625 Watchill Road, Munhall, PA 15120, U.S.A.

Abbreviations used: AM, acetoxymethyl ester; BAF, butoxy-carbonyl-aspartate-fluoromethyl ketone; BAPTA, 1,2-bis(2-aminophenoxy)ethane-*N,N,N′,N′*-tetraacetic acid; $[Ca^{2+}]_i$, intracellular free Ca^{2+} concentration; DTDP, 2,2′-dithiodipyridine; LDH, lactate dehydrogenase; $[Mg^{2+}]_i$, intracellular free Mg^{2+} concentration; MT, metallothionein; TEA, tetraethylammonium; TPEN, *N,N,N′,N′*-tetrakis(2-pyridylmethyl)ethylenediamine; $[Zn^{2+}]_i$, intracellular free Zn^{2+} concentration.

L-lysine-treated tissue culture plates in a growth medium composed of 80% Dulbecco's modified Eagle's medium, 10% Ham's F12-nutrients, and 10% bovine calf serum (heat-inactivated and iron-supplemented) with 25 m*M* HEPES, 24 U/ml penicillin, 24 μg/ml streptomycin, and 2 m*M* L-glutamine. Medium was partially replaced three times a week. Glial cell proliferation was inhibited after 2 weeks in culture with 1–2 μ*M* cytosine arabinoside, at which time the culture medium was reduced to 2% serum without F12-nutrients. At 3–5 weeks in vitro these cultures contain ~10–20% neurons (Rosenberg and Aizenman, 1989; Rosenberg, 1991). Toxicity assays were performed on 4-week-old cultures (25–29 days in vitro). Immediately before drug treatment, the cells were rinsed (200:1) in minimum essential medium with Earle's salts containing 0.01% bovine serum albumin and 25 m*M* HEPES. Cells were exposed to DTDP for 10 min at 37°C in 5% CO_2. Treatment was removed by serial dilution (200:1), and the cells were returned to the incubator.

Neuronal viability was determined 18–20 h following exposure using a lactate dehydrogenase (LDH)-based in vitro toxicology assay kit (Sigma, St. Louis, MO, U.S.A.). Medium samples (40 μl) were analyzed spectrophotometrically (at 490 and 630 nm) according to the manufacturer's protocol, to obtain a measure of cytoplasmic LDH release from dead and dying neurons. Toxicity was assessed as the ratio of LDH_{DTDP} / $LDH_{Vehicle}$. LDH activity can be measured from neurons undergoing apoptosis because phagocytosis of dead cells does not take place in our culture system. Relative neuroprotection provided by the various agents tested was expressed as neuronal protection, which was derived by the following equation: $100 - \{[(LDH_{DTDP+treatment} / LDH_{Vehicle+treatment}) / (LDH_{DTDP} / LDH_{Vehicle})] \times 100\}$.

Forebrain neuronal-enriched cultures were prepared from embryonic day 17 rat fetuses as previously described (McLaughlin et al., 1998). Dissociated cells were plated on poly-L-ornithine-treated tissue culture plates in a growth medium composed of 80% Dulbecco's modified Eagle's medium (high glucose with L-glutamine and without sodium pyruvate; GibcoBRL, Grand Island, NY, U.S.A.), 10% Ham's F12-nutrients, 10% bovine calf serum (heat-inactivated), and 1× antimycotic/antibiotic mixture (with amphotericin B and streptomycin sulfate; GibcoBRL). Cultures were maintained in an incubator at 37°C in 5% CO_2. Glial cell proliferation was inhibited after 48 h in culture with 1–2 μ*M* cytosine arabinoside. After 3 days in vitro, the serum-containing medium was replaced with a serum-free solution comprised of Neurobasal medium (without L-glutamine; GibcoBRL), 1× B27 supplement (GibcoBRL), and 1× antimycotic/antibiotic mixture. Toxicity assays on neuron-enriched cultures were performed in tissue culture plates containing plastic grid coverslips at 6–8 days following dissociation. Cells were rinsed (200:1) with HEPES-buffered salt solution before a 10-min exposure to 10 μ*M* DTDP. Treatment was terminated first by rinsing (200:1) and then by adding serum-free Neurobasal medium (containing 1× antimycotic/antibiotic mixture but without the B27 supplement) to the cultures. Cultures were maintained overnight at 37°C in 5% CO_2. Viability was determined 18–20 h following exposure using trypan blue exclusion staining and viability counts. Cells were counted (three to five areas of the labeled plastic grid) both before and following treatment by a person blinded to the arrangement of the treatment groups. Counts are expressed as percentages of the pre-exposure counts obtained from the same grid areas.

To determine the extent of asymmetric chromatin condensation induced by DTDP, Hoechst 33342 staining was performed on neuron-enriched cultures. Toxicity assays were performed in tissue culture plates containing glass coverslips. Hoechst staining was performed 18–20 h following DTDP exposure. Cultures were washed briefly in phosphate-buffered saline, fixed in 10% formaldehyde for 10 min, and incubated in 5 μg/ml Hoechst 33342 dye (Sigma) for an additional 10 min. Cultures were washed twice with phosphate-buffered saline, and the coverslips were mounted onto slides using Mowoil mounting medium. Fluorescence was visualized using a Nikon Eclipse E600 microscope with a fluorescent light source and bright-field illumination, and the percentage of apoptotic nuclei from three to five fields per coverslip was calculated by a person blinded to the treatment conditions.

Induction of DNA laddering by DTDP in cortical neurons was evaluated as described by McLaughlin et al. (1998). In brief, cells previously exposed to DTDP were scraped from their dishes in a lysis solution (0.1 *M* sodium EDTA, 1% sodium dodecyl sulfate, 200 m*M* Tris, and 0.5 mg of proteinase K). Proteins were removed by centrifugation, and DNA was precipitated with 100% ethanol. DNA samples were electrophoresed on a 1.8% agarose gel, which was later stained with ethidium bromide.

Fluorescence imaging

Changes in intracellular free Zn^{2+} concentration ($[Zn^{2+}]_i$) in cultured neurons were monitored with the zinc-selective fluorescent indicator Newport Green. In addition, previous studies in this and other laboratories have demonstrated the usefulness of the fluorescent indicators magfura-5, magfura-2, fura-2, and fluo-3 for measurement of $[Zn^{2+}]_i$ under conditions in which the intracellular free Ca^{2+} concentration ($[Ca^{2+}]_i$) does not change (Sensi et al., 1997; Cheng and Reynolds, 1998). $[Zn^{2+}]_i$ was measured using methods and equipment previously described for measuring increases in $[Ca^{2+}]_i$ (Stout and Reynolds, 1999). In brief, neurons were loaded with dye via incubation in HEPES-buffered salt solution containing 5 μ*M* Newport Green acetoxymethyl ester (AM), magfura-2 AM, fura-2 AM, or fluo-3 AM, 5 mg/ml bovine serum albumin, and 0.5% dimethyl sulfoxide at 37°C for ~30 min. Following loading, coverslips were rinsed with HEPES-buffered salt solution, mounted in a recording chamber, and perfused with HEPES-buffered salt solution at a rate of 20 ml/min. All recordings were made at room temperature (20–25°C). Background fluorescence values (determined from cell-free regions of each coverslip) were subtracted from all signals. The imaging system used in these studies consisted of a Nikon Diaphot 300 microscope fitted with a 40× quartz objective, a Dage-MTI cooled-CCD camera with 640- × 480-pixel resolution in combination with a Dage-MTI Gen II Sys image intensifier, a software package from Compix (Cranberry, PA, U.S.A.), and a 75-W xenon lamp-based monochromator light source from Applied Scientific Instrumentation (Eugene, OR, U.S.A.). Cells were alternately illuminated with 335 and 375 nm light for magfura-2 measurements or with 345 and 375 nm light for fura-2 measurements. Newport Green and fluo-3 were illuminated at 490 or 504 nm, respectively. Attenuation of incident light was achieved with neutral density filters (ND 2 for 1% transmittance; Omega Optical, Brattleboro, VT, U.S.A.). Emitted light passed through a 515 nm dichroic mirror and a 535 ± 12.5 nm band pass filter (Omega Optical). Simultaneous measurements were performed in 16–32 neurons per coverslip.

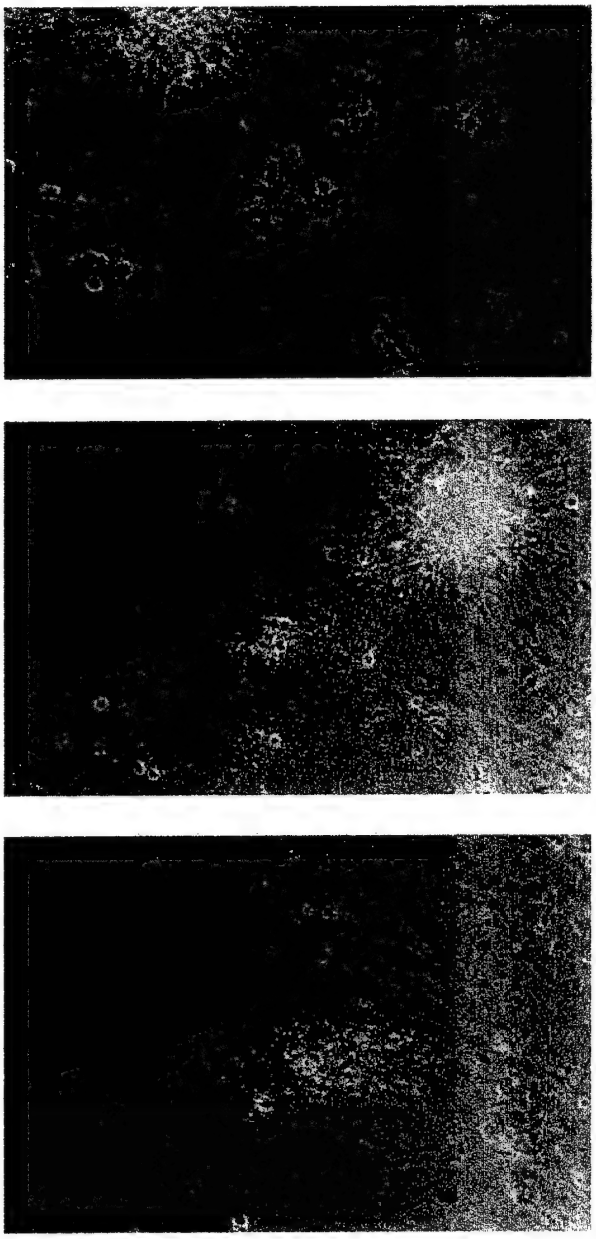

FIG. 1. Neurotoxicity of DTDP. Mixed cultures of neurons and glia were exposed to (**A**) vehicle (minimum essential medium with 0.01% bovine serum albumin and 25 m*M* HEPES, 10 min), (**B**) DTDP (100 μM, 10 min), or (**C**) NMDA (100 μM, 30 min) and photographed 24 h later. Phase-bright neurons appear on top of a glial cell layer. Note the similar pattern of toxicity elicited by DTDP and NMDA.

RESULTS

DTDP is neurotoxic to neurons in culture

Mixed cortical cultures exposed for 10 min to 100 μM DTDP underwent widespread neuronal cell death within 24 h. This toxicity appeared to spare the underlying glial cell layer, a phenomenon that is commonly observed when cells are exposed to NMDA (Fig. 1). Exposure to increasing concentrations of DTDP (10 min) caused the release of LDH from the cultures in a dose-dependent fashion (Fig. 2). Sister cultures that had been previously exposed to 1 m*M* kainate overnight to remove the neuronal component of the cultures also showed a dose-dependent increase in LDH release on DTDP exposure, suggesting that high doses of this agent could promote gliotoxicity. However, this LDH release was much less pronounced that that observed in the presence of neurons (Fig. 2), even though glia constitute ~80–90% of the cellular mass in this preparation (Rosenberg and Aizenman, 1989; Rosenberg, 1991). This argues that neurons are, in fact, appreciably more sensitive than glial cells to the toxic actions of DTDP.

To begin to determine the mechanism of DTDP-induced cell death, we evaluated cultures for hallmark features of apoptosis. First, we extracted DNA from DTDP (100 μM)-treated cultures at various time points to look for the presence of DNA laddering and noted that internucleosomal fragmentation was present 6 h after exposure to the toxin (Fig. 3A). Second, we observed that the broad-spectrum cysteine protease inhibitor butoxy-carbonyl-aspartate-fluoromethyl ketone (BAF; 100 μM) substantially abrogated DTDP toxicity (Fig. 3B). Third, we found that DTDP toxicity was significantly inhibited when high extracellular KCl (25 m*M*) was present during the DTDP exposure (Fig. 3B). These elevated K^+ conditions have previously been shown to block staurosporine-induced apoptosis in cultured neurons by blocking K^+ efflux through tetraethylammonium (TEA)-sensitive channels (Yu et al., 1997). Indeed, we found that 10 m*M* TEA effectively inhibited DTDP toxicity in our cultures (Fig. 3B). Finally, asymmetric chromatin formations were observed following Hoechst staining in neuron-enriched cultures treated for 10 min with 100 μM DTDP (Fig. 4). Given that our neuron-enriched cultures contain <0.5% nonneuronal elements,

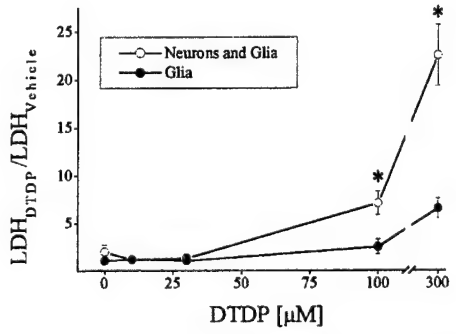

FIG. 2. DTDP kills neurons preferentially over glia. Mixed neuronal and glial cortical cultures were first exposed to minimum essential medium alone or in the presence of 1 m*M* kainate overnight to kill neurons and generate glial cultures. Both cultures were then subsequently exposed to increasing concentrations of DTDP for 10 min. After 18–20 h, LDH release was measured. Results for cell toxicity ($LDH_{DTDP}/LDH_{Vehicle}$) are expressed as mean ± SEM (bars) values of four to seven experiments performed in quadruplicate. *$p < 0.05$ by unpaired two-tailed *t* test, indicating toxicity was significantly different between mixed and glial cultures.

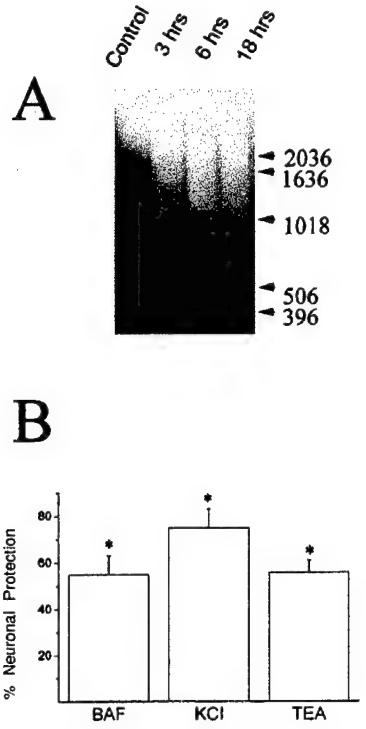

FIG. 3. DTDP induces neuronal apoptosis. **A:** Induction of DNA laddering in cortical cultures by DTDP (100 μM, 10 min). DNA was obtained from control cells and from DTDP-treated cultures at 3, 6, and 18 h following exposure. Note that the lane from control cultures has a high-molecular-weight band representative of intact DNA with no laddering. DNA laddering is observed in DTDP-treated cultures after 6 h. **B:** Inhibition of DTDP neurotoxicity suggests cell death is apoptotic. Mixed cortical cultures were exposed to DTDP (100 μM, 10 min) in the presence or absence of 100 μM BAF, 25 mM KCl, or 10 mM TEA. After 18–20 h, LDH release was measured. Data are mean ± SEM (bars) values for neuroprotection (see text) from experiments performed four to six times in quadruplicate. *$p < 0.001$ by one-sample two-tailed t test, indicating significant neuroprotection.

this observation proved that the apoptotic phenotype following DTDP treatment was present in neurons. We also observed that DTDP-induced chromatin condensation was virtually abolished by 100 μM BAF (Fig. 4D). The percentage of apoptotic nuclei present in these cultures was reduced from 38 ± 7% in the DTDP-treated cultures to 5 ± 4% in cultures treated with DTDP and 100 μM BAF (n = 4; $p < 0.01$ by unpaired t test). In addition, total cell viability was significantly restored in these cultures when 100 μM BAF was included during DTDP exposure (Fig. 5).

DTDP has previously been used to oxidize and activate ryanodine receptors to release Ca^{2+} from intracellular pools (Eager et al., 1997). We thus evaluated whether DTDP toxicity was due to intracellular calcium release or, indirectly, by inducing glutamate release and producing excitotoxicity. Mixed cortical cultures were exposed to DTDP (100 μM, 10 min) in the presence or absence of 50 μM ryanodine, 20 μM dantrolene (to block ryanodine receptors), or 10 μM MK-801 (to block NMDA receptor activation). After 18–20 h, LDH release was measured. No neuroprotection was observed with any of these agents (data not shown).

DTDP releases Zn^{2+} from intracellular stores

Having ruled out intracellular Ca^{2+} release and excitotoxicity as contributors to DTDP toxicity, we next assessed the possibility that the thiol oxidant may be causing Zn^{2+} release from intracellular stores as suggested by prior cell-free studies (Jiang et al., 1998; Maret and Vallee, 1998). To monitor increases in $[Zn^{2+}]_i$ we used a series of fluorescent indicators (Canzoniero et al., 1997; Cheng and Reynolds, 1998; Sensi et al., 1999). Exposure of neurons loaded with the Zn^{2+}-selective dye Newport Green to 100 μM DTDP resulted in a slow increase in the fluorescence signal (4.66 ± 0.39 arbitrary fluorescence units, or 12.8%; n = 43) consistent with an increase in $[Zn^{2+}]_i$. This increase could be rapidly reversed by addition of 25 μM *N,N,N′,N′*-tetrakis(2-pyridylmethyl)ethylenediamine (TPEN) (Fig. 6A). A similar effect was observed when neurons were loaded with magfura-2 (Fig. 6B), which we have previously used to monitor $[Zn^{2+}]_i$ (Cheng and Reynolds, 1998). It is interesting that the increase in magfura-2 ratio was observed in cells bathed in Zn^{2+}-free conditions and previously treated with TPEN, thus suggesting that the DTDP-sensitive pool is not extracellular, nor is it readily chelatable before oxidant treatment. The Zn^{2+}-free solution contained 1 mM Ca^{2+}-saturated disodium EDTA to chelate Zn^{2+}. The $-\log K_D$ of calcium for EDTA is 10.73, whereas the $-\log K_D$ for zinc is 16.8 (MiniSCD Database, version 4; Academic Software, Otley, U.K.).

We performed several additional experiments to investigate further the identity of the ion mobilized by DTDP. By exploiting the high affinity of Zn^{2+} binding to fura-2, magfura-2, and fluo-3, the possibility that dye changes are due to alterations in $[Ca^{2+}]_i$ or another intracellular cation can be addressed. DTDP exposure (100 μM, 10 min) caused an increase in the fluorescence ratio in primary cultures of rat forebrain neurons previously loaded with fura-2 AM (Fig. 7A). The mean ± SEM increase in the fura-2 ratio on DTDP stimulation was 0.21 ± 0.005 over baseline, which was 0.73 ± 0.002 (n = 293). This DTDP-induced increase in the fura-2 signal was relatively small compared with the mean Ca^{2+}-mediated increase in the fura-2 ratio obtained in these cells on stimulation with 100 μM NMDA plus 10 μM glycine for 15 s (1.78 ± 0.030; Fig. 7B). Similar to what we described above, DTDP also caused an increase in the fluorescence ratio in neurons loaded with magfura-2 AM (Fig. 7C). The mean ± SEM increase in the magfura-2 ratio on DTDP stimulation (100 μM, 10 min) was 0.046 ± 0.001 over baseline (0.30 ± 0.001, n = 86). This signal is comparable to that observed following addition of <1 μM extracellular zinc in the presence of pyrithione (Dineley et al., 2000). For comparison, the mean ± SEM increase in the magfura-2 ratio obtained in these cells on stimulation with 100 μM NMDA plus 10 μM glycine for 1 min was 0.23 ± 0.023. DTDP also

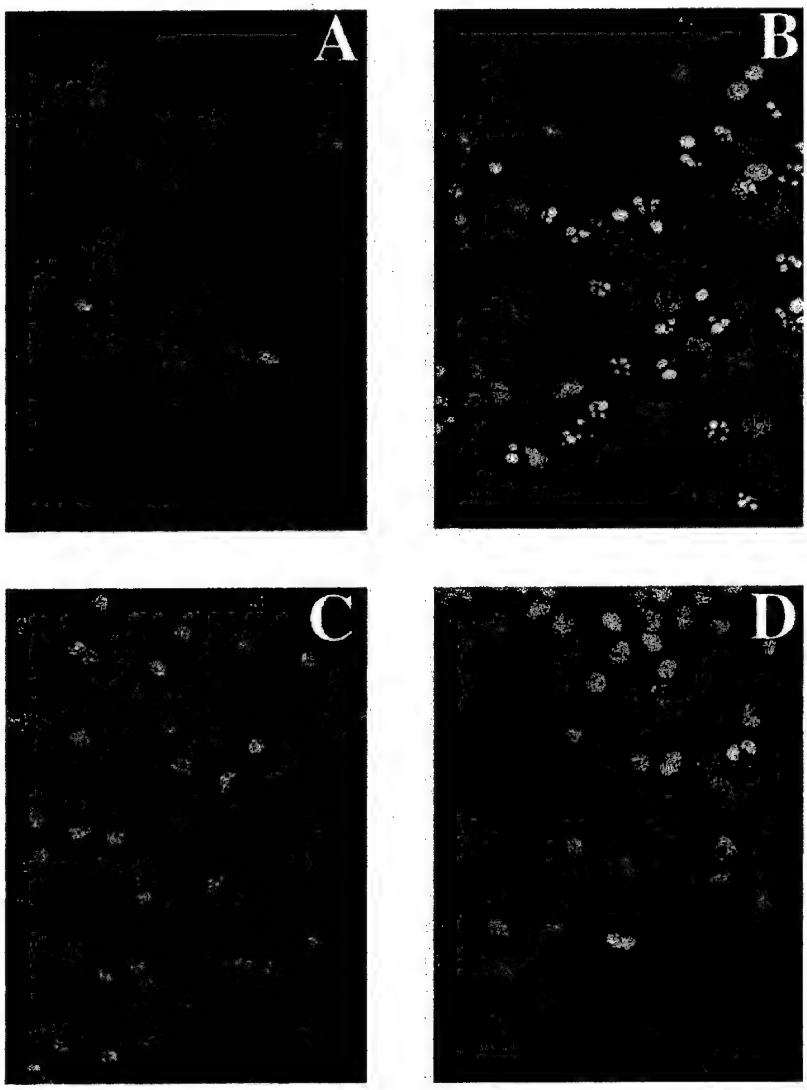

FIG. 4. DTDP-induced caspase-dependent asymmetric chromatin condensation in neurons. Neuron-enriched cultures were exposed to (**A**) vehicle, (**B**) DTDP (10 μM, 10 min), (**C**) BAF (100 μM), or (**D**) DTDP plus BAF. Cultures were fixed at 18–20 h, stained with Hoechst 33342 (5 μg/ml), and visualized with a microscope equipped with a fluorescent light source.

increased the fluorescence signal in fluo-3-loaded neurons (data not shown). DTDP stimulation increased the fluo-3 signal to 2.4 ± 0.05 times the basal level, whereas stimulation with 100 μM NMDA plus 10 μM glycine caused a 7.6 ± 0.2-fold increase in the fluo-3 signal (n = 115; data not shown).

Although three of the four dyes used are typically used to measure increases in $[Ca^{2+}]_i$, the DTDP-induced signal changes reported here likely represent increases in $[Zn^{2+}]_i$. This is supported by three lines of evidence. First, Newport Green shows little or no change in signal in response to increases in $[Ca^{2+}]_i$ or intracellular free Mg^{2+} concentration ($[Mg^{2+}]_i$) (data not shown). Second, increases in $[Ca^{2+}]_i$ of a magnitude sufficient to cause changes in the magfura-2 ratio (K_D for Ca^{2+} of ~25 μM) would cause very large, possibly saturating, responses when measured with the high-affinity indicators fura-2 and fluo-3 [K_D values for Ca^{2+} of 145 and 390 nM, respectively (Stout and Reynolds, 1999)]. Third, the three Ca^{2+}-sensitive dyes undergo fluorescence changes

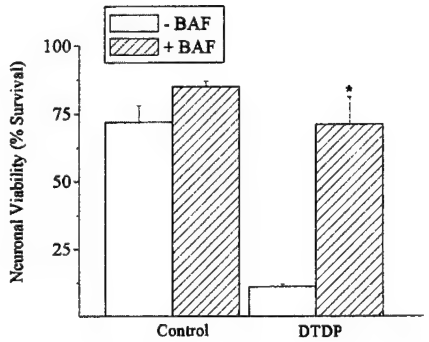

FIG. 5. DTDP toxicity is abolished by BAF in neuronal cultures. Neuron-enriched cultures were exposed to vehicle, BAF (100 μM), DTDP (10 μM, 10 min), or DTDP plus BAF. Viable cells were counted before the treatments and 18–20 h later. Data are mean ± SEM (bars) values from three experiments. *$p < 0.05$ by paired t test, indicating viability is significantly greater in the DTDP + BAF group versus DTDP alone.

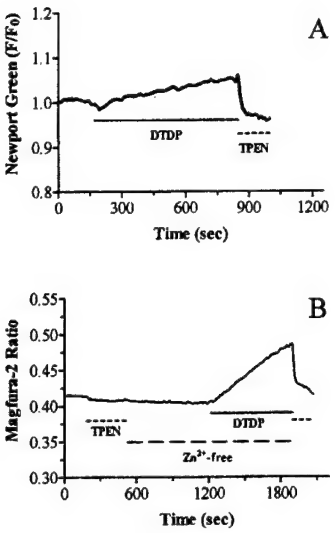

FIG. 6. DTDP causes increases in $[Zn^{2+}]_i$ in neurons. **A:** Neurons loaded with the Zn^{2+}-specific fluorophore Newport Green were exposed to DTDP (100 μM, 10 min; dashed line). DTDP responses were reversed by treatment with TPEN (25 μM, 2.5 min; solid line). The trace depicts the mean change in fluorescence (F/F_0) observed in a field of neurons from a single coverslip and is representative of three separate experiments. DTDP-treated neurons exhibited an increase in Newport Green fluorescence (arbitrary units) of 4.66 ± 0.39 (n = 43), which constituted an average increase of ~12.8%. **B:** DTDP releases Zn^{2+} from tightly bound intracellular stores. Neurons loaded with magfura-2 were exposed to TPEN (25 μM, 5 min; solid line) and subsequently washed with Zn^{2+}-free buffer (large dashed line). After 10 min, DTDP (100 μM; dashed line) was added to the Zn^{2+}-free perfusate for an additional 10 min. The experiment was terminated with application of TPEN (25 μM, 2.5 min; solid line). The trace depicts the mean ratio change observed in a single field of cells and is representative of three separate experiments. Neurons subjected to this series of treatments showed an average magfura-2 ratio increase of 0.072 ± 0.005 units (n = 32).

on Zn^{2+} binding, and the affinities of fura-2, fluo-3, and magfura-2 for Zn^{2+} are similar (low nanomolar K_D values) (Grynkiewicz et al., 1985; Simons, 1993), whereas their affinities for Ca^{2+} and Mg^{2+} vary considerably. Hence, all three dyes detect increases in $[Zn^{2+}]_i$ in the same concentration range. Fourth, the increases in the fluorescence signals observed with magfura-2, fura-2, and fluo-3 were completely reversed by perfusion with TPEN (25 μM; Fig. 7C and D and data not shown). TPEN has a high affinity for Zn^{2+} (K_D = 0.26 fM) but has an affinity for Ca^{2+} that is lower than that of any of the dyes used here [K_D = 40 μM (Arslan et al., 1985)]. Therefore, if the DTDP-induced responses did reflect increases in $[Ca^{2+}]_i$, it is unlikely that TPEN could bind free Ca^{2+} sufficiently to reverse the response. It is also unlikely that these DTDP responses represent increases in $[Mg^{2+}]_i$ because neither fura-2 nor fluo-3 responds to increases in $[Mg^{2+}]_i$ (Stout and Reynolds, 1999) and because the affinity of TPEN for Mg^{2+} [K_D = 20 mM (Arslan et al., 1985)] would not be sufficient to compete with magfura-2 in chelating Mg^{2+} and reversing the response (K_D for Mg^{2+} of 1.9 mM). Thus, both the relative magnitude of the responses measured with the different dyes and the reversibility with TPEN are consistent with the DTDP-induced responses being due to increases in $[Zn^{2+}]_i$.

Previous experiments by our group have demonstrated increases in $[Zn^{2+}]_i$ in the 40–100 nM range on exposure to Zn^{2+} under conditions in which $[Ca^{2+}]_i$ and $[Mg^{2+}]_i$ do not change (Cheng and Reynolds, 1998). When we used this previous Zn^{2+} stimulation paradigm with the imaging system used in the present study, we observed responses similar in magnitude to those induced by DTDP, suggesting DTDP responses are also in the nanomolar range. As DTDP has previously been reported to oxidize and activate ryanodine receptors to release Ca^{2+} from intracellular pools (Eager et al., 1997), our results suggest that intracellular ion changes associated with this reagent might be reevaluated to determine if the observed responses represented increases in $[Zn^{2+}]_i$ instead of $[Ca^{2+}]_i$. The reversal with TPEN observed here could also be consistent with DTDP-induced increases in the intracellular free Cu^{2+} concentration, but the fact that Newport Green does not respond to copper makes this possibility unlikely. Finally, both Fe^{2+} and Fe^{3+} produce a concentration-dependent quenching of fura-2 and magfura-2 in vitro (data not shown). Thus, it is also highly unlikely that the fluorescent changes observed in this study represent alterations in intracellular free iron levels.

As further evidence that the neuronal DTDP responses were mediated by increases in $[Zn^{2+}]_i$ and not $[Ca^{2+}]_i$, we showed that the DTDP-induced increases in the fura-2 signal were completely blocked when cells were loaded with a low concentration of 1,2-bis(2-aminophenoxy)ethane-*N,N,N',N'*-tetraacetic acid (BAPTA) AM before DTDP exposure (10 μM for 10 min; Fig. 7D). Although BAPTA can chelate both Zn^{2+} and Ca^{2+}, it has a higher affinity for Zn^{2+} (Csermely et al., 1989), and BAPTA had only a minor effect on the NMDA-stimulated increases in $[Ca^{2+}]_i$ in these cells at the concentration used here (Fig. 7D). DTDP-induced increases in the fura-2, magfura-2, and fluo-3 responses were also reversed by the sulfhydryl reducing agent dithiothreitol (Fig. 7A and data not shown). Reversal with dithiothreitol is also consistent with the responses being due to increases in $[Zn^{2+}]_i$ because this agent can act as a Zn^{2+} chelator (Cornell and Crivaro, 1972) and could also act to reduce MT back to the form that has high affinity for Zn^{2+} (Jiang et al., 1998; Maret and Vallee, 1998).

Low concentrations of a zinc chelator abolishes DTDP neurotoxicity

Given that our fluorescent dye experiments indicated that zinc released from an oxidation-sensitive store was observed following DTDP exposure, we next evaluated the contribution of this free Zn^{2+} to DTDP-induced apoptosis. We found that DTDP toxicity in neuron-enriched cultures was substantially inhibited by very low concentrations of TPEN (10 nM). The use of low concentrations of TPEN for a very limited exposure time

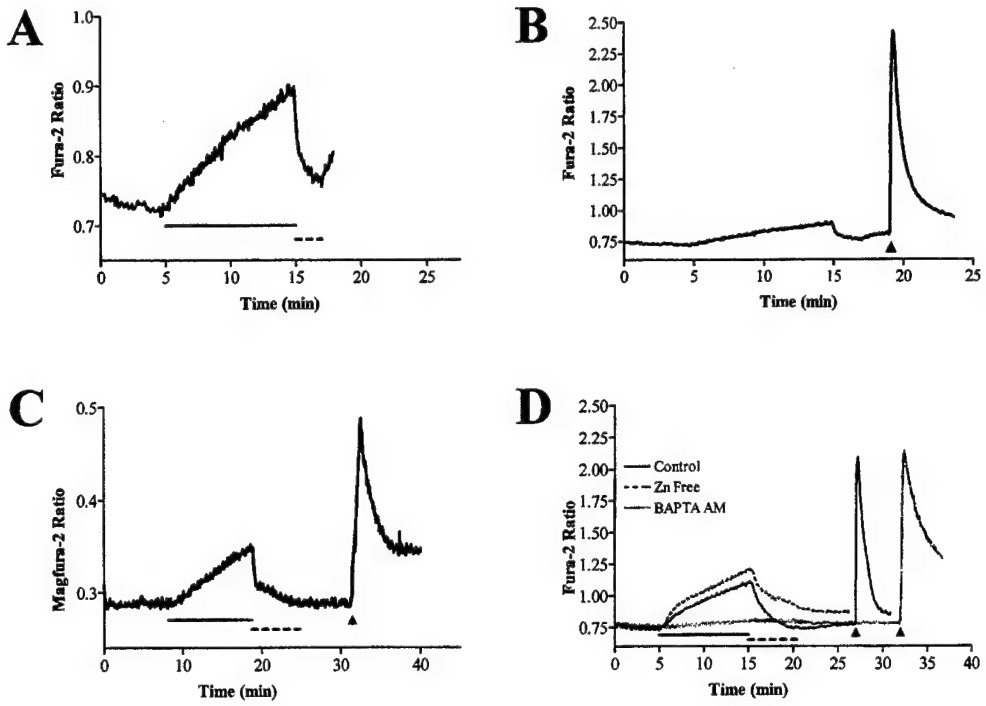

FIG. 7. Further characterization of DTDP-induced zinc release. **A:** Neurons loaded with the fluorescent indicator fura-2 AM were exposed to DTDP (100 μM, 10 min; solid line). DTDP responses were reversed by exposure to dithiothreitol (5 m*M*, 2 min; dashed line). **B:** For comparison, the responses obtained on stimulation with NMDA + glycine (100 μM + 10 μM, 15 s, arrowhead) in the same fura-2-loaded neurons are shown. **C:** Neurons loaded with the fluorescent indicator magfura-2 AM were exposed to DTDP (100 μM, 10 min; solid line). DTDP responses were reversed by exposure to TPEN (25 μM, 6 min). For comparison, the responses obtained on stimulation with NMDA + glycine (100 μM + 10 μM, 1 min, arrowhead) are also shown. **D:** Neurons loaded with the fluorescent indicator fura-2 AM were exposed to DTDP (100 μM, 10 min; solid line). Zn^{2+}-free buffer was present during DTDP stimulation as indicated. Cells were preloaded with BAPTA AM (10 μM, 10 min) as indicated. DTDP responses were reversed by exposure to TPEN (25 μM, 6 min; dashed line). For comparison, the responses obtained on stimulation with NMDA + glycine (100 μM + 10 μM, 15 s, arrowheads) in the same fura-2-loaded neurons are also shown. Each trace represents the mean results from a field of 16–32 neurons from separate coverslips. Similar results were obtained with two to 14 additional coverslips for each condition.

avoided any potential neurotoxic actions of the chelating agent itself, which have been reported by other investigators using very high concentrations of this substance (Ahn et al., 1998; Adler et al., 1999; Virag and Szabo, 1999; although see Shumaker et al., 1998). These neuroprotective actions of TPEN were detected both by Hoechst staining and by cell counting (Fig. 8). In addition, two other metal chelators, BAPTA AM (3 μM) and magfura-2 AM (5 μM) also induced significant neuroprotection against a 100 μM DTDP exposure (BAPTA, 35.0 ± 13.4% neuroprotection, n = 7; magfura-2, 57.8 ± 1.2%, n = 3; $p < 0.05$ and $p < 0.001$, respectively, by two-tailed one-sample *t* test). Although it is conceivable that all these metal chelators block DTDP toxicity by other mechanisms, such as preventing DTDP from inducing Zn^{2+} release from MT, we believe that the simplest explanation to account for these findings is that the chelating agents quickly scavenge any Zn^{2+} released by DTDP. The fact that nanomolar concentrations of TPEN were protective in these studies further supports our contention that DTDP toxicity is due to Zn^{2+} and not Ca^{2+} because the low concentration of TPEN used would not be effective at buffering even resting $[Ca^{2+}]_i$ in these cells.

DISCUSSION

Prior studies have found that elevated $[Zn^{2+}]_i$ may be toxic to neurons following transport into cells via various entry routes (Choi et al., 1988; Weiss et al., 1993; Koh and Choi, 1994; Manev et al., 1997; Sensi et al., 1997; Cuajungco and Lees, 1998*a*). Recent reports by Vallee and colleagues suggest that Zn^{2+} binding and release inside the cell are dynamic processes that are intrinsically linked to the redox status of cell (Jacob et al., 1998; Jiang et al., 1998). The results presented in this study suggest that Zn^{2+} released from such intracellular stores may contribute to neuronal injury under conditions of oxidative stress. These studies thus provide evidence for a previously unrecognized link between oxidative stress and neuronal apoptosis. Furthermore, because there is a substantial body of evidence that links oxidative stress to chronic neurodegenerative disease states, our findings suggest that neuronal injury following intracellular release of Zn^{2+} may be of considerable significance. Given the ubiquitous expression of MT and the fact that zinc is the second most abundant transition metal in the CNS, metalloprotein-bound zinc could be an important component of neurodegeneration throughout the brain. The

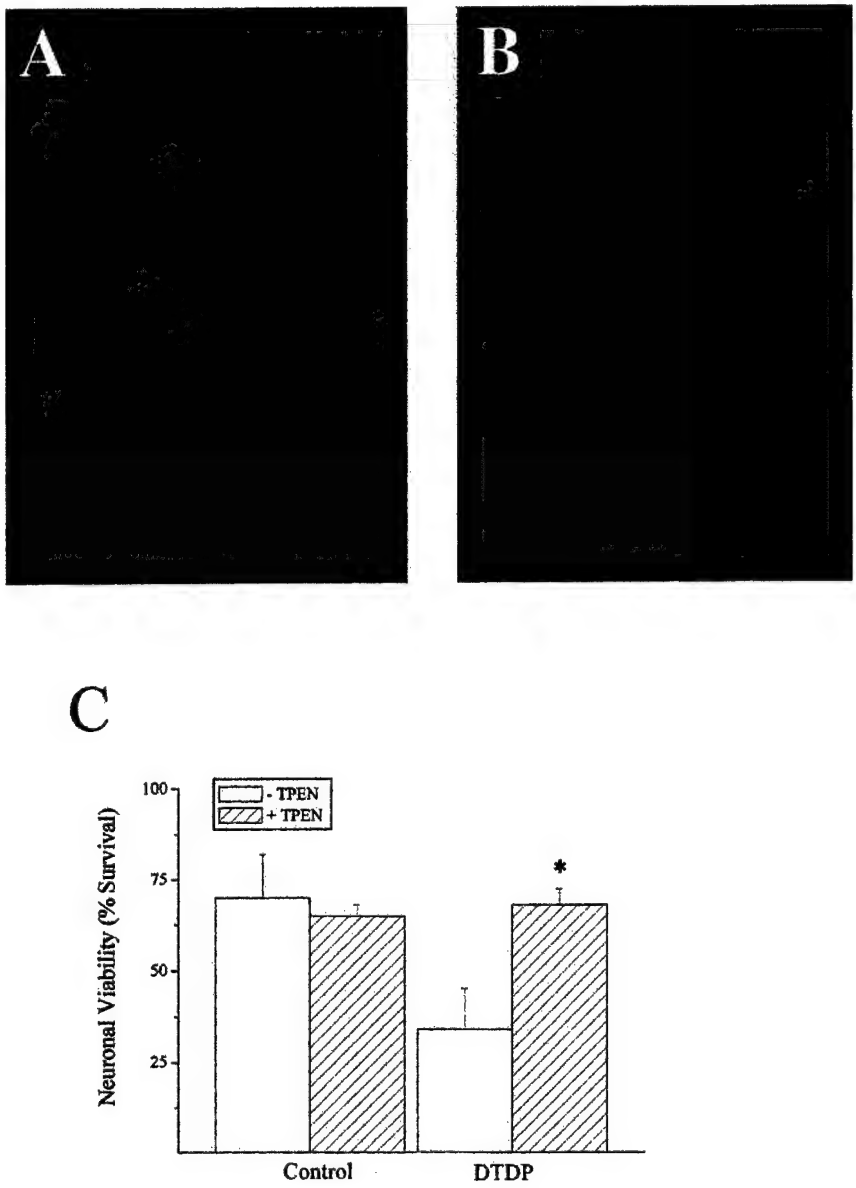

FIG. 8. Low concentrations of a zinc chelator are neuroprotective against DTDP. Neuron-enriched cultures were exposed to vehicle or DTDP (10 μM, 10 min) in the (**A**) absence or (**B**) presence of 10 n*M* TPEN. Cultures were fixed at 18–20 h, stained with Hoechst 33342 (5 μg/ml), and visualized with a microscope equipped with a fluorescent light source. **C:** Neuron-enriched cultures were exposed to vehicle or DTDP (10 μM, 10 min) in the presence or absence of TPEN (10 n*M*). Viable cells were counted before treatments and 18–20 h later to calculate neuronal viability. Data are mean ± SEM (bars) values from three experiments. $^*p < 0.05$ by paired *t* test, indicating viability is significantly greater in the DTDP + TPEN group versus DTDP alone.

use of DTDP thus provides a means to induce zinc release from a physiologically relevant and highly toxic pool.

We recognize that in our present studies we have used an oxidizing agent that, although well characterized for its effects on releasing zinc from MT (Jiang et al., 1998; Maret and Vallee, 1998), is hardly a relevant pathophysiological oxidation stimulus. Nonetheless, many endogenous oxidants are well known for their ability to cross-link or modify disulfide bonds and modify protein function (Aizenman et al., 1990). Therefore, the cell death pathway we describe here may have far-reaching implications in neuronal injury. Oxidative stress has been shown to induce rapidly MT gene expression following the activation of a metal response promoter that is selective for zinc [metal-responsive transcription factor (Dalton et al., 1996; Andrews, 1999)], providing indirect evidence that oxidative stress can lead to a rise in the intracellular concentration of this metal. Also, MT expression following a hypoxic challenge is abolished in nonneuronal cell lines that are deficient in this promoter but not in their wild-type counterparts (Murphy et al., 1999). Furthermore, nitric oxide, an important mediator of cell death in many models of neurodegeneration (Aizenman et al., 1998), has been shown to mobilize intracellular zinc, most likely through its release from MT (Kroncke et al., 1994; Berendji et al., 1997; Cuajungco and Lees, 1998*b*; Aravindakumar et al., 1999; Pearce et al., 2000). Finally, peroxynitrite-induced cytotoxicity in isolated thymocytes was recently shown to be abolished by zinc chelation (Virag and Szabo, 1999).

Zn^{2+}-induced neurotoxicity exhibits features of both apoptosis and necrosis (E. Y. Kim et al., 1999; Y. H. Kim et al., 1999). In the present study we demonstrate that the putative Zn^{2+}-mediated DTDP toxicity likely involves the loss of intracellular potassium and is caspase-dependent, and it induces DNA laddering, all of which are associated with apoptotic processes. Although other studies have previously shown that there are increases in $[Zn^{2+}]_i$ in lymphocytes undergoing apoptosis (Zalewski et al., 1994), the mechanisms by which Zn^{2+} activates cell death pathways are not clear. Indeed, there are several reports suggesting that Zn^{2+} can also inhibit apoptosis (Zalewski et al., 1993; Perry et al., 1997; Chai et al., 1999; Ho et al., 2000), especially at high concentrations (Fraker and Telford, 1997). In those studies Zn^{2+} was shown to inhibit directly both caspase and endonuclease activity as well as prevent apoptosis due to Zn^{2+} deficiency induced by membrane-permeable chelators or dietary deprivation. These studies do not exclude the possibility that the impact of Zn^{2+} on cell viability is critically dependent on the intracellular Zn^{2+} concentration and subcellular localization, as has previously been suggested for Ca^{2+} in neural cells (Lipton and Kater, 1989; Gwag et al., 1999).

We show here that DTDP-induced cell death can be abrogated by high extracellular KCl levels and TEA, presumably be preventing the depletion of intracellular potassium. The efflux of this ion from cells has been implicated in neuronal apoptosis (Lee et al., 1999) and has been associated with activation of caspase-3 (Bortner et al., 1997). This enzyme, in turn, has been shown to activate selectively a caspase-dependent DNase, which causes the apoptotic fragmentation of DNA (Enari et al., 1998) and chromatin condensation (Sahara et al., 1999), both of which were observed in our studies. However, the mechanism by which Zn^{2+} may initiate this putative cascade process is not known.

Zn^{2+} may compromise energy production in neurons by depleting cellular levels of NAD and thereby inhibiting glycolysis (Sheline et al., 2000). Another possibility is that Zn^{2+} may mediate alterations in the function of the mitochondrion, an organelle that has been tightly linked to apoptosis on its dysfunction. In fact, Zn^{2+} has been suggested to inhibit the electron transport chain (Kleiner, 1974) and induce the production of mitochondrial-derived reactive oxygen species (Sensi et al., 1999). Therefore, inhibition of mitochondrial function and respiration may be a causative factor in Zn^{2+}-mediated DTDP toxicity (Brown et al., 2000). Consistent with this notion, Manev et al. (1997) previously associated mitochondrial dysfunction with neuronal Zn^{2+} toxicity. Zn^{2+} has also been shown to activate sphingomyelinase (Spence et al., 1989; Schissel et al., 1996), which leads to generation of ceramide, a known apoptogen (Hannun, 1994; Brugg et al., 1996), and can trigger the activation of mitogen-activated protein kinase pathways (Park and Koh, 1999). Zn^{2+} influx can induce expression of genes with MT promoters (Atar et al., 1995), and it is possible that oxidation-induced Zn^{2+} release from Zn^{2+}-containing DNA-binding proteins, including p53 (Fojta et al., 1999), might alter gene expression. Both of these effects could also contribute to DTDP-induced apoptotic cell death. In conclusion, our findings suggest that DTDP-induced Zn^{2+} release from intracellular stores can result in neuronal apoptosis. Given that oxidative stress is a common mechanism associated with cell death in several acute and chronic neurodegenerative conditions, we believe that oxidant-induced Zn^{2+} release may initiate a previously overlooked pathological cascade.

Acknowledgment: We thank D. Leszkiewicz, S. Du, and M. Tran for suggestions and help with some of the experiments and Dr. P. Land for many helpful discussions. This work was supported by grants NS29365 (to E.A.) and NS34138 (to I.J.R.) from the National Institutes of Health, a Grant-in Aid from the American Heart Association (to E.A.), grant 98292027 (to I.J.R.) from the USAMRMC, and the University of Pittsburgh Alzheimer's Disease Research Center (to B.A.M.). I.J.R. is an Established Investigator of the American Heart Association.

REFERENCES

Adler M., Shafer H., Hamilton T., and Petrali J. P. (1999) Cytotoxic actions of the heavy metal chelator TPEN on NG108–15 neuroblastoma–glioma cells. *Neurotoxicology* **20,** 571–582.

Ahn Y. H., Kim Y. H., Hong S. H., and Koh J. Y. (1998) Depletion of intracellular zinc induces protein synthesis-dependent neuronal apoptosis in mouse cortical culture. *Exp. Neurol.* **154,** 47–56.

Aizenman E., Hartnett K. A., and Reynolds I. J. (1990) Oxygen free radicals regulate NMDA receptor function via a redox modulatory site. *Neuron* **5,** 841–846.

Aizenman E., Brimecombe J. C., Potthoff W. K., and Rosenberg P. A. (1998) Why is the role of nitric oxide in NMDA receptor function and dysfunction so controversial? *Prog. Brain Res.* **118,** 53–71.

Andrews G. K. (1999) Regulation of metallothionein gene expression by oxidative stress and metal ions. *Biochem. Pharmacol.* **59,** 95–104.

Anikstejn L., Charton G., and Ben-Ari Y. (1987) Selective release of endogenous zinc from the hippocampal mossy fibers in situ. *Brain Res.* **404,** 58–64.

Aravindakumar C. T., Ceulemans J., and DeLey M. (1999) Nitric oxide induces Zn^{2+} release from metallothionein by destroying zinc–sulfur clusters without concomitant formation of *S*-nitrosothiol. *Biochem. J.* **344,** 253–258.

Arslan P., Virgilio F. D., Beltrame M., Tsien R. Y., and Pozzan T. (1985) Cytosolic Ca^{2+} homeostasis in Ehrlich and Yoshida carcinomas. A new, membrane permeant chelator of heavy metals reveals that these ascites tumor cell lines have normal cytosolic free Ca^{2+}. *J. Biol. Chem.* **260,** 2719–2727.

Assaf S. Y. and Chung S. H. (1984) Release of endogenous Zn^{2+} from brain tissue during activity. *Nature* **308,** 734–736.

Atar D., Backx P. H., Appel M. M., Gao W. D., and Marban E. (1995) Excitation–transcription coupling mediated by zinc influx through voltage dependent calcium channels. *J. Biol. Chem.* **270,** 2473–2477.

Berg J. M. (1990) Zinc fingers and other metal-binding domains. Elements for interactions between macromolecules. *J. Biol. Chem.* **265,** 6513–6516.

Berendji D., Kolb-Bachofen V., Meyer K. L., Grapenthin O., Weber H., Wahn V., and Kroncke K. D. (1997) Nitric oxide mediates intracytoplasmic and intranuclear zinc release. *FEBS Lett.* **405,** 37–41.

Bortner C. D., Hughes F. M. J. Jr., and Cidlowsky J. A. A. (1997) A primary role for K^+ and Na^+ efflux in the activation of apoptosis. *J. Biol. Chem.* **272,** 32436–32442.

Brown A. M., Kristal B. S., Effron M. S., Shestopalov A. I., Ulucci P. A., Sheu K.-F. R., Blass J. P., and Cooper A. J. L. (2000) Zn^{2+}

inhibits α-ketoglutarate-stimulated mitochondrial respiration and the isolated α-ketoglutarate dehydrogenase complex. *J. Biol. Chem.* **275,** 13441–13447.

Brugg B., Michel P. P., Agid Y., and Ruberg M. (1996) Ceramide induces apoptosis in cultured mesencephalic neurons. *J. Neurochem.* **66,** 733–739.

Canzoniero L. M., Sensi S. L., and Choi D. W. (1997) Measurement of intracellular free zinc in living neurons. *Neurobiol. Dis.* **4,** 275–279.

Chai F., Truong-Tran A. Q., Ho L. H., and Zalewski P. D. (1999) Regulation of caspase activation and apoptosis by cellular zinc fluxes and zinc deprivation: a review. *Immunol. Cell. Biol.* **77,** 272–278.

Cheng C. and Reynolds I. J. (1998) Calcium-sensitive fluorescent dyes can report increases in intracellular free zinc concentration in cultured forebrain neurons. *J. Neurochem.* **71,** 2401–2410.

Choi D. W., Yokoyama M., and Koh J. (1988) Zinc neurotoxicity in cortical cell culture. *Neuroscience* **24,** 67–79.

Cornell N. W. and Crivaro K. E. (1972) Stability constant for the zinc–dithiothreitol complex. *Anal. Biochem.* **47,** 203–208.

Csermely P., Sandor P., Radics L., and Somogyi J. (1989) Zinc forms complexes with higher kinetical stability than calcium, 5-F-BAPTA as a good example. *Biochem. Biophys. Res. Commun.* **165,** 838–844.

Cuajungco M. P. and Lees G. J. (1998*a*) Diverse effects of metal chelating agents on the neuronal cytotoxicity of zinc in the hippocampus. *Brain Res.* **799,** 97–107.

Cuajungco M. P. and Lees G. J. (1998*b*) Nitric oxide generators produce accumulations of chelatable zinc in hippocampal neuronal perikarya. *Brain Res.* **799,** 118–129.

Dalton T. P., Li Q., Bittel D., Liang L., and Andrews G. K. (1996) Oxidative stress activates metal-responsive transcription factor-1 binding activity. Occupancy in vivo of metal response elements in the metallothionein-I gene promoter. *J. Biol. Chem.* **271,** 26233–26241.

Dineley K. E., Scanlon J. M., Kress G. J., Stout A. K., and Reynolds I. J. (2000) Astrocytes are more resistant than neurons to the cytotoxic effects of increased $[Zn^{2+}]_i$. *Neurobiol. Dis.* (in press).

Eager K. R., Roden L. D., and Dulhunty A. F. (1997) Actions of sulfhydryl reagents on single ryanodine receptor Ca^{2+}-release channels from sheep myocardium. *Am. J. Physiol.* **272,** C1908–C1918.

Enari M., Sakahira H., Yokoyama H., Okawa K., Iwamatsu A., and Nagata S. (1998) A caspase-dependent DNase that degrades DNA during apoptosis, and its inhibitor ICAD. *Nature* **391,** 43–50.

Fojta M., Kubicarova T., Vojtesek B., and Palecek E. (1999) Effect of p53 protein redox states on binding to supercoiled and linear DNA. *J. Biol. Chem.* **274,** 25749–25755.

Fraker P. J. and Telford W. G. (1997) A reappraisal of the role of zinc in life and death decisions of cells. *Proc. Soc. Exp. Biol. Med.* **215,** 229–236.

Frederickson C. J. (1989) Neurobiology of zinc and zinc-containing neurons. *Int. Rev. Neurobiol.* **31,** 145–238.

Frederickson C. J., Hernandez M. D., Goik S. A., Morton J. D., and McGinty J. F. (1988) Loss of zinc staining from hippocampal mossy fibers during kainic acid induced seizures: a histofluorescence study. *Brain Res.* **446,** 383–386.

Grynkiewicz G., Poenie M., and Tsien R. Y. (1985) A new generation of Ca^{2+} indicators with greatly improved fluorescence properties. *J. Biol. Chem.* **260,** 3440–3450.

Gwag B. J., Canzoniero L. M., Sensi S. L., Demaro J. A., Koh J. Y., Goldberg M. P., Jacquin M., and Choi D. W. (1999) Calcium ionophores can induce either apoptosis or necrosis in cultured cortical neurons. *Neuroscience* **90,** 1339–1348.

Hannun Y. A. (1994) The sphingomyelin cycle and the second messenger function of ceramide. *J. Biol. Chem.* **269,** 3125–3128.

Hartnett K. A., Stout A. K., Rajdev S., Rosenberg P. A., Reynolds I. J., and Aizenman E. (1997) NMDA receptor-mediated neurotoxicity: a paradoxical requirement for extracellular Mg^{2+} in Na^+/Ca^{2+}-free solutions in rat cortical neurons in vitro. *J. Neurochem.* **68,** 1836–1845.

Ho L. H., Ratnaike R. N., and Zalewski P. D. (2000) Involvement of intracellular labile zinc in suppression of DEVD-caspase activity in human neuroblastoma cells. *Biochem. Biophys. Res. Commun.* **268,** 148–154.

Howell G. A., Welch M. G., and Frederickson C. J. (1984) Stimulation-induced uptake and release of zinc in hippocampal slices. *Nature* **308,** 736–738.

Jacob C., Maret W., and Vallee B. L. (1998) Control of zinc transfer between thionein, metallothionein and zinc proteins. *Proc. Natl. Acad. Sci. USA* **95,** 3489–3494.

Jiang L. J., Maret W., and Vallee B. L. (1998) The glutathione redox couple modulates zinc transfer from metallothionein to zinc-depleted sorbitol dehydrogenase. *Proc. Natl. Acad. Sci. USA* **95,** 3483–3488.

Kim E. Y., Koh J. Y., Kim Y. H., Sohn S., Joe E., and Gwag B. J. (1999) Zn^{2+} entry produces oxidative neuronal necrosis in cortical cell cultures. *Eur. J. Neurosci.* **11,** 327–334.

Kim Y. H., Kim E. Y., Gwag B. J., Sohn S., and Koh J. Y. (1999) Zinc-induced cortical neuronal death with features of apoptosis and necrosis: mediation by free radicals. *Neuroscience* **89,** 175–182.

Kleiner D. (1974) The effect of Zn^{2+} ions on mitochondrial electron transport. *Arch. Biochem. Biophys.* **165,** 121–125.

Koh J.-Y. and Choi D. W. (1994) Zinc toxicity on cultured cortical neurons: involvement of *N*-methyl-D-aspartate receptors. *Neuroscience* **60,** 1049–1057.

Koh J.-Y., Suh S. W., Gwag B. J., He Y. Y., Hsu C. Y., and Choi D. W. (1996) The role of zinc in selective neuronal death after transient global cerebral ischemia. *Science* **272,** 1013–1016.

Kroncke K. D., Fehsel K., Schmidt T., Zenke F. T., Dasting I., Wesener J. R., Betterman H., Breunig K. D., and Kolb-Bachofen V. (1994) Nitric oxide destroys zinc–sulfur clusters inducing zinc release from metallothionein and inhibition of the zinc finger-type yeast transcription activator LAC9. *Biochem. Biophys. Res. Commun.* **200,** 1105–1110.

Lee J.-M., Zipfel G. J., and Choi D. W. (1999) The changing landscape of ischaemic brain injury mechanisms. *Nature* **399** (Suppl.), A7–A14.

Lee J.-Y., Park J., Kim Y.-H., Kim D. H., Kim C. G., and Koh J.-Y. (2000) Induction by synaptic zinc of heat shock protein-70 in hippocampus after kainate seizures. *Exp. Neurol.* **161,** 433–441.

Lipton S. A. and Kater S. B. (1989) Neurotransmitter regulation of neuronal outgrowth, plasticity and survival. *Trends Neurosci.* **12,** 265–270.

Manev H., Kharlamov E., Uz T., Mason R. P., and Cagnoli C. M. (1997) Characterization of zinc-induced neuronal death in primary cultures of rat cerebellar granule cells. *Exp. Neurol.* **146,** 171–178.

Maret W. and Vallee B. L. (1998) Thiolate ligands in metallothionein confer redox activity on zinc clusters. *Proc. Natl. Acad. Sci. USA* **95,** 3478–3482.

McLaughlin B. A., Nelson D., Silver I. A., Erecińska M., and Chesselet M. F. (1998) Methylmalonate toxicity in primary neuronal cultures. *Neuroscience* **86,** 279–290.

Murphy B. J., Andrews G. K., Bittel D., Discher D. J., McCue J., Green C. J., Yanovsky M., Giaccia A., Sutherland R. M., Laderoute K. R., and Webster K. A. (1999) Activation of metallothionein gene expression by hypoxia involves metal response elements and metal transcription factor-1. *Cancer Res.* **59,** 1315–1322.

Park J. A. and Koh J. Y. (1999) Induction of an immediate early gene egr-1 by zinc through extracellular signal-regulated kinase activation in cortical culture: its role in zinc-induced neuronal death. *J. Neurochem.* **73,** 450–456.

Pearce L. L., Gandley R. E., Han W., Wasserloos K., Stitt M., Kanai A. J., McLaughlin M. K., Pitt B. R., and Levitan E. S. (2000) Role of metallothionein in nitric oxide signaling as revealed by a green fluorescent fusion protein. *Proc. Natl. Acad. Sci. USA* **97,** 477–482.

Perry D. K., Smyth M. J., Stennicke H. R., Salvesen G. S., Duriez P., Poirier G. G., and Hannun Y. A. (1997) Zinc is a potent inhibitor of the apoptotic protease, caspase-3. A novel target for zinc in the inhibition of apoptosis. *J. Biol. Chem.* **272,** 18530–18533.

Rosenberg P. A. (1991) Accumulation of extracellular glutamate and neuronal death in astrocyte-poor cortical cultures exposed to glutamine. *Glia* **4,** 91–100.

Rosenberg P. A. and Aizenman E. (1989) Hundred-fold increase in neuronal vulnerability to glutamate toxicity in astrocyte-poor cultures of rat cerebral cortex. *Neurosci. Lett.* **103,** 162–168.

Sahara S., Aoto M., Eguchi Y., Imamoto N., Yoneda Y., and Tsujimoto Y. (1999) Acinus is a caspase-3-activated protein required for apoptotic chromatin condensation. *Nature* **401,** 168–173.

Schissel S. L., Schuchman E. H., Williams K. J., and Tabas I. (1996) Zn^{2+}-stimulated sphingomyelinase is secreted by many cell types and is a product of the acid sphingomyelinase gene. *J. Biol. Chem.* **271,** 18431–18436.

Sensi S. L., Canzoniero L. M., Yu S. P., Ying H. S., Koh J. Y., Kerchner G. A., and Choi D. W. (1997) Measurement of intracellular free zinc in living cortical neurons: routes of entry. *J. Neurosci.* **17,** 9554–9564.

Sensi S. L., Yin H. Z., Carriedo S. G., Rao S. S., and Weiss J. H. (1999) Preferential Zn^{2+} influx through Ca^{2+}-permeable AMPA/kainate channels triggers prolonged mitochondrial superoxide production. *Proc. Natl. Acad. Sci. USA* **96,** 2414–2419.

Sheline C. T., Behrens M. M., and Choi D. W. (2000) Zinc-induced cortical neuronal death: contribution of energy failure attributable to loss of NAD^+ and inhibition of glycolysis. *J. Neurosci.* **20,** 3139–3146.

Shumaker D. K., Vann L. R., Goldberg M. W., Allen T. D., and Wilson K. L. (1998) TPEN, a Zn^{2+}/Fe^{2+} chelator with low affinity for Ca^{2+}, inhibits lamin assembly, destabilizes nuclear architecture and may independently protect nuclei from apoptosis in vitro. *Cell Calcium* **23,** 151–164.

Simons T. J. B. (1993) Measurement of free Zn^{2+} ion concentration with the fluorescent probe mag-fura-2 (furaptra). *J. Biochem. Biophys. Methods* **27,** 25–37.

Sloviter R. S. (1985) A selective loss of hippocampal mossy fiber Timm stain accompanies granule cell seizure activity induced by perforant path stimulation. *Brain Res.* **330,** 150–153.

Spence M. W., Byers D. M., Palmer F. B., and Cook H. W. (1989) A new Zn^{2+}-stimulated sphingomyelinase in fetal bovine serum. *J. Biol. Chem.* **264,** 5358–5363.

Stout A. K. and Reynolds I. J. (1999) High-affinity calcium indicators underestimate increases in intracellular calcium concentrations associated with excitotoxic glutamate stimulations. *Neuroscience* **89,** 91–100.

Virag L. and Szabo C. (1999) Inhibition of poly(ADP-ribose) synthetase (PARS) and protection against peroxynitrite-induced cytotoxicity by zinc chelation. *Br. J. Pharmacol.* **126,** 769–777.

Vogt K., Mellor J., Tong G., and Nicoll R. (2000) The actions of synaptically released zinc at hippocampal mossy fibers. *J. Neurosci.* **26,** 187–196.

Weiss J. H., Hartley D. M., Koh J.-Y., and Choi D. W. (1993) AMPA receptor activation potentiates zinc neurotoxicity. *Neuron* **10,** 43–49.

Yu S. P., Yeh C. H., Sensi S., Gwag B. J., Canzoniero L. M., Farhangrazi Z. S., Ying H. S., Tian M., Dugan L. L., and Choi D. W. (1997) Mediation of neuronal apoptosis by enhancement of outward potassium current. *Science* **278,** 114–117.

Zalewski P. D., Forbes I. J., and Betts W. H. (1993) Correlation of apoptosis with change in intracellular labile Zn(II) using zinquin [(2-methyl-8-*p*-toluenesulphonamido-6-quinolyloxy)acetic acid], a new specific fluorescent probe for Zn(II). *Biochem. J.* **296,** 403–408.

Zalewski P. D., Forbes I. J., Seamark R. F., Borlinghaus R., Betts W. H., Lincoln S. F., and Ward A. D. (1994) Flux of intracellular labile zinc during apoptosis (gene-directed cell death) revealed by a specific chemical probe, Zinquin. *Chem. Biol.* **1,** 153–161.

Journal of Neurochemistry
Lippincott Williams & Wilkins, Inc., Philadelphia

Dopamine Oxidation Alters Mitochondrial Respiration and Induces Permeability Transition in Brain Mitochondria: Implications for Parkinson's Disease

*Sarah B. Berman and *†Teresa G. Hastings

*Departments of *Neuroscience and †Neurology, University of Pittsburgh, Pittsburgh, Pennsylvania, U.S.A.*

Abstract: Both reactive dopamine metabolites and mitochondrial dysfunction have been implicated in the neurodegeneration of Parkinson's disease. Dopamine metabolites, dopamine quinone and reactive oxygen species, can directly alter protein function by oxidative modifications, and several mitochondrial proteins may be targets of this oxidative damage. In this study, we examined, using isolated brain mitochondria, whether dopamine oxidation products alter mitochondrial function. We found that exposure to dopamine quinone caused a large increase in mitochondrial resting state 4 respiration. This effect was prevented by GSH but not superoxide dismutase and catalase. In contrast, exposure to dopamine and monoamine oxidase-generated hydrogen peroxide resulted in a decrease in active state 3 respiration. This inhibition was prevented by both pargyline and catalase. We also examined the effects of dopamine oxidation products on the opening of the mitochondrial permeability transition pore, which has been implicated in neuronal cell death. Dopamine oxidation to dopamine quinone caused a significant increase in swelling of brain and liver mitochondria. This was inhibited by both the pore inhibitor cyclosporin A and GSH, suggesting that swelling was due to pore opening and related to dopamine quinone formation. In contrast, dopamine and endogenous monoamine oxidase had no effect on mitochondrial swelling. These findings suggest that mitochondrial dysfunction induced by products of dopamine oxidation may be involved in neurodegenerative conditions such as Parkinson's disease and methamphetamine-induced neurotoxicity. **Key Words:** Dopamine—Mitochondria—Permeability transition—Parkinson's disease—Quinone—Respiration.
J. Neurochem. **73,** 1127–1137 (1999).

In Parkinson's disease (PD), the cause of the degeneration of dopaminergic neurons of the substantia nigra is unknown, but evidence suggests that oxidative stress is involved (for review, see Fahn and Cohen, 1992). One source of oxidative stress that is unique to dopaminergic neurons is the presence of dopamine (DA) itself, as DA can form reactive oxygen species (ROS) and quinones through two different pathways. First, DA is metabolized via monoamine oxidase (MAO) to produce hydrogen peroxide (H_2O_2) and dihydroxyphenylacetic acid (Maker et al., 1981). H_2O_2, if not reduced by cellular antioxidant mechanisms such as GSH and GSH peroxidase, can react with transition metals such as iron to form hydroxyl radical (Halliwell, 1992). This molecule will immediately react with lipids, DNA, and susceptible amino acids in proteins, thus causing cellular damage (Halliwell, 1992). Second, the catechol ring of DA can undergo oxidation to form DA quinone and ROS such as H_2O_2 and superoxide anion ($O_2^{\bullet -}$) in a reaction that can occur either spontaneously in the presence of transition metals or enzymatically (Graham, 1978; Hastings, 1995). The DA quinone is electron-deficient and reacts readily with cellular nucleophiles such as sulfhydryl groups on free cysteine, GSH, and cysteinyl residues in proteins (Tse et al., 1976; Graham, 1978). The reaction between the DA quinone and sulfhydryl groups leads to covalent modification of protein and free thiols, forming cysteinyl–DA conjugates (Tse et al., 1976; Graham, 1978; Fornstedt et al., 1990; Hastings and Zigmond, 1994). Because free thiols are important antioxidants in cells and protein cysteinyl residues often play critical roles in protein function, alterations of either free or protein thiols could lead to cellular toxicity.

DA is known to be toxic both in vitro (Graham, 1978; Michel and Hefti, 1990) and in vivo (Filloux and Townsend, 1993; Hastings et al., 1996), and we have shown that the formation of cysteinyl–DA conjugates

Received February 19, 1999; revised manuscript received May 3, 1999; accepted May 3, 1999.

Address correspondence and reprint requests to Dr. T. G. Hastings at Department of Neurology, S-505 Biomedical Science Tower, University of Pittsburgh, Pittsburgh, PA 15261, U.S.A.

Preliminary reports of these findings were presented at the 27th Annual Meeting of the Society for Neuroscience, New Orleans, LA, U.S.A., October 25–30, 1997.

Abbreviations used: CsA, cyclosporin A; DA, dopamine; H_2O_2, hydrogen peroxide; MAO, monoamine oxidase; $O_2^{\bullet -}$, superoxide anion; 6-OHDA, 6-hydroxydopamine; PD, Parkinson's disease; PTP, permeability transition pore; ROS, reactive oxygen species; SOD, superoxide dismutase; TMPD, *N,N,N′,N′*-tetramethyl-*p*-phenylenediamine.

correlates with DA-induced neurotoxicity (Hastings et al., 1996). In addition, we have shown that DA oxidation products can inhibit the function of specific proteins, the DA and glutamate transporters (Berman et al., 1996; Berman and Hastings, 1997), and others have recently reported similar effects on the activities of tryptophan hydroxylase (Kuhn and Arthur, 1998) and tyrosine hydroxylase (Xu et al., 1998).

The protein targets that are critical to the toxicity induced by DA are not yet known, but likely candidates include many of the proteins important in mitochondrial processes. The critical role of mitochondria for cellular survival is well known, and mitochondrial dysfunction has recently been elucidated as an essential target in the induction of apoptosis as well as in excitotoxic neuronal death (Deckwerth and Johnson, 1993; Vayssiére et al., 1994; Zamzami et al., 1995*a*,*b*; Petit et al., 1995; Liu et al., 1996; Schinder et al., 1996; Susin et al., 1996; White and Reynolds, 1996; Ellerby et al., 1997). These findings have led to a focus on potential contributions of mitochondrial dysfunction to neurodegenerative diseases (see Bowling and Beal, 1995). Mitochondria are of particular interest in PD, where evidence has suggested that an underlying deficit of complex I enzyme activity in the mitochondrial electron transport chain exists (Parker et al., 1989; Schapira et al., 1990*a*,*b*; Shoffner et al., 1991; Mann et al., 1992; Martin et al., 1996; Sheehan et al., 1997). Whether this plays a causative role in PD has not yet been elucidated, but it suggests that deficiencies in mitochondrial function could be involved in the degeneration of DA neurons.

Several mitochondrial processes can be disrupted by oxidants such as ROS and quinones. One such process is mitochondrial respiration, which is responsible for generating ATP through oxidative phosphorylation. Several enzymes in the electron transport chain have been shown to be inhibited following exposure to ROS or sulfhydryl-modifying agents (Kenney, 1975; Yagi and Hatefi, 1987; Zhang et al., 1990; Benard and Balasubramanian, 1995). Because both ROS and quinones, formed as a result of DA oxidation, are capable of modifying critical sulfhydryl groups on proteins, these electron transport enzymes may be susceptible to damage by DA oxidation products.

Another potential target of DA oxidation products is the mitochondrial permeability transition pore (PTP). The PTP is a calcium-dependent, proteinaceous pore that allows the normally impermeable inner membrane of mitochondria to become permeable to solutes of <1,500 Da. The change in membrane permeability leads to depolarization of the transmembrane potential, release of small solutes and then proteins, osmotic swelling, and a loss of oxidative phosphorylation (for review, see Gunter and Pfeiffer, 1990). Opening of the PTP has been implicated in several forms of neuronal death including apoptosis, excitotoxicity, ischemia, and toxicity due to the parkinsonian neurotoxin MPTP (Uchino et al., 1995; Nieminen et al., 1996; Packer et al., 1996; Schinder et al., 1996; White and Reynolds, 1996; Zamzami et al., 1996; Ouyang et al., 1997; Cassarino et al., 1998). Many oxidants and toxic quinones are known inducers of PTP opening (e.g., see Gunter and Pfeiffer, 1990). Likewise, sulfhydryl modification has been shown to induce PTP opening, and critical cysteinyl residues have been implicated in regulation of the PTP (Bernardi et al., 1992; Valle et al., 1993; Petronilli et al., 1994). Therefore, the PTP is also a potential target of ROS and quinones formed through both DA oxidation pathways.

In this study, we examined the effects of DA oxidation products on both mitochondrial respiration and the PTP, using isolated respiring brain mitochondria. We report that MAO-catalyzed oxidation of DA and production of H_2O_2 inhibit active mitochondrial respiration, whereas DA quinone production leads to a large increase in resting respiration, indicative of an increase in inner membrane permeability. In addition, we found that the oxidation of DA to DA quinone results in a cyclosporin A (CsA)-inhibitable increase in mitochondrial swelling, suggestive of the opening of the PTP. These effects on mitochondrial function could contribute to DA-induced toxicity and to the neurodegenerative process in PD.

MATERIALS AND METHODS

Mitochondrial isolation

Brain mitochondria were isolated from male Sprague–Dawley rats (300–350 g) by the method of Rosenthal et al. (1987). This method uses 0.02% digitonin to free mitochondria from the synaptosomal fraction. In brief, one rat was decapitated, and the whole brain minus the cerebellum was rapidly removed, washed, minced, and homogenized in a Dounce glass tissue homogenizer (via six strokes each with a loose-fitting pestle and then a tight-fitting pestle) at 4°C in 10 ml of isolation medium (225 m*M* mannitol, 75 m*M* sucrose, 5 m*M* HEPES, 1 m*M* EGTA, 1 mg/ml bovine serum albumin, pH 7.4) containing 5 mg of the bacterial protease Nagarse. Single brain homogenates were brought to 30 ml, divided equally into three tubes, and then centrifuged at 2,000 *g* for 3 min. Pellets were resuspended to 10 ml and recentrifuged as above, and the supernatants were pooled and centrifuged in four tubes at 12,000 *g* for 8 min. The pellets, including the fluffy synaptosomal layer, were resuspended in two tubes to 10 ml each in isolation medium containing 0.02% digitonin and centrifuged at 12,000 *g* for 10 min. The brown mitochondrial pellets without the synaptosomal layer were then resuspended again in 10 ml of medium and recentrifuged at 12,000 *g* for 10 min. The mitochondrial pellets were resuspended in 50 μl of medium/tube and combined. Mitochondrial protein yields, determined by the method of Bradford (1976), were ~8–12 mg per rat brain. When utilized, liver mitochondria were isolated from 1.5–1.75 g of liver tissue using the identical procedure, which produced 20–25 mg of mitochondrial protein.

Mitochondrial respiration

Respiration measurements were determined polarographically with a thermostatically controlled (37°C) Clark oxygen electrode (Yellow Springs Instrument Co., Yellow Springs, OH, U.S.A.) according to the method of Rosenthal et al. (1987) in standard respiration medium containing 125 m*M* KCl, 2 m*M* K_2HPO_4, 1 m*M* $MgCl_2$, 5 m*M* K-HEPES (pH 7.0), 1 m*M* EGTA, 5 m*M* glutamate, and 5 m*M* malate. Mitochondria (0.5 mg of protein/ml) were added to 1.6 ml of medium in a water-jacketed chamber (Gilson, Middleton, WI, U.S.A.). Ac-

tive state 3 respiration rates were determined by the addition of ADP (0.25 m*M*), and resting state 4 respiration rates were determined after consumption of ADP and the addition of oligomycin (2 μg/ml) to inhibit ATP synthase. Rates are expressed as nanograms of oxygen atoms consumed per minute per milligram of protein and were calculated based on the solubility of oxygen in the air-saturated, temperature-equilibrated medium of 390 ng of O/ml at 37°C and 760 mm Hg. Evaluation of state 3 and state 4 rates occurred over ~3–5 min for each sample. Prior to the initiation of every experiment, respiration rates of the mitochondrial preparation were determined, and mitochondria were used for these studies when the ratio of state 3 respiration to state 4 respiration was determined to be at least 7.0, signifying healthy, well-coupled mitochondria.

For experiments examining the effects of DA oxidation products on mitochondrial respiration, mitochondria (0.5 mg of protein/ml) were incubated in medium alone or medium containing the indicated compounds for 5 min in the electrode chamber at 37°C, with air bubbled into the chamber to maintain O_2 saturation. All control incubations were performed in an identical manner. At the end of the incubation period, state 3 and state 4 respiration was measured as described above. In experiments examining succinate-linked respiration, the medium contained 125 m*M* KCl, 2 m*M* K_2HPO_4, 1 m*M* $MgCl_2$, 5 m*M* K-HEPES (pH 7.0), 1 m*M* EGTA, 5 m*M* succinate, and 2 μ*M* rotenone. For experiments using ascorbate and *N,N,N′,N′*-tetramethyl-*p*-phenylenediamine (TMPD) to examine complex IV activity, mitochondria were incubated for 5 min in the standard respiration medium containing malate (5 m*M*) and glutamate (5 m*M*). After the incubation period, rotenone (2 μ*M*) was added, followed by the addition of antimycin A (1 μ*M*), ascorbate (2 m*M*), and TMPD (0.1 m*M*), and state 3 respiration was measured with the addition of ADP (0.25 m*M*).

Mitochondrial swelling

Mitochondrial swelling was measured spectrophotometrically (Beckman DU-640, Fullerton, CA, U.S.A.) by monitoring the decrease in absorbance at 540 nm over 10 min similar to previously described methods (Broekemeier et al., 1989). Mitochondria (1 mg of protein) were incubated in 2 ml of medium containing 213 m*M* mannitol, 70 m*M* sucrose, 3 m*M* HEPES (pH. 7.4), 10 m*M* succinate, and 1 μ*M* rotenone. $CaCl_2$ (70 μ*M*) was added after 30 s, and other indicated compounds were added at 2 min. When CsA or GSH was used, it was added to the buffer prior to the addition of the mitochondria. When tyrosinase was used to oxidize DA and when 6-hydroxydopamine (6-OHDA) was used, interfering absorbance due to colored oxidative products was subtracted from measurements using blanks containing only buffer with DA and tyrosinase or buffer with 6-OHDA. Data were quantified and compared by calculating the total decrease in absorbance from 2 to 10 min.

Statistical analysis

Analyses were performed by one-way ANOVA followed by Tukey's post hoc comparisons. A probability of $p < 0.05$ was considered significant. The n values reported refer to data obtained from n separate experiments.

RESULTS

Mitochondrial respiration

A typical measure of oxygen consumption in our isolated brain mitochondrial preparation is shown in Fig. 1. Mitochondrial respiration is conventionally classified into several states, which can be measured via oxygen consumption (Chance and Williams, 1956). State 3, termed active respiration, is defined as respiration in the presence of an oxidizable substrate and ADP and thus is a measure of the respiration that is coupled to ATP synthesis. State 4, or resting, respiration is the rate of respiration in the presence of substrate, but without ADP, and thus is a measure of the rate of respiration that is not coupled to ATP synthesis. Mean rates of active ADP-linked state 3 respiration and resting state 4 respiration were 216 ± 17 and 23 ± 2 ng of O/min/mg of protein, respectively, in untreated brain mitochondria (n = 28; mean ± SEM). The ratio of state 3 to state 4 can be used to evaluate the functional health of the preparation by giving an indication of the degree to which respiration is coupled to ATP synthesis. The average ratio of state 3 to state 4 was 10.2. For experiments in which liver mitochondria were used, mean state 3 and state 4 respiration was 219 ± 44 and 21 ± 5.6 ng of O/min/mg of protein, respectively, and did not differ significantly from that in isolated brain mitochondria (n = 6; mean ± SEM).

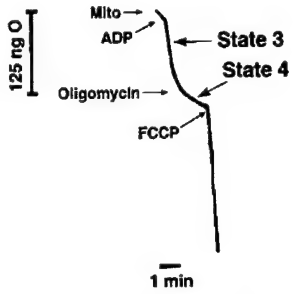

FIG. 1. Representative measure of baseline mitochondrial respiration. For each isolated mitochondrial preparation, oxygen consumption was first measured in isolated brain mitochondria (0.5 mg of protein/ml) with glutamate and malate as substrates, prior to any experimentation, as described in Materials and Methods. State 3 respiration was measured after addition of ADP (0.25 m*M*), and state 4 respiration was measured after addition of oligomycin (2 μg/ml). The rate of uncoupled respiration was recorded after the addition of FCCP (carbonyl cyanide *p*-trifluoromethoxyphenylhydrazone; 150 n*M*). Mean rates of oxygen consumption were 216 ± 17 and 23 ± 2 ng of O/min/mg of protein for state 3 and state 4, respectively.

Effects of DA oxidation on mitochondrial respiration

We first examined the effect of DA alone on mitochondrial respiration. When mitochondria were incubated for 5 min in the control respiration buffer, mean state 3 respiration was 86 ± 5 ng of O/min/mg of protein, and mean state 4 respiration was 18 ± 3 ng of O/min/mg of protein (Fig. 2). The reduction in state 3 respiration is typical for isolated brain mitochondria after incubation periods at 37°C. When brain mitochondria were incubated for 5 min in respiration buffer containing DA (100 μ*M*), state 3 respiration was reduced by 24% as compared with respiration after incubation in buffer alone (Fig. 2). However, state 4 respiration was unaffected by the presence of DA (Fig. 2). To determine whether the

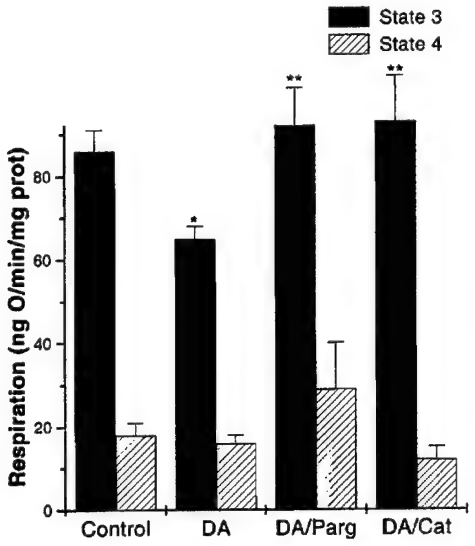

FIG. 2. Effect of DA on mitochondrial respiration. Isolated brain mitochondria were incubated for 5 min as described in Materials and Methods in buffer alone or buffer containing DA (100 μM), DA + pargyline (Parg; 10 μM), or DA + catalase (Cat; 1 U/ml), and then oxygen consumption was measured, utilizing glutamate and malate as substrates. Under control conditions, mean state 3 respiration was 86 ± 5 ng of O/min/mg of protein, and mean state 4 respiration was 18 ± 3 ng of O/min/mg of protein. *Significantly less than respiration under control conditions; **significantly greater than respiration after exposure to DA alone (mean ± SEM; n = 5–16).

state 3 inhibition caused by DA was due to H_2O_2 formed during MAO-catalyzed oxidation of DA, we examined the effects of adding the nonselective MAO inhibitor pargyline (10 μM) or the H_2O_2-scavenging enzyme catalase (1 U/ml) to the incubation medium. We found that the addition of either pargyline or catalase during the incubation with DA completely prevented the inhibition of state 3 respiration (Fig. 2). Neither pargyline nor catalase alone had any effect on mitochondrial respiration (data not shown).

To begin to determine which enzyme complexes of the electron transport chain were affected by DA, we utilized various substrates that donate electrons at different points in the electron transport chain, thereby hoping to bypass the DA-induced inhibition. We observed that when succinate and rotenone were utilized to bypass complex I and donate electrons via complex II to complex III, the decrease in state 3 respiration following incubation with DA was still observed (Fig. 3). Under these conditions, state 3 respiration was inhibited by 37% in the presence of DA as compared with control, an inhibition that was completely prevented by pargyline. However, when ascorbate and TMPD were utilized to donate electrons directly to cytochrome *c*, bypassing complexes I and III, incubation with DA no longer had any effect on state 3 respiration as compared with incubation under the same conditions without DA (Fig. 3).

To examine whether the products resulting from oxidation of the catechol ring would alter mitochondrial respiration, we utilized the enzyme tyrosinase to directly oxidize DA to DA quinone. Mitochondria were incubated for 5 min in standard respiration medium or medium containing DA (20 or 100 μM) and a concentration of tyrosinase (200 mU/ml) that was determined to oxidize all of the DA within 2 min (Berman and Hastings, 1997). Tyrosinase alone had no effect on respiration (data not shown). Following the incubation, we found that incubation with either concentration of DA quinone had no significant effect on state 3 respiration (Fig. 4A). However, we observed a dramatic increase in state 4 respiration with both the lower and the higher DA concentrations (+202 and +280%, respectively; Fig. 4B). Coincubation with GSH (500 μM), which can either reduce the DA quinone to DA or act as a nucleophile to bind DA, prevented the DA oxidation-induced increase in state 4 respiration at both concentrations of DA (Fig. 4B). GSH at this concentration had no effect on respiration (data not shown). When superoxide dismutase (SOD; 1 U/ml) and catalase (1 U/ml) were present, they did not prevent the increase in state 4 respiration caused by DA and tyrosinase (Fig. 4B).

Effects of DA oxidation products on mitochondrial permeability transition

Induction of permeability transition has been shown to lead to swelling of mitochondria (Gunter and Pfeiffer, 1990), which can be measured spectrophotometrically. Figure 5A shows the results of a representative swelling experiment. Exposure of brain mitochondria to control

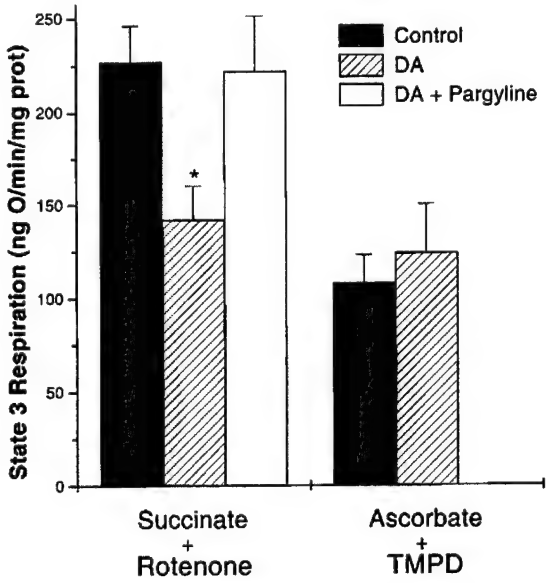

FIG. 3. Effect of bypassing steps in the electron transport chain on DA-induced inhibition of state 3 respiration. Mitochondria were incubated in buffer alone or buffer containing DA (100 μM) or DA + pargyline (10 μM) as described in Materials and Methods. Succinate (5 mM) + rotenone (2 μM) were utilized to donate electrons to complex II, and ascorbate (2 mM) + TMPD (100 μM) + antimycin A (1 μM) were utilized to donate electrons to cytochrome *c*. *Significantly less than respiration under control conditions (mean ± SEM; n = 3–8).

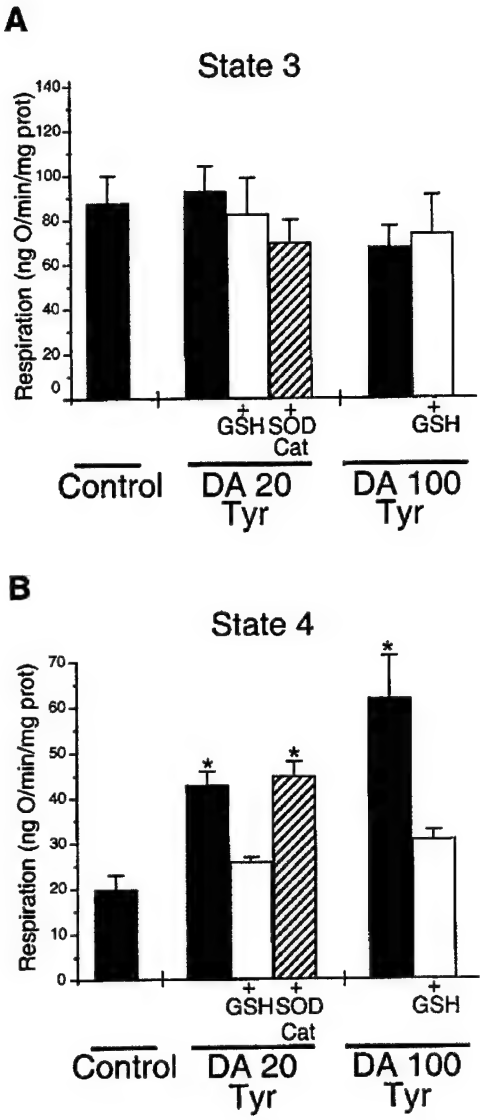

FIG. 4. Effect of enzymatic oxidation of DA on mitochondrial respiration. Mitochondria were incubated for 5 min in buffer or buffer containing DA (20 or 100 μM) + tyrosinase (Tyr; 200 U/ml) with or without GSH (500 μM) or SOD (1 U/ml) + catalase (Cat; 1 U/ml), and then respiration was measured using glutamate and malate as substrates. **A:** State 3 respiration. **B:** State 4 respiration. *Significantly different from control respiration (mean ± SEM; n = 3–13).

conditions (70 μM $CaCl_2$) led to a small degree of mitochondrial swelling. Exposure to 70 μM $CaCl_2$, followed by the addition of DA (100 μM), did not lead to an increase in the amount of mitochondrial swelling. However, exposure to the rapidly oxidizing catecholamine 6-OHDA (100 μM) significantly increased mitochondrial swelling. The results of these experiments, expressed as a change in absorbance, are quantified in Fig. 5B, demonstrating that 6-OHDA caused a threefold increase in mitochondrial swelling above control levels. CsA (850 nM), known to prevent the opening of the PTP in liver and heart mitochondria (Fournier et al., 1987; Crompton et al., 1988; Broekemeier et al., 1989), did not significantly prevent the swelling caused by 6-OHDA (Fig. 5B). CsA alone has no effect on swelling (data not shown).

We also examined the effects of DA quinone production using tyrosinase (Fig. 6). We found that brain mitochondria exposed to $CaCl_2$ (70 μM) followed by DA (100 μM) and tyrosinase (200 U/ml) led to a significant increase in mitochondrial swelling. In contrast to the findings with 6-OHDA, CsA (850 nM) was able to completely prevent the increase in swelling. Similar results were observed when a lower concentration of DA (20 μM) was utilized (Fig. 6). The addition of GSH (1

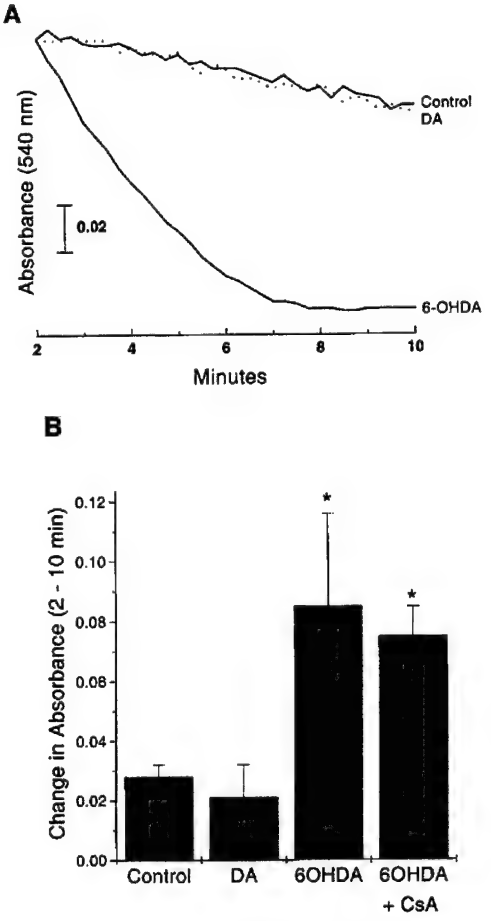

FIG. 5. Effect of DA and 6-OHDA on swelling of brain mitochondria. **A:** Representative traces of the change in absorbance at 540 nm, indicative of swelling in brain mitochondria, are shown following exposure to $CaCl_2$ (70 μM) alone (Control), $CaCl_2$ + DA (100 μM), or $CaCl_2$ + 6-OHDA (100 μM). $CaCl_2$ was added after 0.5 min, and DA or 6-OHDA was added at 2 min. When utilized, CsA (850 nM) was present at the beginning of the experiment. Absorbance changes due to the autoxidation of 6-OHDA were subtracted using blanks containing only buffer and 6-OHDA. **B:** Quantification of swelling measured as the absolute change in absorbance from the time the inducer was added (2 min) to 10 min (mean ± SEM; n = 3–6). *Significantly different from control values ($p < 0.05$).

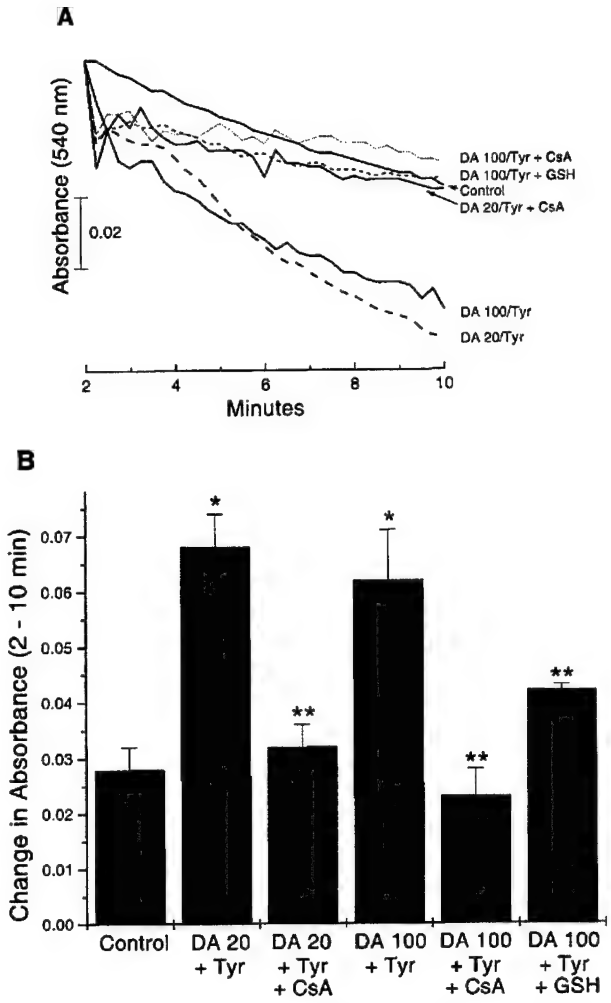

FIG. 6. Effect of tyrosinase (Tyr)-catalyzed oxidation of DA on swelling of brain mitochondria. **A:** Representative traces of swelling after exposure to $CaCl_2$ (70 μM) alone (Control) or + DA and tyrosinase (200 U/ml), with or without the addition of GSH (1 mM) or CsA (850 nM). $CaCl_2$ was added after 30 s, and then DA and tyrosinase were added at 2 min. When utilized, CsA and GSH were present at the beginning of the experiment. **B:** Quantification of swelling, measured as described in Fig. 5 (mean ± SEM; n = 3–6). *Significantly different from control values; **significantly different from the same condition without CsA or GSH.

mM) also significantly reduced the amount of swelling induced by DA and tyrosinase to levels similar to controls (Fig. 6).

The degree of swelling induced by DA oxidation in brain mitochondria is much smaller than that classically observed in studies of inducers of the transition pore. Most compounds have been tested in liver mitochondria, and we have noted that brain mitochondria respond to a much smaller degree to classic inducers of the PTP than do liver mitochondria (S. B. Berman, S. C. Watson, and T. G. Hastings, unpublished data). Therefore, we also examined the effect of DA quinone production on liver mitochondria. We observed that exposure of liver mitochondria to $CaCl_2$ (70 μM) followed by DA (100 μM) and tyrosinase (200 U/ml) resulted in large-amplitude swelling that was also prevented by the addition of CsA (Fig. 7). The change in absorbance induced in liver mitochondria by DA and tyrosinase was 11-fold higher than that observed in brain mitochondria (Figs. 6B and 7B) and was of similar magnitude to that observed for classic inducers of the PTP in liver mitochondria (e.g., Savage et al., 1991; Bernardi et al., 1992; S. B. Berman, S. C. Watson, and T. G. Hastings, unpublished data).

DISCUSSION

In this study, we provide evidence that both oxidation of the DA catechol ring and MAO-catalyzed DA oxidation can negatively affect the function of isolated brain mitochondria. We found that exposure of brain mitochondria to DA oxidation products altered both state 3 and state 4 mitochondrial respiration and caused mito-

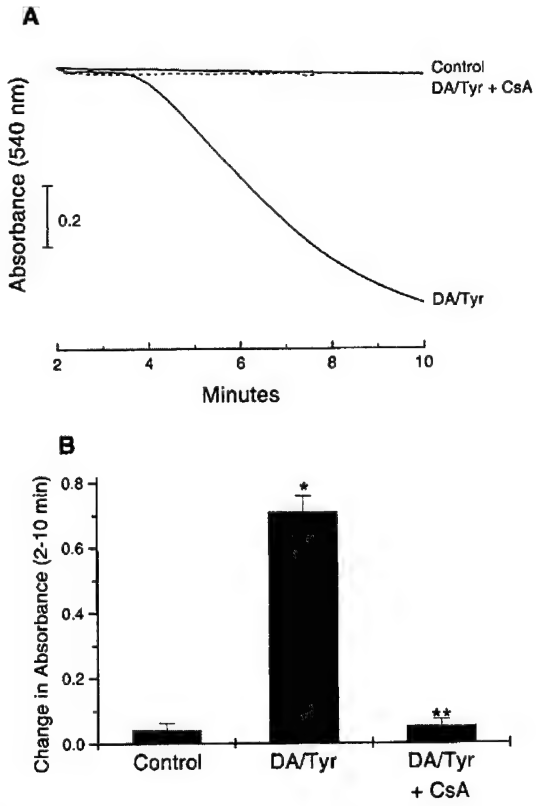

FIG. 7. Effect of tyrosinase (Tyr)-catalyzed oxidation of DA on swelling of liver mitochondria. **A:** Representative traces of swelling after exposure to $CaCl_2$ (70 μM) alone (Control) or + DA and tyrosinase (200 U/ml), with or without CsA (850 nM). Experiments were conducted as described in Fig. 6, except utilizing mitochondria isolated from liver. **B:** Quantification of swelling, measured as described in Fig. 5 (mean ± SEM; n = 3–6). *Significantly different from control values ($p < 0.05$); **significantly different from the same condition without CsA ($p < 0.05$). Note the different scale indicating absorbance change as compared with Fig. 6.

chondrial swelling that may be indicative of the opening of the PTP.

Mitochondrial respiration

DA oxidation to DA quinone. We provide the first evidence that oxidation of DA to DA quinone can lead to changes in mitochondrial respiration. We found that exposure of mitochondria to DA quinone resulted in a large increase in the resting rate of mitochondrial respiration (state 4). Normally, the transport of electrons through the electron transport chain is coupled to the pumping of protons from the matrix across the inner mitochondrial membrane, which is generally impermeable to protons (Brand et al., 1994). This establishes a proton gradient across the membrane, and protons are driven back into the matrix through the ATP synthase, providing the energy to convert ADP to ATP. In this way, mitochondrial respiration and its resultant oxygen consumption are coupled to ATP synthesis. If mitochondrial respiration were completely coupled to ATP synthesis, resting state 4 respiration would be zero, as ATP synthesis is not occurring. In healthy mitochondria, a low rate of respiration persists under state 4 conditions, and this is thought to be indicative of a low rate of proton leakage back across the inner membrane (Hafner et al., 1990). An increase in state 4 respiration therefore implies an increase in the proton leak across the membrane. After exposure to DA quinone, the rate of state 4 respiration increases nearly to the level of respiration measured in the presence of ADP (state 3). In other words, after exposure to DA quinone, respiration in the mitochondria proceeded without being coupled to ATP synthesis, an unproductive use of cellular energy.

It is possible that tyrosinase-catalyzed oxidation of DA produces not only the DA quinone but also $O_2^{\bullet -}$, albeit at a much lower level (Tomita et al., 1984; however, see Koga et al., 1992). To begin to determine whether the quinone is important in the effect on mitochondrial respiration that was observed, we investigated protection by either GSH or SOD plus catalase. GSH can reduce the quinone to DA or utilize its sulfhydryl group to covalently bind to DA quinone (Tse et al., 1976), thus scavenging the quinone and preventing it from binding to mitochondrial proteins. GSH was largely able to prevent the effect of DA and tyrosinase, suggesting that DA quinone is involved in the increase in resting respiration. SOD and catalase, which would detoxify any $O_2^{\bullet -}$ that might be formed, showed no protection against the effect caused by DA plus tyrosinase, further supporting the hypothesis that it is the DA quinone that is responsible for the uncoupling of respiration from ATP production.

Although the mechanism associated with the stimulation of resting respiration by DA quinone is not known, a similar effect on brain mitochondria was recently reported after exposure to the oxidant peroxynitrite (Brookes et al., 1998). This effect was prevented in the presence of the antioxidant Trolox. Although lipid peroxidation was suggested as a possible cause of the peroxynitrite effect, peroxynitrite, like DA quinone, can also modify sulfhydryl groups (Radi et al., 1991). Thus, it is also possible that covalent modification of sulfhydryl-containing proteins in the mitochondrial membrane contributes to the increase in proton permeability.

MAO-catalyzed oxidation of DA. We also found that MAO-catalyzed oxidation of DA, producing H_2O_2, led to an inhibition of active state 3 mitochondrial respiration. As both catalase and pargyline could prevent the inhibition, the production of H_2O_2 appears to be responsible for the effect. To determine where in the electron transport chain the inhibition was occurring, we utilized compounds that donate electrons directly to specific points along the chain, bypassing others. We found that inhibition of state 3 persisted when complex I was bypassed, suggesting that a process downstream of complex I is being affected. Furthermore, the inhibition disappeared when electrons were directly donated to cytochrome *c* just prior to complex IV, thus bypassing complex I and III. These findings suggest the possibility that the ubiquinone–complex III component of the electron transport chain is the target of the H_2O_2-induced inhibition. However, we cannot exclude the possibility that both complex I and II are inhibited by the H_2O_2. Both succinate dehydrogenase (complex II) and NADH dehydrogenase (complex I) have been shown to have thiol-dependent activity (Kenney, 1975; Benard and Balasubramanian, 1995) and thus may be susceptible to oxidation by H_2O_2.

This is the first study to examine the effect of DA on the oxygen consumption of well-coupled, healthy, intact mitochondria. Several previous studies examined only the effect of DA on complex I enzyme activity in tissue homogenates and reported conflicting results such as complete inhibition of complex I by 10 μM DA (Ben-Shachar et al., 1995), 25–50% inhibition with 1–100 m*M* DA (Przedborski et al., 1993), and 10% inhibition by 10 m*M* DA (Morikawa et al., 1996). The reasons for the discrepancies are not clear but may reflect different assay conditions. The two studies that began to investigate the role of DA oxidation in the enzyme inhibition noted prevention by antioxidants (Przedborski et al., 1993) and iron chelation (Ben-Shachar et al., 1995) but not by MAO inhibition (Ben-Shachar et al., 1995). All of these studies utilized only disrupted mitochondrial preparations to examine enzyme activities. However, studies utilizing intact, actively respiring mitochondria are likely to be more closely related to physiological circumstances, as the electron transport chain enzymes are normally coupled to ATP synthesis. In fact, studies have suggested that in nonsynaptic brain mitochondria, at least 70% inhibition of complex I is required before changes in state 3 respiration or ATP production are observed (Davey and Clark, 1996). Thus, the small inhibitory effect on respiration observed in our study may be indicative of larger changes in enzyme function. One other recent study utilized intact mitochondria but used extended incubation periods, and therefore less-coupled mitochondria, and utilized dye reduction rather than oxygen consumption as a measure of respiration, which does not allow examination of ATP synthesis-coupled

respiration (Cohen et al., 1997). It also studied only one of the two physiologic pathways of DA oxidation, MAO-catalyzed oxidation of DA, and reported an inhibition of respiration dependent on this oxidation, similar to our results. With avoidance of some of these limitations in our methods, the results of the current study confirm this finding as well as demonstrate significant effects on respiration by DA oxidation to DA quinone.

Mitochondrial permeability transition

Opening of the mitochondrial PTP has been suggested to play a critical role in several forms of neuronal cell death, including excitotoxicity, ischemia, MPP^+-induced toxicity, and hypoglycemia (Uchino et al., 1995; Nieminen et al., 1996; Packer et al., 1996; Schinder et al., 1996; White and Reynolds, 1996; Ouyang et al., 1997; Friberg et al., 1998). The increase in inner mitochondrial membrane permeability that is induced by PTP opening leads to mitochondrial membrane depolarization, release of small solutes and proteins, osmotic swelling, and a loss of oxidative phosphorylation (see Gunter and Pfeiffer, 1990; Bernardi, 1995). The PTP has been shown to contain critical thiol residues (Chernyak and Bernardi, 1996), and it has been induced by many oxidants including quinones (Gunter and Pfeiffer, 1990; Henry and Wallace, 1995; Henry et al., 1995). Therefore, we also examined effects of DA oxidation products on the PTP in mitochondria, and we conclude that DA quinone production resulted in the opening of the mitochondrial PTP. Mitochondrial swelling was induced in brain mitochondria after exposure to DA quinone that was completely prevented by the presence of the PTP inhibitor CsA, suggesting involvement of the PTP. GSH, which can inhibit DA quinone from reacting with sulfhydryl-containing mitochondrial proteins by covalently binding it as well as reducing it, was also able to prevent the swelling induced by DA quinone production.

Classically, most studies of the pore are performed in liver mitochondria, where a robust response has been well characterized (see Bernardi, 1995). To further investigate the effect of DA quinone production on classic pore characteristics, we also examined liver mitochondria. We found that enzymatic oxidation of DA produced large-amplitude swelling of liver mitochondria that was completely prevented by CsA, similar to that observed with other known pore inducers (e.g., Broekemeier et al., 1989; Bernardi et al., 1992). The magnitude of the swelling response in brain mitochondria was much smaller than that observed in liver (~10% of liver response) but is consistent with comparisons of PTP opening in brain and liver mitochondria after exposure to classic pore inducers such as calcium with phosphate (S. B. Berman, S. C. Watson, and T. G. Hastings, unpublished data).

The opening of the PTP induced by DA oxidation to DA quinone is interesting, given recent mechanistic studies of the transition pore. Evidence suggests that two sites exist on pore proteins that are important regulators of PTP function (Chernyak and Bernardi, 1996). One site contains vicinal thiols, which, when oxidized to disulfides, induce PTP opening. This site can be protected from oxidation by compounds that bind monothiols and prevent disulfide formation (Petronilli et al., 1994; Chernyak and Bernardi, 1996). One might expect that binding of DA quinone could protect similarly, binding directly to the monothiols. Benzoquinone has been suggested to inhibit PTP opening through this mechanism (Palmeira and Wallace, 1997). In contrast, there is also evidence that high concentrations of a monothiol-binding compound, *N*-ethylmaleimide, increased rather than decreased PTP opening (Petronilli et al., 1994), similar to the results with DA quinone.

A second important regulatory modulation involves the redox status of pyridine nucleotides. Oxidation of NADH and NADPH also increases pore opening, through an unknown mechanism that has been shown to be independent of the dithiol site (Chernyak and Bernardi, 1996). Oxidation of pyridines (both NADH and NADPH) can occur enzymatically through the cytosolic and mitochondrial enzyme DT-diaphorase, which reduces quinones via a two-electron reduction (Cadenas, 1995), and it has been shown that quinone substrates of DT-diaphorase can induce PTP opening (Chernyak and Bernardi, 1996). PTP opening by DA quinone could also be explained by this enzyme converting DA quinone to DA, oxidizing pyridine nucleotides in the process and increasing the probability of pore opening.

Availability of DA

For DA oxidation products to exert effects on mitochondrial function, DA must be available to mitochondrial proteins. Although the majority of DA in DA neurons is stored in vesicles, much of the DA clearly has access to mitochondria, because MAO, the major metabolizing enzyme of DA, is located on the outer mitochondrial membrane (Greenawalt and Schnaitman, 1970). One could hypothesize that under conditions of increased availability of cytoplasmic DA or increased synthesis and metabolism of DA, the potential for DA oxidation-induced effects on mitochondria would increase. Such conditions are thought to exist both in PD, where there is an increase in DA turnover (Bernheimer et al., 1973), and following high doses of methamphetamine, resulting in the redistribution of DA from vesicular storage to the cytoplasm (Cubbells et al., 1994; Sulzer et al., 1995). In fact, DA oxidation products have been shown to be increased in the substantia nigra of postmortem brain tissue from parkinsonian patients (Fornstedt et al., 1989; Spencer et al., 1998) and in rat striatum following exposure to methamphetamine (LaVoie and Hastings, 1999). Thus, these conditions may lead to an increase in cytoplasmic DA and subsequent increase in DA oxidation products, resulting in eventual dysfunction of mitochondria. Although this study was performed in vitro with isolated mitochondria and relatively high concentrations of DA, it raises the possibility that DA oxidation-induced alterations in mitochondrial function could occur under pathological conditions.

Conclusions

The alterations in mitochondrial function due to DA oxidation have several potential implications for neuronal cell death and neurodegenerative disease. As mentioned previously, it has been reported that individuals with PD exhibit a deficiency in the activity of complex I of the electron transport chain. It is not entirely clear whether this is a deficiency in all cells (Parker et al., 1989; Shoffner et al., 1991; Martin et al., 1996; Sheehan et al., 1997) or is limited to the substantia nigra (Schapira et al., 1990*b*; Mann et al., 1992), but the majority of evidence seems to point to a global deficiency. Therefore, the question arises as to the mechanism by which an underlying enzyme deficiency in all cells would lead to the specific loss of DA neurons. Our evidence suggests that one potential contributing factor may be the presence of DA. It is possible that an underlying deficiency, which alone does not cause cell death, is exacerbated by the presence of reactive DA metabolites. Other factors that have been implicated in PD, such as decreased antioxidant ability or increased iron (see Fahn and Cohen, 1992), also will contribute to increases in DA oxidation.

The effects of DA oxidation on mitochondrial function may also contribute to more acute neurotoxic events in which DA has been implicated. In methamphetamine toxicity, for example, DA is known to be important to the toxicity (Cubbels et al., 1994; Stephans and Yamamoto, 1994), and DA oxidation products have been shown to correlate with methamphetamine toxicity (LaVoie and Hastings, 1999). Thus, DA-induced mitochondrial dysfunction may also play a role in this neurotoxicity.

Acknowledgment: This study was supported in part by USPHS grants DA09601 and NS19068 and USAMRMC grant 98292027.

REFERENCES

Benard O. and Balasubramanian K. A. (1995) Effect of oxidized glutathione on intestinal mitochondria and brush border membrane. *Int. J. Biochem. Cell Biol.* **27,** 589–595.

Ben-Shachar D., Zuk R., and Glinka Y. (1995) Dopamine neurotoxicity: inhibition of mitochondrial respiration. *J. Neurochem.* **64,** 718–723.

Berman S. B. and Hastings T. G. (1997) Inhibition of glutamate transport in synaptosomes by dopamine oxidation and reactive oxygen species. *J. Neurochem.* **69,** 1185–1195.

Berman S. B., Zigmond M. J., and Hastings T. G. (1996) Modification of dopamine transporter function: effect of reactive oxygen species and dopamine. *J. Neurochem.* **67,** 593–600.

Bernardi P. (1995) The permeability transition pore. History and perspectives of a cyclosporin A-sensitive mitochondrial channel. *Prog. Cell Res.* **5,** 119–123.

Bernardi P., Vassanelli S., Veronese P., Raffaele C., Szabo I., and Zoratti M. (1992) Modulation of the mitochondrial permeability transition pore: effect of protons and divalent cations. *J. Biol. Chem.* **267,** 2934–2939.

Bernheimer H., Birkmayer W., Hornykiewicz O., Jellinger K., and Seitelberger F. (1973) Brain dopamine and the syndromes of Parkinson and Huntington. Clinical, morphological and neurochemical correlations. *J. Neurol. Sci.* **20,** 415–455.

Bowling A. C. and Beal M. F. (1995) Bioenergetic and oxidative stress in neurodegenerative diseases. *Life Sci.* **56,** 1151–1171.

Bradford M. A. (1976) A rapid and sensitive method for the quantitation of microgram quantities of protein utilizing the principle of protein-dye binding. *Anal. Biochem.* **72,** 248–254.

Brand M. D., Chien L.-F., Ainscow E. D., Rolfe D. F. S., and Porter R. K. (1994) The causes and functions of mitochondrial proton leak. *Biochim. Biophys. Acta* **1187,** 132–139.

Broekemeier K. M., Dempsey M. E., and Pfeiffer D. R. (1989) Cyclosporin A is a potent inhibitor of the inner membrane permeability transition in liver mitochondria. *J. Biol. Chem.* **264,** 7826–7830.

Brookes P. S., Land J. M., Clark J. B., and Heales S. J. R. (1998) Peroxynitrite and brain mitochondria: evidence for increased proton leak. *J. Neurochem.* **70,** 2195–2202.

Cadenas E. (1995) Antioxidant and prooxidant functions of DT-diaphorase in quinone metabolism. *Biochem. Pharmacol.* **49,** 127–140.

Cassarino D. S., Fall C. P., Smith T. S., and Bennett J. P. Jr. (1998) Pramipexole reduces reactive oxygen species production in vivo and in vitro and inhibits the mitochondrial permeability transition produced by the parkinsonian neurotoxin methylpyridinium ion. *J. Neurochem.* **71,** 295–301.

Chance B. and Williams G. R. (1956) The respiratory chain and oxidative phosphorylation. *Adv. Enzymol.* **17,** 65–134.

Chernyak B. V. and Bernardi P. (1996) The mitochondrial permeability transition pore is modulated by oxidative agents through both pyridine nucleotides and glutathione at two separate sites. *Eur. J. Biochem.* **238,** 623–630.

Cohen G., Farooqui R., and Kesler N. (1997) Parkinson disease: a new link between monoamine oxidase and mitochondrial electron flow. *Proc. Natl. Acad. Sci. USA* **94,** 4890–4894.

Crompton M., Ellinger H., and Costi A. (1988) Inhibition by cyclosporin A of a Ca^{2+}-dependent pore in heart mitochondria activated by inorganic phosphate and oxidative stress. *Biochem. J.* **255,** 357–360.

Cubbells J. F., Rayport S., Rajendran G., and Sulzer D. (1994) Methamphetamine neurotoxicity involves vacuolation of endocytic organelles and dopamine-dependent intracellular oxidative stress. *J. Neurosci.* **14,** 2260–2271.

Davey G. P. and Clark J. B. (1996) Threshold effects and control of oxidative phosphorylation in nonsynaptic rat brain mitochondria. *J. Neurochem.* **66,** 1617–1624.

Deckwerth T. L. and Johnson E. M. (1993) Temporal analysis of events associated with programmed cell death (apoptosis) of sympathetic neurons deprived of nerve growth factor. *J. Cell Biol.* **123,** 1207–1222.

Ellerby H. M., Martin S. J., Ellerby L. M., Naiem S. S., Rabizadeh S., Salvesen G. S., Casiano C. A., Cashman N. R., Green D. R., and Bredesen D. E. (1997) Establishment of a cell-free system of neuronal apoptosis: comparison of premitochondrial, mitochondrial, and postmitochondrial phases. *J. Neurosci.* **17,** 6165–6178.

Fahn S. and Cohen G. (1992) The oxidant stress hypothesis in Parkinson's disease: evidence supporting it. *Ann. Neurol.* **32,** 804–812.

Filloux F. and Townsend J. J. (1993) Pre- and postsynaptic neurotoxic effects of dopamine demonstrated by intrastriatal injection. *Exp. Neurol.* **119,** 79–88.

Fornstedt B., Brun A., Rosengren E., and Carlsson A. (1989) The apparent autoxidation rate of catechols in dopamine-rich regions of human brains increases with the degree of depigmentation of substantia nigra. *J. Neural Transm.* **1,** 279–295.

Fornstedt B., Bergh I., Rosengren E., and Carlsson A. (1990) An improved HPLC-electrochemical detection method for measuring brain levels of 5-*S*-cysteinyldopamine, 5-*S*-cysteinyl-3,4-dihydroxyphenylalanine, and 5-*S*-cysteinyl-3,4-dihydroxyphenylacetic acid. *J. Neurochem.* **54,** 578–586.

Fournier N., Ducet G., and Crevat A. (1987) Action of cyclosporine on mitochondrial calcium fluxes. *J. Bioenerg. Biomembr.* **19,** 297–303.

Friberg H., Ferrand-Drake M., Bengtsson F., Halestrap A. P., and Wieloch T. (1998) Cyclosporin A, but not FK506, protects mitochondria and neurons against hypoglycemic damage and implicates the mitochondrial permeability transition in cell death. *J. Neurosci.* **18,** 5151–5159.

Graham D. G. (1978) Oxidative pathways for catecholamines in the genesis of neuromelanin and cytotoxic quinones. *Mol. Pharmacol.* **14,** 633–643.

Greenawalt J. W. and Schnaitman C. (1970) An appraisal of the use of monoamine oxidase as an enzyme marker for the outer membrane of rat liver mitochondria. *J. Cell Biol.* **46,** 173–179.

Gunter T. E. and Pfeiffer D. R. (1990) Mechanisms by which mitochondria transport calcium. *Am. J. Physiol.* **258,** C755–C786.

Hafner R. P., Brown G. C., and Brand M. D. (1990) Analysis of the control of respiration rate, phosphorylation rate, proton leak rate and protonmotive force in isolated mitochondria using the "top-down" approach. *Eur. J. Biochem.* **188,** 313–319.

Halliwell B. (1992) Reactive oxygen species and the central nervous system. *J. Neurochem.* **59,** 1609–1623.

Hastings T. G. (1995) Enzymatic oxidation of dopamine: the role of prostaglandin H synthase. *J. Neurochem.* **64,** 919–924.

Hastings T. G. and Zigmond M. J. (1994) Identification of catechol–protein conjugates in neostriatal slices incubated with [^{3}H]dopamine: impact of ascorbic acid and glutathione. *J. Neurochem.* **63,** 1126–1132.

Hastings T. G., Lewis D., and Zigmond M. J. (1996) Role of oxidation in the neurotoxic effects of intrastriatal dopamine injections. *Proc. Natl. Acad. Sci. USA* **93,** 1956–1961.

Henry T. R. and Wallace K. B. (1995) Differential mechanisms of induction of the mitochondrial permeability transition by quinones of varying chemical reactivities. *Toxicol. Appl. Pharmacol.* **134,** 195–203.

Henry T. R., Solem L. E., and Wallace K. B. (1995) Channel-specific induction of the cyclosporine A-sensitive mitochondrial permeability transition by menadione. *J. Toxicol. Environ. Health* **45,** 489–504.

Kenney W. C. (1975) The reaction of *N*-ethylmaleimide at the active site of succinate dehydrogenase. *J. Biol. Chem.* **250,** 3089–3094.

Koga S., Nakano M., and Tero-Kuboto S. (1992) Generation of superoxide during the enzymatic action of tyrosinase. *Arch. Biochem. Biophys.* **292,** 570–575.

Kuhn D. M. and Arthur R. (1998) Dopamine inactivates tryptophan hydroxylase and forms a redox-cycling quinoprotein—possible endogenous toxin to serotonin neurons. *J. Neurosci.* **18,** 7111–7117.

LaVoie M. J. and Hastings T. G. (1999) Dopamine quinone formation and protein modification associated with the striatal neurotoxicity of methamphetamine: evidence against a role for extracellular dopamine. *J. Neurosci.* **19,** 1484–1491.

Liu X., Kim C. N., Yang J., Jemmerson R., and Wang X. (1996) Induction of apoptotic program in cell-free extracts: requirement for dATP and cytochrome c. *Cell* **86,** 147–157.

Maker H. S., Weiss C., Silides D. J., and Cohen G. (1981) Coupling of dopamine oxidation (monoamine oxidase activity) to glutathione oxidation via the generation of hydrogen peroxide in rat brain homogenates. *J. Neurochem.* **36,** 589–593.

Mann V. M., Cooper J. M., Krige D., Daniel S. E., Schapira A. H., and Marsden C. D. (1992) Brian, skeletal muscle and platelet homogenate mitochondrial function in Parkinson's disease. *Brain* **115,** 333–342.

Martin M. A., Molina J. A., Jimenez-Jimenez F. J., Benito-Leon J., Orti-Pareja M., Campos Y., and Arenas J. (1996) Respiratory chain enzyme activities in isolated mitochondria of lymphocytes from untreated Parkinson's disease patients. *Neurology* **46,** 1343–1346.

Michel P. P. and Hefti F. (1990) Toxicity of 6-hydroxydopamine and dopamine for dopaminergic neurons in culture. *J. Neurosci. Res.* **26,** 428–435.

Morikawa N., Nakagawa-Hattori Y., and Mizuno Y. (1996) Effect of dopamine, dimethoxyphenylethylamine, papaverine, and related compounds on mitochondrial respiration and complex I activity. *J. Neurochem.* **66,** 1174–1181.

Nieminen A.-L., Petrie T. G., LeMasters J. J., and Selman W. R. (1996) Cyclosporin A delays mitochondrial depolarization induced by *N*-methyl-D-aspartate in cortical neurons: evidence of the mitochondrial permeability transition. *Neuroscience* **75,** 993–997.

Ouyang Y. B., Kuroda S., Kristian T., and Siesjö B. K. (1997) Release of mitochondrial aspartate aminotransferase (MAST) following transient focal cerebral ischemia suggests the opening of a mitochondrial permeability transition pore. *Neurosci. Res. Commun.* **20,** 167–173.

Packer M. A., Miesel R., and Murphy M. P. (1996) Exposure to the parkinsonian neurotoxin 1-methyl-4-phenylpyridinium (MPP^+) and nitric oxide simultaneously causes cyclosporin A-sensitive mitochondrial calcium efflux and depolarisation. *Biochem. Pharmacol.* **51,** 267–273.

Palmeira C. M. and Wallace K. B. (1997) Benzoquinone inhibits the voltage-dependent induction of the mitochondrial permeability transition caused by redox-cycling naphthoquinones. *Toxicol. Appl. Pharmacol.* **143,** 338–347.

Parker W. D., Boyson S. J., and Parks J. K. (1989) Abnormalities of the electron transport chain in idiopathic Parkinson's disease. *Ann. Neurol.* **26,** 719–723.

Petit P. X., LeCoeur H., Zorn E., Duguet C., Mignotte B., and Gougeon M. L. (1995) Alterations of mitochondrial structure and function are early events of dexamethasone-induced thymocyte apoptosis. *J. Cell Biol.* **130,** 157–167.

Petronilli V., Costantini P., Scorrano L., Colonna R., Passamonti S., and Bernardi P. (1994) The voltage sensor of the mitochondrial permeability transition pore is tuned by the oxidation–reduction state of vicinal thiols: increase of the gating potential by oxidants and its reversal by reducing agents. *J. Biol. Chem.* **269,** 16638–16642.

Przedborski S., Jackson-Lewis V., Muthane U., Jiang H., Ferreira M., Naini A. B., and Fahn S. (1993) Chronic levodopa administration alters cerebral mitochondrial respiratory chain activity. *Ann. Neurol.* **34,** 715–723.

Radi R., Bechman J. S., Bush K. M., and Freeman B. A. (1991) Peroxynitrite oxidation of sulfhydryls: the cytotoxic potential of superoxide and nitric oxide. *J. Biol. Chem.* **206,** 4244–4250.

Rosenthal R. E., Hamud F., Fiskum G., Varghese P. J., and Sharpe S. (1987) Cerebral ischemia and reperfusion: prevention of brain mitochondrial injury by lidoflazine. *J. Cereb. Blood Flow Metab.* **7,** 752–758.

Savage M. K., Jones D. P., and Reed D. J. (1991) Calcium- and phosphate-dependent release and loading of glutathione by liver mitochondria. *Arch. Biochem. Biophys.* **290,** 51–56.

Schapira A. H. V., Cooper J. M., Dexter D., Clark J. B., Jenner P., and Marsden C. D. (1990*a*) Mitochondrial complex I deficiency in Parkinson's disease. *J. Neurochem.* **54,** 823–827.

Schapira A. H. V., Mann V. M., Cooper J. M., Dexter D., Daniel S. E., Jenner P., Clark J. B., and Marsden C. D. (1990*b*) Anatomic and disease specificity of NADH CoQ_1 reductase (complex I) deficiency in Parkinson's disease. *J. Neurochem.* **55,** 2142–2145.

Schinder A. F., Olson E. C., Spitzer N. C., and Montal M. (1996) Mitochondrial dysfunction is a primary event in glutamate neurotoxicity. *J. Neurosci.* **16,** 6125–6133.

Sheehan J. P., Swerdlow R. H., Parker W. D., Miller S. W., Davis R. E., and Tuttle J. B. (1997) Altered calcium homeostasis in cells transformed by mitochondria from individuals with Parkinson's disease. *J. Neurochem.* **68,** 1221–1233.

Shoffner J. M., Watts R. L., Juncos J. L., Torroni A., and Wallace D. C. (1991) Mitochondrial oxidative phosphorylation defects in Parkinson's disease. *Ann. Neurol.* **30,** 332–339.

Spencer J. P. E., Jenner P., Daniel S. E., Lees A. J., Marsden D. C., and Halliwell B. (1998) Conjugates of catecholamines with cysteine and GSH in Parkinson's disease: possible mechanisms of formation involving reactive oxygen species. *J. Neurochem.* **71,** 2112–2122.

Stephans S. E. and Yamamoto B. K. (1994) Methamphetamine-induced neurotoxicity: roles for glutamate and dopamine efflux. *Synapse* **17,** 203–209.

Sulzer D., Chen T.-K., Lau Y. Y., Kristensen H., Rayport S., and Ewing A. (1995) Amphetamine redistributes dopamine from synaptic vesicles to the cytosol and promotes reverse transport. *J. Neurosci.* **15,** 4102–4108.

Susin S. A., Zamzami N., Castedo M., Hirsch T., Marchetti P., Macho A., Daugas E., Geuskens M., and Kroemer G. (1996) Bcl-2 inhibits the mitochondrial release of an apoptogenic protease. *J. Exp. Med.* **184,** 1331–1341.

Tomita Y., Hariu A., Kato C., and Seiji M. (1984) Radical production during tyrosinase reaction, dopa–melanin formation, and photoirradiation of dopa–melanin. *J. Invest. Dermatol.* **82,** 573–576.

Tse D. C. S., McCreery R. L., and Adams R. N. (1976) Potential oxidative pathways of brain catecholamines. *J. Med. Chem.* **19,** 37–40.

Uchino H., Elmér E., Uchino K., Lindvall O., and Siesjö B. K. (1995) Cyclosporin A dramatically ameliorates CA1 hippocampal damage following transient forebrain ischaemia in the rat. *Acta Physiol. Scand.* **155,** 469–471.

Valle V. G. R., Fagian M. M., Parentoni L. S., Meinicke A. R., and Vercesi A. E. (1993) The participation of reactive oxygen species and protein thiols in the mechanism of mitochondrial inner membrane permeabilization by calcium plus prooxidants. *Arch. Biochem. Biophys.* **307,** 1–7.

Vayssiére J.-L., Petit P. X., Risler Y., and Mignotte B. (1994) Commitment to apoptosis is associated with changes in mitochondrial biogenesis and activity in cell lines conditionally immortalized with simian virus 40. *Proc. Natl. Acad. Sci. USA* **91,** 11752–11756.

White R. J. and Reynolds I. J. (1996) Mitochondrial depolarization in glutamate-stimulated neurons: an early signal specific to excitotoxin exposure. *J. Neurosci.* **16,** 5688–5697.

Xu Y. M., Stokes A. H., Roskoski R., and Vrana K. E. (1998) Dopamine, in the presence of tyrosinase, covalently modifies and inactivates tyrosine hydroxylase. *J. Neurosci. Res.* **54,** 691–697.

Yagi T. and Hatefi Y. (1987) Thiols in oxidative phosphorylation: thiols in the F_0 of ATP synthase essential for ATPase activity. *Arch. Biochem. Biophys.* **254,** 102–109.

Zamzami N., Marchetti P., Castedo M., Zanin C., Vayssiere J.-L., Petit P. X., and Kroemer G. (1995*a*) Reduction in mitochondrial potential constitutes an early irreversible step of programmed lymphocyte death in vivo. *J. Exp. Med.* **181,** 1661–1672.

Zamzami N., Marchetti P., Castedo M., Decaudin D., Macho A., Hirsch T., Susin S. A., Petit P. X., Mignotte B., and Kroemer G. (1995*b*) Sequential reduction of mitochondrial transmembrane potential and generation of reactive oxygen species in early programmed cell death. *J. Exp. Med.* **182,** 367–377.

Zamzami N., Susin S. A., Marchetti P., Hirsch T., Gómez-Monterrey I., Castedo M., and Kroemer G. (1996) Mitochondrial control of nuclear apoptosis. *J. Exp. Med.* **183,** 1533–1544.

Zhang Y., Marcillat O., Giulivi C., Ernster L., and Davies K. J. A. (1990) The oxidative inactivation of mitochondrial electron transport chain components and ATPase. *J. Biol. Chem.* **265,** 16330–16336.

Experimental Neurology **164**, 415–425 (2000)
doi:10.1006/exnr.2000.7438, available online at http://www.idealibrary.com on IDEAL®

Quantitative Biochemical and Ultrastructural Comparison of Mitochondrial Permeability Transition in Isolated Brain and Liver Mitochondria: Evidence for Reduced Sensitivity of Brain Mitochondria

Sarah B. Berman,* Simon C. Watkins,† and Teresa G. Hastings*,‡

*Department of Neuroscience, †Department of Cell Biology and Physiology, and ‡Department of Neurology, University of Pittsburgh, Pittsburgh, Pennsylvania 15213

Received November 15, 1999; accepted March 23, 2000

Opening of the mitochondrial permeability transition pore has increasingly been implicated in excitotoxic, ischemic, and apoptotic cell death, as well as in several neurodegenerative disease processes. However, much of the work directly characterizing properties of the transition pore has been performed in isolated liver mitochondria. Because of suggestions of tissue-specific differences in pore properties, we directly compared isolated brain mitochondria with liver mitochondria and used three quantitative biochemical and ultrastructural measurements of permeability transition. We provide evidence that brain mitochondria do not readily undergo permeability transition upon exposure to conditions that rapidly induce the opening of the transition pore in liver mitochondria. Exposure of liver mitochondria to transition-inducing agents led to a large, cyclosporin A-inhibitable decrease in spectrophotometric absorbance, a loss of mitochondrial glutathione, and morphologic evidence of matrix swelling and disruption, as expected. However, we found that similarly treated brain mitochondria showed very little absorbance change and no loss of glutathione. The absence of response in brain was not simply due to structural limitations, since large-amplitude swelling and release of glutathione occurred when membrane pores unrelated to the transition pore were formed. Additionally, electron microscopy revealed that the majority of brain mitochondria appeared morphologically unchanged following treatment to induce permeability transition. These findings show that isolated brain mitochondria are more resistant to induction of permeability transition than mitochondria from liver, which may have important implications for the study of the mechanisms involved in neuronal cell death.

Key Words: **mitochondria; permeability transition; neurodegeneration; apoptosis; excitotoxicity; oxidative stress.**

INTRODUCTION

The important role of mitochondria in normal cellular functioning has long been recognized, and not surprisingly, abnormalities in mitochondrial function are increasingly found to play a significant role in cell death. This has become of particular importance in the brain, where investigations into the mechanisms responsible for neurodegenerative diseases and neurotoxic events have begun to focus on the potential contributions of mitochondrial dysfunction (for review, see 23, 37). Mitochondrial dysfunction has been associated with the mechanisms of several forms of neuronal cell death, including excitotoxicity, apoptosis, ischemia, and hypoglycemia-induced death (20, 22, 27–28, 34, 42, 45, 48, 53, 57, 59, 61–64). Mitochondrial alterations have also been implicated in several neurodegenerative diseases, including Parkinson's disease, Alzheimer's disease, and amyotrophic lateral sclerosis (see 12).

One mitochondrial process that has been increasingly implicated in many of these neurotoxic and neurodegenerative conditions is the opening of a proteinaceous pore in the inner mitochondrial membrane, the permeability transition pore (PTP). The opening of the PTP, termed permeability transition, allows the normally impermeable inner membrane of mitochondria to become nonselectively permeable to solutes with a molecular mass of 1500 Daltons or less. This leads to mitochondrial membrane depolarization, release of small solutes and proteins, osmotic swelling, and a loss of oxidative phosphorylation (see 6, 31). Much of the early work characterizing the properties of the mitochondrial PTP has been performed in liver and heart cells, and opening of the PTP has been linked to many forms of cell death (7). Interest in potential involvement of the PTP in neuronal cell death led to investigations of permeability transition in glial and neuronal cells (21, 32), under conditions of glutamate exposure (53, 62), hypoglycemia (27), and ischemia (42, 59). In

0014-4886/00 $35.00

these studies, the pharmacological PTP inhibitor cyclosporin A (CsA) was shown to be protective against the neurotoxic insults. However, interpretation is complicated by the fact that CsA has other cellular effects such as inhibiting calcineurin (56), which may also play an important role in cell death (2, 54).

To avoid such confounds, PTP properties have been characterized directly, by utilizing preparations of isolated mitochondria, most often liver mitochondria, where environmental factors can be controlled and actions of CsA are less ambiguous (see 6, 31 and references therein). Factors that affect pore opening such as calcium concentration, phosphate (Pi), pH, surface potential, oxidants, and free fatty acids have been well described in this system, and many more regulators of the PTP are being actively studied (6). Investigations have also shown different tissue-specific properties. For example, heart mitochondria are much less sensitive than liver to permeability transition induced by calcium alone, and require either higher concentrations of calcium or an additional inducer such as Pi (40, 44). In addition, permeability transition in skeletal muscle mitochondria has been shown to have different sensitivity than liver to modulation by Complex I substrates of the electron transport chain (24).

These data suggest that differences may also exist in pore properties in brain mitochondria. In fact, many variations in mitochondrial function and the cellular environment of brain and liver mitochondria would support this hypothesis. We have previously shown that dopamine oxidation induced opening of the PTP, as evidenced by CsA-inhibitable mitochondrial swelling (4). However, this occurs to a far lesser extent in isolated brain mitochondria than in liver mitochondria (4). Other studies of the PTP in brain utilizing whole cells (21, 32) or isolated mitochondria (1, 32) also report findings that differ from previously noted properties in liver mitochondria. These data suggest the possibility that assumptions about the role of the PTP in brain based on properties developed in liver mitochondria, which has occurred, for example, in studies of the parkinsonian neurotoxin 1-methyl-4-phenylpyridinium (13–14, 43), may not be entirely valid. Thus, it is critical to more fully elucidate PTP characteristics in brain mitochondria, given the growing interest in its involvement in neuronal degeneration. However, no systematic characterization of pore properties in brain mitochondria had been undertaken, nor had any direct comparison of brain mitochondria to the very well-characterized properties of the PTP in liver mitochondria been performed.

Therefore, in this study, we directly compared the effects of exposure to known inducers of the PTP in liver mitochondria to those in identically isolated brain mitochondria. Using three different measures of pore opening: mitochondrial swelling, glutathione (GSH) release, and ultrastructural changes, we provide evidence that the majority of brain mitochondria do not readily undergo permeability transition after exposure to conditions that rapidly induce permeability transition in liver mitochondria. These findings present the possibility that regulatory processes in brain differ from those in liver mitochondria and have important implications for the study of the mechanisms involved in neuronal cell death.

MATERIALS AND METHODS

Mitochondrial isolation. Brain mitochondria from male Sprague–Dawley rats (300–350 g; Hilltop Laboratories, Scottdale, PA), were isolated by differential centrifugation using a medium containing 225 mM mannitol, 75 mM sucrose, 5 mM K-Hepes, 1 mg/ml BSA, and 1 mM EGTA (pH 7.4), according to the method of Rosenthal *et al.* (49). This method uses 0.02% digitonin to free mitochondria from the synaptosomal fraction. Digitonin binds cholesterol and permeabilizes cell membranes such as those of synaptosomes, but has little effect on mitochondria, which contain less cholesterol than cellular membranes (e.g., 55). In order to maintain identical conditions, liver mitochondria were isolated from rat liver (1.5–1.75 g tissue) using the exact procedure as that for brain mitochondria. Mitochondrial protein yields for a single rat, determined by the method of Bradford (10), were approximately 8–12 mg protein for brain and 20–25 mg protein for liver.

To ensure that the preparation contained healthy, functioning mitochondria, mitochondrial respiration was measured prior to the start of experiments (49). Respiration measurements were determined polarographically with a thermostatically controlled (37°C) Clark oxygen electrode (Yellow Springs Instrument Co., Yellow Springs, OH) in medium containing 125 mM KCl, 2 mM K_2HPO_4, 1 mM $MgCl_2$, 5 mM K-Hepes (pH 7.0), 1 mM EGTA, 5 mM glutamate, and 5 mM malate. Mitochondria were only used if the ratios of State 3 respiration (using 0.25 mM ADP) to State 4 respiration (using 2 μg/ml oligomycin) were determined to be at least 7.5. Rates of respiration (ng O/min/mg protein) were similar in brain and liver mitochondria.

Mitochondrial swelling. Mitochondrial swelling was measured spectrophotometrically by monitoring the decrease in absorbance at 540 nm over 10 min similar to previously described methods (11). Mitochondria (1 mg protein) were incubated in 2 ml of media containing 213 mM mannitol, 70 mM sucrose, 3 mM Hepes (pH 7.4), 10 mM succinate, and 1 μM rotenone. In studies of the transition pore, $CaCl_2$ (70 μM) was added after 30 s, and other indicated compounds were added at 2 min. When cyclosporin A (CsA; 850 nM) was used, it was added to the buffer prior to the addition of the mitochondria. Data were quantified and

compared by calculating the total decrease in absorbance from 2 min (the time the indicated inducers were added) to 10 min. In studies utilizing mastoparan, it was added after 30 s, and data were quantified by calculating the total decrease in absorbance from 30 s to 10 min.

GSH measurements. Mitochondria were incubated as described for the swelling measurements. After the 10-min incubation, mitochondria were reisolated via centrifugation at 12,000*g* for 10 min at 4°C. The supernatant was removed, and protein was precipitated from the mitochondrial pellet via sonication in 0.1 N perchloric acid with 0.2 mM sodium bisulfite followed by centrifugation at 18,000*g* for 10 min at 4°C. The resulting supernatant, containing GSH from inside the mitochondria, was removed and stored at −70°C until the time of the GSH assay. Total GSH (oxidized and reduced) was measured via the enzyme-coupled spectrophotometric method of Griffith (29).

Electron microscopy. Mitochondria were prepared for electron microscopy either directly after the final centrifugation of the isolation procedure or following treatment with $CaCl_2$ and Pi as described for swelling experiments, followed by centrifugation at 12,000*g* for 10 min. Electron microscopy methods are well established and only will be discussed briefly. Mitochondrial pellets were prepared and fixed in 2.5% glutaraldehyde in PBS. Following fixation, the samples were cut into small (1 mm^3) cubes, postfixed with 1% osmium tetroxide, dehydrated, and embedded in Epon. Sections were cut using a Reichert Ultracut E ultramicrotome (Leica, Deerfield, IL), mounted on grids, and double-stained with 2% uranyl acetate (7 min) and 1% lead citrate (3 min). Observation was with either a Jeol 100CXII or Jeol 1210 TEM (Peabody, MA). To quantify the proportion of mitochondria affected by treatment with $CaCl_2$ and Pi, mitochondrial profiles were counted from randomly selected images collected at 25,000. Negatives from the two populations were coded and mixed and examined. The mitochondrial profiles were assigned either a normal or aberrant morphology by an experienced microscopist (SCW).

Statistical analysis. Analyses were performed by one-way ANOVA followed by Tukey's *post hoc* comparisons. A probability of $P < 0.05$ was considered significant. *N* values reported refer to data obtained from separate experiments.

RESULTS

Mitochondrial swelling. Induction of permeability transition has been shown to lead to swelling of mitochondria (31), which can be measured spectrophotometrically. In this study, known inducers of the PTP were tested for their ability to cause mitochondrial swelling in liver and brain mitochondria isolated by identical procedures. Similar to previously reported studies (see 31), exposure of liver mitochondria to 70 μM $CaCl_2$, followed by the addition of the inducers, Pi (3 mM K_2HPO_4), phenylarsenoxide (PhAsO, 5 μM), or tert-butylhydroperoxide (tBOOH, 1 mM) led to large decreases in absorbance, indicative of mitochondrial swelling (Fig. 1A). Cyclosporin A (CsA) has been shown to prevent the opening of the PTP in liver and heart mitochondria (11, 19, 25). We also found that pretreatment of liver mitochondria with CsA (850 nM) largely prevented the swelling caused by the pore inducers (Fig. 1A). In contrast, exposure of brain mitochondria to the same compounds led to much smaller changes in absorbance (Fig. 1B), with less potent inhibition by CsA. Expansion of the scale, as shown in Fig. 1C, clearly reveals that the inducers caused some changes in absorbance in brain mitochondria albeit much smaller than those in liver.

Table 1 shows the quantified results of these treatments. The change in absorbance from the time the inducing agent was added (2 min) until the end of the experiments (10 min) was determined for each condition in liver and brain mitochondria. All of the inducers tested led to a significantly larger absorbance change over time in liver mitochondria as compared to control conditions. CsA pretreatment significantly reduced the absorbance change after exposure to the inducers, by 89% with Pi, 72% with PhAsO, and 74% with tBOOH, indicative of a decrease in the amount of swelling. Exposure to the inducers in brain resulted in changes in absorbance that were 10–14% of responses observed in liver. However, the small responses were still statistically significant for Pi and PhAsO, although not for exposure to tBOOH (Table 1). Effects of CsA pretreatment also differed in brain as compared to liver, preventing only 46% of the change in absorbance caused by Pi and 51% of the change caused by PhAsO (Table 1).

Increasing the mitochondrial calcium load either by the presence of CGP 37157, an inhibitor of sodium-dependent calcium efflux from mitochondria (16, 18), or by exposure to higher concentrations of calcium did not increase the amount of swelling in brain mitochondria (data not shown). These results were also similar whether Complex I substrates in a KCl-based respiration medium, longer incubation times, or combinations of inducers were utilized (data not shown).

Loss of GSH. To begin to determine whether the differences between liver and brain swelling were due to differences in pore function or simply in the swelling properties of the different types of mitochondria, a second measure of pore opening, loss of mitochondrial GSH, was investigated. GSH is a small molecule that is accumulated in the mitochondrial matrix, and the loss of GSH from the matrix has been shown to occur upon pore opening (51). Although GSH exists in both a re-

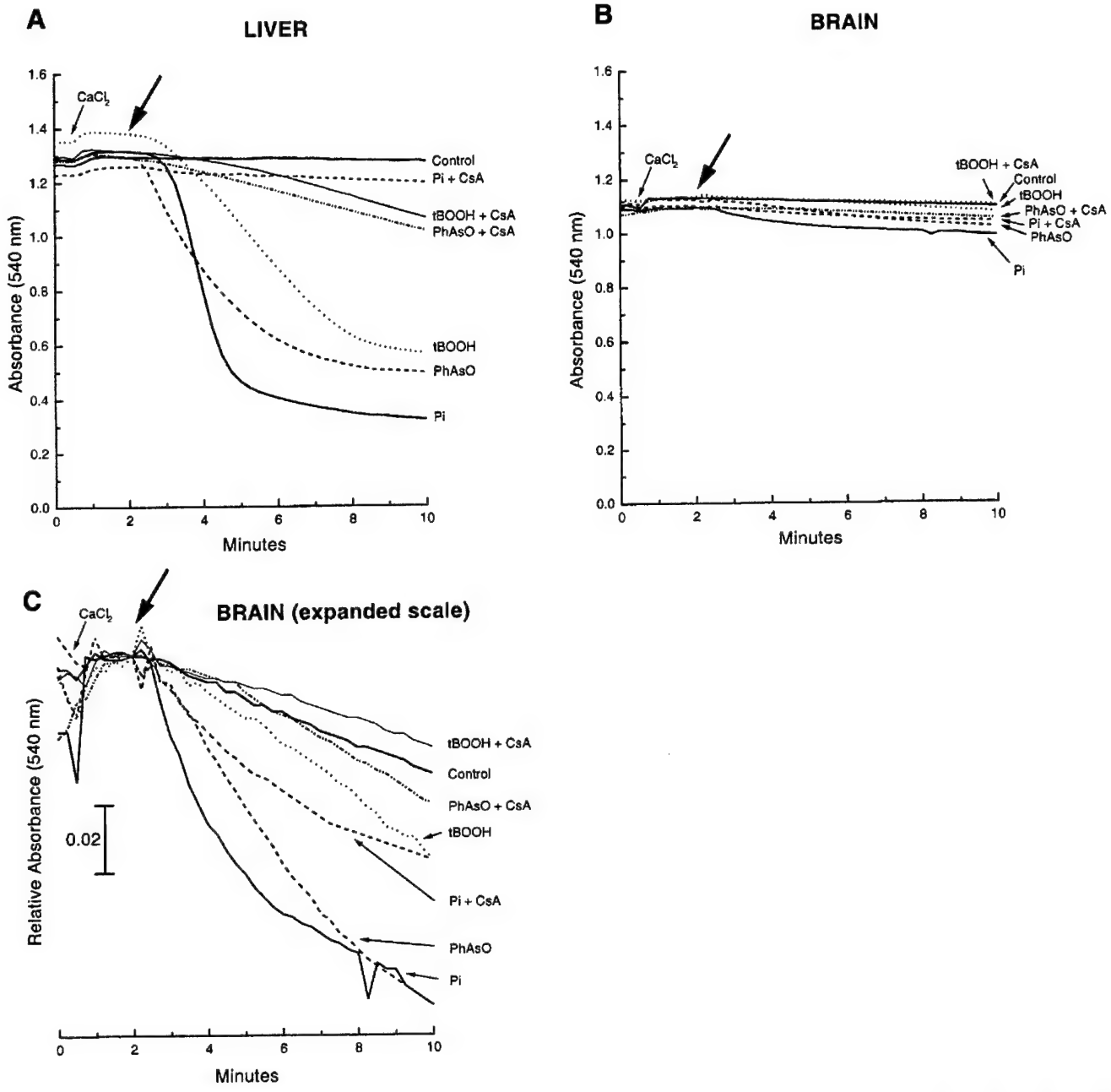

FIG. 1. Representative traces of mitochondrial swelling induced by various agents, assessed spectrophotometrically. $CaCl_2$ (70 μM) was added after 30 s, and other compounds were added at 2 min [phosphate (Pi; 3 mM), phenylarsenoxide (PhAsO; 5 μM), and tert-butylhydroperoxide (tBOOH; 1 mM)]. When used, cyclosporin A (CsA; 850 nM) was present at the beginning of the incubation. Control samples were exposed only to $CaCl_2$. (A) Liver; (B) brain; (C) brain (expanded scale). Arrow indicates the time that the inducers were added.

duced and oxidized form, nearly all of the intramitochondrial GSH has been shown to be in the reduced state (58). Liver and brain mitochondria contain comparable amounts of GSH following isolation and exposure to control conditions containing only $CaCl_2$ (Fig. 2). We found that treatment of liver mitochondria with $CaCl_2$ (70 μM) followed by Pi (3 mM) resulted in a profound loss (−82%) of mitochondrial GSH (Fig. 2). CsA (850 nM) was able to completely prevent this effect. In brain mitochondria, however, $CaCl_2$ and Pi did not result in any loss of GSH (Fig. 2). Incubation with $CaCl_2$ (70 μM) and CsA had no significant effect on GSH levels in either brain or liver mitochondria as compared to controls.

Effects of mastoparan on swelling and GSH release. As a positive control, we tested the effects of the peptide mastoparan on mitochondrial swelling and GSH

TABLE 1

Quantification of Mitochondrial Swelling after Exposure to Permeability Transition Inducing Agents

Treatment[a]	Liver n	Liver Decrease in absorbance (540 nm)[b]	Brain n	Brain Decrease in absorbance (540 nm)[b]
Control	3	0.024 ± 0.003	8	0.032 ± 0.003
Pi (3 mM)	5	0.958 ± 0.014[c]	3	0.130 ± 0.012[c]
Pi (3 mM) + CsA	4	0.095 ± 0.019[d]	4	0.074 ± 0.006[d]
PhAsO (5 μM)	3	0.853 ± 0.069[c]	3	0.099 ± 0.007[c]
PhAsO (5 μM) + CsA	3	0.230 ± 0.030[d]	3	0.049 ± 0.002[d]
tBOOH (1 mM)	3	0.550 ± 0.150[c]	3	0.052 ± 0.003
tBOOH (1 mM) + CsA	3	0.143 ± 0.059[d]	2	0.024 ± 0.004

[a] Mitochondria were exposed to $CaCl_2$ (70 μM) at 30 s, followed by the indicated agents at 2 min. When utilized, CsA (850 nM) was present prior to the addition of mitochondria.

[b] Values are the absolute change in absorbance from the time the inducing agent was added (2 min) to 10 min (mean ± SEM).

[c] Significantly different than control values ($P < 0.05$).

[d] Significantly different than the same condition without CsA ($P < 0.05$).

release in liver and brain. Although at lower concentrations, mastoparan can induce the PTP (46), at higher concentrations, such as the concentration used in this study (20 μM), mastoparan produces pores in the mitochondrial membrane in a non-CsA-dependent manner, thought to be unrelated to PTP opening (38, 46). We observed that mastoparan caused large-amplitude swelling in both liver and brain mitochondria (Figs. 3A and 3B). In liver, maximal change in absorbance approximated that induced by permeability transition, whereas in brain, the change in absorbance was approximately threefold greater than with presumed inducers of the pore and averaged 40% that of liver (Fig. 3B). In addition, mastoparan caused the complete loss of GSH from both brain and liver mitochondria. Levels of GSH in brain and liver mitochondria under the same control conditions as in the swelling experiments were 2.94 ± 0.17 and 3.03 ± 0.33 nmol/mg protein, respectively (mean ± SEM; $n = 3$). Levels of GSH following exposure to mastoparan (20 μM) were nondetectable in both tissues.

Electron microscopy. Figure 4 shows the typical fine structural morphology of mitochondrial preparations used within this study. In untreated preparations of brain mitochondria (Fig. 4A), the predominant morphology shows small mitochondria with numerous electron dense branching cristae (arrow). The only contaminant in these preparations is free synaptosomes (chevron). In approximately 10% of mitochondria, vesiculated cristae may be seen (arrowhead). Following exposure to $CaCl_2$ (70 μM) and Pi (3 mM) (Fig. 4B), large numbers of normal brain mitochondria are still seen (arrow) as well as synaptosomes. However, mitochondria showing fragmentation and vesiculation of cristae (arrowhead) now represent a larger (quantitatively 45%) proportion of the mitochondrial fraction in these preparations. Liver mitochondria prepared in the same fashion show a somewhat different morphology (Fig. 4C): the intracristal volume appears reduced when compared with the brain mitochondria, principally due to an increased volume fraction of matrix within the mitochondria. Apart from occasional free membrane derived from the endoplasmic reticulum, there is very little contamination of this preparation. Treatment of liver mitochondria with $CaCl_2$ and Pi completely disrupts the mitochondrial morphology (Fig. 4D). Although discrete membrane bound profiles persist, no recognizable structures are present within the mitochondria apart from free protein aggregates.

DISCUSSION

This study is the first to directly compare properties of the mitochondrial PTP in brain mitochondria with those of the well-characterized liver mitochondria, using both biochemical and ultrastructural measurements. We found that brain and liver mitochondria behave biochemically and morphologically different after exposure to agents that have previously been shown to induce permeability transition in liver mitochondria.

Using three different measures, we provide evidence that isolated brain mitochondria are more resistant to undergoing permeability transition upon exposure to conditions that rapidly induce the opening of the PTP in liver mitochondria. Exposure to transition-inducing agents led to a large, CsA-inhibitable decrease in spectrophotometric absorbance, a loss of mitochondrial GSH, and morphologic evidence of matrix swelling and disruption in liver mitochondria, as has been reported

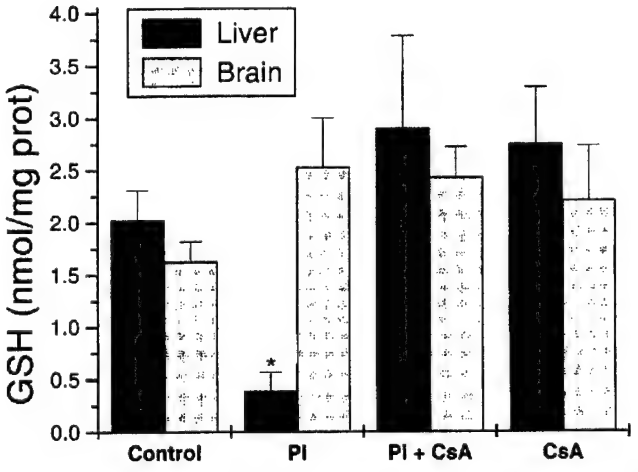

FIG. 2. GSH remaining in the mitochondria was measured following a 10-min incubation period (mean ± SEM; $n = 3$–9). $CaCl_2$ (70 μM) was added to all samples after 30 s of incubation, and Pi (3 mM) was added where indicated after 2 min.

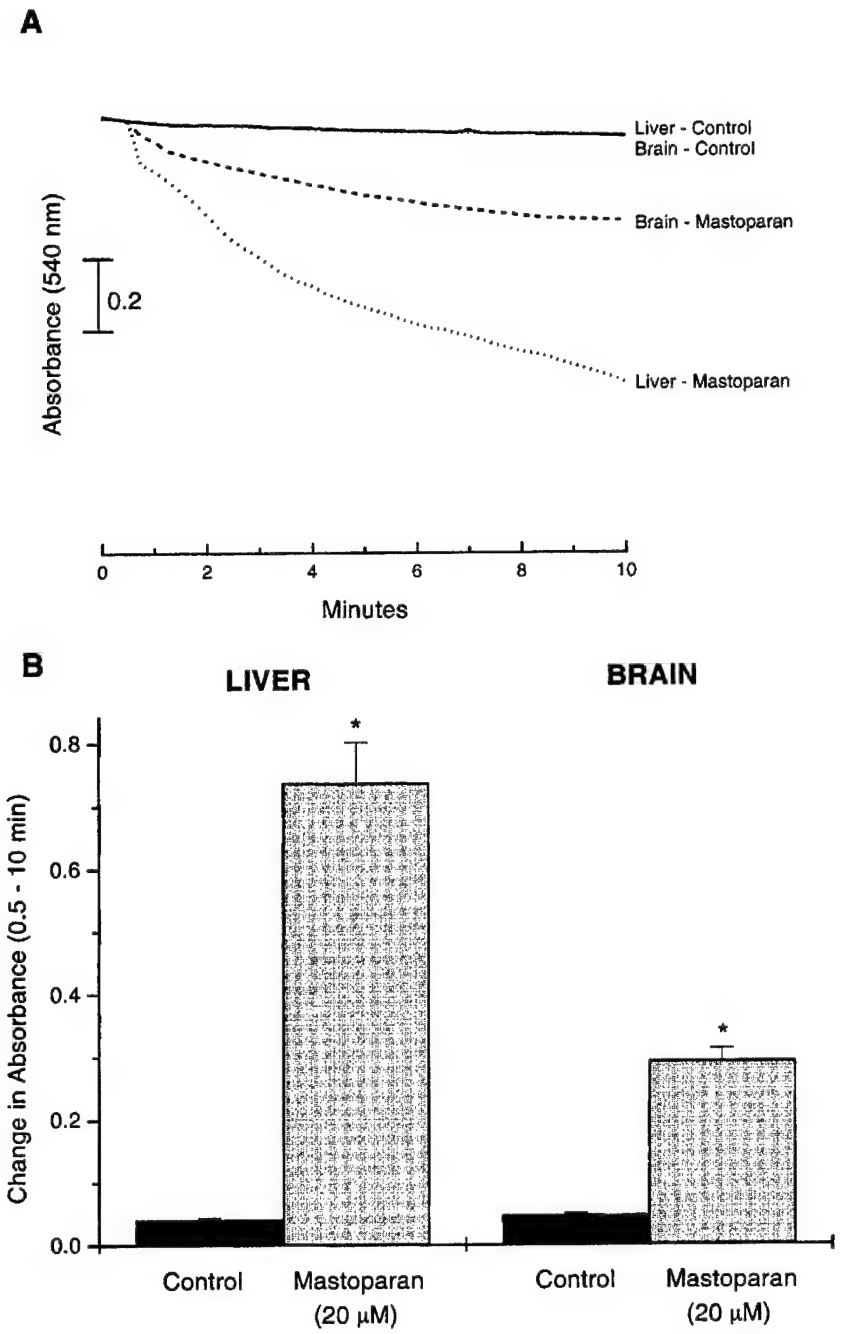

FIG. 3. (A) Representative traces of mitochondrial swelling induced by mastoparan (20 μM), added at 30 s compared to control. (B) Quantification of absorbance changes calculated as the absolute change in absorbance from 30 s to 10 min (mean ± SEM; n = 3–4).

previously (e.g., 8, 51, 52). However, we found that similarly treated brain mitochondria showed very little absorbance change as compared to liver and no loss of GSH. The absence of these responses in brain was not simply due to structural limitations, since large-amplitude swelling and release of GSH were induced when membrane pores unrelated to the PTP were formed by high concentrations of mastoparan. As additional evidence, electron microscopy revealed that the majority of the brain mitochondria appeared morphologically unchanged following treatments to induce PTP. The morphological changes that did occur were more subtle and did not reflect the complete disruption of structure that was observed in liver mitochondria.

Comparison to previous studies of isolated brain mitochondria. We have previously noted a similar differential swelling response of liver and brain mitochon-

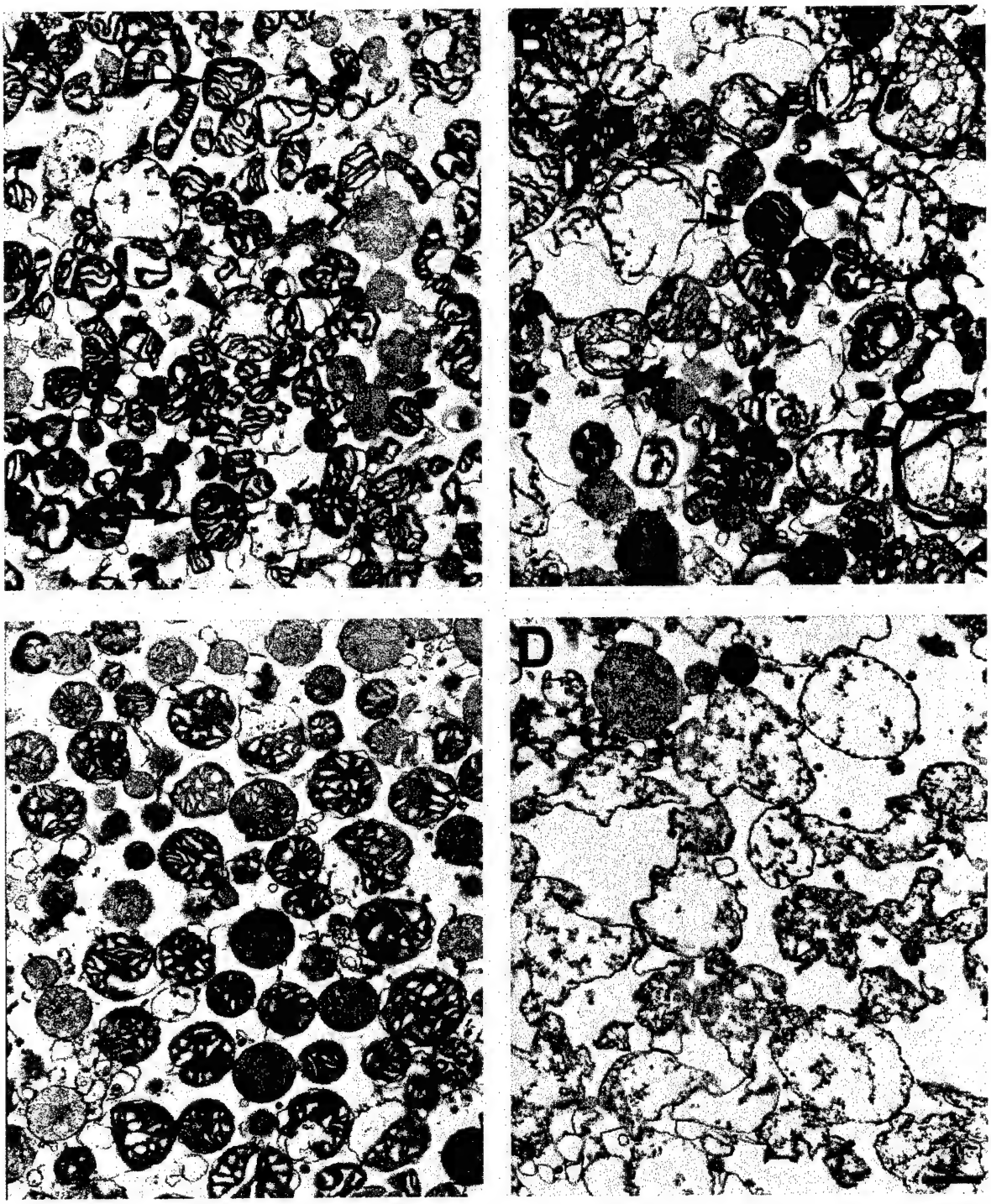

FIG. 4. Electron micrographs of mitochondria from brain (A and B) and liver (C and D), isolated and prepared as described under Materials and Methods. Mitochondria either were untreated (A and C) or were incubated with $CaCl_2$ (70 μM) and Pi (3 mM) for 10 min as described in the legend of Fig. 2 (B and D). In A and B, normal brain mitochondria (arrow), larger mitochondria with fragmented cristae (arrowhead), and a small amount of contaminating synaptosomes (chevron) are observed. In liver mitochondria (C and D), nearly all mitochondria appear normal when untreated (C) and are completely disrupted when treated (D). Bar, 0.5 μm.

dria after exposure to the products of dopamine oxidation (4). Many other recent studies have provided evidence for swelling of isolated brain mitochondria after exposure to pore-inducing agents (1, 26, 27, 32). However, none of these studies quantified the degree of swelling, nor compared it to the degree of swelling observed in liver mitochondria. Where quantitative inferences can be made (32), it appears that the degree of

swelling observed is similar to the small amount of swelling found in our study. In fact, Andreyev *et al.* (1) also noted that when swelling did occur upon exposure to pore inducers, the degree of swelling was incomplete. Thus, these studies support our findings of decreased sensitivity of brain mitochondria to permeability transition.

Similar to findings reported by Kristal and Dubinsky (32), we also found that inhibition of mitochondrial swelling by CsA was incomplete in brain mitochondria, yet we observed a much greater degree of inhibition of swelling and GSH release by CsA in liver. In contrast to our results, Andreyev *et al.* (1) reported release of GSH from brain mitochondria upon pore induction. Although the reason for this apparent difference is unclear, the total mitochondrial GSH in that study was not determined, and thus, it is not known what fraction of the total GSH was released.

Possible mechanisms involved in tissue-specific differences. Our evidence suggests, then, that brain mitochondria do not readily undergo permeability transition under the same conditions that have been well-characterized for liver mitochondria. The reason for this difference is not known, but several possible explanations exist. One possibility is that only a fraction of mitochondria in the brain preparation are able to undergo permeability transition. Although the degree of swelling in brain mitochondria after exposure to Pi or PhAsO was small compared to liver, approximately half of the swelling was prevented by CsA, suggesting that this portion may be due to the PTP. The accompanying release of GSH from the mitochondria that undergo transition would then be only a very small amount compared to that still remaining inside the intact mitochondria and therefore, may be difficult to detect. In addition, since mitochondria are able to take up GSH (30, 33, 36), any released GSH could potentially be transported into the intact mitochondria, masking a small effect.

The heterogeneous brain preparation includes mitochondria from both glia and neurons, and it is not known which population of mitochondria might be more susceptible to PTP induction. It is possible that one cell type or cells from specific regions in brain contain mitochondria that will undergo permeability transition, while others do not. The proportion of mitochondria from glial and neuronal cells in our preparation is not definitively known, but it is likely that there is a substantial proportion from both cell types. The method utilized in our studies is similar to isolation procedures for brain mitochondria which isolate both glial and neuronal (nonsynaptosomal) mitochondria (e.g., 17). However, the current method adds digitonin to the synaptosomal/mitochondrial fraction, which permeabilizes synaptosomal membranes, increasing the neuronal mitochondrial yield (49). The overall mitochondrial yield increases from approximately 3–4 mg mitochondrial protein/brain in standard procedures (e.g., 17) to 8–10 mg mitochondrial protein/brain in this preparation. Thus, it is likely that there is a substantial population of neuronal mitochondria as well as glial mitochondria. It is interesting to speculate whether the small degree of swelling observed in our study reflects the population of mitochondria from specific regions of the brain or from specific cell types that are susceptible to degeneration via mechanisms suggested to involve the PTP. In fact, Friberg *et al.* (26) found that sensitivity to calcium-induced mitochondrial swelling varies in different regions of the brain, correlating with sensitivity to ischemic damage.

It is also possible that differences in protein expression between liver and brain could be responsible for the differences observed in this study. For example, recent evidence suggests that creatine kinase, which is present in high amounts in brain but not liver mitochondria, is a potent inhibitor of the PTP (9, 41). In addition, members of the bcl-2 family of proteins are known to be inhibitors and activators of permeability transition (47), and thus, differential expression of these proteins in liver and brain could contribute to altered sensitivity. Protein expression may also indirectly affect pore opening by altering environmental factors that are known to regulate the PTP, such as intramitochondrial pH, the oxidation state of pyridine nucleotides and GSH, calcium load, or matrix magnesium (5). For example, oxidized pyridine nucleotides are known to increase the probability of PTP opening (15), and evidence suggests that the ability of pyridine nucleotides to be oxidized may be lower in brain mitochondria than in other tissues, due to differences in peroxidase activity (3, 35, 50).

Certainly, other differences in mitochondria from liver and brain have been identified. For example, liver and brain mitochondria use diverse mechanisms to transport calcium; calcium efflux from brain mitochondria is primarily through sodium-dependent transport, whereas liver mainly utilizes a sodium-independent mechanism (31). Likewise, as stated previously, different PTP characteristics have also been identified in other tissues, such as heart mitochondria, which are less sensitive than liver (40, 44) and skeletal muscle mitochondria, which show differential sensitivity to substrate modulators (24). Brain mitochondria appear to be even less sensitive than heart, since exposure to calcium with inducers, higher concentrations of calcium, calcium efflux blockade, or even combinations of several inducers over longer periods of time did not result in large-scale opening of the PTP. The composition of the PTP and its regulatory proteins is still under debate (see 6), and until it is fully defined, it will be difficult to specifically determine the potential mechanisms leading to these tissue-specific differences.

Conclusions. This study is the first to directly examine pore properties in brain mitochondria and compare them to the properties that have previously been well-described in other tissues. It is clear from our findings that considerable differences exist in measures of PTP properties between isolated brain and liver mitochondria and that sensitivity to variations in mitochondria from one tissue to another is critical. This is important to note, since previously it has been thought that pore properties are similar, and studies of isolated liver mitochondria have been utilized to extrapolate to brain (13, 14, 43).

In addition, it is very likely that heterogeneity exists between glial and neuronal mitochondria, between mitochondria from different regions of the brain, or even within different regions of a single neuron. With reports suggesting a potential role for the PTP in neuronal injury due to excitotoxicity (39, 53, 62), ischemia (42, 59, 60), dopamine-induced toxicity (4), the parkinsonian neurotoxin, 1-methyl-4-phenylpyridinium (13, 14, 43), and some forms of apoptosis (65), better characterization of the properties and regulatory mechanisms of the PTP specific to brain mitochondria is critical.

ACKNOWLEDGMENTS

Preliminary reports of these findings were presented at the 28th meeting of the Society for Neuroscience, Los Angeles, CA, November 7–12, 1998 (Berman *et al.*, 1998). We thank Dr. Anne Murphy for her helpful discussions and technical expertise and Dr. Ian Reynolds for critical reading of the manuscript. In addition, we thank Dr. Donna Beer Stolz for providing the EM analysis. This work was supported in part by USPHS Grants NS19068 and DA09601 and USAMRMC Grant 98292027.

REFERENCES

1. Andreyev, A. Y., B. Fahy, and G. Fiskum. 1998. Cytochrome *c* release from brain mitochondria independent of the mitochondrial permeability transition. *FEBS Lett.* **439:** 373–376.
2. Ankarcrona, M., J. M. Dypbukt, S. Orrenius, and P. Nicotera. 1996. Calcineurin and mitochondrial function in glutamate-induced neuronal cell death. *FEBS Lett.* **439:** 321–324.
3. Beatrice, M. C., D. L. Stiers, and D. R. Pfeiffer. 1984. The role of glutathione in the retention of Ca^{2+} by liver mitochondria. *J. Biol. Chem.* **259:** 1279–1287.
4. Berman, S. B., and T. G. Hastings. 1999. Dopamine oxidation alters mitochondrial respiration and induces permeability transition in brain mitochondria: Implications for Parkinson's disease. *J. Neurochem.* **73:** 1127–1137.
5. Bernardi, P. 1995. The permeability transition pore. History and perspectives of a cyclosporin A-sensitive mitochondrial channel. *Prog. Cell Res.* **5:** 119–123.
6. Bernardi, P. 1999. Mitochondrial transport of cations: Channels, exchangers, and permeability transition. *Physiol. Rev.* **79:** 1127–1155.
7. Bernardi, P., L. Scorano, R. Colonna, V. Petronilli, and F. Di Lisa. 1999. Mitochondria and cell death: Mechanistic aspects and methodological issues. *Eur. J. Biochem.* **264:** 687–701.
8. Bernardi, P., S. Vassanelli, P. Veronese, R. Colonna, I. Szabó, and M. Zoratti. 1992. Modulation of the mitochondrial permeability transition pore: Effect of protons and divalent cations. *J. Biol. Chem.* **267:** 2934–2939.
9. Beutner, G., A. Ruck, B. Riede, and D. Brdiczka. 1998. Complexes between porin, hexokinase, mitochondrial creatine kinase and adenylate translocator display properties of the permeability transition pore. Implication for regulation of permeability transition by the kinases. *Biochim. Biophys. Acta.* **1368:** 7–18.
10. Bradford, M. A. 1976. A rapid and sensitive method for the quantitation of microgram quantities of protein utilizing the principle of protein-dye binding. *Anal. Biochem.* **72:** 248–254.
11. Broekemeier, K. M., M. E. Dempsey, and D. R. Pfeiffer. 1989. Cyclosporin A is a potent inhibitor of the inner membrane permeability transition in liver mitochondria. *J. Biol. Chem.* **264:** 7826–7830.
12. Cassarino, D. S., and J. P. Bennett. 1999. An evaluation of the role of mitochondria in neurodegenerative diseases: Mitochondrial mutations and oxidative pathology, protective nuclear responses, and cell death in neurodegeneration. *Brain Res. Rev.* **29:** 1–25.
13. Cassarino, D. S., C. P. Fall, T. S. Smith, and J. P. Bennett. 1998. Pramipexole reduces reactive oxygen species production *in vivo* and *in vitro* and inhibits the mitochondrial permeability transition produced by the parkinsonian neurotoxin methylpyridinium ion. *J. Neurochem.* **71:** 295–301.
14. Cassarino, D. S., J. K. Parks, W. D. Parker Jr., and J. P. Bennett Jr. 1999. The parkinsonian neurotoxin MPP+ opens the mitochondrial permeability transition pore and releases cytochrome c in isolated mitochondria via an oxidative mechanism. *Biochim. Biophys. Acta.* **1453:** 49–62.
15. Chernyak, B. V., and P. Bernardi. 1996. The mitochondrial permeability transition pore is modulated by oxidative agents through both pyridine nucleotides and glutathione at two separate sites. *Eur. J. Biochem.* **238:** 623–630.
16. Chiesi, M., R. Schwaller, and K. Eichenberger. 1988. Structural dependency of the inhibitory action of benzodiazepines and related compounds on the mitochondrial Na^{+}-Ca^{2+} exchanger. *Biochem. Pharmacol.* **37:** 4399–4403.
17. Clark, J. B., and W. J. Nicklas. 1970. The metabolism of rat brain mitochondria: Preparation and characterization. *J. Biol. Chem.* **245:** 4724–4731.
18. Cox, D. A., L. Conforti, N. Sperelakis, and M. A. Matlib. 1993. Selectivity of inhibition of $Na(^{+})$-Ca^{2+} exchange of heart mitochondria by benzothiazepine CGP-37157. *J. Cardiovasc. Pharmacol.* **21:** 595–599.
19. Crompton, M., H. Ellinger, and A. Costi. 1988. Inhibition by cyclosporin A of a Ca^{2+}-dependent pore in heart mitochondria activated by inorganic phosphate and oxidative stress. *Biochem. J.* **255:** 357–360.
20. Deckwerth, T. L., and E. M. Johnson. 1993. Temporal analysis of events associated with programmed cell death (apoptosis) of sympathetic neurons deprived of nerve growth factor. *J. Cell Biol.* **123:** 1207–1222.
21. Dubinsky, J. M., and Y. Levi. 1998. Calcium-induced activation of the mitochondrial permeability transition in hippocampal neurons. *J. Neurosci. Res.* **53:** 728–741.
22. Ellerby, M. H., S. J. Martin, L. M. Ellerby, S. S. Naiem, S. Rabizadeh, G. S. Salvesen, C. A. Casiano, N. R. Cashman, D. R. Green, and D. E. Bredesen. 1997. Establishment of a cell-free

system of neuronal apoptosis: Comparison of premitochondrial, mitochondrial, and postmitochondrial phases. *J. Neurosci.* **17:** 6165–6178.

23. Fiskum, G., A. N. Murphy, and M. F. Beal. 1999. Mitochondria in neurodegeneration: Acute ischemia and chronic neurodegenerative diseases. *J. Cereb. Blood Flow Metab.* **19:** 351–369.
24. Fontaine, E., O. Eriksson, F. Ichas, and P. Bernardi. 1998. Regulation of the permeability transition pore in skeletal muscle mitochondria: Modulation by electron flow through the respiratory chain complex I. *J. Biol. Chem.* **273:** 12662–12668.
25. Fournier, N., G. Ducet, and A. Crevat. 1987. Action of cyclosporine on mitochondrial calcium fluxes. *J. Bioenerg. Biomembr.* **19:** 297–303.
26. Friberg, H., C. Connern, A. P. Halestrap, and T. Wieloch. 1999. Differences in the activation of the mitochondrial permeability transition among brain regions in the rat correlate with selective vulnerability. *J. Neurochem.* **72:** 2488–2497.
27. Friberg, H., M. Ferrand-Drake, F. Bengtsson, A. P. Halestrap, and T. Wieloch. 1998. Cyclosporin A, but not FK506, protects mitochondria and neurons against hypoglycemic damage and implicates the mitochondrial permeability transition in cell death. *J. Neurosci.* **18:** 5151–5159.
28. Green, D. R., and J. C. Reed. 1998. Mitochondria and apoptosis. *Science* **281:** 1309–1312.
29. Griffith, O. W. 1980. Determination of glutathione and glutathione disulfide using glutathione reductase and 2-vinylpyridine. *Anal. Biochem.* **106:** 207–212.
30. Griffith, O. W., and A. Meister. 1985. Origin and turnover of mitochondrial glutathione. *Proc. Natl. Acad. Sci. USA* **82:** 4668–4672.
31. Gunter, T. E., and D. R. Pfeiffer. 1990. Mechanisms by which mitochondria transport calcium. *Am. J. Physiol.* **258:** C755–786.
32. Kristal, B. S., and J. M. Dubinsky. 1997. Mitochondrial permeability transition in the central nervous system: Induction by calcium cycling-dependent and -independent pathways. *J. Neurochem.* **69:** 524–538.
33. Kurosawa, K., N. Hayashi, N. Sato, T. Kamada, and K. Tagawa. 1990. Transport of glutathione across the mitochondrial membranes. *Biochem. Biophys. Res. Commun.* **167:** 367–372.
34. Liu, X., C. N. Kim, J. Yang, R. Jemmerson, and X. Wang. 1996. Induction of apoptotic program in cell-free extracts: Requirement for dATP and cytochrome c. *Cell* **86:** 147.
35. Lötscher, R. R., K. H. Winterhalter, E. Carafoli, and C. Richter. 1979. Hydroperoxides can modulate the redox state of pyridine nucleotides and the calcium balance in rat liver mitochondria. *Proc. Natl. Acad. Sci. USA* **76:** 4340–4344.
36. Martensson, J., J. C. K. Lai, and A. Meister. 1990. High-affinity transport of glutathione is part of a multicomponent system essential for mitochondrial function. *Proc. Natl. Acad. Sci. USA* **87:** 7185–7189.
37. Murphy, A. N., G. Fiskum, and M. F. Beal. 1999. Mitochondria in neurodegeneration: Bioenergetic function in cell life and death. *J. Cereb. Blood Fl. Metab.* **19:** 231–245.
38. Nicolay, K., F. D. Laterveer, and W. Laurens Van Heerde. 1994. Effects of amphipathic peptides, including presequences, on the functional integrity of rat liver mitochondrial membranes. *J. Bioenerg. Biomembr.* **26:** 327–334.
39. Nieminen, A-L., T. G. Petrie, J. J. Lemasters, and W. R. Selman. 1996. Cyclosporin A delays mitochondrial depolarization induced by *N*-methyl-D-aspartate in cortical neurons: Evidence of the mitochondrial permeability transition. *Neuroscience* **75:** 993–997.
40. Novgorodov, S. A., T. I. Gudz, Y. M. Milfrom, and G. P. Brierley. 1992. The permeability transition in heart mitochondria is regulated synergistically by ADP and cyclosporin A. *J. Biol. Chem.* **267:** 16274–16282.
41. O'Gorman, E., G. Beutner, M. Dolder, A. P. Koretsky, D. Brdiczka, and T. Wallimann. 1997. The role of creatine kinase in inhibition of mitochondrial permeability transition. *FEBS Lett.* **414:** 253–257.
42. Ouyang, Y. B., S. Kuroda, T. Kristian, and B. K. Siesjö. 1997. Release of mitochondrial aspartate aminotransferase (MAST) following transient focal cerebral ischemia suggests the opening of a mitochondrial permeability transition pore. *Neurosci. Res. Commun.* **20:** 167–173.
43. Packer, M. A., R. Miesel, and M. P. Murphy. 1996. Exposure to the parkinsonian neurotoxin 1-methyl-4-phenylpyridinium (MPP^+) and nitric oxide simultaneously causes cyclosporin A-sensitive mitochondrial calcium efflux and depolarization. *Biochem. Pharmacol.* **51:** 267–273.
44. Palmer, J. W., and D. R. Pfeiffer. 1981. The control of Ca^{2+} release from heart mitochondria. *J. Biol. Chem.* **256:** 6742–6750.
45. Petit, P. X., H. Lecoeur, E. Zorn, C. Duguet, B. Mignotte, and M. L. Gougeon. 1995. Alterations of mitochondrial structure and function are early events of dexamethasone-induced thymocyte apoptosis. *J. Cell Biol.* **130:** 157–167.
46. Pfeiffer, D. R., T. I. Gudz, S. A. Novgorodov, and W. L. Erdahl. 1995. The peptide mastoparan is a potent facilitator of the mitochondrial permeability transition. *J. Biol. Chem.* **270:** 4923–4932.
47. Reed, J. C., J. M. Jurgensmeier, and S. Matsuyama. 1998. Bcl-2 family proteins and mitochondria. *Biochim. et Biophys. Acta.* **1366:** 127–137.
48. Reynolds, I. J., J. M. Scanlon, and A. K. Stout. 1998. Mitochondrial mechanisms of neuronal injury. In *Pharmacology of Cerebral Ischemia 1998* (Krieglstein, J., Ed), pp. 89–95. Elsevier Science, New York.
49. Rosenthal, R. E., F. Hamud, G. Fiskum, P. J. Varghese, and S. Sharpe. 1987. Cerebral ischemia and reperfusion: Prevention of brain mitochondrial injury by lidoflazine. *J. Cereb. Blood Flow Metab.* **7:** 752–758.
50. Satrustegui, J., and C. Richter. 1984. The role of hydroperoxides as calcium release agents in rat brain mitochondria. *Arch. Biochem. Biophys.* **233:** 736–740.
51. Savage, M. K., D. P. Jones, and D. J. Reed. 1991. Calcium- and phosphate-dependent release and loading of glutathione by liver mitochondria. *Arch. Biochem. Biophys.* **290:** 51–56.
52. Savage, M. K., and D. J. Reed. 1994. Release of mitochondrial glutathione and calcium by a cyclosporin A-sensitive mechanism occurs without large amplitude swelling. *Arch. Biochem. Biophys.* **315:** 142–152.
53. Schinder, A. F., E. C. Olson, N. C. Spitzer, and M. Montal. 1996. Mitochondrial dysfunction is a primary event in glutamate neurotoxicity. *J. Neurosci.* **16:** 6125–6133.
54. Shibasaki, F., and F. McKeon. 1995. Calcineurin functions in Ca^{2+}-activated cell death in mammalian cells. *J. Cell Biol.* **131:** 735–743.
55. Sims, N. R., and J. P. Blass. 1986. Expression of classical mitochondrial respiratory responses in homogenates of rat forebrain. *J. Neurochem.* **47:** 496–505.
56. Snyder, S. H., and D. M. Sabatini. 1995. Immunophilins and the nervous system. *Nature Med.* **1:** 32–37.
57. Susin, S. A., N. Zamzami, M. Castedo, T. Hirsh, P. Marchetti, A. Macho, E. Daugas, M. Geuskens, and G. Kroemer. 1996. Bcl-2 inhibits the mitochondrial release of an apoptogenic protease. *J. Exp. Med.* **184:** 1331–1341.

58. Traber, J., M. Suter, P. Walter, and C. Richter. 1992. *In vivo* modulation of total and mitochondrial glutathione in rat liver: Depletion by phorone and rescue by *N*-acetylcysteine. *Biochem. Pharmacol.* **43:** 961–964.

59. Uchino, H., E. Elmér, K. Uchino, O. Lindvall, and B. K. Siesjö. 1995. Cyclosporin A dramatically ameliorates CA1 hippocampal damage following transient forebrain ischaemia in the rat. *Acta Physiol. Scand.* **155:** 469–471.

60. Uchino, H., E. Elmer, K. Uchino, P. A. Li, Q. P. He, M. L. Smith, and B. K. Siesjo. 1998. Amelioration by cyclosporin A of brain damage in transient forebrain ischemia in the rat. *Brain Res.* **812:** 216–226.

61. Vayssière, J-L., P. X. Petit, Y. Risler, and B. Mignotte. 1994. Commitment to apoptosis is associated with changes in mitochondrial biogenesis and activity in cell lines conditionally immortalized with simian virus 40. *Proc. Natl. Acad. Sci. USA* **91:** 11752–11756.

62. White, R. J., and I. J. Reynolds. 1996. Mitochondrial depolarization in glutamate-stimulated neurons: An early signal specific to excitotoxin exposure. *J. Neurosci.* **16:** 5688–5697.

63. Zamzami, N., P. Marchetti, M. Castedo, C. Zanin, J-L. Vayssière, P. X. Petit, and G. Kroemer. 1995a. Reduction in mitochondrial potential constitutes an early irreversible step of programmed lymphocyte death in vivo. *J. Exp. Med.* **181:** 1661–1672.

64. Zamzami, N., P. Marchetti, M. Castedo, D. Decaudin, A. Maho, T. Hirsch, S. A. Susin, P. X. Petit, B. Mignotte, and G. Kroemer. 1995b. Sequential reduction of mitochondrial transmembrane potential and generation of reactive oxygen species in early programmed cell death. *J. Exp. Med.* **182:** 367–377.

65. Zamzami, N., S. A. Susin, P. Marchetti, T. Hirsch, I. Gómez-Monterrey, M. Castedo, and G. Kroemer. 1996. Mitochondrial control of nuclear apoptosis. *J. Exp. Med.* **183:** 1533–1544.

ELSEVIER

Journal of Neuroscience Methods 104 (2001) 165–176

JOURNAL OF NEUROSCIENCE METHODS

www.elsevier.com/locate/jneumeth

MitoTracker labeling in primary neuronal and astrocytic cultures: influence of mitochondrial membrane potential and oxidants

Jennifer F. Buckman, Hélène Hernández, Geraldine J. Kress, Tatyana V. Votyakova, Sumon Pal, Ian J. Reynolds *

Department of Pharmacology, University of Pittsburgh, E1351 Biomedical Science Tower, Pittsburgh, PA 15261, USA

Received 31 July 2000; received in revised form 3 October 2000; accepted 3 October 2000

Abstract

MitoTracker dyes are fluorescent mitochondrial markers that covalently bind free sulfhydryls. The impact of alterations in mitochondrial membrane potential ($\Delta\Psi_m$) and oxidant stress on MitoTracker staining in mitochondria in cultured neurons and astrocytes has been investigated. *p*-(Trifluoromethoxy) phenyl-hydrazone (FCCP) significantly decreased MitoTracker loading, except with MitoTracker Green in neurons and MitoTracker Red in astrocytes. Treatment with FCCP after loading increased fluorescence intensity and caused a relocalization of the dyes. The magnitude of these effects was contingent on which MitoTracker, cell type and dye concentration were used. H_2O_2 pretreatment led to a consistent increase in neuronal MitoTracker Orange and Red and astrocytic MitoTracker Green and Orange fluorescence intensity. H_2O_2 exposure following loading increased MitoTracker Red fluorescence in astrocytes. In rat brain mitochondria, high concentrations of MitoTracker dyes uncoupled respiration in state 4 and inhibited maximal respiration. Thus, loading and mitochondrial localization of the MitoTracker dyes can be influenced by loss of $\Delta\Psi_m$ and increased oxidant burden. These dyes can also directly inhibit respiration. Care must be taken in interpreting data collected using MitoTrackers dyes as these dyes have several potential limitations. Although MitoTrackers may have some value in identifying the location of mitochondria within cultured neurons and astrocytes, their sensitivity to $\Delta\Psi_m$ and oxidation negates their use as markers of mitochondrial dynamics in healthy cultures.

Keywords: Fluorescence imaging; Mitochondria; Oxidative stress

1. Introduction

There is an emerging appreciation for a role of mitochondria in excitotoxic injury pathways as well as injury mechanisms manifested as apoptotic or necrotic death processes. The development of novel mitochondrion-specific fluorescent dyes is necessary to explore the significance of mitochondria in these cell death pathways. Although some mitochondrial fluorescent probes are available that allow the assessment of mitochondrial membrane potential ($\Delta\Psi_m$), most fluorescent dyes that measure ions, such as calcium, magnesium and zinc, or reactive oxygen species (ROS) generation and pH are not specific to mitochondria. Moreover, dyes that can detect activity at the elusive permeability transition pore (PTP) in cultured neurons are currently unavailable.

The MitoTracker dyes, developed commercially by Molecular Probes (Eugene, OR), are structurally novel fluorescent probes that have been used to measure $\Delta\Psi_m$ (Macho et al., 1996), $\Delta\Psi_m$-independent mitochondrial mass (Krohn et al., 1999) and photosensitization (Minamikawa et al., 1999). The MitoTracker dyes (MitoTracker Green FM, MitoTracker Orange CMTMRos, MitoTracker Red CMXRos) contain chloromethyl moieties that are thought to react with free sulfhydryls within the cell. MitoTracker Green has been suggested to be $\Delta\Psi_m$-insensitive and capable of loading and remaining within depolarized mitochondria, which implies that it would be an exceptional tool for assessing mitochondrial mass (Poot et al., 1996). MitoTrackers Orange and Red are positively charged rosamine

* Corresponding author. Tel.: +1-412-6482134; fax: +1-412-6240794.

E-mail address: iannmda + @pitt.edu (I.J. Reynolds).

0165-0270/01/$ - see front matter
PII: S0165-0270(00)00340-X

derivatives that are rapidly taken up into the negatively charged mitochondria, suggesting that their loading would be dependent on $\Delta\Psi_m$, but their localization should be mitochondrial specific. However, MitoTracker Orange and Red, at least in their reduced state, may be strongly influenced by the presence of ROS (Poot and Pierce, 1999a,b) and MitoTracker Orange may directly inhibit the respiratory chain at complex I and induce permeability transition (PT) (Scorrano et al., 1999). All three MitoTracker probes are believed to be retained following fixation due to the membrane-impermeant dye complex that is created when the dyes enters the mitochondria. However, the sensitivity of these dyes to $\Delta\Psi_m$ and oxidant status and their permeability through the mitochondrial membrane has not been fully explored in unfixed cultured neurons and astrocytes.

This laboratory is interested in identifying fluorescent dyes that can specifically label mitochondria in the central nervous system under a variety of conditions. The aim of the present study was to characterize the MitoTracker dyes in primary forebrain neurons and astrocytes to determine their dependency on $\Delta\Psi_m$ and oxidant status, especially given the widespread interest in using these dyes as fixable markers of $\Delta\Psi_m$. In addition, one addressed whether the MitoTrackers altered respiratory chain activity in isolated brain mitochondria to determine whether these dyes altered mitochondrial physiology.

2. Materials and methods

2.1. Cell culture

All procedures were in strict accordance with the NIH Guide for the Care and Use of Laboratory Animals and were approved by the University of Pittsburgh's Institutional Animal Care and Use Committee. Primary forebrain neurons were prepared as previously described (White and Reynolds, 1995). Briefly, forebrains from embryonic day-17 Sprague Dawley rats were removed and dissociated. Cells were plated on poly-D-lysine coated 31 mm glass coverslips at a density of 450 000/ml (1.5 ml/coverslip) and inverted after 24 h to decrease glial growth. Experiments were performed when cells were 14–17 days in culture.

Primary forebrain astrocytes were prepared as described by McCarthy and de Vellis (1980) with minor modifications. Briefly, forebrains from postnatal day-1 Sprague Dawley rats were dissociated and plated in 75 cm^2 plastic flasks at a density of 860 000 cells/ml (10 ml/flask). Media was changed every other day. Cells were grown to the point of confluency, at which point the flasks were orbitally shaken for 15–18 h at 37°C. Adherent cells were then plated onto poly-D-lysine coated 31 mm glass coverslips and fed every other day and used for up to 5 days in culture.

2.2. Solutions

Coverslips were perfused with a HEPES-buffered salt solution (HBSS) with (in mM): NaCl (137), KCl (5), $NaHCO_3$ (10), HEPES (20), glucose (5.5), KH_2PO_4 (0.6), Na_2HPO_4 (0.6), $CaCl_2$ (1.4), $MgSO_4$ (0.9), pH adjusted to 7.4 with NaOH. The protonophore and mitochondrial uncoupler carbonyl cyanide *p*-(trifluoromethoxy) phenyl-hydrazone (FCCP) was used at a concentration of 750 nM (diluted in HBSS from a 750 μM stock in methanol). Hydrogen peroxide (H_2O_2) was diluted in HBSS to concentrations ranging from 10 μM to 3 mM (from a 30% w/w stock solution). Oligomycin was used at a 2 μM concentration (diluted from a 10 mM stock in methanol).

2.3. Fluorescence imaging

For all experiments, individual coverslips were rinsed twice in HBSS and loaded with 10–500 nM concentrations of MitoTracker Green FM, MitoTracker Orange (CMTMRos) or MitoTracker Red (CMXRos) (Molecular Probes, Eugene, OR) for 15 min at 37°C. Dyes were diluted in HBSS from a 1 mM stock in anhydrous dimethyl sulfoxide. Coverslips were rinsed for 15 min in HBSS at room temperature. Loading parameters were tested and optimized for assessing fluorescence intensity and localization.

Experiments were performed at room temperature on two light microscope-based imaging systems with 40 × quartz objectives. Cells were illuminated using a Xenon lamp-based monochromator (TILL, Photonics, Germany) and light detected using a CCD camera. Data acquisition was controlled using Simple PCI software (Compix, Cranberry, PA). Cells were illuminated with a 490, 550 or 575 nm light depending on the dye and incidence light was attenuated with neutral density filters (Omega Optical, Brattleboro, VT). Emitted fluorescence from MitoTracker Green was passed through a 500 or 515 long pass (LP) dichroic mirror and a 535, 25 band pass (BP) or 535, 40BP emission filter (depending on the imaging system used). For MitoTracker Orange, a 570 or 575LP dichroic and a 590, 35BP or 605, 35BP emission filter was used. For MitoTracker Red, a 590LP dichroic with a 600LP emission filter was used. Coverslips were placed on the microscope stage, a field of cells (with at least ten viable neurons or five viable astrocytes in the field) was chosen and a bright field image was captured. From this image, cell bodies were circled and used as regions of interest from which cellular fluorescence intensity was measured. Three small cell-free regions on the coverslip were also chosen to assess background fluorescence

intensity. Images were collected once every 15 s for baseline and once every 5 s for the remainder of the experiment. Data were collected as background subtracted fluorescence intensity. All experiments were performed on at least three different culture dates. For most experiments, data were converted to percent baseline or percent of untreated control. The number of cells analyzed are presented with each graph, however in order to insure stringency in the statistical analyses, all cells from a single coverslip were combined and statistics were performed with the more conservative '*n*' of the number of coverslips. Where pertinent, data were statistically analyzed using a two-tailed *t*-test or a one-way ANOVA and a Dunnett post-hoc test (when $P < 0.05$).

2.4. FCCP experiments

To determine the effect of $\Delta\Psi_m$ depolarization on MitoTracker-loaded cells, individual coverslips were loaded with 10–500 nM concentrations of MitoTracker dye (Green, Orange or Red) and imaged to observe changes in the intensity and/or pattern of fluorescence. Coverslips were perfused with HBSS for 5 min, with FCCP (750 nM) for 5 min, and then with HBSS again for 5 min. The effect of $\Delta\Psi_m$ on loading was assessed by comparing fluorescence intensity (over 5 min, 1 frame/15 s) from coverslips incubated with 50 nM MitoTracker alone to coverslips incubated in 750 nM FCCP + 50 nM MitoTracker.

2.5. H_2O_2 experiments

As with the FCCP experiments, the effect of an oxidant burden on pre-loaded cells was tested by loading coverslips with 50 nM MitoTracker dye and imaging. Coverslips were perfused with HBSS, H_2O_2 (500 μM in neurons, 3 mM in astrocytes) and HBSS again. The effect of an oxidant burden on loading was assessed by incubating coverslips in H_2O_2 (10–500 μM in neurons, 500 μM–3 mM in astrocytes) for 15 min, then immediately loading 50 nM MitoTracker dye (Green, Orange or Red) and imaging for 5 min.

2.6. Isolated brain mitochondria preparation

Rat brain mitochondria were isolated according to Rosenthal et al. (1987). Briefly, a rat forebrain was removed, homogenized and suspended in 10 ml of isolation buffer (pH 7.4, containing 225 mM mannitol, 75 mM sucrose, 1 mg/ml BSA, 1 mM EDTA, 5 mM HEPES-KOH). The brain homogenates were subjected to differential centrifugation and the final suspensions contained a heterogeneous population of synaptosomal and non-synaptosomal mitochondria. Protein concentration in the mitochondrial suspensions was determined according to Bradford (1976). Only mitochondria that had a respiration ratio of 6 or higher (phosphorylating state 3 to resting state 4 with glutamate and malate as substrates) were used.

2.7. Respiratory experiments

Mitochondrial respiration rates were measured polarographically at 37°C with a Clark oxygen electrode (Yellow Springs Instrument, Yellow Springs, OH) in a buffer containing 125 mM KCl, 2 mM K_2HPO_4, 4 mM $MgCl_2$, 3 mM ATP, 5 mM glutamate, 5 mM malate, 5 mM HEPES-KOH (pH 7.0). This buffer exhibits similarities to the intracellular environment and is believed to decrease the probability of PT (Andreyev et al., 1998; Andreyev and Fiskum, 1999). Energized brain mitochondria (0.25 mg protein/ml), oligomycin (2 μM) and the MitoTracker dyes (at concentrations of 50 nM (low) or 3.12 μM (high) concentrations) were incubated in a 1.6 ml water-jacketed glass chamber (Gilson, Middletown, WI). The experiment was initiated in an open chamber (to maintain oxygen concentration close to saturation) and mitochondrial suspension was stirred at 37°C for 10 min. The chamber was then sealed, state 4 (resting) respiration was measured and 1 min later the uncoupling agent, FCCP (200 nM) was added and the rate of uncoupled (maximal) respiration was determined.

Data were collected as nanograms of oxygen atoms consumed per minute per milligram of protein. Data were then transformed into percent of control respiration (in the absence of MitoTracker dye) and three separate one-way ANOVAs (for each MitoTracker dye), comparing respiration in control mitochondria to that in mitochondria incubated with the low and high concentration of dye. A Bonferroni post-hoc test was performed when $P < 0.05$.

3. Results

3.1. FCCP-induced changes in dye labeling

All three MitoTrackers labeled neurons and astrocytes in a punctate fashion anticipated for a mitochondrion-specific dye. Staining was typically observed in perinuclear regions and processes, while the nucleus was typically devoid of staining (Fig. 1A,B, top panels). The fluorescence intensity of the MitoTrackers was concentration dependent with maximal staining seen with 200–500 nM (data not shown). To determine the effect of $\Delta\Psi_m$ on fluorescence intensity, cells were loaded with different dye concentrations and then exposed the cells to FCCP. At high concentrations, the MitoTracker dyes showed an increase in fluorescence intensity upon loss of $\Delta\Psi_m$, suggesting that they be-

come so tightly packed within mitochondria at these concentrations that fluorescence intensity is underestimated due to the phenomenon of quenching (see Section 4). MitoTracker Green showed the smallest increase in fluorescence intensity during treatment with FCCP, however, in both neurons and astrocytes, no return to baseline was observed during a 5-min wash period (Fig. 2A,D). MitoTracker Orange showed the most robust increase in fluorescence intensity in neurons and this was observed at concentrations of 50–500 nM. A slow, delayed decrease in fluorescence was observed during the wash period, indicating either re-sequestration as mitochondria repolarize or a leakage of the dye from the cell (Fig. 2B,E). MitoTracker Red showed variability in the time course of the FCCP-induced fluorescence increases, however, every concentration of MitoTracker Red tested was influenced by mitochondrial depolarization. In addition, a rapid return to basal fluorescence was observed during the recovery period (Fig. 2C,F). All three MitoTrackers showed a diffusion of fluorescence upon mitochondrial depolarization (Fig. 1A,B, bottom panels). Interestingly, the redistribution of dye was apparent even when there was no overall change in fluorescence intensity. Taken together these data suggest that MitoTrackers are membrane-permeable and diffuse out of mitochondria during a depolarizing stimulus. It also appears that MitoTrackers, at concentrations as low as 25 nM (in MitoTracker Red), are quenched in mitochondria as evidenced by the increase in fluorescence signal seen when the dyes are released from mitochondria.

3.2. FCCP-induced changes in dye loading

A concentration of 50 nM, the lowest concentration that reliably gave a good signal:noise ratio, was used

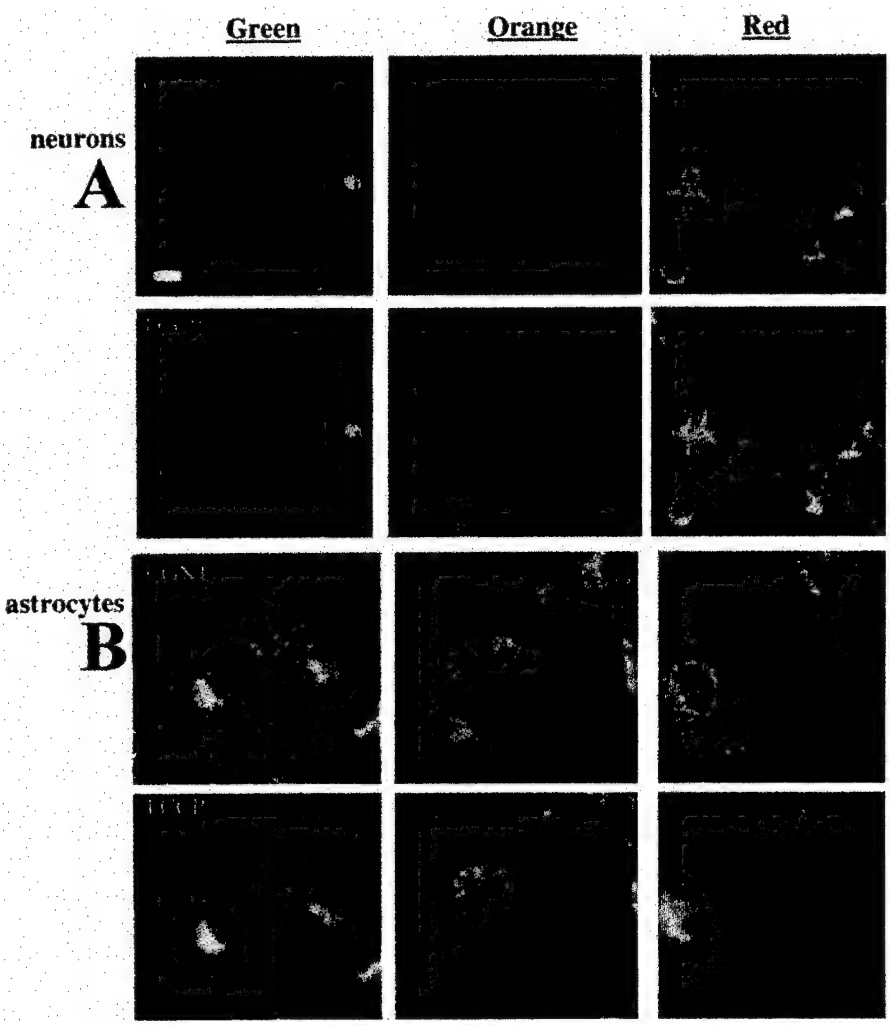

Fig. 1. Representative micrographs of fluorescence intensity and distribution of the MitoTracker dyes prior to and during treatment with *p*-(trifluoromethoxy) phenyl-hydrazone (FCCP) in (A) primary neurons and (B) astrocytes. In both (A) and (B), the upper row of images shows baseline fluorescence in cells loaded with 50 nM MitoTracker Green, Orange and Red (from left to right). The lower row of images shows fluorescence in cells treated with a mitochondrial depolarizing stimulus (images collected after approximately 3 min of FCCP treatment). Bar, 25 μM.

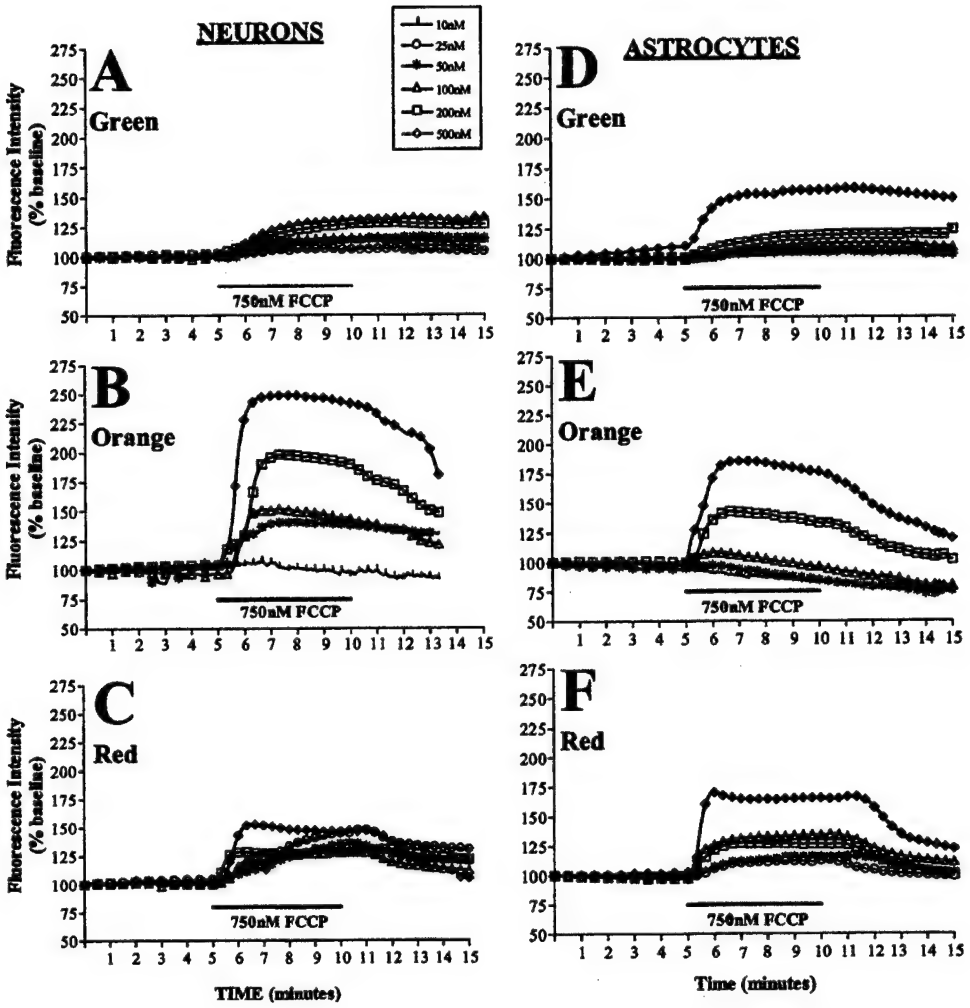

Fig. 2. Intensity of MitoTracker fluorescence during mitochondrial depolarization. (A–C) Primary neurons and (D–F) astrocytes were loaded with varying concentrations of MitoTracker (A,D) Green, (B,E) Orange or (C,F) Red and the fluorescence intensity was measured. Baseline fluorescent images were recorded for 5 min, then the MitoTracker response to a depolarizing concentration (750 nM) of the uncoupling agent, *p*-(trifluoromethoxy) phenyl-hydrazone (FCCP) was measured for 5 min. Following treatment, cells were allowed to recover for 5 min. Data are presented as percent of baseline fluorescence intensity.

for all MitoTrackers in this experiment. Neurons or astrocytes were loaded with MitoTracker dyes alone or in the presence of 750 nM FCCP. This concentration of FCCP has been shown to result in a profound, but reversible depolarization of the $\Delta\Psi_m$ (White and Reynolds, 1996). In neurons, MitoTracker Green appeared to load equally well into polarized or depolarized mitochondria, however MitoTracker Orange and Red showed considerably lower fluorescence intensity when loaded into neurons treated with FCCP (Fig. 3A). In astrocytes, MitoTracker Green loading appeared to depend on the $\Delta\Psi_m$, with lower fluorescence intensity observed in the presence of FCCP. Similarly, MitoTracker Orange loading into astrocytes was compromised when mitochondria were depolarized. In contrast, MitoTracker Red appeared to load into astrocytic mitochondria regardless of $\Delta\Psi_m$ (Fig. 3B). A less punctate label (vs. Fig. 1A,B, upper panels) was observed under these loading conditions, except with MitoTracker Red in astrocytes (Fig. 4). These data reflect the different loading behaviors of the MitoTrackers and point to the significance of cell model for the appropriate use of these dyes.

3.3. H_2O_2-induced changes in dye loading

Cells were incubated with H_2O_2 for 15 min prior to loading with 50 nM MitoTracker in order to induce an oxidant stress. H_2O_2-induced oxidative stress was seen in neurons at concentrations as low as 10 μM and at concentrations greater than 500 μM considerable cell death was evident. Astrocytes were more resistant to oxidant stress and thus higher concentrations of H_2O_2 were utilized. The chloromethyl moieties of the MitoTracker dyes have been suggested to react with free sulfhydryls (Haugland, 1996). Thus, an oxidative stress

was expected to change the loading and stability of the MitoTrackers labeling. Comparison of the mean fluorescence intensity following pretreatment, using unpaired t tests, showed that some concentrations of H_2O_2 increased neuronal MitoTracker Green fluorescence (Fig. 5A) and astrocytic MitoTracker Red fluorescence (Fig. 5F); however, with MitoTracker Orange and Red in neurons (Fig. 5B,C) and MitoTracker Green and Orange in astrocytes (Fig. 5D,E) statistically significant increases in fluorescence were more broadly seen and appeared, in some cases, to correspond to an H_2O_2 concentration-dependence. The changes in fluorescence intensity did not correlate with a relocalization of the dyes (Fig. 6), in that H_2O_2 increased fluorescence intensity without the migration of the dye into parts of the cell not normally labeled. This may be consistent with an alteration of the interaction of the dyes with cellular sulfhydryl moieties.

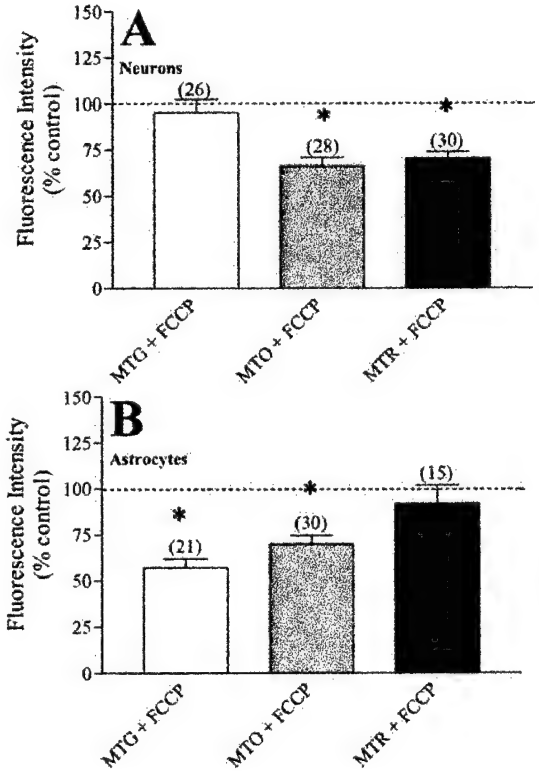

Fig. 3. Effect of mitochondrial depolarization on MitoTracker loading. (A) Neurons and (B) astrocytes were loaded with 50 nM MitoTracker dye in the presence of 750 nM p-(trifluoromethoxy) phenyl-hydrazone (FCCP) and the fluorescence intensity (averaged over 5 min) was compared to cells loaded without FCCP. The loading of MitoTracker Green (MTG) in astrocytes [$t = 2.6$, df = 5, $P < 0.05$], MitoTracker Orange (MTO) in neurons [$t = 3.7$, df = 4, $P < 0.05$] and astrocytes [$t = 2.8$, df = 6, $P < 0.05$] and Red (MTR) in neurons [$t = 3.6$, df = 4, $P < 0.05$] was sensitive to $\Delta\psi_m$, as evidenced by the significant decrease in fluorescence intensity when FCCP was present. The number of cells analyzed (n) is presented above each bar. Average fluorescence from each coverslip was then computed and used as degrees of freedom in unpaired t tests (see Section 2). [* $P < 0.05$].

3.4. H_2O_2-induced changes in dye labeling

Neurons and astrocytes were loaded with 50 nM MitoTracker dye and imaged for 5 min to achieve stable baseline fluorescence. Neurons were then treated with 500 μM H_2O_2 for 5 min and the intensity of fluorescence was measured. MitoTracker Green was unaffected by treatment with H_2O_2 and MitoTracker Orange and Red fluorescence were only very modestly increased by this short-term oxidative stress, with no return to baseline observed. In astrocytes treated with 3 mM H_2O_2, only MitoTracker Red fluorescence was increased (Fig. 7). No apparent relocalization of the dyes was observed (data not shown). These data suggest that once MitoTrackers, especially MitoTracker Green, are loaded into primary neuronal or astrocytic cultures, they are only mildly influenced by a change in the production of ROS and/or oxidation of sulfhydryl groups. However, the effect of a longer exposure to H_2O_2 (i.e. 15 min) may be necessary to see the more profound effect seen during pretreatment with H_2O_2.

3.5. Respiration in isolated brain mitochondria

Isolated rat brain mitochondria were incubated in the presence of 50 nM or 3.12 μM MitoTracker Green, Orange or Red and state 4 (resting) and uncoupled (maximal) respiration were recorded. Since dye distribution between the aqueous phase and the mitochondrial membranes is not homogeneous, MitoTracker concentrations are also denoted as nmoles of dye per mg of mitochondrial protein (50 nM corresponds to 0.2 nmol/mg protein and 3.12 μM corresponds to 12.5 nmol/mg protein). Initially mitochondria and the fluorescent dyes were incubated for 2–4 min prior to uncoupling, however, there was no inhibition seen at either concentration tested (data not shown). Because the MitoTrackers contain sulfhydryl-reactive moieties they may bind more slowly, therefore the incubation time was extended to 10 min. Under these conditions, high concentrations of MitoTracker Green (3.12 μM) significantly increased resting respiration, suggesting its ability to uncouple respiratory chain activity from ATP synthesis, and decreased maximal respiration rates, suggesting its ability to inhibit respiration (Fig. 8). MitoTracker Orange did not significantly impact respiration rate, however it exhibited trends towards increased state 4 respiration rate ($P = 0.07$) and decreased maximal respiration rate ($P = 0.13$) (Fig. 8). MitoTracker Red exhibited a trend towards increased resting respiration rate ($P = 0.09$) and significantly decreased the rate of maximal respiration rate (at 3.12 μM, but not at 50 nM). Taken together, these data suggest that all of the MitoTracker dyes are capable of inhibiting normal mitochondrial respiration at μM concentrations.

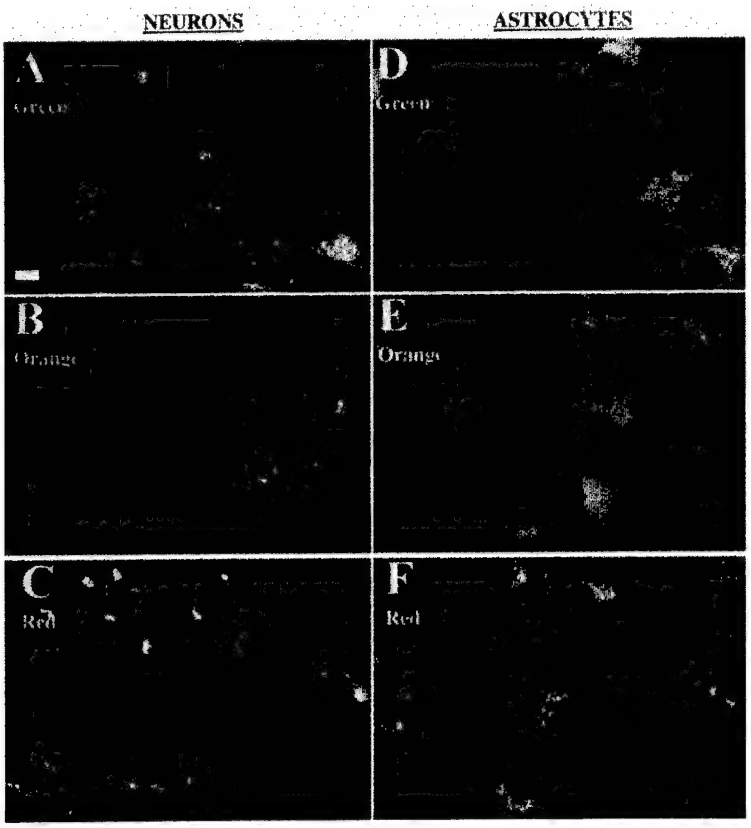

Fig. 4. Representative micrographs of distribution of the MitoTracker fluorescence when loaded in the presence of a mitochondrial depolarizing stimulus. (A–C) Primary neurons and (D–F) astrocytes were loaded with 50 nM MitoTracker (A,D) Green, (B,E) Orange or (C,F) Red in the presence of 750 nM *p*-(trifluoromethoxy) phenyl-hydrazone (FCCP). Bar, 25 μM.

4. Discussion

The MitoTracker dyes are being used with increasing frequency for morphological and functional measurements of mitochondria. While the pattern of their fluorescence strongly suggests mitochondrial specificity, parameters that influence their loading and/or labeling are still controversial and have not been fully explored in neural cells. For example, reports that during apoptosis the release of cytochrome c can occur independent of changes in mitochondrial membrane potential have been partially based on the lack of change in MitoTracker Orange fluorescence (which was being used as a $\Delta\Psi_m$ sensor) during cytochrome c release (Bossy-Wetzel et al., 1998; Li et al., 1998; Finucane et al., 1999). However, the present experiments suggest that there are numerous factors to consider prior to using the MitoTracker dyes and, in agreement with Scorrano et al. (1999) and Keij et al. (2000), that these aforementioned data must be interpreted with caution. It has been noted that not only are MitoTracker Green, Orange and Red different from one another, but also that each MitoTracker behaves differently in neurons and astrocytes.

For all three MitoTrackers, in both neurons and astrocytes, a concentration of 50 nM was sufficient to produce a bright, punctate label that appears to be associated with mitochondria. However, at this concentration, neurons and astrocytes treated with FCCP during or after loading showed a diffusion of the dye into the cytoplasm, nucleus and/or other organelles. In human osteosarcoma cells, a redistribution of MitoTracker Green was observed following a 30-min treatment with another uncoupler, CCCP (Minamikawa et al., 1999). However, these authors used high-resolution confocal microscopy and the observed redistribution appeared to coincide with mitochondrial swelling, not diffusion into cytoplasm (Minamikawa et al., 1999). Whether this observation is associated with confocal versus light microscopy or osteosarcomas versus primary neurons and astrocytes is unclear.

In addition to a relocalization of fluorescence observed in association with mitochondrial depolarization, an increase in fluorescence intensity was frequently seen, especially at higher concentrations and most intensely with MitoTracker Orange (Fig. 2). This increased fluorescence has been interpreted as an unquenching of dye. Quenching occurs as the result of

molecular interactions that inhibit the ability of a fluorophore to emit a photon. For example, rhodamine dyes aggregate based on $\Delta\Psi_m$ but these aggregates are non-fluorescent due to quenching. Quenching becomes most apparent with these rhodamine dyes when the mitochondria are depolarized and the intensity of fluorescence dramatically increases (Chen and Smiley, 1993). It is possible that MitoTrackers aggregate within mitochondria without truly quenching, however, due to the similarities of the current observations with those seen with rhodamine derivatives this phenomen will be tentatively referred to as quenching.

The use of quenching concentrations of MitoTracker dyes impacts a number of possible interpretations of the data. During washout after FCCP treatment, a slow decrease in fluorescence is observed (Fig. 2). This may be due to the movement of the dye back into the mitochondria as they repolarize (requenching) or due to slow leakage of the dye through the plasma membrane. As quenching interferes with linear measurements of fluorescence, it is not possible to determine whether one or both of these phenomena have occurred. However at the beginning and end of this experiment, small punctate spots of labeling can be observed within the cells. This suggests that some of the dye remains within the mitochondria, but quenching prohibits direct quantitation of a $\Delta\Psi_m$-insensitive pool, an irreversibly bound pool or re-sequestered pool of dye.

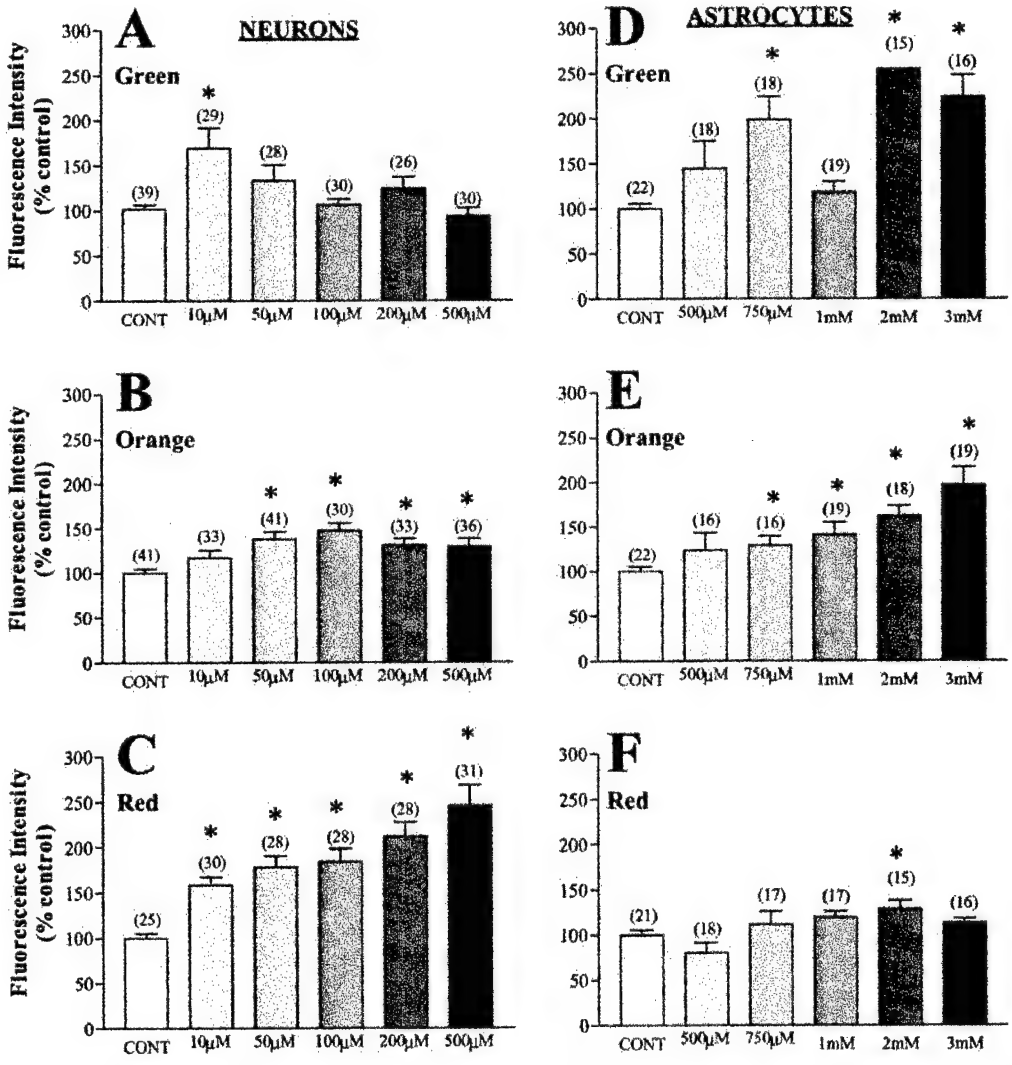

Fig. 5. Effect of H_2O_2 pretreatment on MitoTracker loading. (A–C) Neurons and (D–F) astrocytes were incubated with 10 μM–3 mM of H_2O_2 for 15 min, then loaded with 50 nM MitoTracker (A,D) Green, (B,E) Orange or (C,F) Red. The intensity of fluorescence was measured (over 5 min) and the mean ± S.E.M. was calculated. Data are expressed as percent of untreated control and the number of cells analyzed is presented above each bar. Unpaired *t* tests were performed to determine whether H_2O_2 pretreatment led to significant changes in fluorescence intensity. All points were individually compared to the untreated control. MitoTracker Orange and Red in neurons and MitoTracker Green and Orange in astrocytes exhibited H_2O_2 concentration-dependent changes in fluorescence [* $P < 0.05$].

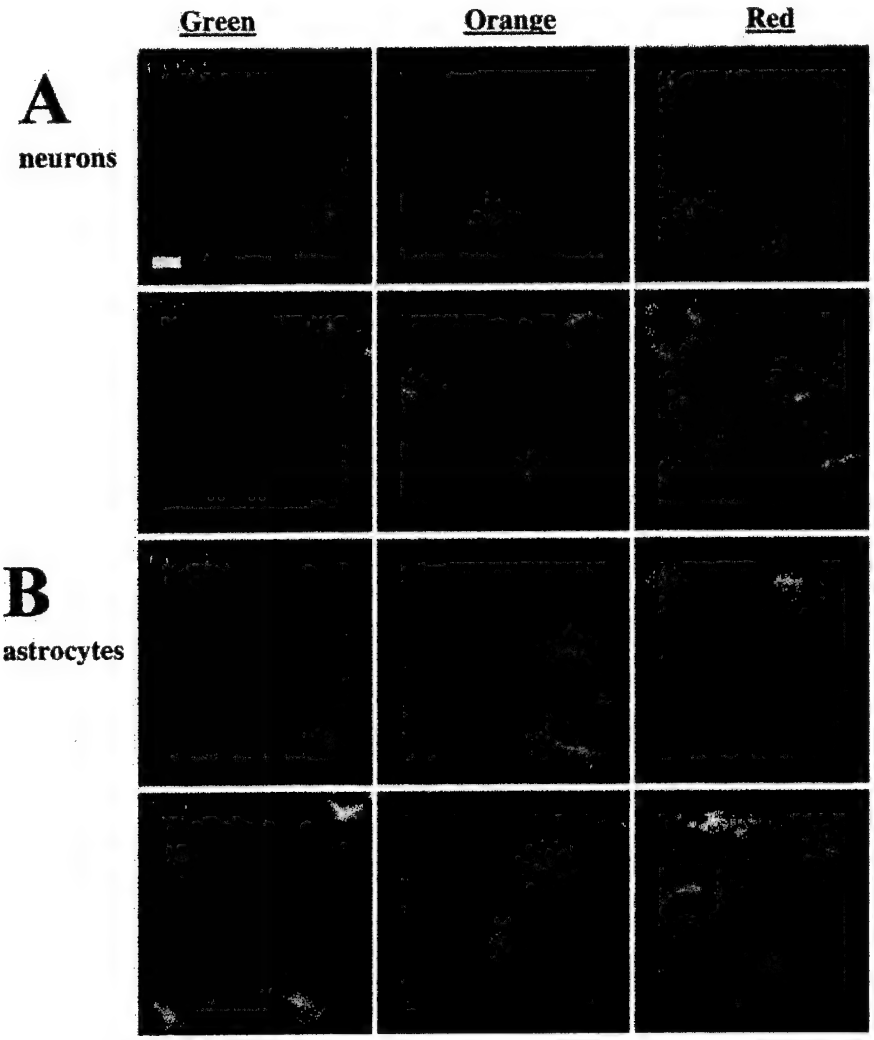

Fig. 6. Representative micrographs of distribution of the MitoTracker loading in cells pretreated with H_2O_2. (A,B) The upper rows of images show neurons loaded with 50 nM MitoTracker Green, Orange and Red (from left to right) without any pretreatment. In the lower rows, (A) neurons were preincubated with 500 μM H_2O_2 and then loaded with 50 nM MitoTracker (B) astrocytes were preincubated with 3 mM H_2O_2 and then loaded with 50 nM MitoTracker. Bar, 25 μM.

4.1.1. MitoTracker Green

MitoTracker Green is now commonly being used for measurement of mitochondrial shape changes, mass or swelling (Bowser et al., 1998; Funk et al., 1999; Krohn et al., 1999; Minamikawa et al., 1999; Monteith and Blaustein, 1999). At low concentrations (≤ 50 nM), MitoTracker Green may be useful for these measures, however several features of this dye must be acknowledged prior to use. There are cell type- and concentration-specific differences in MitoTracker Green labeling. At 50 nM, MitoTracker Green loading appeared $\Delta\Psi_m$- and oxidation-sensitive in astrocytes, but not neurons. At concentrations greater than 50 nM, MitoTracker Green exhibits a tendency to quench and, upon depolarization, exhibits an irreversible increase in fluorescence. Moreover, in isolated brain mitochondria, μM concentrations of MitoTracker Green appeared capable of acting as an uncoupler and inhibiting respiration. Taken together, the present data support the use of MitoTracker Green at low concentrations for assessing mitochondrial size, localization and structure. However, determination of the appropriate concentration of MitoTracker in individual cell models will be necessary for interpretable results.

4.1.2. MitoTracker Orange

MitoTracker Orange has been used as a marker for $\Delta\Psi_m$ (Matylevitch et al., 1998) and, in its reduced form, as a marker for ROS generation (Karbowski et al., 1999). Scorrano et al. (1999) characterized this dye in MH1C1 rat hepatoma cells and in agreement with the present findings, found that the fluorescence was punctate and stable. However, in their cell model, a redistribution of the dye was observed following pretreatment with agents that decrease free sulfhydryls, but not with FCCP. In the present paper, pretreatment with FCCP,

but not H_2O_2, caused a redistribution of MitoTracker Orange into neuronal and astrocytic cultures. H_2O_2 pretreatment, however, did appear to increase MitoTracker Orange fluorescence in neurons and astrocytes. Moreover, Scorrano et al. (1999) did not observe quenching or relocalization of MitoTracker Orange when cells were treated with FCCP following loading. In the present experiments, neurons and astrocytes treated with FCCP following loading showed increased fluorescence intensity (suggestive of quenching) as well as a relocalization of fluorescence. In isolated rat liver mitochondria, MitoTracker Orange inhibited complex I of the respiratory chain, induced PT and caused depolarization, swelling and the release of cytochrome c in liver mitochondria (Scorrano et al., 1999). However, in isolated brain mitochondria, no inhibition of complex I by MitoTracker Orange was observed, even at concentrations exceeding 3 μM. Again, these observed differences suggest that care must be taken in extrapolating MitoTracker data obtained in different cell models. In addition, MitoTracker Orange should be used with caution and that the interpretation of data with MitoTracker Orange must consider their effects on mitochondrial function and their sensitivity to $\Delta\Psi_m$ and free sulfhydryls.

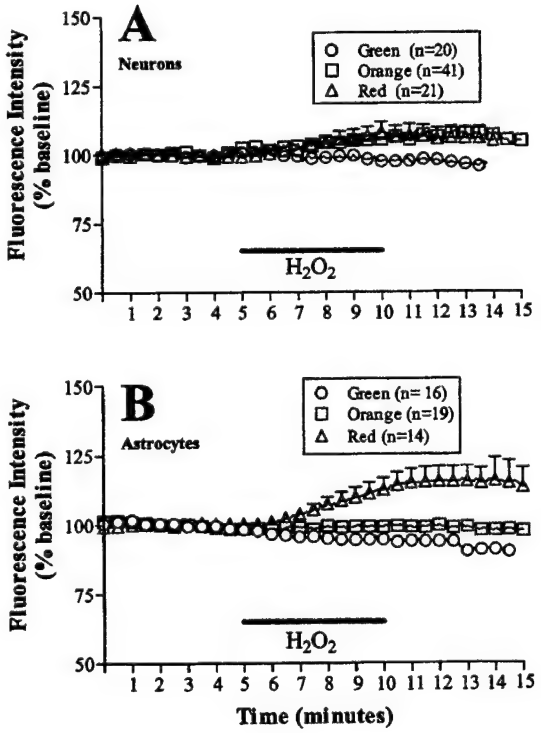

Fig. 7. Intensity of MitoTracker fluorescence in response to H_2O_2. (A) Neurons and (B) astrocytes were loaded with 50 nM MitoTracker and their response to 500 μM (neurons) or 3 mM (astrocytes) H_2O_2 was measured. Baseline fluorescent images were recorded for 5 min, followed by a 5-min H_2O_2 treatment and a 5-min recovery period. Data are expressed as percent of basal fluorescence (± S.E.M.). The number of cells analyzed in presented in the figure legend.

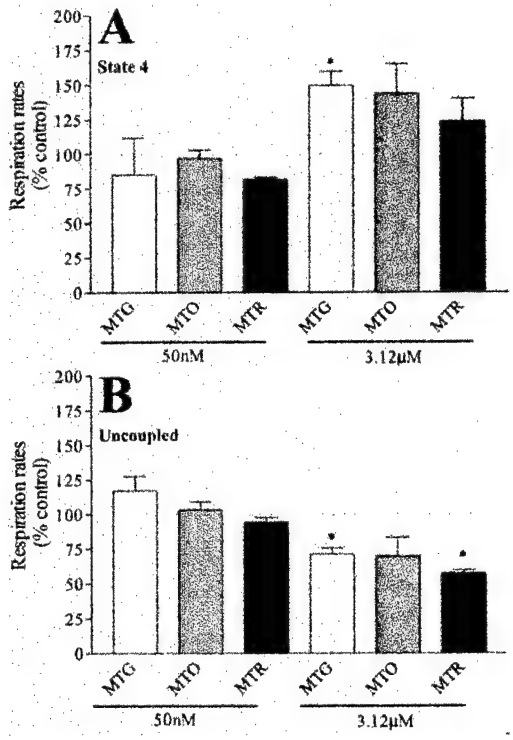

Fig. 8. Respiration of isolated rat brain mitochondria. (A) State 4 (resting) respiration rate was determined following a 10 min preincubation of isolated mitochondria with 2 μM oligomycin and 50 nM or 3.12 μM MitoTracker Green (MTG), Orange (MTO) or Red (MTR). The mean (± S.E.M.) respiration rates were computed and data were transformed into percent of respiration rate of control (without MitoTracker dyes). Statistical analysis using a one-way ANOVA and a Bonferroni's post-hoc test showed the following: MTG: $F_{(2, 10)} = 7.5$, $P < 0.05$ with the high concentration being significantly different from both the control and 50 nM group ($P < 0.05$). MTO: $F_{(2, 8)} = 3.7$, $P > 0.05$. MTR: $F_{(2, 8)} = 3.3$, $P > 0.05$. (B) Following assessment of resting respiration, 200 nM *p*-(trifluoromethoxy) phenyl-hydrazone (FCCP) was added and the maximal respiration rate was determine in the same isolated mitochondria. The mean (± S.E.M.) respiration rate was computed and data were transformed into percent of respiration rate of control (without MitoTracker dyes). Statistical analysis showed the following: MTG: $F_{(2, 8)} = 16.2$, $P < 0.05$ with the high concentration being significantly different from both the control and 50 nM group ($P < 0.05$). MTO: $F_{(2, 6)} = 2.9$, $P > 0.05$. MTR: $F_{(2, 6)} = 130.1$, $P < 0.05$ with the high concentration being significantly different from both the control and 50 nM group ($P < 0.05$).

4.1.3. MitoTracker Red

MitoTracker Red has been utilized as a $\Delta\Psi_m$-sensitive dye, since being reported as one by Macho et al. (1996). The linearity between $\Delta\Psi_m$ and MitoTracker Red fluorescence has been brought into question due to thiol binding of MitoTracker Red (Ferlini et al., 1998; Poot and Pierce, 1999a). It seems unlikely that this dye would offer advantages over JC-1, TMRE or rhodamine 123 for assessing $\Delta\Psi_m$. However, MitoTracker Red can be fixed and maintain a mitochondrial-specific localization, as observed in double labeling experiments with cytochrome c oxidase (Poot et al., 1996). Gilmore and Wilson (1999) used flow cytometry to show that

MitoTracker Red was $\Delta\Psi_m$-sensitive because it decreased with depolarizing stimuli, but it could not reliably indicate $\Delta\Psi_m$ at the time of fixation. Moreover, MitoTracker Red has been implicated as a mitochondrial-specific photosensitiser, due to the laser-induced mitochondrial damage observed in osteosarcomas (Minamikawa et al., 1999). In light of these observations, clear understanding of how MitoTracker Red influences neuronal and astrocytic mitochondria is necessary. In the present experiments, the loading of MitoTracker Red appeared $\Delta\Psi_m$- and oxidant-dependent in neurons, but not astrocytes. Following loading, MitoTracker Red fluorescence relocalized during mitochondrial depolarization and increased following treatment with FCCP and H_2O_2 in astrocytes, and to a lesser degree, neurons. It also appears to inhibit normal respiratory activity through complex I. These data illustrate that MitoTracker Red loading, stability and mitochondrial localization is contingent on cell type, $\Delta\Psi_m$, ROS and/or free sulfhydryl groups. Therefore, in addition to being less than ideal as a $\Delta\Psi_m$ marker, MitoTracker Red seems incapable of functionally characterizing mitochondria in intact cells and should be used only as a marker for the localization of normal, energized mitochondria.

To determine whether MitoTracker dyes directly influenced bioenergetics, isolated rat brain mitochondria were examined for resting and uncoupled (maximal) respiration rates through complex I in the presence of the different MitoTrackers. It was observed that MitoTracker Green acted as both a weak uncoupler and inhibitor of respiration and MitoTracker Red significantly decreased the rate of maximal respiration. MitoTracker Orange showed similar trends. These data suggest that the MitoTracker dyes are capable of inhibiting normal mitochondrial respiration at μM concentrations. Previously, MitoTracker Orange was found to inhibit complex I in isolated liver mitochondria and was observed to induce PT and swelling and release cytochrome c (Scorrano et al., 1999). In the present experiments, the respiration buffer contained physiological concentrations of Mg^{2+} and ATP and had a pH of 7.0 to minimize the likelihood of PT. The opening of the PTP can lead to the loss of respiratory substrates, such as NADH, as well as cytochrome c, thereby confounding the assessment of the MitoTracker dyes on respiratory chain activity. Moreover, since the MitoTracker dyes are sulfhydryl agents, they may increase the probability of opening the PTP (Zoratti and Szabo, 1995). The respiration experiments were therefore designed to enhance a straightforward assessment of respiratory chain activity through complex I and did not test the MitoTracker dyes' ability to induce transition. In keeping with Scorrano et al. (1999), however, preliminary experiments were performed in isolated liver mitochondria and observed inhibition of respiration with MitoTracker Red, and to a lesser extent with MitoTracker Orange (data not shown).

Potential problems associated with the use of the MitoTracker dyes, including their sensitivity to changes in $\Delta\Psi_m$, oxidant status and quenching have been addressed in these experiments. Although these features of the MitoTracker dyes makes data interpretation difficult, it should be noted that numerous other mitochondrial-specific dyes (e.g. $\Delta\Psi_m$-sensitive JC-1 and TMRM) also suffer from several of the same caveats in interpretation. For example, both JC-1 and TMRM can respond to changes in the plasma membrane potential, although fluorescence changes caused by mitochondrial versus plasma membrane depolarizations appear differently (Nicholls and Ward, 2000). Similar plasma membrane potential contributions cannot be ruled out with MitoTracker fluorescence. TMRM, being a rhodamine-based dye, is capable of quenching, in a similar fashion to the MitoTrackers, and may be sensitive to photo-oxidation (Nicholls and Ward, 2000). JC-1, however, is a dual emission dye that exhibits fluorescent monomers and aggregates. Although quenching per se may not occur, JC-1 aggregates localized specifically in mitochondria can disband during depolarization and cause a transient increase in monomer signal. It is also interesting to note that using JC-1, Chinopoulos et al. (1999) have reported a slight mitochondrial depolarization resulting from H_2O_2 treatment. However, Scanlon and Reynolds (1998) noted that H_2O_2 alters JC-1 fluorescence in a manner distinct from other known depolarizing agents. Typical depolarizing agents, such as FCCP, lead to increases in JC-1 monomer signal, whereas H_2O_2 leads to a decrease in the aggregate signal. Thus, although it seems that most mitochondrial dyes must be used with caution, a direct relationship between $\Delta\Psi_m$ and fluorescence intensity has been demonstrated with JC-1 and TMRM (Ward et al., 2000). This direct relationship does not appear to be as clear with the MitoTracker dyes.

There are clearly some potential limitations to the present studies. The resolution obtainable with wide-field microscopy precludes the ready assessment of the fluorescence signal at the single mitochondrion level, so that relocalization of dye is difficult to quantitatively measure. Indeed, it is even difficult to conclusively establish that the punctate staining that has been observed is associated with mitochondria, because any correlative co-staining approach would also require assumptions about the localization of the co-stain. The impact of permeability transition on the localization of the dyes was not monitored because of the lack of an unequivocal method for inducing robust and measurable transition in intact neurons or astrocytes. Nevertheless, the characterization provided by this study will help to establish suitable methods for the use of these dyes, and suggests caution when using the MitoTrackers for even a semi-quantitative determination of $\Delta\Psi_m$.

Acknowledgements

The authors gratefully acknowledge Teresa Hastings for her collaboration with the respiration experiments. This work was supported by USAMRMC grant DAMD-17-98-1-8627 (IJR), the Scaife Family Foundation (IJR) and an NIH grant T32NS07391 (JFB).

References

Andreyev A, Fiskum G. Calcium induced release of mitochondrial cytochrome c by different mechanisms selective for brain versus liver. Cell Death Differ 1999;6:825–32.

Andreyev AY, Fahy B, Fiskum G. Cytochrome c release from brain mitochondria is independent of the mitochondrial permeability transition. FEBS Lett 1998;439:373–6.

Bossy-Wetzel E, Newmeyer DD, Green DR. Mitochondrial cytochrome c release in apoptosis occurs upstream of DEVD-specific caspase activation and independently of mitochondrial transmembrane depolarization. EMBO J 1998;17:37–49.

Bowser DN, Minamikawa T, Nagley P, Williams DA. Role of mitochondria in calcium regulation of spontaneously contracting cardiac muscle cells. Biophys J 1998;75:2004–14.

Bradford MM. A rapid and sensitive method for the quantitation of microgram quantities of protein utilizing the principle of protein-dye binding. Anal Biochem 1976;72:248–54.

Chen LB, Smiley ST. Probing mitochondrial membrane potential in living cells by a J-aggregate-forming dye. In: Fluorescent and Luminescent Probes for Biological Activity. London: Academic Press, 1993:124–31.

Chinopoulos C, Tretter L, Adam-Vizi V. Depolarization of in situ mitochondria due to hydrogen peroxide-induced oxidative stress in nerve terminals: inhibition of alpha-ketoglutarate dehydrogenase. J Neurochem 1999;73:220–8.

Ferlini C, Scambia G, Fattorossi A. Is chloromethyl-X-rosamine useful in measuring mitochondrial transmembrane potential? Cytometry 1998;31:74–5.

Finucane DM, Bossy-Wetzel E, Waterhouse NJ, Cotter TG, Green DR. Bax-induced caspase activation and apoptosis via cytochrome c release from mitochondria is inhibitable by Bcl-xL. J Biol Chem 1999;274:2225–33.

Funk RH, Nagel F, Wonka F, Krinke HE, Golfert F, Hofer A. Effects of heat shock on the functional morphology of cell organelles observed by video-enhanced microscopy. Anat Rec 1999;255:458–64.

Gilmore K, Wilson M. The use of chloromethyl-X-rosamine (Mitotracker red) to measure loss of mitochondrial membrane potential in apoptotic cells is incompatible with cell fixation. Cytometry 1999;36:355–8.

Haugland RP. Handbook of Fluorescent Probes and Research Chemicals. Eugene, OR: Molec. Probes, 1996.

Karbowski M, Kurono C, Wozniak M, Ostrowski M, Teranishi M, Soji T, Wakabayashi T. Cycloheximide and 4-OH-TEMPO suppress chloramphenicol-induced apoptosis in RL-34 cells via the suppression of the formation of megamitochondria. Biochim Biophys Acta 1999;1449:25–40.

Keij JF, Bell-Prince C, Steinkamp JA. Staining of mitochondrial membranes with 10-nonyl acridine orange, MitoFluor Green, and MitoTracker Green is affected by mitochondrial membrane potential altering drugs. Cytometry 2000;39:203–10.

Krohn AJ, Wahlbrink T, Prehn JH. Mitochondrial depolarization is not required for neuronal apoptosis. J Neurosci 1999;19:7394–404.

Li N, Oberley TD, Oberley LW, Zhong W. Inhibition of cell growth in NIH/3T3 fibroblasts by overexpression of manganese superoxide dismutase: mechanistic studies. J Cell Physiol 1998;175:359–69.

Macho A, Decaudin D, Castedo M, Hirsch T, Susin SA, Zamzami N, Kroemer G. Chloromethyl-X-Rosamine is an aldehyde-fixable potential-sensitive fluorochrome for the detection of early apoptosis. Cytometry 1996;25:333–40.

Matylevitch NP, Schuschereba ST, Mata JR, Gilligan GR, Lawlor DF, Goodwin CW, Bowman PD. Apoptosis and accidental cell death in cultured human keratinocytes after thermal injury. Am J Pathol 1998;153:567–77.

McCarthy KD, de Vellis J. Preparation of separate astroglial and oligodendroglial cell cultures from rat cerebral tissue. J Cell Biol 1980;85:890–902.

Minamikawa T, Williams DA, Bowser DN, Nagley P. Mitochondrial permeability transition and swelling can occur reversibly without inducing cell death in intact human cells. Exp Cell Res 1999;246:26–37.

Monteith GR, Blaustein MP. Heterogeneity of mitochondrial matrix free Ca2+: resolution of Ca2+ dynamics in individual mitochondria in situ. Am J Physiol 1999;276:C1193–204.

Nicholls DG, Ward MW. Mitochondrial membrane potential and neuronal glutamate excitotoxicity: mortality and millivolts. Trends Neurosci 2000;23:166–74.

Poot M, Pierce RC. Detection of apoptosis and changes in mitochondrial membrane potential with chloromethyl-X-rosamine. Cytometry 1999a;36:359–60.

Poot M, Pierce RH. Detection of changes in mitochondrial function during apoptosis by simultaneous staining with multiple fluorescent dyes and correlated multiparameter flow cytometry. Cytometry 1999b;35:311–7.

Poot M, Zhang YZ, Kramer JA, Wells KS, Jones LJ, Hanzel DK, Lugade AG, Singer VL, Haugland RP. Analysis of mitochondrial morphology and function with novel fixable fluorescent stains. J Histochem Cytochem 1996;44:1363–72.

Rosenthal RE, Hamud F, Fiskum G, Varghese PJ, Sharpe S. Cerebral ischemia and reperfusion: prevention of brain mitochondrial injury by lidoflazine. J Cereb Blood Flow Metab 1987;7:752–8.

Scanlon JM, Reynolds IJ. Effects of oxidants and glutamate receptor activation on mitochondrial membrane potential in rat forebrain neurons. J Neurochem 1998;71:2392–400.

Scorrano L, Petronilli V, Colonna R, Di Lisa F, Bernardi P. Chloromethyltetramethylrosamine (Mitotracker Orange) induces the mitochondrial permeability transition and inhibits respiratory complex I. Implications for the mechanism of cytochrome c release. J Biol Chem 1999;274:24657–63.

Ward MW, Rego AC, Frenguelli BG, Nicholls DG. Mitochondrial membrane potential and glutamate excitotoxicity in cultured cerebellar granule cells. J Neurosci 2000;20:7208–19.

White RJ, Reynolds IJ. Mitochondria and Na+/Ca2+ exchange buffer glutamate-induced calcium loads in cultured cortical neurons. J Neurosci 1995;15:1318–28.

White RJ, Reynolds IJ. Mitochondrial depolarization in glutamate-stimulated neurons: an early signal specific to excitotoxin exposure. J Neurosci 1996;16:5688–97.

Zoratti M, Szabo I. The mitochondrial permeability transition. Biochim Biophys Acta 1995;1241:139–76.

The Journal of Neuroscience, July 15, 2001, 21(14):5054–5065

Spontaneous Changes in Mitochondrial Membrane Potential in Cultured Neurons

Jennifer F. Buckman and Ian J. Reynolds

Department of Pharmacology, University of Pittsburgh, Pittsburgh, Pennsylvania 15261

Using the mitochondrial membrane potential ($\Delta\Psi_m$)-sensitive fluorescent dyes 5,5′,6,6′-tetrachloro-1,1′,3,3′-tetraethylbenzimidazolocarbocyanine iodide (JC-1) and tetramethylrhodamine methyl ester (TMRM), we have observed spontaneous changes in the $\Delta\Psi_m$ of cultured forebrain neurons. These fluctuations in $\Delta\Psi_m$ appear to represent partial, transient depolarizations of individual mitochondria. The frequency of these $\Delta\Psi_m$ fluctuations can be significantly lowered by exposure to a photo-induced oxidant burden, an ATP synthase inhibitor, or a glutamate-induced sodium load, without changing overall JC-1 fluorescence intensity. These spontaneous fluctuations in JC-1 signal were not inhibited by altering plasma membrane activity with tetrodotoxin or MK-801 or by blocking the mitochondrial permeability transition pore (PTP) with cyclosporin A. Neurons loaded with TMRM showed similar, low-amplitude, spontaneous fluctuations in $\Delta\Psi_m$. We hypothesize that these $\Delta\Psi_m$ fluctuations are dependent on the proper functioning of the mitochondria and reflect mitochondria alternating between the active and inactive states of oxidative phosphorylation.

Key words: mitochondria; membrane potential; ATP; JC-1; TMRM; F_1F_O *ATPase*

Mitochondria have been implicated in excitotoxic injury pathways, as well as injury mechanisms manifested as apoptotic or necrotic death processes. The mitochondrial membrane potential ($\Delta\Psi_m$) has often been used as a marker for mitochondrial activity and neuronal viability during the various cell death cascades (for review, see Kroemer et al., 1998; Nicholls and Ward, 2000). Injurious stimuli, leading to either excitotoxicity or apoptosis, can lead to profound depolarization of $\Delta\Psi_m$ resulting from abnormalities in neuronal processes, including alterations in intracellular calcium dynamics and the opening of the mitochondrial permeability transition pore (PTP) (Ankarcrona et al., 1995; Nieminen et al., 1996; Schinder et al., 1996; White and Reynolds, 1996; Vergun et al., 1999; Budd et al., 2000). Although a loss of $\Delta\Psi_m$ may be linked to various inducers of cell death, these are observed as large and possibly catastrophic changes in mitochondrial function.

Mitochondria under physiological conditions also play active roles in the maintenance of normal cellular functioning. A key feature of mitochondria that allows them to participate in cell survival is proton pumping across the impermeable inner membrane. This generates an electrochemical gradient, composed of $\Delta\Psi_m$ and ΔpH, which is used for ATP synthesis, ADP–ATP exchange, uptake of respiratory substrates and inorganic phosphate, transport of K^+, Na^+, and anions to regulate volume, and regulation of protons to control heat production (for review, see Bernardi, 1999). Mitochondria also play protective roles by buffering cells against high concentrations of calcium (Budd and Nicholls, 1996; White and Reynolds, 1997; Stout et al., 1998) and sequestering proapoptotic agents, such as cytochrome c (for review, see Green and Reed, 1998; Desagher and Martinou, 2000). Compared with the catastrophic changes in acute injury states, healthy mitochondria may exhibit smaller functional changes in ion transport, ATP production or consumption, volume, and permeability, all of which may impact $\Delta\Psi_m$, to optimize the balance between the need for respiration and ATP synthesis and the production of free radicals (Nicholls and Budd, 2000). In the present experiments, the physiological activity of mitochondria has been assessed using $\Delta\Psi_m$-sensitive fluorescent dyes. These dyes exhibit exceptional sensitivity to small changes in $\Delta\Psi_m$ (Ward et al., 2000) and offer the opportunity to study subtle activities inherent in mitochondria.

Several laboratories have reported fluctuations in $\Delta\Psi_m$ in isolated mitochondria (Ichas et al., 1997; Huser and Blatter, 1999), cardiomyocytes (Duchen et al., 1998), neuroblastoma (Loew et al., 1994; Fall and Bennett, 1999), vascular endothelial (Huser and Blatter, 1999), and pancreatic B-cells (Krippeit-Drews et al., 2000). We report here that spontaneous, low-amplitude changes in the $\Delta\Psi_m$ occur in neuronal mitochondria. The widespread occurrence of these spontaneous fluctuations have prompted us to hypothesize that mitochondria exhibit partial, transient depolarizations that represent an inherent physiological function of mitochondria thus far undescribed in neurons. A significant role for the functional state of mitochondria in these fluctuations in $\Delta\Psi_m$ is discussed.

MATERIALS AND METHODS

Cell culture

All procedures were in strict accordance with the *NIH Guide for the Care and Use of Laboratory Animals* and were approved by the Institutional Animal Care and Use Committee of the University of Pittsburgh. Primary forebrain neurons were prepared as described previously (White and Reynolds, 1995). Briefly, forebrains from embryonic day 17 Sprague Dawley rats were removed and dissociated. Cells were plated on poly-D-lysine-coated 31 mm glass coverslips at a density of 450,000 per

Received March 8, 2001; revised April 25, 2001; accepted April 30, 2001.

This work was supported by United States Army Medical Research and Materiel Command Grant DAMD-17-98-1-8627 (I.J.R.), the Scaife Family Foundation (I.J.R.), and National Institutes of Health Grants T32NS07391 (J.F.B.) and F32NS11147 (J.F.B.). We thank Jacques Brocard, Gareth Dewalt, Kirk Dineley, and Yong Yun Han for their assistance in data collection and analysis.

Correspondence should be addressed to Dr. Ian J. Reynolds, Department of Pharmacology, University of Pittsburgh, W1351 Biomedical Sciences Tower, Pittsburgh, PA 15261. E-mail: iannmda+@pitt.edu.

milliliter (1.5 ml/coverslip) and inverted after 24 hr to decrease glial growth. Experiments were performed when cells were 12–14 d in culture.

Solutions

Coverslips were perfused with HBSS containing (in mM): 137 NaCl, 5 KCl, 10 $NaHCO_3$, 20 HEPES, 5.5 glucose, 0.6 KH_2PO_4, 0.6 Na_2HPO_4, 1.4 $CaCl_2$, and 0.9 $MgSO_4$, pH adjusted to 7.4 with NaOH. (+)-5-Methyl-10,11-dihydro-5H-dibenzo [a,d] cyclohepten-5,10-imine maleate (MK-801) (10 mM stock in dH_2O) was purchased from Research Biochemicals (Natick, MA), cyclosporin A (20 mM stock in methanol) from Calbiochem (San Diego, CA), kainic acid (10 mM stock in dH_2O), oligomycin (10 mM stock in ethanol), and *p*-(trifluoromethoxy)phenylhydrazone (FCCP) (750 μM in methanol) from Sigma (St. Louis, MO), and tetrodotoxin (TTX) (200 mM stock in dH_2O) from Alomone Labs (Jerusalem, Israel). Tetramethylrhodamine methyl ester (TMRM) and 5,5′,6,6′-tetrachloro-1,1′,3,3′-tetraethylbenzimidazolocarbocyanine iodide (JC-1) were purchased from Molecular Probes (Eugene, OR).

Fluorescence imaging

Coverslips were mounted on a BX50WI Olympus Optical (Tokyo, Japan) light microscope fitted with an Olympus Optical LUMPlanFI 60× water immersion quartz objective. All recordings were made at room temperature while cells were perfused with 10 ml/min HBSS (alone or containing various drugs, as described below). Imaging was performed using a 75 W xenon lamp-based monochromator light source (T.I.L.L. Photonics GmbH, Martinsried, Germany), and light was detected using a CCD camera (Orca; Hamamatsu, Shizouka, Japan). Data acquisition was controlled using Simple PCI software (Compix, Cranberry, PA). For JC-1 (see below), cells were illuminated with a 485 ± 12 nm light (incident light is attenuated with neutral density filters; Omega Optical, Brattleboro, VT), and emitted fluorescence was passed through 500 nm long-pass dichroic mirror. The aggregate signal was obtained using a 605/55 nm filter, and the monomer signal was collected using a 535/25 nm filter. For TMRM (see below), cells were illuminated with a 550 ± 12 nm light, emitted fluorescence was passed through a 570 nm long-pass dichroic mirror, and the single emission signal was obtained using a 605/55 nm filter. An image was collected every 5 sec for the duration of the 10 min experiment.

JC-1. Coverslips were incubated for 20 min at 37°C with a 3 μM JC-1 and then rinsed in HBSS for 15 min at room temperature. Coverslips were mounted on the microscope and perfused with HBSS. A region of cell processes (adjacent to healthy cell bodies) was chosen, and a differential interference contrast image of this field was digitally captured. Mitochondria within neuronal processes, but not cell bodies, were used in these analyses because the dimensions of these processes are such that the movement of mitochondria is constrained to the *x–y* plane (no *z*-plane depth) and mitochondrial movement is readily observable.

The length of time cells were illuminated was minimized and kept constant across coverslips. The coverslip was briefly illuminated with 485 nm light, an image of the aggregate signal was captured, and the monomer signal was focused. The coverslip was then left unilluminated for 3 min while the dye reequilibrated (after light exposure). For post-treated coverslips, basal fluorescence was recorded for 4 min, followed by a 5 min drug exposure and a 1 min recovery. Data were collected from neurons from at least four separate culture dates (except for BAPTA experiments, in which two culture dates were tested).

TMRM. Optimal conditions for TMRM were observed when cells were loaded for 30 min with 200 nM TMRM in HBSS and perfused with 20 nM TMRM during the experiment. At this concentration of TMRM, the dye that accumulates in the mitochondria becomes quenched and a depolarization leads to an increase in fluorescence (Ward et al., 2000). The TMRM experiments were identical to those with JC-1, except that cells were not exposed to light before the initiation of the experiment because TMRM does not appear to reequilibrate after light exposure as JC-1 does.

Data analysis

A 640 × 512 pixel field of neuronal processes was imaged, and a "mask" that identified regions of interest (ROIs) that correlated with the expected number, appearance, and distribution of mitochondria within these neuronal processes was generated. The mask was made using a single JC-1 aggregate image taken before the initiation of the monomer imaging or from a stacking of TMRM images. The mask isolated individual spots of fluorescence that had a fluorescence intensity indicative of physiological $\Delta\Psi_m$ and were more than eight contiguous pixels. Cell bodies present in the imaged field were excluded from the mask to prevent analysis of mitochondrial clusters often observed within these regions. Using the fluorescence images from these dyes, ~1000 ROIs per field were detected. The ROIs generated from the punctate JC-1 aggregate signal were transferred onto the diffuse JC-1 monomer signal, and the fluorescence intensity within each individual ROI was analyzed over time. TMRM, unlike JC-1, is a single wavelength dye that has nonfluorescent, quenching aggregates. Thus, to locate mitochondria, fluorescent images collected during the 10 min experiment were stacked, and a mask was generated based on the brightest spots of fluorescence. ROIs were further qualified based on size, as they were with JC-1 (more than eight pixels, not within cell bodies).

The differences in the techniques used to identify mitochondria with JC-1 and TMRM were useful in determining whether mitochondrial motility was a significant factor in the assessment of $\Delta\Psi_m$ fluctuations. With JC-1, mitochondrial location was identified only at the onset of the experiment, a percentage of mitochondria moved during the experiment (for review, see Overly et al., 1996), and a decrease in the number of $\Delta\Psi_m$ fluctuations was observed. This decrease was at least partially attributable to mitochondria moving out of the defined ROI. Using an image-stacking procedure to identify mitochondria in TMRM-loaded cells, the number of mitochondria was overestimated because the same mitochondrion could be identified at more than one location. With TMRM, we corrected for mitochondrial motility (there was no decrease in the number of fluctuations) but, in turn, underestimated the number of fluctuations occurring per 1000 ROIs. By using both dyes, we were thus able to determine the overall pattern of spontaneous $\Delta\Psi_m$ fluctuations.

The fluorescence intensity data from each ROI were analyzed separately, allowing us to determine $\Delta\Psi_m$ in individual mitochondria within cultured neuronal processes and measure changes in that $\Delta\Psi_m$ over the course of 10 min. Several mathematical criteria were set to detect the spontaneous fluctuations in mitochondrial fluorescence intensity. The first criterion was set to determine whether the changes in the raw fluorescence values exceeded basal fluctuations. Preliminary data suggested that inherent variability within the system accounted for fluorescent fluctuations of 4 units or less. Therefore, the first criterion was that changes in raw fluorescence between two sequential images (taken 5 sec apart) were >4 fluorescent units. The second criterion for detection of a spontaneous $\Delta\Psi_m$ fluctuation was that the slope of the fluorescence change had to be >0.3 fluorescent units per second for both the rise and fall of the fluctuation. The slope was determined using a moving average of three sequential images. This criterion was set to distinguish fluctuations from changes in basal fluorescence attributable to photo-oxidation, focus drifts, debris in the field temporarily impeding fluorescence detection, or other spurious changes in signal. Using these two criteria, preliminary analysis showed substantial correspondence between the observation of changes in fluorescence (on the computer screen) and the statistical detection of a spontaneous $\Delta\Psi_m$ fluctuation.

The number of a spontaneous $\Delta\Psi_m$ fluctuation detected in a field of neuronal processes was determined and normalized as the number of spontaneous $\Delta\Psi_m$ fluctuations occurring per minute per 1000 ROIs. Data were graphed as either the percentage of fluctuations in a drug-treated field versus an untreated control field (for pretreatment experiments) or as a ratio of the number of spontaneous $\Delta\Psi_m$ fluctuations per minute per 1000 ROIs before versus after drug treatment (for post-treatment experiments). Presentation of a ratio was chosen because, as a result of mitochondrial motility, all JC-1-loaded neuronal fields analyzed showed a decreasing number of fluctuations with time. For the post-treatment experiments, the number of fluctuations occurring per minute per 1000 ROIs was counted, and the average of minutes 2–4 (baseline) and minutes 6–8 (treatment) were calculated. This corrected for any instability in the baseline at the onset of the experiment and allowed treatment effects to stabilize for 2 min before analysis. Data from controls and individual drug treatments were averaged across coverslip and culture date and statistically compared using a *t* test or ANOVA.

To distinguish between long-term, global mitochondrial depolarizations and the spontaneous, small-amplitude fluctuations in $\Delta\Psi_m$, the average fluorescence intensity in all mitochondria in a field of neurons was calculated. This enabled us to determine whether there was an association between average $\Delta\Psi_m$ and the occurrence of spontaneous fluctuations. Average fluorescence intensity (in arbitrary units) is presented for all pharmacological experiments.

RESULTS

Under physiological conditions, mitochondria located within cultured neuronal processes exhibit a great deal of spontaneous activity, including repetitive, small-amplitude depolarizations. Our previous measurements of $\Delta\Psi_m$ were limited in both spatial and temporal resolution (White and Reynolds, 1996; Scanlon and Reynolds, 1998), and thus these phenomena were undetected. Using the wide-field imaging system described here, we captured images at 0.2 Hz with resolution adequate to monitor signals from neuronal processes. Replaying these images at a rate of 6 Hz revealed some unappreciated dynamics in the dye signal. Mitochondria traverse several tens of micrometers and, more surprisingly, exhibit extensive spontaneous alterations in dye signal consistent with depolarization of $\Delta\Psi_m$ over the period of the experiment. With real-time imaging (0.2 Hz), fluctuations in $\Delta\Psi_m$ could occasionally be observed; however, on playback (6 Hz), this phenomenon was observed throughout the field of neurons during the entirety of the experiment.

Figure 1 illustrates the spontaneous $\Delta\Psi_m$ fluctuations in JC-1-loaded (Fig. 1*A*) and TMRM-loaded (Fig. 1*B*) neurons. This figure shows small regions of fluorescence (*arrowheads*) within untreated neuronal processes that appear to be spontaneously increasing and decreasing in intensity. We were unable to determine whether there was a propagation of this signal down a process, although this did not appear to be the case. The fluctuations in fluorescence within individual mitochondria appear independent, and no wave-like activity was noted. Movies of JC-1- and TMRM-loaded neurons illustrating this phenomenon are included in the supplemental data section located in the on-line version of this article. For details of these movies, see the legend for Figure 1.

Measurement of spontaneous $\Delta\Psi_m$ fluctuations

To provide a quantitative analysis of this phenomenon, we developed a technique for identifying individual mitochondria within a field of neuronal cell bodies and processes (Fig. 2). The majority of the data presented were collected using the potentiometric dye JC-1, although qualitatively similar results were obtained with TMRM. JC-1 was preferred for these experiments because its aggregates accumulate within the mitochondria based on $\Delta\Psi_m$ and are fluorescent. This allowed us to use the aggregate fluorescent signal to locate individual mitochondria and the monomer signal to detect changes in $\Delta\Psi_m$. A loss of $\Delta\Psi_m$ results in an increase in JC-1 monomer fluorescence in the regions in and around the mitochondria.

A differential interference contrast image was taken (Fig. 2*A*), followed by a single fluorescent image of the JC-1 aggregate signal (Fig. 2*B*). We then isolated each individual fluorescent area and identified it as an ROI depicting what is likely to be a single mitochondrion (Fig. 2*C*). Because of the thickness of the cell bodies and the wide-field microscopy used, it was difficult to distinguish individual mitochondria within the soma. This is evidenced by the large regions of aggregate fluorescence present in the cell body (*arrowhead*), most likely resulting from numerous mitochondria overlapping in the *z*-axis. These large regions of fluorescence, most typically seen in cell bodies, were excluded from analysis based on size. The mask containing the ROIs (Fig. 2*C*) was overlaid onto the JC-1 monomer signal (Fig. 2*D*), and the fluorescence intensity from each individual ROI was recorded (Fig. 2*E*). This technique allowed us to measure the fluorescence intensity of ~1000 ROIs per field from images collected every 5 sec for 10 min.

A graphical illustration of the spontaneous $\Delta\Psi_m$ fluctuations is presented in Figure 3, *A* and *B*. There appears to be no regularity in amplitude or frequency of the spontaneous depolarizations. Note that the individual mitochondria in each of these graphs (*traces A–D*) exhibit numerous spontaneous depolarizations and repolarizations over the course of the experiments, with the overall basal fluorescence intensity remaining relatively stable. However, not all mitochondria exhibit spontaneous fluctuations (*trace E* on both graphs). Over 35,000 mitochondria from untreated cells were assessed for spontaneous $\Delta\Psi_m$ fluctuations in these experiments. The percentage of mitochondria that exhibit at least one $\Delta\Psi_m$ fluctuation was calculated from ~15,600 mitochondria in JC-1-loaded control fields, and 55% of these mitochondria were inherently active.

From Figure 3, it is evident that the fluctuations appear different in JC-1- and TMRM-loaded mitochondria. The $\Delta\Psi_m$ fluctuations appear slower in JC-1-loaded neurons, probably because of the differences in the properties of the dyes. TMRM equilibrates faster across membranes, and thus the fluctuations appear more rapid. This difference in the rate of reequilibration of these dyes thus results in the same phenomenon having a somewhat different appearance, depending on the dye used (Nicholls and Ward, 2000).

JC-1- and TMRM-loaded mitochondria can also be distinguished by the fluctuation frequency, which appears to decrease over time with JC-1 but remain stable or increase with TMRM (Fig. 3*C*). This may be explained by the rapid distribution of TMRM across membranes, which necessitated the addition of TMRM into the perfusate to maintain the level of fluorescence within the neurons (Fig. 3*B*, note the stability of the basal fluorescence within the ROIs). In contrast, JC-1 was not included in the perfusate, making it likely that there is only a partial reaggregation of the dye during repolarization, with some dye diffusing out of the cell. This could lead to a decrease in JC-1 aggregate fluorescence, which could imply less monomer release until eventually the magnitude of the increase in monomer fluorescence would fall below the criterion needed to indicate a fluctuation. This explanation however seems unlikely because, when JC-1 aggregate fluorescence in neurons was decreased by high-light exposure, depolarization could still be observed as a rise in monomer fluorescence (data not shown).

Another factor that may impact the number of fluctuations is that a percentage of mitochondria are known to be motile within neurons (Overly et al., 1996). In fact, we note that a fraction of the mitochondria move throughout the processes of our cultured neurons, regardless of which dye we used. With JC-1, mitochondria were located and ROIs identified only at the onset of the experiment, using the JC-1 aggregate signal. Thus, over time, the regions being analyzed may no longer correlate with the regions exhibiting the changes in fluorescence (i.e., a mitochondrion may move out of the defined ROI). TMRM-loaded mitochondria were located using image stacking; thus, when a mitochondrion moves, each location may be associated with an independent ROI. This would suggest that TMRM overestimates the number of ROIs and thus underestimates the number of fluctuations per 1000 ROIs. These technical differences can explain why TMRM-loaded mitochondria appear more active than JC-1-loaded mitochondria, a fact that is not reflected in the average number of fluctuations reported in Figure 3*C*. In addition, they suggest that the percentage of mitochondria that move is stable because the decrease in fluctuations observed with JC-1 is very consistent. It is important to note, however, that regardless of the cause, we have corrected for this loss of fluctuation detection in subsequent

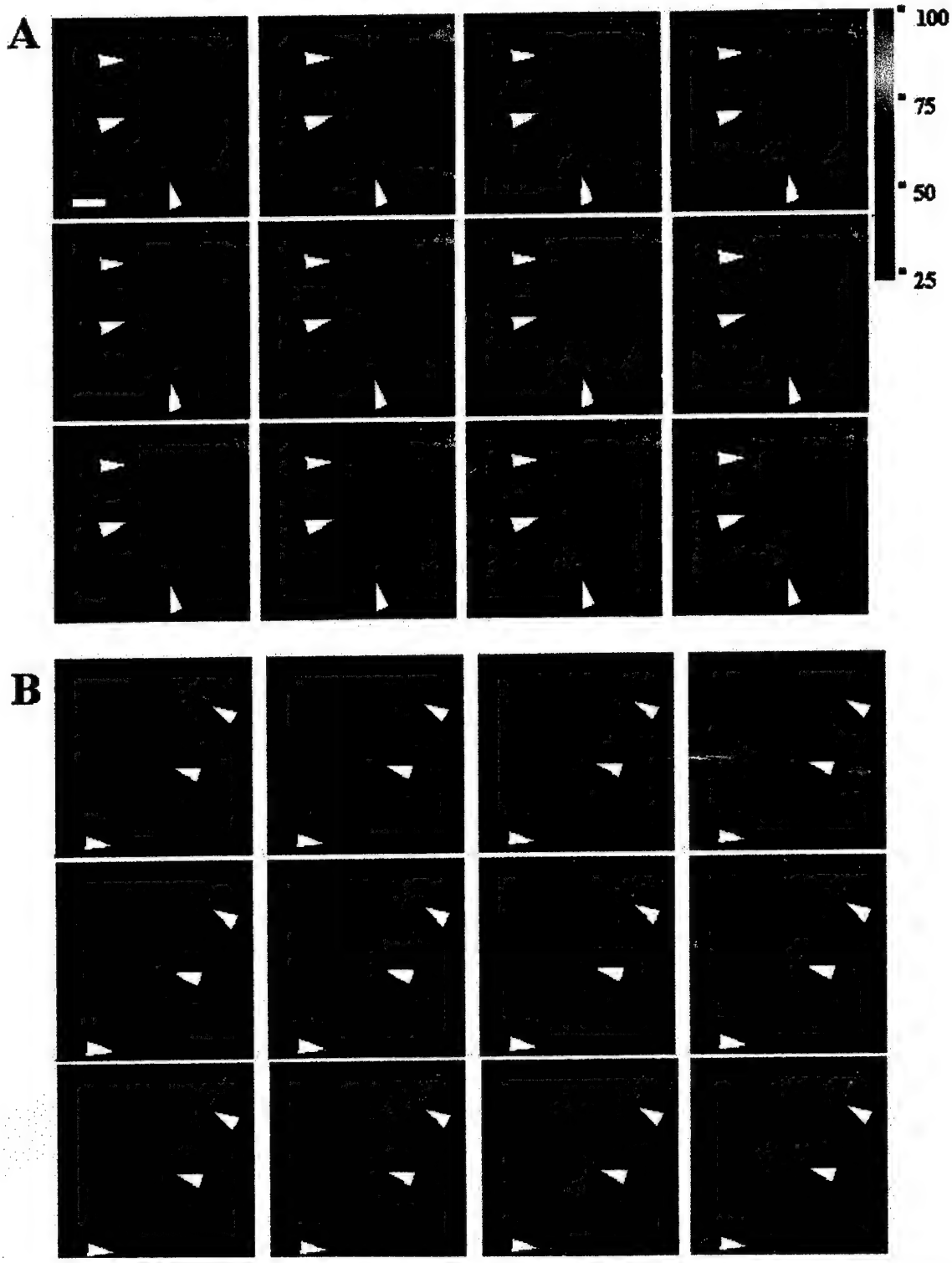

Figure 1. Representative fluorescent images of $\Delta\Psi_m$ fluctuations. *A*, JC-1-loaded neuronal processes. *B*, TMRM-loaded processes. These *panels* show spontaneous changes in fluorescent intensity occurring in small regions of neuronal processes. Images show a 200 × 200 pixel field. Images were taken 30 sec apart. *Arrowheads* identify examples of regions of fluorescence that correspond to the expected size and shape of neuronal mitochondria and show readily observed fluctuations in intensity. Increases in fluorescence imply depolarization. TMRM-loaded cells have lower basal fluorescence because light levels were kept low to avoid light-induced increase in fluorescence. Scale bar, 10 μM. Movie files corresponding to JC-1-loaded (*A*) and TMRM-loaded (*B*) neurons have been included in the supplemental data section located in the on-line version of this article. Movie images were taken 5 sec apart, and time is shown in minutes and seconds. Both spontaneous fluctuations and dye intensity and mitochondrial motility are evident.

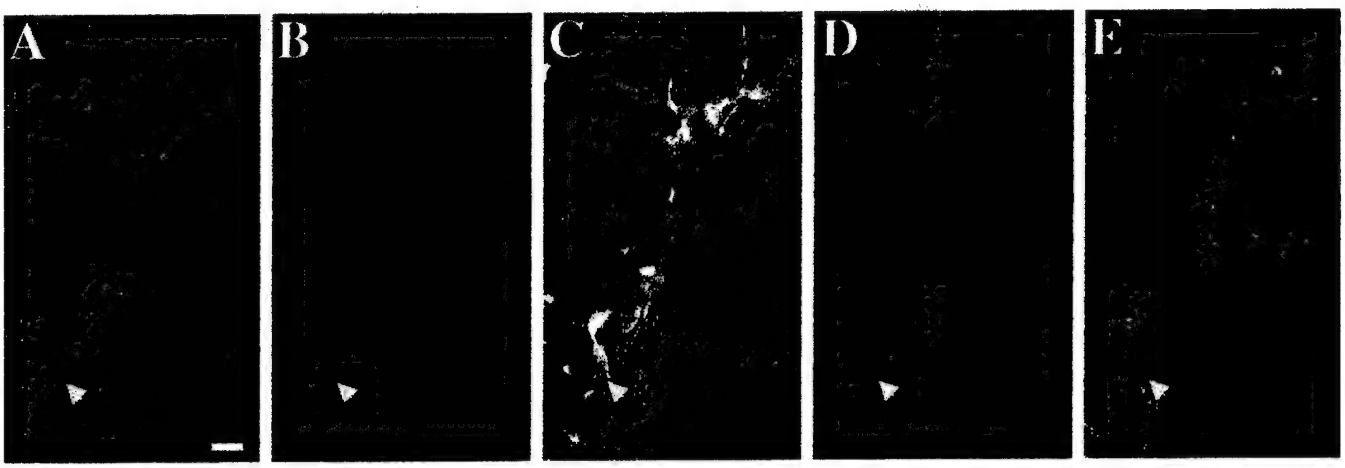

Figure 2. Imaging technique used to measure spontaneous changes in mitochondrial membrane potential using JC-1. *A*, Bright-field image, using differential interference contrast. The *arrow* shows a healthy neuronal cell body with processes within a field of neurites. *B–E* represent fluorescent images from this same field. *B*, The JC-1 aggregate image. Note the punctate nature of the label within the processes. *C*, The mask (*red*) created to discern ROIs thought to correspond to mitochondria. The bright fluorescent spots observed with the JC-1 aggregate image (same as *B*, now *white*) are detected using image analysis software based on size criteria. Regions uniformly labeled (e.g., cell bodies) are excluded from the mask based on size. *D*, The JC-1 monomer image. Note the diffuse nature of the label within the processes. *E*, The "overlay." The mask generated in *C* (*red*) is overlaid onto the JC-1 monomer image from *D* (*green*). Scale bar, 20 μM.

pharmacological experiments by analyzing only the ratio of spontaneous $\Delta\Psi_m$ fluctuations at the beginning versus end of the experiment.

It was important to rule out nonphysiological influences on the fluctuations in $\Delta\Psi_m$. Fluorescence imaging of organelles as small as mitochondria requires careful maintenance of the correct focal plane. Drifts in focus could lead to the appearance and/or disappearance of $\Delta\Psi_m$ fluctuations. To minimize inclusion of focus changes in our quantitation of $\Delta\Psi_m$ fluctuations, we used a moving average paradigm to smooth out brief irregularities in whole-field fluorescence (see Materials and Methods). However, because the cells were also being perfused throughout the experiment, it was possible that smaller regions of the field were drifting in and out of focus, thus leading to the graphical appearance of fluctuations. To show that the $\Delta\Psi_m$ fluctuations were not attributable to focus drift, we identified three adjacent mitochondria located within a single neuronal process and analyzed them for spontaneous $\Delta\Psi_m$ fluctuations (Fig. 4). If the $\Delta\Psi_m$ fluctuations were the result of drifts in focus, then mitochondria in close proximity to one another should all exhibit simultaneous fluctuations. This was not observed. Three neighboring ROIs were identified using the JC-1 aggregate signal (Fig. 4*A*, *red*), and the fluorescence intensity of JC-1 monomer signal (Fig. 4*A*, *green*) within each ROI was determined. As the monomer signal increases (indicating depolarization), the ROIs appear increasingly *yellow* (Fig. 4*A*) and an increase in fluorescence intensity is observed graphically (Fig. 4*B*). The fluctuations in fluorescence intensity observed qualitatively and quantitatively appear to correspond, with no evidence of changes in focus in any of the ROIs. Moreover, two mitochondria demonstrate fluctuations (ROIs 1 and 3), whereas the ROI in the middle does not (ROI 2). This strongly argues against a drift in focus or movement of the process as the underlying mechanism of this phenomenon.

Illumination of mitochondria loaded with cationic fluorescence dyes has been reported to lead to the generation of reactive oxygen species (ROS) and thus mitochondrial damage (Bunting, 1992). Photo damage to the mitochondria could therefore be a potential cause of the observed fluctuations in $\Delta\Psi_m$. Typically, during imaging, neurons were exposed to attenuated fluorescent light (5% transmitted light) for ~0.1 sec every 5 sec over the course of a 10 min experiment. To determine the relative contribution of light, we took JC-1-loaded neurons and exposed a portion of the field to a brief, intense light. For our high-light conditions, we maintained the exposure time of 0.1 sec (per 5 sec) but increased transmitted light to 100%. In these experiments, JC-1-loaded neuronal processes were imaged under standard conditions for 50 frames (one frame per 5 sec). The microscope aperture size was then decreased so that light exposure was limited to the center of the neuronal field and the processes in this central region were illuminated, for 20 frames (one frame per 5 sec), with a 20-fold higher light intensity. Light conditions were then returned to normal. We separated the imaged field into the exposed center region (illuminated under high-light conditions) and the peripheral, control region (unilluminated for the same 20 frames). The ratio of fluctuations occurring before versus after intense light exposure were compared across the control and exposed regions. The region exposed to high-light conditions showed significantly fewer spontaneous $\Delta\Psi_m$ fluctuations (Fig. 5*A*), without a concurrent change in average fluorescence intensity (Fig. 5*B*). Thus, photo damage cannot account for the observation of these phenomena; in fact, these data suggest that light exposure can lead to the loss of $\Delta\Psi_m$ fluctuations, potentially through a photo-induced oxidant burden.

Pharmacological analysis of spontaneous $\Delta\Psi_m$ fluctuations

Having established methods to measure spontaneous fluctuations in fluorescence intensity in JC-1-loaded mitochondria in untreated neurons, we explored mechanisms underlying this phenomenon. We first tested the possibility that the $\Delta\Psi_m$ fluctuations were the result of synaptic activity and thus were reflecting plasma membrane potential changes or calcium influx. Neurons were treated with TTX (200 nM), a sodium channel blocker, to inhibit spontaneous synaptic activity. We also tested an NMDA receptor antagonist, MK-801 (10 μM), to block a major route of calcium entry. JC-1-loaded neurons were perfused with HBSS for

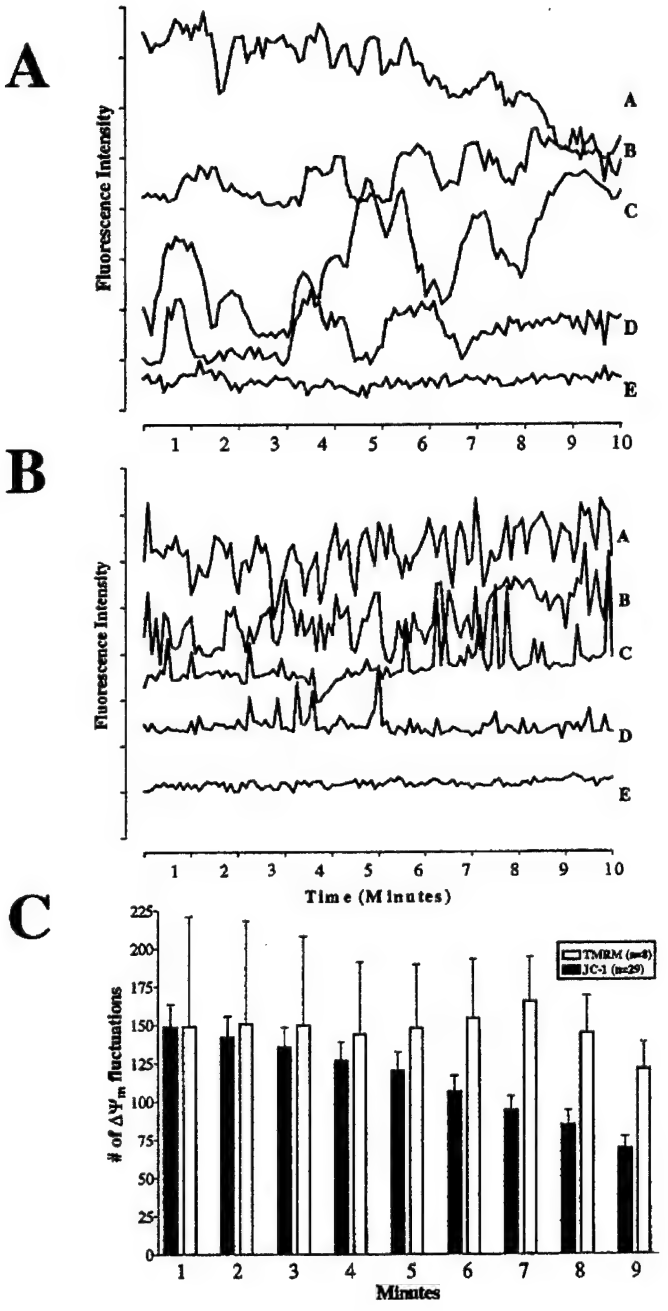

Figure 3. Quantification of $\Delta\Psi_m$ fluctuations within individual mitochondria. *A*, JC-1 monomer traces. *B*, TMRM fluorescence traces. Each *trace* represents in a single ROI corresponding to an individual mitochondrion. An increase in fluorescence is associated with depolarization. Note that the basal fluorescence in both graphs remains stable and that fluctuations are not all of the same magnitude or of regular frequency. Approximately 1000 such traces were collected per field. The *y*-axis represents arbitrary fluorescence units, with each *tick mark* equaling 10 units. *Traces* have been offset from one another for display purposes. *A*, *Trace* A shows a mitochondrion that fluctuates repeatedly followed by a loss of fluorescence, most likely indicating the movement of the mitochondrion out of the ROI. *Trace* B shows a mitochondrion that fluctuates especially as the experiment continues. *Trace* C shows large fluctuations and then a slow increase in fluorescence suggesting a gradual depolarization. *Trace* D initially exhibits fluctuations, but by 7 min activity ceases. *B*, *Traces* A and B show mitochondria that fluctuate repeatedly throughout the experiment. *Trace* C shows a mitochondrion that fluctuates especially as the experiment continues. *Trace* D initially has fluctuations, but by 5 min activity ceases. *Trace* E from both figures shows background noise in the system and reflects mitochondria that do not exhibit spontaneous fluctuations. *C*, Average number of spontaneous $\Delta\Psi_m$ fluctuations in JC-1- or TMRM-loaded neurons from *traces* such as those presented in *A* and *B*. Criteria for a spontaneous fluctuation in $\Delta\Psi_m$ were set a priori: fluorescence changes >4 fluorescent units and a slope >0.3 fluorescent units per second. The number of $\Delta\Psi_m$ fluctuations that occurred per minute per 1000 ROIs is presented. A decrease in the number of $\Delta\Psi_m$ fluctuations over time was observed in JC-1-loaded, but not in TMRM-loaded, neurons (see Results). Data are presented as means ± SEM. The number of fields (*n*) imaged (~1000 ROIs per field) is presented in the key.

4 min to establish basal activity. Neurons were then exposed to the inhibitors for 5 min. The ratio of fluctuations occurring before versus those occurring after drug treatment was graphed to correct for the decrease in the number of fluctuations that occurs even in untreated control mitochondria (Fig. 3*C*). There was no difference in the ratio of fluctuations between control mitochondria and those treated with TTX or MK-801 (Fig. 6*A*). These treatments did not alter the average fluorescence intensity of the JC-1 monomer signal within the mitochondria (Fig. 6*B*). This suggests that drugs that inhibit plasma membrane activities do not inhibit spontaneous fluctuations or change the resting level of $\Delta\Psi_m$.

There are several additional routes of calcium entry beyond NMDA receptor activation. Mitochondria are intricately involved in shaping calcium dynamics (Duchen, 1999), and calcium has also been suggested to regulate $\Delta\Psi_m$ fluctuation in other cells (Loew et al., 1994; Ichas et al., 1997; Duchen, 1999; Krippeit-Drews et al., 2000). BAPTA, an intracellular calcium chelator, interrupts calcium-mediated events that result from calcium influx and release from intracellular stores. Because of the close apposition of mitochondria to endoplasmic reticulum, release of calcium from the reticular stores can alter mitochondrial function by creating microdomains of high calcium (Rizzuto et al., 1993, 1998; Hajnoczky et al., 1995). Thus, any involvement of calcium-mediated activity in the observed spontaneous mitochondrial depolarizations should become evident with BAPTA treatment. Neurons were preincubated with BAPTA-AM (50 μM) showed a dramatic decrease in the number of spontaneous fluctuations compared with controls (Fig. 7*A*). However, this BAPTA-induced inhibition was associated with a dramatic rise in fluorescence intensity (Fig. 7*B*). This implies that BAPTA-AM, at this concentration, leads to mitochondrial depolarization. The mechanism by which this occurs is unclear and cannot necessarily be attributed to calcium chelation. Respiratory complex inhibitors and the uncoupler FCCP depolarized $\Delta\Psi_m$ and decreased the number of spontaneous fluctuations (data not shown). This raises the possibility that the effects of BAPTA are attributable to general mitochondrial depolarization, which occludes the smaller fluctuations rather than a result of modifying intrinsic calcium changes.

Activity of the respiratory chain complexes leads to the extrusion of protons from the mitochondrial matrix, whereas synthesis of ATP through the F_1F_O ATPase (ATP synthase) is driven by proton reentry. Thus, whereas inhibition at the respiratory chain complexes may lead to a slow loss of $\Delta\Psi_m$, inhibition at the ATP synthase should lead to a subtle hyperpolarization in healthy, ATP-generating mitochondria and a depolarization in damaged, ATP-consuming mitochondria (Scott and Nicholls, 1980; Nicholls and Ward, 2000). Neurons pretreated with oligomycin (15 min) showed a significant decrease in the number of spontaneous $\Delta\Psi_m$ fluctuations compared with untreated control mitochondria (Fig. 8*A*) but no significant change in initial basal fluorescence (Fig. 8*B*). Because it is unlikely that all mitochondria within a field of

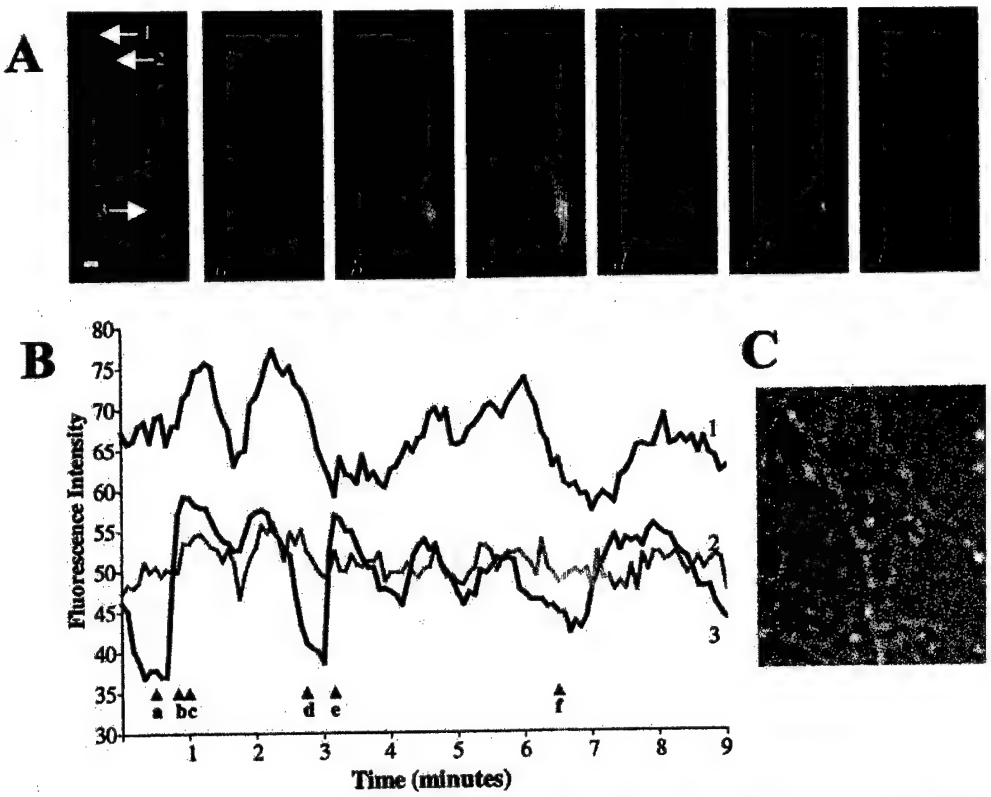

Figure 4. $\Delta\Psi_m$ fluctuations are not attributable to focus drift. Three individual ROIs located within a single neuronal process analyzed for spontaneous $\Delta\Psi_m$ fluctuations. *A*, In this series of images, the JC-1 aggregate signal (*red*, depicting individual ROIs) has been overlaid on the corresponding JC-1 monomer (*green*) images (as shown in Fig. 2*E*). The first image in this series identifies three mitochondria at the onset of imaging (*arrows*). The *numbers* associated with each mitochondrion correspond to the *traces* in *B*. In images *a–f*, a static aggregate (*red*) image has been used; thus, changes in the ratio of *green* to *red* represent changes in JC-1 monomer fluorescence. (i.e., when mitochondria appear *yellow*, monomer signal has increased, suggesting depolarization). Note that fluctuations in JC-1 monomer fluorescence intensity can be observed qualitatively over time. *B*, Fluorescence intensity of the JC-1 monomer signal within each of the three ROIs identified in *A* was quantified (*arrowheads a–f* show the time points when the images in *A* were taken). Note that *traces 1* and *3* show significant fluctuations in fluorescence intensity, but *trace 2* does not. This illustrates that changes in fluorescence intensity are not simply attributable to a drift in focus or movement of the process. If this were the case, then all three mitochondria within this process should exhibit similar $\Delta\Psi_m$ fluctuations. *C*, A differential interference contrast image showing the neuronal process from which the fluorescent images were taken. The *arrows* correspond to the ROIs analyzed. Scale bar, 5 μM.

neurons are of equivalent membrane potential and ATP synthase activity and ~1000 mitochondria were averaged per field, small changes in overall fluorescence intensity were not detected.

The PTP is thought to regulate matrix Ca^{2+}, pH, $\Delta\Psi_m$, and volume (Susin et al., 1998). Its opening is triggered by a wide variety of treatments, including increased Ca^{2+} (Zoratti and Szabo, 1995), and is inhibited by cyclosporin A (Crompton et al., 1988). Two open states for this pore have been proposed, with the low-conductance state causing transient openings that aid in stabilizing $\Delta\Psi_m$ and volume (Ichas et al., 1997) and the high-conductance state involved in irreversible openings, complete dissipation of the $\Delta\Psi_m$, extensive swelling, and cell death (Petit et al., 1996; Susin et al., 1997). Transient depolarizations in $\Delta\Psi_m$ have been reported to coincide with activation of the low-conductance state of the PTP in isolated mitochondria, which could represent a physiological process necessary for regulating $\Delta\Psi_m$ (Ichas et al., 1997) and limiting the generation of ROS in hyperpolarized mitochondria (Skulachev, 1996). We tested whether cyclosporin A influenced the frequency of the $\Delta\Psi_m$ fluctuations in our cultured neurons. No effect was observed at any concentration tested (Fig. 9*A*); however, cyclosporin A caused a modest decrease in fluorescence intensity at lower concentrations (Fig. 9*B*).

Taxing neurons by increasing synaptic activity may lead to an increase in mitochondrial activity. Stimulation of neurons by high concentrations of glutamate causes large calcium fluxes that directly influence mitochondrial function (White and Reynolds, 1995) and have been proposed to increase ATP demand by the plasma membrane ATPases. Although inhibition of basal synaptic activity with a sodium channel blocker or a glutamate receptor antagonist did not alter the frequency of $\Delta\Psi_m$ fluctuations (Fig. 6*A*), we tested whether increasing synaptic activity, and presumably increasing the demand placed on the mitochondria, would alter the frequency of fluctuations. Treatment with glutamate in the presence of extracellular calcium leads to an increase in fluorescence intensity in a similar manner to that observed with BAPTA-AM. In fact, stimulation with glutamate is known to cause mitochondrial calcium influx and depolarization (Ankarcrona et al., 1995; White and Reynolds, 1996). We attempted to circumvent the problem of the superimposition of the catastrophic depolarization on the smaller spontaneous changes using two approaches. First, we treated neurons with kainic acid, an agonist of the AMPA–kainate subtype of glutamate receptors. Activation of glutamate receptors with kainic acid results in increased intracellular sodium and calcium but does not lead to mitochondrial depolarization (Courtney et al., 1995, Hoyt et al., 1998). Accumulation of calcium within mitochondria is also significantly lower using kainic acid than it is with NMDA (Budd and Nicholls, 1996; Stout et al., 1998). Therefore, neurons were treated with 100 μM kainic acid for 5 min, in either the presence or absence of calcium, but no evidence of altered $\Delta\Psi_m$ fluctuation frequency (Fig. 10*A*) or overall fluorescence intensity (Fig. 10*B*) was observed.

We then attempted to increase synaptic activity and mitochondrial demand without flooding mitochondria with calcium and depolarizing them by treating neurons with glutamate (in the presence of its coagonist glycine) in buffer that is nominally calcium free. This should lead to the activation of the glutamate receptors without the concurrent increase in intracellular and intramitochondrial calcium concentrations. Receptor activation should, however, lead to an influx of sodium and thus manipulate mitochondrial ion concentrations through sodium-related path-

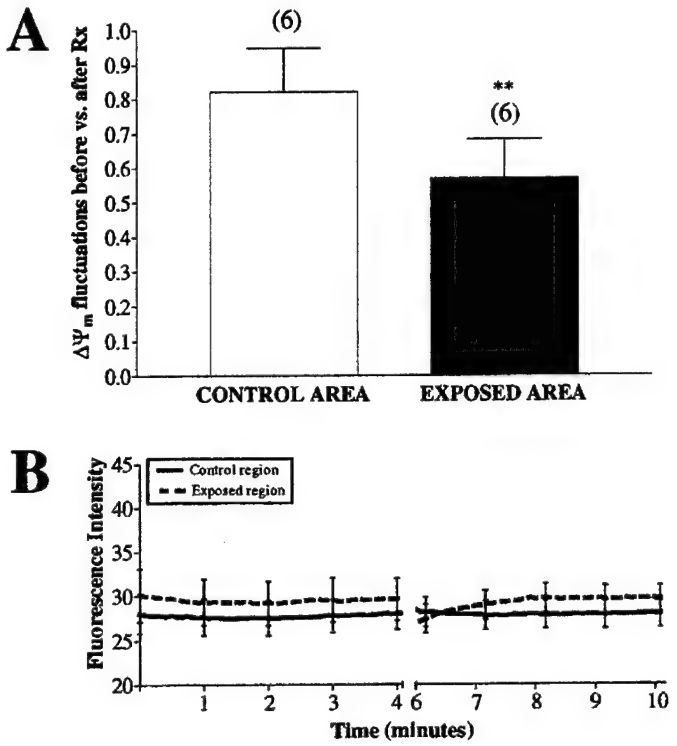

Figure 5. $\Delta\Psi_m$ fluctuations in JC-1-loaded neurons are not caused by light. Untreated neurons were loaded with JC-1 and imaged under our standard light conditions for 50 frames (neutral density attenuating transmitted light to 5%). The aperture on the microscope was then closed to allow light to hit only the center portion of the field, and the cells were imaged for 20 frames. Under this condition, the middle portion of the coverslip was exposed to intense light (100% transmitted light; *EXPOSED AREA*), whereas the periphery of the coverslip was left unexposed (*CONTROL AREA*). The imaging conditions were then returned to the standard conditions from the beginning of the experiment for 50 more frames. *A*, The number of fluctuations in $\Delta\Psi_m$ per minute per 1000 ROIs was determined in the control and exposed regions, and the ratio of fluctuations occurring before versus after intense light exposure are presented (note that the control area received no light during this period). Data are presented as means ± SEM, and the *numbers* above each *bar* equal the number of fields imaged. The region exposed to high-light conditions showed significantly fewer spontaneous $\Delta\Psi_m$ fluctuations (paired *t* test; $t = 3.77$; df = 5; $p < 0.05$). *B*, Average fluorescence intensity of all mitochondria imaged, with representative error bars indicating SEM. Basal fluorescence did not change after light exposure.

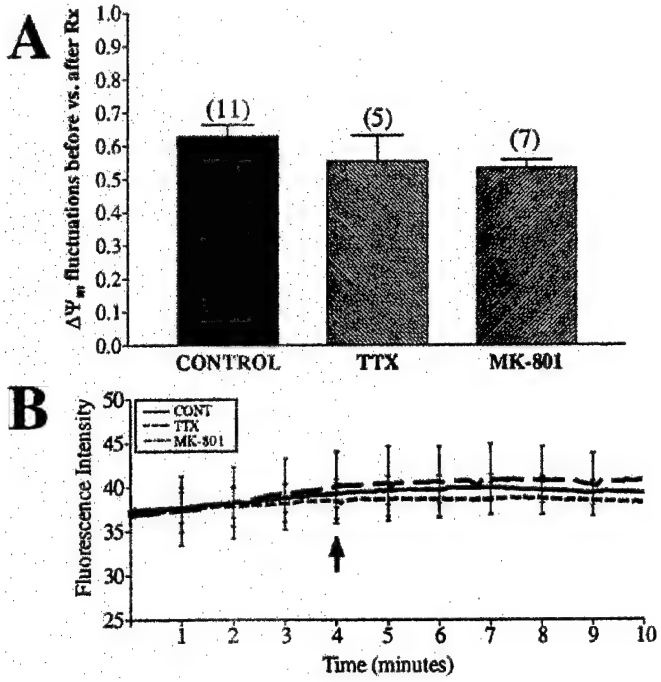

Figure 6. $\Delta\Psi_m$ fluctuations are not attributable to synaptic activity. Untreated neurons were loaded with JC-1 and imaged for 4 min before the addition of drugs (*arrow*). TTX (200 nM) (a Na^+ channel blocker) or 10 μM MK-801 (NMDA antagonist) were perfused over the cells for 5 min, and fluorescence intensity and number of fluctuations per minute per 1000 ROIs were calculated. *A*, The ratio of fluctuations occurring during the baseline to those occurring after drug treatment. This corrected for the consistent decrease in fluctuations observed in untreated mitochondria (see Fig. 3). Data are presented as means ± SEM, and the *numbers* above each *bar* equal the number of fields imaged (~1000 ROIs per field). Neither treatment had a significant impact on $\Delta\Psi_m$ fluctuations (TTX, $t = 1.03$, df = 14, $p > 0.05$; MK-801, $t = 1.98$, df = 16, $p > 0.05$). *B*, Average fluorescence intensity of all mitochondria imaged, with representative error bars indicating SEM. Neither treatment altered basal fluorescence.

ways. JC-1-loaded neurons were treated with 100 μM glutamate and 10 μM glycine in calcium-free buffer for 5 min. This treatment led to a significant decrease in $\Delta\Psi_m$ fluctuations (Fig. 11*A*) without a concomitant rise in fluorescence intensity (Fig. 11*B*). The differences between glutamate and kainate on $\Delta\Psi_m$ fluctuations are not surprising in light of the observation that their ability to activate glutamate receptors is not equivalent qualitatively or quantitatively (Hoyt et al., 1998; Sattler et al., 1998; Brocard et al., 2001).

DISCUSSION

In this study, we report that mitochondria in neuronal cultures display small, spontaneous fluctuations in $\Delta\Psi_m$ and that these fluctuations can be dramatically decreased, without a concurrent change in basal fluorescence, by treatments that alter mitochondrial activity. Although there has been a great deal of recent interest in large-scale changes in mitochondrial function associated with neuronal injury, the present findings reveal a previously unappreciated property of mitochondria in resting, uninjured neurons.

The $\Delta\Psi_m$ is a key marker of mitochondrial function, generated by the pumping of protons across the inner mitochondrial membrane in association with electron transport. In turn, $\Delta\Psi_m$ drives many key mitochondrial functions, including ATP synthesis, calcium accumulation, and maintenance of ion gradients that permit the influx of substrates and egress of metabolic products. Clearly, $\Delta\Psi_m$ has a number of important functions, and thus a variety of activities could account for the spontaneous changes in $\Delta\Psi_m$ reported here. Our observations of $\Delta\Psi_m$ fluctuations could reflect inherent changes in mitochondrial ion transport, ATP production–consumption, respiration, or volume, all of which are essential for proper mitochondrial function. We believe that spontaneous $\Delta\Psi_m$ fluctuations represent a normal physiological feature of neuronal mitochondria such that the presence or absence of these fluctuations may be useful as a novel marker for mitochondrial activity.

The pharmacological approach of using tetrodotoxin or MK-801 clearly excludes alterations in plasma membrane potential and ion fluxes as the basis for the change in the mitochondrial dye signal. However, the mitochondrial mechanism that causes the fluctuations is less clear. Attempts to regulate the permeability transition pore with cyclosporin A had no effect on either $\Delta\Psi_m$ fluctuations or fluorescence intensity, which ostensibly excludes

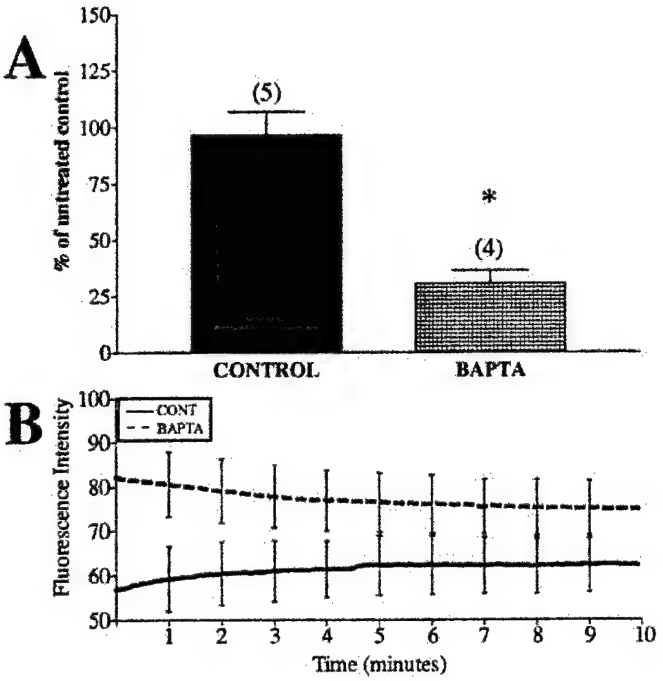

Figure 7. An intracellular calcium chelator alters $\Delta\Psi_m$ fluctuations and basal fluorescence. Neurons loaded with JC-1 were treated with 50 μM BAPTA-AM for 15 min before imaging. The fluorescence intensity and number of fluctuations per minute per 1000 ROIs were calculated. *A*, The percentage of fluctuations occurring in BAPTA-pretreated mitochondria to untreated mitochondria. Data are presented as means ± SEM. *Numbers* above each *bar* equal the number of fields imaged (~1000 ROIs per field). BAPTA decreased $\Delta\Psi_m$ fluctuations ($t = 5.17$; df = 7; $^*p < 0.05$; but see Discussion). *B*, Average fluorescence intensity of all mitochondria imaged, with representative error bars indicating SEM. BAPTA increased the average fluorescence intensity. (Note that the scale is twice that of Figs. 8–10).

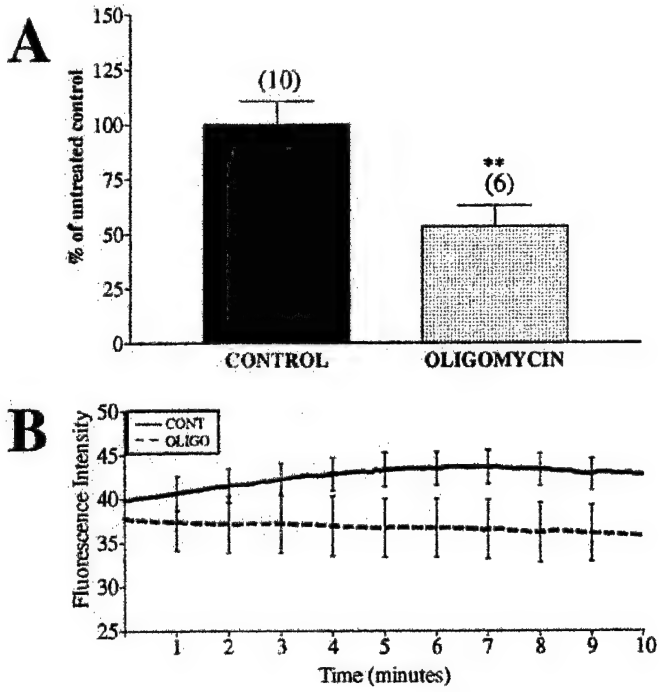

Figure 8. $\Delta\Psi_m$ fluctuations are decreased by pretreatment with an ATP synthase inhibitor. Neurons loaded with JC-1 were treated with 10 μM oligomycin (*OLIGO*) for 15 min before imaging to ensure substantial inhibition of the synthase. Fluorescence intensity and number of fluctuations per minute per 1000 ROIs were calculated. *A*, Percentage of fluctuations in oligomycin-pretreated to untreated mitochondria (means ± SEM). Oligomycin significantly decreased $\Delta\Psi_m$ fluctuations ($t = 3.03$; $df = 14$; $^{**}p < 0.01$). *Numbers* above *bars* equals the number of fields imaged (~1000 ROIs per field). *B*, Average fluorescence intensity of all mitochondria, with representative error bars indicating SEM. Oligomycin had no effect.

low-amplitude transition as a basis for these changes (Ichas et al., 1997). Oligomycin, however, significantly decreased the frequency of fluctuations, which argues that the fluctuations are associated with oxidative phosphorylation.

Oxidative phosphorylation may impact $\Delta\Psi_m$ fluctuations by one of two mechanisms. The first mechanism would suggest that, as mitochondria go from a resting state to active phosphorylation (state 4 to state 3), the fluctuations reflect the transient loss of $\Delta\Psi_m$ as proton flux increases (Nicholls and Ferguson, 1992). In this case, the increase in dye signal would be attributable to the disaggregation and subsequent dissipation of dye from mitochondria. Alternatively, because state 3 mitochondria adopt a condensed configuration whereas state 4 mitochondria adopt the larger orthodox configuration (Scalettar et al., 1991), the fluctuations would reflect changes in mitochondrial matrix volume. In this case, the increase in dye signal attributable to the increased volume would lead to a disaggregation of dye that is retained within the mitochondrial matrix. Although these mechanisms are contradictory in that the first proposes that a fluctuation is associated with the onset of phosphorylation whereas the second suggests that the signal should be associated with the termination of active phosphorylation, the key feature of both mechanisms is that the fluctuations represent an on–off transition. Thus, either mechanism could explain the decrease in fluctuations observed with a glutamate-induced sodium load. In this condition, an increase in ATP demand presumably occurs causing the mitochondria to spend a greater fraction of the time engaged in active phosphorylation rather than switching on and off. One could also argue that light-induced damage places greater demands on the mitochondria to be met by increasing ATP synthesis (or perhaps by decreasing synthetic capacity).

Predicting manipulations that increase the frequency of fluctuations is harder. We have observed differences in the number fluctuations on a culture-to-culture basis but have not yet established a mechanism for these differences. We are not aware of any previous studies that have suggested that individual mitochondria can be observed to change between states of resting and active phosphorylation. However, the architecture of neurons is uniquely suited to making such observations because optically isolating individual mitochondria in neuronal processes is straightforward (Figs. 1, 2).

Cationic dyes used to measure $\Delta\Psi_m$ (such as JC-1 and TMRM) can lead to toxicity resulting from light-induced singlet oxygen generation (Bunting, 1992) and inhibition of respiration. Although light exposure was carefully controlled and minimized to that necessary for adequate recordings, some effects of light exposure were observed even under these low-light conditions. With JC-1, exposure to light before recording stabilized the baseline, and with TMRM, increasing light exposure tended to increase the overall fluorescent signal. Both of these light-induced changes in dye signal could be indicative of a potential impact of phototoxicity in $\Delta\Psi_m$ measurements. A more immediate concern was that the spontaneous changes were triggered by light expo-

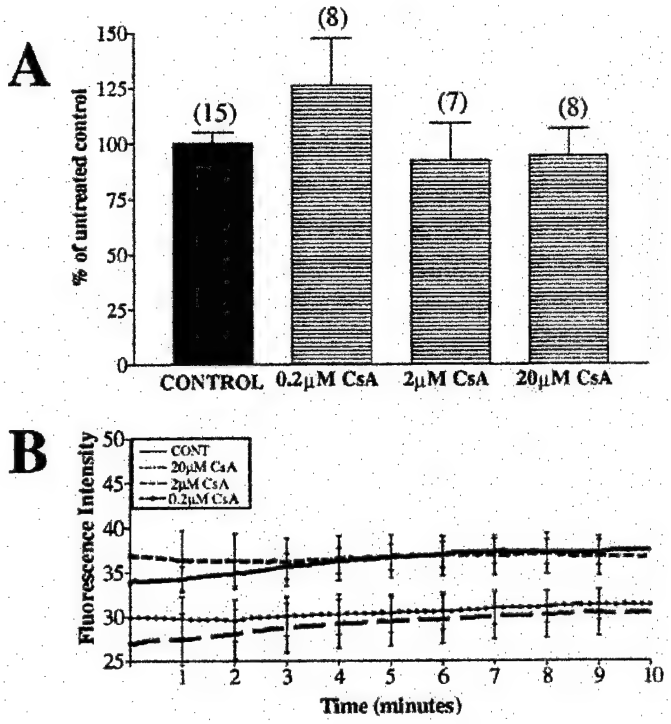

Figure 9. $\Delta\Psi_m$ fluctuations are not altered by treatment with cyclosporin A. Neurons loaded with JC-1 were treated with 0.2–20 μM cyclosporin A (*CsA*) for 15 min before imaging. Fluorescence intensity and number of fluctuations per minute per 1000 ROIs were calculated. *A*, Percentage of fluctuations in cyclosporin A-pretreated mitochondria to untreated mitochondria. Cyclosporin A did not significantly alter $\Delta\Psi_m$ fluctuations ($F_{(3,34)} = 1.27$; $p > 0.05$). Data are presented as means ± SEM, and the *numbers* above *bars* equal the number of fields imaged (~1000 ROIs per field). *B*, Average fluorescence intensity, with representative error bars indicating SEM. Cyclosporin A did not substantially alter the average fluorescence intensity.

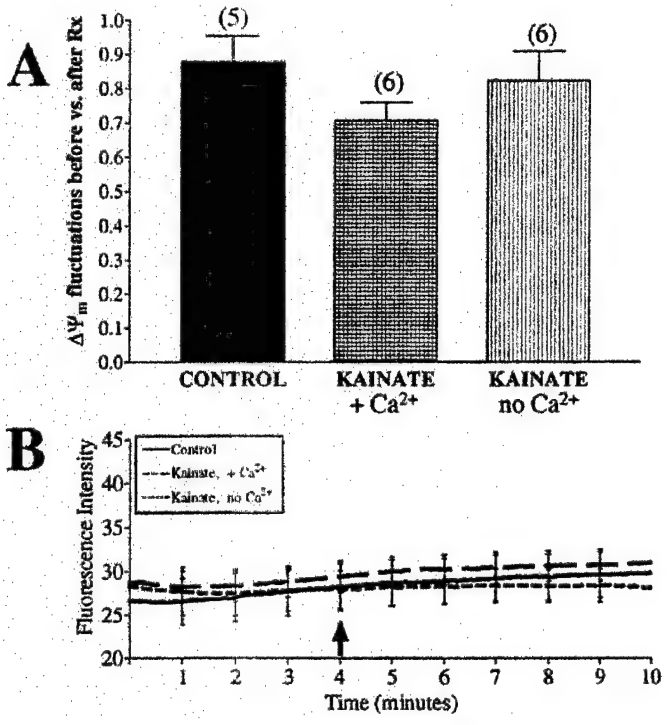

Figure 10. $\Delta\Psi_m$ fluctuations are not altered by treatment with kainic acid. Untreated neurons were loaded with JC-1 and imaged for 4 min before the addition of drug (*arrow*). Kainic acid (100 μM) was perfused over the cells in a buffer containing 1.4 mM (*+Ca^{2+}*) or 0 mM (*no Ca^{2+}*) calcium for 5 min, and fluorescence intensity and number of fluctuations per minute per 1000 ROIs were calculated. *A*, The ratio of fluctuations occurring during baseline to those occurring after drug treatment. Data are presented as means ± SEM, and the *numbers* above each *bar* equal the number of fields imaged (~1000 ROIs per field). Neither treatment had a significant impact on $\Delta\Psi_m$ fluctuations (with Ca^{2+}, $t = 1.90$, df = 9, $p > 0.05$; without Ca^{2+}, $t = 0.48$, df = 9, $p > 0.05$). *B*, Average fluorescence intensity of all mitochondria imaged, with representative error bars indicating SEM. Neither treatment altered basal fluorescence.

sure. Thus, if a brief, intense light augmented the frequency of $\Delta\Psi_m$ fluctuations, it would suggest that these fluctuations were merely reflecting photo damage. We saw, however, a decrease in the number of fluctuations under high-light conditions, suggesting that dye-loaded mitochondria exhibit spontaneous fluctuations in $\Delta\Psi_m$, which were not a consequence of illumination. These high-light conditions led to a decrease in the JC-1 aggregate signal without a concurrent change in the monomer signal (data not shown), similar to what is observed with oxidant treatments, such as hydrogen peroxide (Scanlon and Reynolds, 1998; Chinopoulos et al., 1999). However, treatment with the uncoupler FCCP at the end of the high-light experiments led to an increase in monomer fluorescence of the same magnitude in both the exposed and unexposed regions (data not shown). This supports the hypothesis that JC-1 aggregate fluorescence responds to more than just changes in $\Delta\Psi_m$ (Scanlon and Reynolds, 1998; Chinopoulos et al., 1999) but indicates that light-induced changes in aggregate fluorescence do not change the ability of the JC-1 monomer signal to respond to changes in $\Delta\Psi_m$.

Calcium may have a profound impact on mitochondrial function in general and on membrane potential in particular. Small transient changes in $\Delta\Psi_m$ observed in cardiomyocytes were reported to be the result of mitochondrial calcium transport (Duchen et al., 1998; Fall and Bennett, 1999). Furthermore, calcium can induce the generation of ROS, alter respiration (McCormack et al., 1990), and possibly open the large, nonselective PTP (Zoratti and Szabo, 1995). This suggests that calcium could be a key mediator of changes in $\Delta\Psi_m$. Inhibiting the NMDA receptor, thus decreasing the entry accumulation of calcium (Fig. 6*A*), chelating extracellular calcium with EGTA (data not shown), and inhibiting the PTP with cyclosporin A (Fig. 9) all failed to change $\Delta\Psi_m$ fluctuations, which argues against this possibility. Chelating intracellular calcium with BAPTA (Fig. 7*A*) did decrease fluctuations, but this occurred in conjunction with a considerable mitochondrial depolarization. The large rise in monomer fluorescence induced by BAPTA most likely occluded our ability to detect small fluctuations and was similar to the effects of the protonophore FCCP. However, it remains unclear how adding BAPTA influences the free calcium because, under resting conditions, the calcium concentration in both the cytoplasm and mitochondria of these neurons is low (Brocard et al., 2001).

We believe that these are the first experiments that illustrate spontaneous changes in $\Delta\Psi_m$ in neurons. Previous studies have suggested cyclosporin A-stimulated changes in whole-cell TMRM signal in neuroblastoma cells (Fall and Bennett, 1999), which are obviously distinct from the single organelle signals reported here. In cardiomyocytes, transient depolarizations in single mitochondria have been seen (Duchen et al., 1998), but these changes were the consequence of calcium movements.

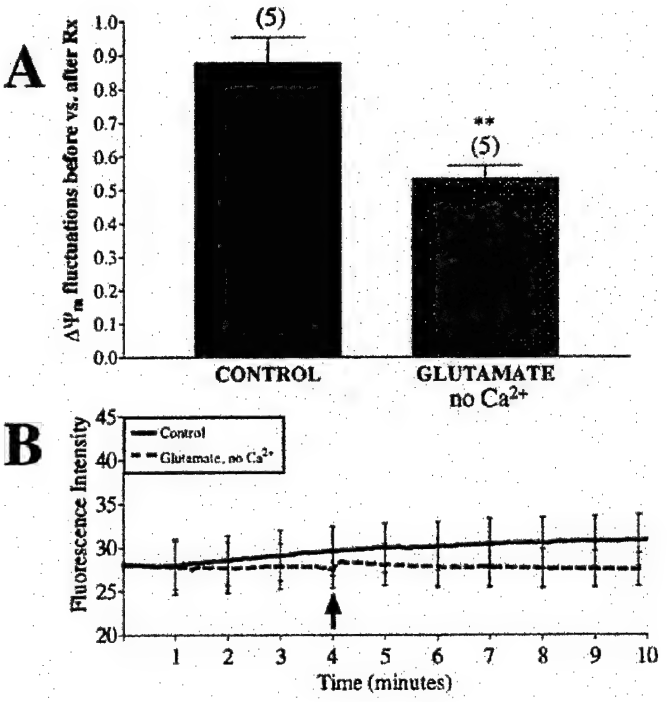

Figure 11. $\Delta\Psi_m$ fluctuations are decreased after treatment with glutamate in a calcium-free buffer. Untreated neurons were loaded with JC-1 and imaged for 4 min before the addition of drug (*arrow*). Glutamate (100 μM, with 10 μM glycine) was perfused over the cells in a Ca^{2+}-free buffer for 5 min. Fluorescence intensity and number of fluctuations per minute per 1000 ROIs were calculated. Glutamate in the presence of Ca^{2+} caused mitochondrial depolarization and thus was not tested. *A*, The ratio of fluctuations occurring during baseline to those occurring after drug treatment. Data are presented as means ± SEM, and the *numbers* above each *bar* equal the number of fields imaged (~1000 ROIs per field). Glutamate in Ca^{2+}-free buffer significantly decreased the number of spontaneous fluctuations ($t = 4.04$; df = 8; $^{**}p < 0.01$). *B*, Average fluorescence intensity of all mitochondria imaged, with representative error bars indicating SEM. Glutamate (*no* Ca^{2+}) treatment did not alter basal fluorescence.

Other studies have investigated single mitochondria but only after their isolation from cells (Ichas et al., 1997; Huser and Blatter, 1999). Apparently none of these studies have reported oligomycin sensitivity of the fluctuations.

Herein, we have documented a novel feature of mitochondrial physiology in neurons. Unlike previous studies that have reported large changes in $\Delta\Psi_m$ associated with neuronal injury, the spontaneous changes in $\Delta\Psi_m$ reported here appear to be a normal characteristic of mitochondrial function in neurons and may reflect alterations in the activity of individual mitochondria associated with the transition between rest and active oxidative phosphorylation. We suggest that this phenomenon that may prove to be a useful marker of mitochondrial function in neurons and hypothesize that these fluctuations in $\Delta\Psi_m$ reflect variations in the cellular environment associated with altered states of respiratory control or ion-induced matrix swelling.

REFERENCES

Ankarcrona M, Dypbukt JM, Bonfoco E, Zhivotovsky B, Orrenius S, Lipton SA, Nicotera P (1995) Glutamate-induced neuronal death: a succession of necrosis or apoptosis depending on mitochondrial function. Neuron 15:961–973.

Bernardi P (1999) Mitochondrial transport of cations: channels, exchangers, and permeability transition. Physiol Rev 79:1127–1155.

Brocard JB, Tassetto M, Reynolds IJ (2001) Quantitative evaluation of mitochondrial calcium content following a glutamate stimulation in rat cortical neurones. J Physiol (Lond) 531:793–805.

Budd SL, Nicholls DG (1996) Mitochondria, calcium regulation, and acute glutamate excitotoxicity in cultured cerebellar granule cells. J Neurochem 67:2282–2291.

Budd SL, Tenneti L, Lishnak T, Lipton SA (2000) Mitochondrial and extramitochondrial apoptotic signaling pathways in cerebrocortical neurons. Proc Natl Acad Sci USA 97:6161–6166.

Bunting JR (1992) A test of the singlet oxygen mechanism of cationic dye photosensitization of mitochondrial damage. Photochem Photobiol 55:81–87.

Chinopoulos C, Tretter L, Adam-Vizi V (1999) Depolarization of in situ mitochondria due to hydrogen peroxide-induced oxidative stress in nerve terminals: inhibition of alpha-ketoglutarate dehydrogenase. J Neurochem 73:220–228.

Courtney MJ, Enkvist MO, Akerman KE (1995) The calcium response to the excitotoxin kainate is amplified by subsequent reduction of extracellular sodium. Neuroscience 68:1051–1057.

Crompton M, Ellinger H, Costi A (1988) Inhibition by cyclosporin A of a Ca^{2+}-dependent pore in heart mitochondria activated by inorganic phosphate and oxidative stress. Biochem J 255:357–360.

Desagher S, Martinou JC (2000) Mitochondria as the central control point of apoptosis. Trends Cell Biol 10:369–377.

Duchen MR (1999) Contributions of mitochondria to animal physiology: from homeostatic sensor to calcium signalling and cell death. J Physiol (Lond) 516:1–17.

Duchen MR, Leyssens A, Crompton M (1998) Transient mitochondrial depolarizations reflect focal sarcoplasmic reticular calcium release in single rat cardiomyocytes. J Cell Biol 142:975–988.

Fall CP, Bennett Jr JP (1999) Visualization of cyclosporin A and Ca^{2+}-sensitive cyclical mitochondrial depolarizations in cell culture. Biochim Biophys Acta 1410:77–84.

Green DR, Reed JC (1998) Mitochondria and apoptosis. Science 281:1309–1312.

Hajnoczky G, Robb-Gaspers LD, Seitz MB, Thomas AP (1995) Decoding of cytosolic calcium oscillations in the mitochondria. Cell 82:415–424.

Hoyt KR, Stout AK, Cardman JM, Reynolds IJ (1998) The role of intracellular Na^+ and mitochondria in buffering of kainate-induced intracellular free Ca^{2+} changes in rat forebrain neurones. J Physiol (Lond) 509:103–116.

Huser J, Blatter LA (1999) Fluctuations in mitochondrial membrane potential caused by repetitive gating of the permeability transition pore. Biochem J 343:311–317.

Ichas F, Jouaville LS, Mazat JP (1997) Mitochondria are excitable organelles capable of generating and conveying electrical and calcium signals. Cell 89:1145–1153.

Krippeit-Drews P, Dufer M, Drews G (2000) Parallel oscillations of intracellular calcium activity and mitochondrial membrane potential in mouse pancreatic B-cells. Biochem Biophys Res Commun 267:179–183.

Kroemer G, Dallaporta B, Resche-Rigon M (1998) The mitochondrial death/life regulator in apoptosis and necrosis. Annu Rev Physiol 60:619–642.

Loew LM, Carrington W, Tuft RA, Fay FS (1994) Physiological cytosolic Ca^{2+} transients evoke concurrent mitochondrial depolarizations. Proc Natl Acad Sci USA 91:12579–12583.

McCormack JG, Halestrap AP, Denton RM (1990) Role of calcium ions in regulation of mammalian intramitochondrial metabolism. Physiol Rev 70:391–425.

Nicholls DG, Budd SL (2000) Mitochondria and neuronal survival. Physiol Rev 80:315–360.

Nicholls DG, Ferguson SJ (1992) Bioenergetics 2. San Diego: Academic.

Nicholls DG, Ward MW (2000) Mitochondrial membrane potential and neuronal glutamate excitotoxicity: mortality and millivolts. Trends Neurosci 23:166–174.

Nieminen AL, Petrie TG, Lemasters JJ, Selman WR (1996) Cyclosporin A delays mitochondrial depolarization induced by *N*-methyl-D-aspartate in cortical neurons: evidence of the mitochondrial permeability transition. Neuroscience 75:993–997.

Overly CC, Rieff HI, Hollenbeck PJ (1996) Organelle motility and metabolism in axons vs dendrites of cultured hippocampal neurons. J Cell Sci 109:971–980.

Petit PX, Susin SA, Zamzami N, Mignotte B, Kroemer G (1996) Mitochondria and programmed cell death: back to the future. FEBS Lett 396:7–13.

Rizzuto R, Brini M, Murgia M, Pozzan T (1993) Microdomains with high Ca^{2+} close to IP3-sensitive channels that are sensed by neighboring mitochondria. Science 262:744–747.

Rizzuto R, Pinton P, Carrington W, Fay FS, Fogarty KE, Lifshitz LM, Tuft RA, Pozzan T (1998) Close contacts with the endoplasmic reticulum as determinants of mitochondrial Ca^{2+} responses. Science 280:1763–1766.

Sattler R, Charlton MP, Hafner M, Tymianski M (1998) Distinct influx pathways, not calcium load, determine neuronal vulnerability to calcium neurotoxicity. J Neurochem 71:2349–2364.

Scalettar BA, Abney JR, Hackenbrock CR (1991) Dynamics, structure, and function are coupled in the mitochondrial matrix. Proc Natl Acad Sci USA 88:8057–8061.

Scanlon JM, Reynolds IJ (1998) Effects of oxidants and glutamate receptor activation on mitochondrial membrane potential in rat forebrain neurons. J Neurochem 71:2392–2400.

Schinder AF, Olson EC, Spitzer NC, Montal M (1996) Mitochondrial dysfunction is a primary event in glutamate neurotoxicity. J Neurosci 16:6125–6133.

Scott ID, Nicholls DG (1980) Energy transduction in intact synaptosomes. Influence of plasma-membrane depolarization on the respiration and membrane potential of internal mitochondria determined in situ. Biochem J 186:21–33.

Skulachev VP (1996) Role of uncoupled and non-coupled oxidations in maintenance of safely low levels of oxygen and its one-electron reductants. Q Rev Biophys 29:169–202.

Stout AK, Raphael HM, Kanterewicz BI, Klann E, Reynolds IJ (1998) Glutamate-induced neuron death requires mitochondrial calcium uptake. Nat Neurosci 1:366–373.

Susin SA, Zamzami N, Castedo M, Daugas E, Wang HG, Geley S, Fassy F, Reed JC, Kroemer G (1997) The central executioner of apoptosis: multiple connections between protease activation and mitochondria in Fas/APO-1/CD95- and ceramide-induced apoptosis. J Exp Med 186:25–37.

Susin SA, Zamzami N, Kroemer G (1998) Mitochondria as regulators of apoptosis: doubt no more. Biochim Biophys Acta 1366:151–165.

Vergun O, Keelan J, Khodorov BI, Duchen MR (1999) Glutamate-induced mitochondrial depolarisation and perturbation of calcium homeostasis in cultured rat hippocampal neurones. J Physiol (Lond) 519:451–466.

Ward MW, Rego AC, Frenguelli BG, Nicholls DG (2000) Mitochondrial membrane potential and glutamate excitotoxicity in cultured cerebellar granule cells. J Neurosci 20:7208–7219.

White RJ, Reynolds IJ (1995) Mitochondria and Na^+/Ca^{2+} exchange buffer glutamate-induced calcium loads in cultured cortical neurons. J Neurosci 15:1318–1328.

White RJ, Reynolds IJ (1996) Mitochondrial depolarization in glutamate-stimulated neurons: an early signal specific to excitotoxin exposure. J Neurosci 16:5688–5697.

White RJ, Reynolds IJ (1997) Mitochondria accumulate Ca^{2+} following intense glutamate stimulation of cultured rat forebrain neurones. J Physiol (Lond) 498:31–47.

Zoratti M, Szabo I (1995) The mitochondrial permeability transition. Biochim Biophys Acta 1241:139–176.

0022-3565/00/2932-0480$03.00/0
THE JOURNAL OF PHARMACOLOGY AND EXPERIMENTAL THERAPEUTICS
Copyright © 2000 by The American Society for Pharmacology and Experimental Therapeutics
JPET 293:480–486, 2000 /2189/817868

Vol. 293, No. 2
Printed in U.S.A.

Inhibition of Glutamate-Induced Mitochondrial Depolarization by Tamoxifen in Cultured Neurons[1]

KARI R. HOYT,[2] BETH ANN MCLAUGHLIN, DONALD S. HIGGINS JR., and IAN J. REYNOLDS[3]

Departments of Pharmacology (K.R.H, I.J.R.) and Neurobiology (B.A.M.), University of Pittsburgh School of Medicine, Pittsburgh, Pennsylvania; and Department of Neurology (D.S.H.), The Ohio State University College of Medicine, Columbus, Ohio

Accepted for publication January 9, 2000 This paper is available online at http://www.jpet.org

ABSTRACT

In central neurons, glutamate receptor activation causes massive calcium influx and induces a mitochondrial depolarization, which is partially blocked by cyclosporin A, suggesting a possible activation of the mitochondrial permeability transition pore (PTP) as a mechanism. It has been recently reported that tamoxifen (an antiestrogen chemotherapeutic agent) blocks the PTP in isolated liver mitochondria, similar to cyclosporin A. In this study, we tested whether tamoxifen inhibits the mitochondrial depolarization induced by glutamate receptor activation in intact cultured neurons loaded with the fluorescent dye 5,5′,6,6′-tetrachloro-1,1′,3,3′-tetraethylbenzimidazolylcarbocyanine iodide. This dye reports disruptions in mitochondrial membrane potential, which can be caused by PTP activation. We found that glutamate (100 μM for 10 min) causes a robust mitochondrial depolarization that is partially inhibited by tamoxifen. The maximum inhibitory concentration of tamoxifen was 0.3 μM, with concentrations higher and lower than 0.3 μM being less effective. However, although tamoxifen (0.3 μM) blocked glutamate-induced mitochondrial depolarization, it did not inhibit glutamate-induced neuronal death, in contrast to the PTP inhibitor cyclosporin A. A relatively high concentration of tamoxifen (100 μM) caused mitochondrial depolarization itself and was neurotoxic. These data suggest that tamoxifen may be an inhibitor of the PTP in intact neurons. However, the lack of specificity of most PTP inhibitors, and the difficulty in measuring PTP in intact cells, preclude definite conclusions about the role of PTP in excitotoxic injury.

Activation of the mitochondrial permeability transition pore (PTP) has been identified as a possible common effector of the cell death of numerous cell types in response to both necrotic and apoptotic stimuli (Lemasters et al., 1997; Kroemer et al., 1998). The PTP includes proteins located in both the inner and outer mitochondrial membranes and, when opened, allows mitochondrial constituents <1.5 kD to cross the inner membrane. In isolated mitochondria this results in swelling, loss of the protonmotive force, and the loss of low molecular weight compounds such as glutathione (Savage and Reed, 1994; Zoratti and Szabo, 1995). Increases in matrix Ca^{2+} and oxidant levels are important inducers of the PTP. Cyclosporin A is among the most potent inhibitors of the PTP (Broekemeier et al., 1989).

The PTP has been suggested to be involved in the neurotoxicity caused by overactivation of neuronal glutamate receptors (Nieminen et al., 1996; Schinder et al., 1996; White and Reynolds, 1996). Glutamate-induced neurotoxicity is involved in the cell loss caused by stroke and trauma, as well as chronic neurodegenerative diseases (Choi, 1988). Activation of the various subtypes of glutamate receptor leads to opening of an integral ion channel and influx of Na^+, and for the *N*-methyl-D-aspartate (NMDA) subtype and certain α-amino-3-hydroxy-5-methyl-4-isoxazolepropionic acid/kainate subtypes, Ca^{2+} (Mayer and Westbrook, 1987). Robust Ca^{2+} accumulation and the subsequent mitochondrial Ca^{2+} loading are critical for the expression of NMDA receptor-mediated injury, although the events that link mitochondrial Ca^{2+} changes to toxicity have not been firmly established (Budd and Nicholls, 1996; Stout et al., 1998). Reactive oxygen species are generated by mitochondria in response to NMDA receptor-mediated Ca^{2+} influx (Dugan et al., 1995; Reynolds and Hastings, 1995; Bindokas et al., 1996). The massive Ca^{2+} loading caused by NMDA receptor activation also induces a Ca^{2+}-dependent depolarization of the mitochondrial membrane potential ($\Delta\psi_m$) that is partially blocked by the PTP inhibitor cyclosporin A (Ankarcrona et al., 1996; Schinder et

Received for publication October 11, 1999.
[1] This study was supported by DAMD17-98-1-8627 (to I.J.R.), the American Heart Association (to I.J.R.), AG 00751 (to D.S.H.), NS 07391 (to B.A.M.), and NS 07291 (to K.R.H.).
[2] Current address: Department of Neurology, 190 Medical Research Facility, 420 West 12th Ave., The Ohio State University, Columbus, OH 43210. E-mail: hoyt.31@osu.edu
[3] I.J.R. is an Established Investigator of the American Heart Association.

ABBREVIATIONS: PTP, mitochondrial permeability transition pore; NMDA, *N*-methyl-D-aspartate; $\Delta\psi_m$, mitochondrial membrane potential; JC-1, 5,5′,6,6′-tetrachloro-1,1′,3,3′-tetraethylbenzimidazolylcarbocyanine iodide; HBSS, HEPES-buffered salt solution; FCCP, carbonyl cyanide *p*-trifluoromethoxyphenylhydrazone; LDH, lactate dehydrogenase.

al., 1996; White and Reynolds, 1996) as well as other PTP blockers such as trifluoperazine and dibucaine (Hoyt et al., 1997). Cyclosporin A also inhibits toxicity caused by glutamate receptor activation, although this effect may be mediated by calcineurin inhibition rather than PTP activation (Dawson et al., 1993; Ankarcrona et al., 1996; Schinder et al., 1996; White and Reynolds, 1996). Indeed, it has proven difficult to establish the role of the PTP in excitotoxicity because of the lack of potent and selective inhibitors.

It has been recently reported that tamoxifen, a widely used antiestrogen chemotherapeutic and chemoprevention agent, blocks Ca^{2+}-induced PTP activation in isolated liver mitochondria, with effects similar to those caused by cyclosporin A (Custodio et al., 1998). In addition to its estrogen receptor-blocking effects, tamoxifen is a lipophilic peroxyl radical scavenger (Custodio et al., 1994). However, it does not appear that its antioxidant function is related to its ability to block PTP because the PTP-inducing conditions (Ca^{2+} and phosphate treatment) with which tamoxifen was tested did not alter mitochondrial oxidized glutathione levels (an indication of oxidation) (Custodio et al., 1998).

Tamoxifen rapidly induces apoptosis in neural cell lines (Ellerby et al., 1997; Hashimoto et al., 1997). Whole-cell extracts from cultures treated with 100 μM tamoxifen induced assymetric chromatin formations indicative of apoptosis in naïve isolated nuclei within 1 h. This rapid morphological change was accompanied by caspase cleavage of nuclear substrates (Ellerby et al., 1997). These effects were not blocked by inhibitors of caspases 1 and 4 and could not be reproduced if nuclei were treated with only mitochondrial and cytosolic fractions from tamoxifen-primed cells. This apparent requirement for cellular components other than the mitochondria and cytosol would suggest that tamoxifen does not initiate cell death by directly impairing mitochondrial membrane potential, although this hypothesis has not been directly tested. It also remains to be determined if this compound can provide neuroprotection by altering PTP activation in primary neuronal cultures at concentrations similar to those that inhibit PTP in liver mitochondria (5–25 μM) (Custodio et al., 1998).

There are relatively few drugs available to study PTP activation in intact cells, and we were interested to see whether tamoxifen would be as effective in neurons as it is in isolated mitochondria. We tested whether tamoxifen inhibits the $\Delta\psi_m$ depolarization induced by glutamate receptor activation in cultured neurons. $\Delta\psi_m$ was monitored in neurons loaded with the $\Delta\psi_m$-sensitive fluorescent dye 5,5′,6,6′-tetrachloro-1,1′,3,3′-tetraethylbenzimidazolylcarbocyanine iodide (JC-1), as an indirect indication of PTP activation, because PTP activation necessarily results in a loss of $\Delta\psi_m$. We also determined the effect of tamoxifen on glutamate-induced neuronal death, both in vitro and in vivo.

Materials and Methods

Primary Neuronal Culture. Forebrain neurons were cultured from embryonic day 17 Sprague-Dawley rat pups as described in White and Reynolds (1995). Pregnant rats were deeply anesthetized with diethyl ether and were not allowed to regain consciousness. Embryos were then taken and used to obtain forebrain neurons. All animal handling procedures for isolation of neurons for cell culture were approved by the Institutional Animal Care and Use Committee of the University of Pittsburgh. Brain tissue was dissociated with trypsin, and then plated on to poly(D-lysine)-coated glass coverslips at a density of 450,000 cells ml^{-1} in Dulbecco's modified Eagle's medium with 10% fetal bovine serum, 24 U ml^{-1} penicillin, and 24 μg ml^{-1} streptomycin. Twenty-four hours after plating, the media were removed and replaced with Dulbecco's modified Eagle's medium that contained horse serum in place of fetal bovine serum, and the coverslips were inverted to suppress glial proliferation. Neurons were kept in a 37°C, 5% CO_2-humidified incubator for 12 to 18 days until use. All recordings were made with a HEPES-buffered salt solution (HBSS) that contained 137 mM NaCl, 5 mM KCl, 0.9 mM $MgSO_4$, 1.4 mM $CaCl_2$, 3 mM $NaHCO_3$, 0.6 mM Na_2HPO_4, 0.4 mM KH_2PO_4, 5.6 mM glucose, and 20 mM HEPES; pH was adjusted to 7.4 with NaOH. All glutamate solutions contained 1 μM glycine. Tamoxifen was dissolved in methanol (≤0.02% final methanol concentration) and all control conditions contained 0.02% methanol.

Measurements of $\Delta\psi_m$. $\Delta\psi_m$ was estimated in individual neurons loaded with the $\Delta\psi_m$-sensitive fluorescent dye JC-1 (Molecular Probes, Eugene, OR; White and Reynolds, 1996). Neurons were loaded with the JC-1 (3 μM) for 20 min at 37°C, rinsed with dye-free HBSS for 20 min at room temperature, and then mounted in a recording chamber on the stage of an ACAS 570c laser scanning confocal microscope (Meridian Instruments, Okemos, MI). Fields of neurons were illuminated with the 488-nm line of an argon laser, and emission at 530 and 590 nm was monitored. Solution changes in this protocol were made by rapidly aspirating and replacing the contents of the recording chamber. The fluorescence emission wavelength of JC-1 depends on the aggregation of the JC-1 molecules that in turn depends on the $\Delta\psi_m$ (i.e., the greater the $\Delta\psi_m$, the greater the aggregation; Reers et al., 1991). By monitoring JC-1 fluorescence at 590 nm (aggregate) and 530 nm (monomer), one can assess relative changes in $\Delta\psi_m$. Ratio values were obtained by dividing the signal at 590 nm by the signal at 530 nm after background subtraction on a cell-by-cell basis and normalized to a starting value of 1 for comparison between cells. With this approach, a decrease in the normalized ratio represents mitochondrial depolarization, which was confirmed by titration with increasing concentrations of the protonophore carbonyl cyanide *p*-trifluoromethoxyphenylhydrazone (FCCP; 20–750 nM), resulting in graded, concentration-dependent decreases in the JC-1 ratio (K. R. Hoyt and I. J. Reynolds, unpublished observations).

$[Ca^{2+}]_i$ Measurements. $[Ca^{2+}]_i$ was measured from individual neurons loaded with the Ca^{2+}-sensitive fluorescent dye indo-1 (White and Reynolds, 1995). Neurons were rinsed with HBSS and then loaded with 5 μM indo-1 AM (Molecular Probes) in HBSS containing 5 mg/ml BSA for 50 min at 37°C, and incubated in dye-free HBSS for a further 20 min at 37°C to allow for dye cleavage. Coverslips were then mounted in a recording chamber (1-ml volume) on the stage of a Nikon Diaphot microscope. Cells were illuminated at 350 nm with light from a 75-W mercury arc lamp. Indo-1 emission was simultaneously monitored at 405 and 490 nm with a dual photomultiplier system. Background subtracted ratios were converted to $[Ca^{2+}]_i$ with parameters from an in situ calibration.

In Vitro Toxicity Assay. For neuronal viability experiments, coverslips were washed once in HBSS that had been prewarmed to 37°C, inverted, and transferred to new plates. Cells were then washed twice more in HBSS and incubated in toxin. Cells were exposed to glutamate (100 μM) and glycine (1 μM) or HBSS in the presence or absence of tamoxifen (0.3 μM) and returned to the incubator for 10 min. Glutamate exposure was terminated by washing cells twice with HBSS. After rinsing with HBSS, cells were maintained in the presence or absence of tamoxifen (0.3 μM) in minimal essential medium. For high-dose tamoxifen experiments, cells were maintained in 100 μM tamoxifen in minimal essential medium. Neuronal viability was determined 18 to 20 h later for all experiments by measuring lactate dehydrogenase (LDH) release with an in vitro toxicology assay kit (Sigma Chemical Co., St. Louis, MO). Forty-microliter samples of medium were assayed spectrophotometrically according to the manufacturer's protocol to obtain a measure of cytoplasmic LDH released from dead and dying neurons

(Hartnett et al., 1997). LDH results were confirmed qualitatively by visual inspection of the cells. Chromatin staining of tamoxifen-treated cells also was performed as described in McLaughlin et al. (1998). After incubation with tamoxifen, the cultures were washed briefly with PBS, fixed in 4% paraformaldehyde (pH 7.4) for 5 min, and incubated in 5 μg/ml Hoechst 33342 (Molecular Probes) for 10 min. Cells were then washed twice in PBS and mounted on glass slides. Fluorescence of stained chromatin was evaluated with a Nikon Diaphot fluorescence microscope.

Striatal Malonate Lesions. Male Sprague-Dawley rats (275–350 g) were maintained in a 12-h light/dark cycle with free access to standard rat chow and water. All animal procedures were in accordance with the National Institutes of Health Guide for the Care and Use of Laboratory Animals and have been approved by the Institutional Laboratory Animal Care and Use Committee of The Ohio State University. Rats were anesthetized with equithesin, then placed in a Kopf small animal stereotaxic apparatus. A midline incision was made and the confluence of the sagittal and coronal sutures was identified (bregma). Malonate (3 μmol in 2 μl of 0.9 N NaCl) was administered via a 26-gauge Hamilton syringe at a rate of 0.2 μl/min at the following coordinates relative to bregma: 0.7 mm anterior, 2.8 mm lateral, and 5.0 mm ventral. The needle remained in place for an additional 5 min to limit regurgitation up the needle tract. Tamoxifen or vehicle (dimethyl sulfoxide) treatments were administered i.p. 2 h before and 4 h after malonate exposure. Seven days after malonate exposure, all animals were euthanized with chloral hydrate (500 mg/kg) and rapid decapitation. The cranial contents were removed, coated with embedding matrix, frozen under powdered dry ice, and stored at −70°C until sectioning.

Coronal sections (25 μm) were gathered at 250-μm intervals through the rostrocaudal extent of the striatum with a cryostat and were thaw-mounted onto poly(lysine)-treated slides. Tissue sections were then processed for cytochrome oxidase histochemistry.

Cytochrome Oxidase Histochemistry. Sections were incubated in 100 mM sodium phosphate buffer (pH 7.4) with cytochrome *c* (10 μM) and 3,3′-diaminobenzidine (1 mM) for 2 h at 37°C in the dark. Sections were postfixed in 10% formalin (10 min), dehydrated in graded alcohol, and coverslipped from xylene. Analysis of striatal lesion volume of cytochrome oxidase-stained sections was performed on a microcomputer based image analysis program (Imaging Research, St. Catherines, Ontario, Canada) with area standards to provide a calibration from which three-dimensional volume (cubic millimeters) of the lesioned striatum was estimated.

Results

Exposure of neurons to excitotoxic concentrations of glutamate (100 μM) causes a decrease in $\Delta\psi_m$ that can be monitored with the $\Delta\psi_m$-sensitive fluorescent probe JC-1. A decrease in the ratio of JC-1 fluorescence emission at 590 nm relative to the emission at 530 nm indicates $\Delta\psi_m$ depolarization (Fig. 1A). We have previously shown this depolarization is mediated primarily by the NMDA subtype of glutamate receptor and is Ca^{2+}-dependent (White and Reynolds, 1996). When tamoxifen (0.3 μM) was included during the glutamate exposure (Fig. 1A), there was a notable attenuation of the $\Delta\psi_m$ depolarization caused by glutamate. A protonophore FCCP, which collapses the $\Delta\psi_m$, was added at the end of the fluorescence recording and demonstrates a small additional depolarization that was not affected by tamoxifen. A higher tamoxifen concentration (20 μM) did not inhibit glutamate-induced mitochondrial depolarization (Fig. 1B). We tested a range of tamoxifen concentrations (0.001–20 μM) on the glutamate-induced $\Delta\psi_m$ depolarization (Fig. 1, A and B). As an expression of the magnitude of the effect of tamoxifen, we took the difference between the mean normalized JC-1 ratios after 5 min of exposure to glutamate (100 μM) in the presence or absence of tamoxifen (Fig. 1C). The inhibitory effect of tamoxifen on glutamate-induced $\Delta\psi_m$ depolarization was maximal at 0.3 μM. Tamoxifen was less effective at concentrations higher or lower than 0.3 μM, suggesting an additional effect of higher tamoxifen concentrations on $\Delta\psi_m$.

We tested whether tamoxifen alone affected $\Delta\psi_m$ and found no effect of tamoxifen at lower concentrations (<1 μM) and an apparent increase in $\Delta\psi_m$ induced by higher tamoxifen concentrations (10 or 20 μM) (Fig. 2A). Prolonged exposure to a relatively high concentration of tamoxifen (100 μM) resulted in an apparent $\Delta\psi_m$ hyperpolarization followed by a marked depolarization (Fig. 2B).

We tested whether tamoxifen inhibits glutamate receptor activity as a possible mechanism of its inhibition of glutamate-induced $\Delta\psi_m$ depolarization. Tamoxifen (0.3 μM) did not inhibit glutamate-induced increases in $[Ca^{2+}]_i$ measured in indo-1-loaded neurons, indicating that tamoxifen does not directly inhibit glutamate receptor activation (Fig. 3A). Specifically, the glutamate-induced (3 μM for 15 s) peak $[Ca^{2+}]_i$ increase was 2.1 ± 0.4 μM (n = 7 neurons) and 1.7 ± 0.2 μM in the presence of 0.3 μM tamoxifen (n = 7 neurons; not significantly different from control, Student's t test). Tamoxifen (0.3 μM) also did not affect the rate of Ca^{2+} recovery from a longer, more intense glutamate stimulus (100 μM for 5 min) (Fig. 3C). The time required to recover to twice basal Ca^{2+} levels in Ca^{2+}-free HBSS was 47.1 ± 9.5 min (n = 8 neurons) and 42.5 ± 8.3 min in the presence of 0.3 μM tamoxifen for the 2 min after glutamate exposure (n = 6 neurons; not significantly different from control, Student's t test). Agents that alter mitochondrial and plasma membrane Ca^{2+}-buffering mechanisms affect the rate of Ca^{2+} recovery after glutamate (White and Reynolds, 1995, 1997; Hoyt and Reynolds, 1998; Hoyt et al., 1998). The lack of effect of tamoxifen on $[Ca^{2+}]_i$ or on Ca^{2+} recovery suggests that it does not inhibit glutamate-induced $\Delta\psi_m$ depolarization because of major alterations in $[Ca^{2+}]_i$ handling in response to glutamate.

It has been proposed that PTP activation is involved in the neurotoxicity of glutamate receptor activation, so we were interested to see whether tamoxifen had a neuroprotective action. Tamoxifen (0.3 μM; present during and after glutamate exposure) had no effect on the neuronal death caused by glutamate (100 μM for 10 min) as measured by LDH release from damaged neurons into the media during the 20 h after glutamate exposure (Fig. 4A). Because tamoxifen has been reported to rapidly induce apoptosis in neural cell lines, we tested a higher concentration (100 μM) of tamoxifen alone on neuronal viability and found that a 30-min exposure resulted in significant cell loss expressed 20 h later (Fig. 4B). Continuous exposure of neurons to 100 μM tamoxifen for 3 h also caused an increase in the number of apoptotic nuclei visualized with the fluorescent nuclear dye Hoechst 33342 from 3% in controls to 23% for cells treated with tamoxifen, consistent with previous findings in a neural cell line (Ellerby et al., 1997). It appears, therefore, that a low concentration of tamoxifen does not protect cells from excitotoxic injury and that high concentrations of tamoxifen are neurotoxic to primary cultured neurons.

We also tested whether tamoxifen was neuroprotective in an in vivo model of excitotoxic neuronal death. Malonate, an inhibitor of succinate dehydrogenase, causes metabolic inhi-

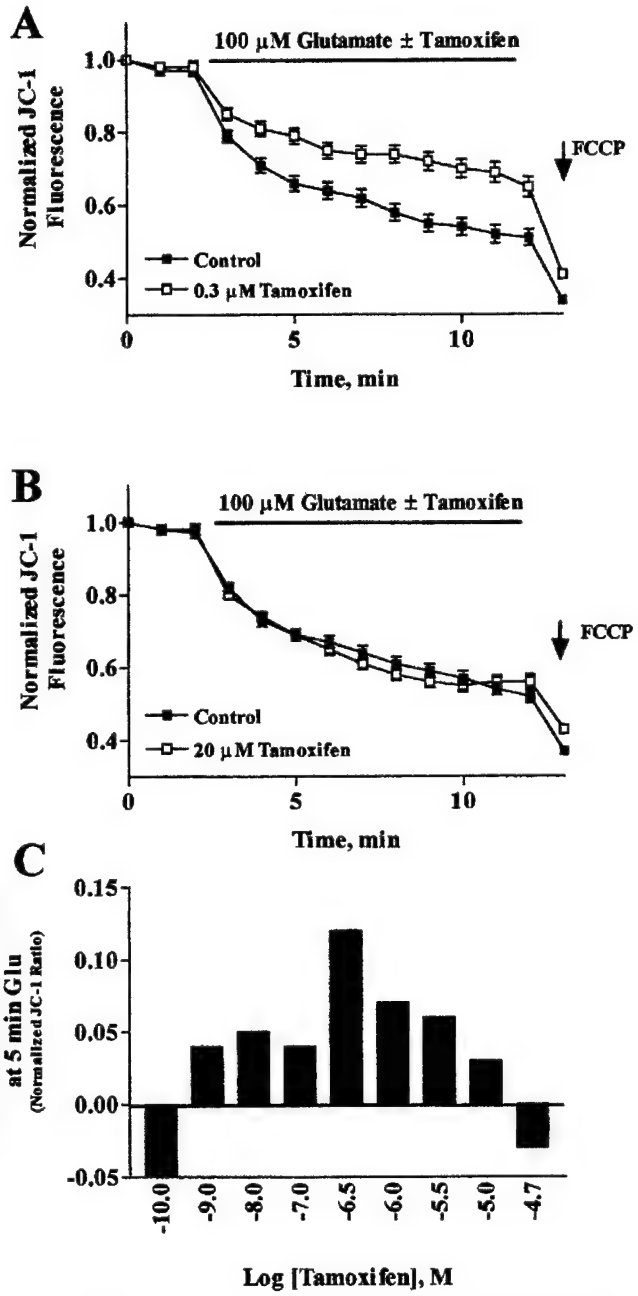

Fig. 1. Tamoxifen inhibits glutamate-induced mitochondrial depolarization in neurons loaded with JC-1. A, application of 100 μM glutamate (■) caused a decrease in the normalized 590:530 nm JC-1 emission ratio, reflecting mitochondrial depolarization. Addition of 0.3 μM tamoxifen (□) during the glutamate exposure substantially reduced the extent of the loss of $\Delta\psi_m$ caused by glutamate. Data represent the mean ± S.E. of 54 to 70 neurons per condition. FCCP (750 nM), a protonophore that depolarizes $\Delta\psi_m$, was added at the end of the experiment for comparison. B, a higher tamoxifen concentration (20 μM) did not inhibit the glutamate-induced decrease in $\Delta\psi_m$ when included during the glutamate exposure. Data represent the mean ± S.E. of 51 to 61 neurons per condition. C, concentration dependence of the inhibition of glutamate-induced mitochondrial depolarization by tamoxifen. Data are expressed as the difference between the normalized JC-1 ratio for tamoxifen-treated versus untreated cells after 5 min of glutamate exposure. Because these data points are not paired, we cannot calculate individual standard error values for these data. As an indication of variability, we report that the range of the standard error for the data points from which the differences were calculated was 0.018 to 0.025 normalized JC-1 fluorescence units. As the tamoxifen concentration was increased, there was a decrease in the inhibitory effect on glutamate-induced depolarization. Data were collected from a total of 41 to 70 neurons.

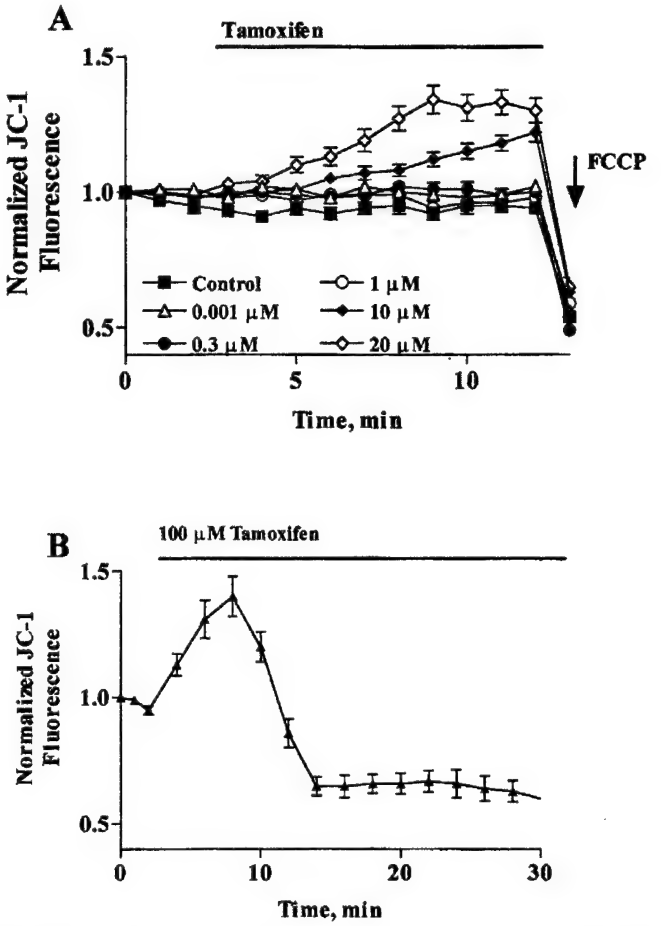

Fig. 2. Tamoxifen, at relatively high concentrations, increases the apparent $\Delta\psi_m$. A, a range of tamoxifen concentrations was tested on the $\Delta\psi_m$ in JC-1-loaded neurons. Concentrations of tamoxifen <1 μM had little direct effect on $\Delta\psi_m$, whereas higher concentrations (>10 μM) caused an increase in the JC-1 ratio, presumably reflecting an increase in $\Delta\psi_m$. Data represent the mean ± S.E. of 21 to 41 neurons per condition. B, a prolonged exposure to tamoxifen (100 μM) causes an increase in the $\Delta\psi_m$ followed by a pronounced decrease in $\Delta\psi_m$. Data represent the mean ± S.E. of 14 neurons from a single culture date and are representative of data collected from a total of three experiments.

bition and neuronal damage when injected into the striatum (Fig. 5A). Glutamate receptor antagonists inhibit this neuronal damage, reflecting an excitotoxic component of this neuronal injury (data not shown) (Greene and Greenamyre, 1995; Schulz et al., 1996). Tamoxifen (2 mg/kg i.p. 2 h before and 4 h after striatal malonate injection) did not reduce the volume of the striatal lesion (Fig. 5B). Doses of tamoxifen from 1 to 20 mg/kg were tested and none prevented the striatal damage caused by malonate (Fig. 5C).

Discussion

We found that glutamate (100 μM) causes a robust mitochondrial depolarization that is partially inhibited by tamoxifen. The maximum inhibitory concentration of tamoxifen was 0.3 μM, with concentrations higher and lower than 0.3 μM being less effective. Tamoxifen (0.3 μM) did not inhibit glutamate receptor-activated increases in intracellular Ca^{2+}, suggesting that it does not directly inhibit receptor activation, nor does it appear to inhibit $[Ca^{2+}]_i$ buffering after a glutamate stimulus. Therefore, a decrease in glutamate-in-

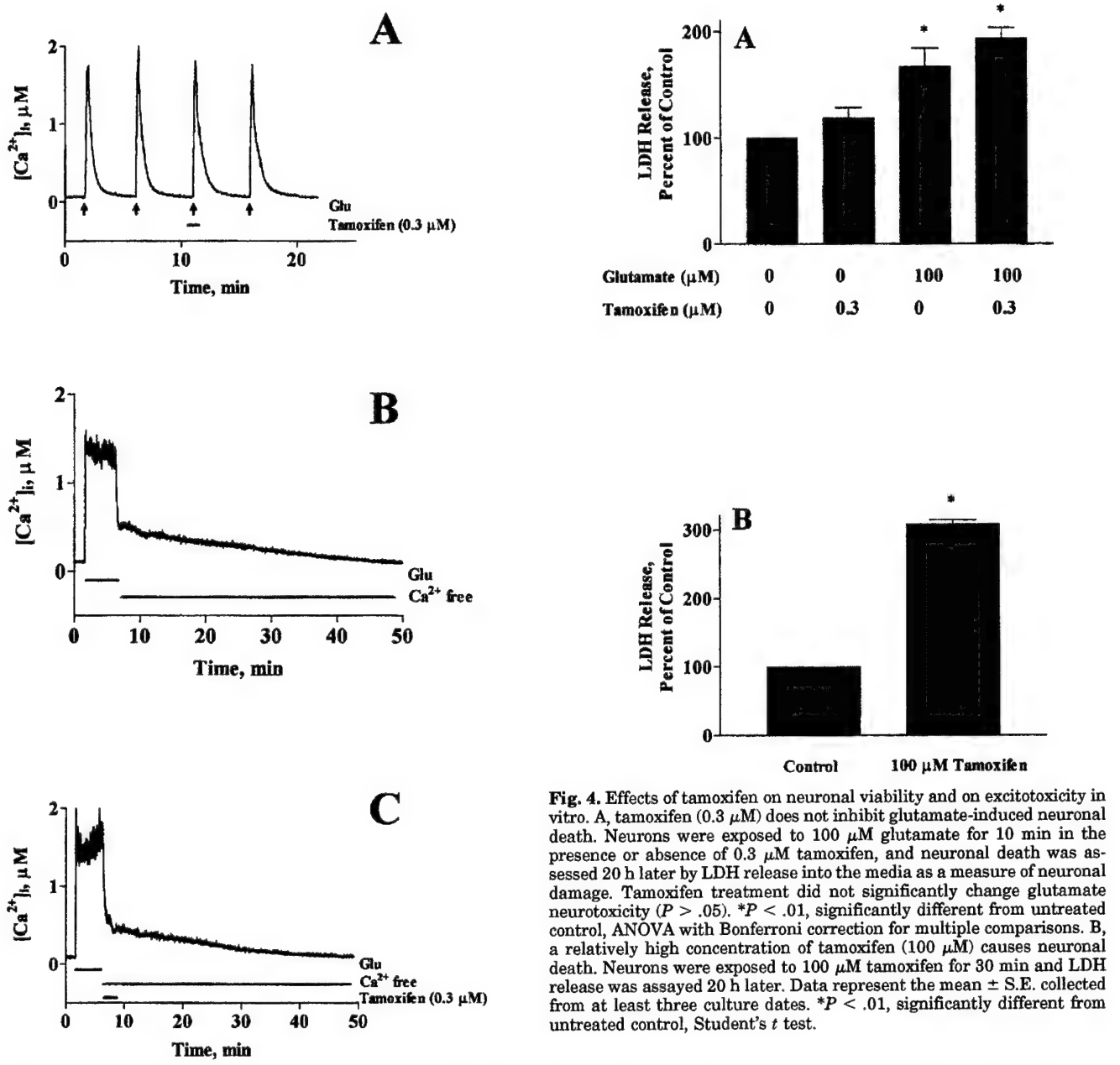

Fig. 3. Tamoxifen did not inhibit glutamate-induced increases in $[Ca^{2+}]_i$. A, indo-1-loaded neurons were exposed to 15-s pulses of 3 μM glutamate/1 μM glycine (arrows). When tamoxifen (0.3 μM) was included before and during the glutamate stimulus, there was no alteration in the $[Ca^{2+}]_i$ increase induced by glutamate. Data are representative of Ca^{2+} traces collected from seven neurons. B, tamoxifen does not affect $[Ca^{2+}]_i$ recovery after a glutamate stimulus. Neurons were exposed to 100 μM glutamate/1 μM glycine for 5 min and then immediately exposed to Ca^{2+}-free HBSS or tamoxifen (0.3 μM) in Ca^{2+}-free HBSS for 2 min immediately after glutamate exposure. Note that there is no apparent effect of tamoxifen on the rate or shape of the $[Ca^{2+}]_i$ recovery. Data are representative of Ca^{2+} traces collected from five to seven additional neurons.

Fig. 4. Effects of tamoxifen on neuronal viability and on excitotoxicity in vitro. A, tamoxifen (0.3 μM) does not inhibit glutamate-induced neuronal death. Neurons were exposed to 100 μM glutamate for 10 min in the presence or absence of 0.3 μM tamoxifen, and neuronal death was assessed 20 h later by LDH release into the media as a measure of neuronal damage. Tamoxifen treatment did not significantly change glutamate neurotoxicity ($P > .05$). *$P < .01$, significantly different from untreated control, ANOVA with Bonferroni correction for multiple comparisons. B, a relatively high concentration of tamoxifen (100 μM) causes neuronal death. Neurons were exposed to 100 μM tamoxifen for 30 min and LDH release was assayed 20 h later. Data represent the mean ± S.E. collected from at least three culture dates. *$P < .01$, significantly different from untreated control, Student's t test.

duced $[Ca^{2+}]_i$ levels by tamoxifen is unlikely to explain the inhibitory effect of tamoxifen on mitochondrial $\Delta\psi_m$ depolarization.

Tamoxifen did not completely inhibit glutamate-induced $\Delta\psi_m$ depolarization. This is similar to what we have previously reported for other PTP inhibitors, namely, cyclosporin A, trifluoperazine, and dibucaine (White and Reynolds, 1996; Hoyt et al., 1997; Scanlon and Reynolds, 1998). This may be a matter of time of onset of action of the particular drug, or its duration of action. There are other Ca^{2+}-stimulated effects on mitochondria in addition to activation of the PTP that would result in dissipation of $\Delta\psi_m$, including mitochondrial Ca^{2+} cycling (Nicholls and Akerman, 1982) and ATP synthesis. Because we are not measuring PTP activation directly and are unable to do so as yet in intact neurons, we cannot differentiate between PTP activation and other direct effects of glutamate receptor activation on $\Delta\psi_m$. Therefore, definitive conclusions about the role of PTP activation in glutamate-induced mitochondrial depolarization cannot be drawn from the results presented herein. The numerous additional effects of these agents on other cellular signal transduction mechanisms such as calcineurin, calmodulin, and protein kinase C complicate the interpretation of effects of these drugs (Levin and Weiss, 1979; Liu et al., 1991; Rowlands et al., 1995; Gundimeda et al., 1996).

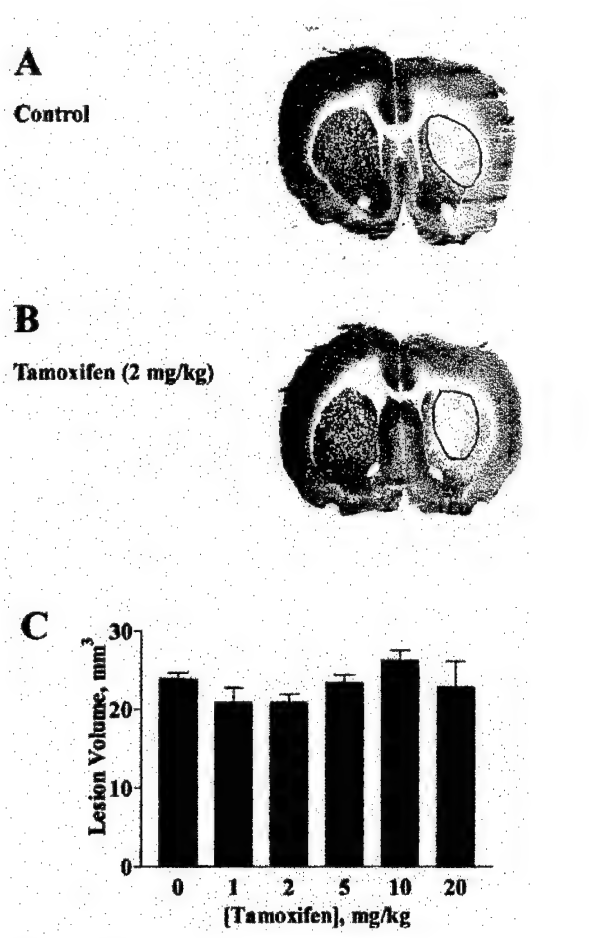

Fig. 5. Tamoxifen does not inhibit formation of striatal lesions induced by malonate. A, injection of malonate into the rat striatum induces a lesion that was visualized 7 days postinjection by staining for cytochrome oxidase. B, treatment with 2 mg/kg tamoxifen 2 h before and 4 h after malonate injection did not decrease the size of the malonate-induced lesion. C, a range of tamoxifen doses (1–20 mg/kg) did not protect against striatal malonate lesion formation. Data represent the mean ± S.E. collected from 3 to 13 rats per condition.

The lack of inhibition of glutamate-induced depolarization by tamoxifen at higher concentrations is puzzling. It is possible that at lower concentrations, tamoxifen has a relatively selective effect on glutamate-mediated $\Delta\psi_m$ depolarization, whereas at higher concentrations, its membrane-disruptive effects interact with the glutamate-induced mitochondrial dysfunction, leading to a lack of inhibition at these tamoxifen concentrations. These higher tamoxifen concentrations caused an increase in $\Delta\psi_m$. It is possible that tamoxifen affects one of a number of mitochondrial functions that could result in hyperpolarization. Among these possibilities are inhibition of the mitochondrial Na^+/Ca^{2+} exchanger, the F_1F_o-ATPase or a direct ionophore effect similar to nigericin (White and Reynolds, 1996; Hoyt et al., 1997), or inhibition of spontaneous depolarizing events (Duchen et al., 1998). These possible mechanisms remain to be tested. High micromolar concentrations of tamoxifen induce rapid apoptotic death in neural cell lines (a finding that we confirmed in our primary cultures) (Ellerby et al., 1997; Hashimoto et al., 1997). The inability of tamoxifen-primed mitochondria to initiate apoptosis in naïve cell extracts suggests that nuclear or cell membrane associated caspases mediate the major component of tamoxifen-induced programmed cell death (Ellerby et al., 1997).

Cyclosporin A inhibits glutamate-induced neuronal death in vitro, although the interpretation of the mechanism of this neuroprotective effect is complicated by the multiple effects that cyclosporin A has on cellular function, including inhibition of PTP as well as calcineurin activation (Dawson et al., 1993; Ankarcrona et al., 1996; Schinder et al., 1996; White and Reynolds, 1996). Because tamoxifen inhibited glutamate-induced $\Delta\psi_m$ depolarization in a manner similar to that of cyclosporin A, we were interested to see whether tamoxifen protected neurons from glutamate-induced injury. Tamoxifen did not inhibit glutamate-induced neuronal death, suggesting that PTP activation is not a major contributor to the death caused by glutamate and that other actions of cyclosporin A explain its neuroprotective effect. We also tested whether tamoxifen could lessen the neuronal injury caused by excitotoxic injury to the striatum in an intact animal. Tamoxifen was not an effective inhibitor of striatal injury at the doses tested (1–20 mg/kg). Clinical doses of tamoxifen in humans are 0.4 to 0.8 mg/kg, causing an acute serum concentration of ~0.07 μM and chronic (after 3 months) steady-state concentrations of ~0.2 μM (Physicians' Desk Reference, 1997). Because tamoxifen is very lipophilic, it is likely that tissue concentrations are higher than the serum concentration. It is possible that a higher and more prolonged tamoxifen exposure than used herein would be neuroprotective. The lack of effect in primary culture argued against further testing this in vivo.

The inhibition of glutamate-induced mitochondrial depolarization by tamoxifen is consistent with its reported action as an inhibitor of PTP activation, although processes other than PTP activation may explain the decrease in $\Delta\psi_m$ caused by glutamate receptor activation. Given the lack of specificity of tamoxifen and other PTP inhibitors and the difficulties in measuring PTP in intact cells, conclusions about the role of PTP in glutamate-induced mitochondrial depolarization and excitotoxic injury are not yet possible and await the development of selective PTP inhibitors, as well as a reliable assay for PTP activation in intact cells.

Acknowledgments

We thank Geraldine Kress for preparation of neuronal cultures and Dr. Kendall Wallace for helpful discussion.

References

Ankarcrona M, Dypbukt JM, Orrenius S and Nicotera P (1996) Calcineurin and mitochondrial function in glutamate-induced neuronal cell death. *FEBS Lett* **394:** 321–324.

Bindokas VP, Jordan J, Lee CC and Miller RJ (1996) Superoxide production in rat hippocampal neurons: Selective imaging with hydroethidine. *J Neurosci* **16:**1324–1336.

Broekemeier KM, Dempsey ME and Pfeiffer DR (1989) Cyclosporin A is a potent inhibitor of the inner membrane permeability transition in liver mitochondria. *J Biol Chem* **264:**7826–7830.

Budd SL and Nicholls DG (1996) Mitochondria, calcium regulation, and acute glutamate excitotoxicity in cultured cerebellar granule cells. *J Neurochem* **67:**2282–2291.

Choi DW (1988) Glutamate neurotoxicity and diseases of the nervous system. *Neuron* **1:**623–634.

Custodio JB, Dinis TC, Almeida LM and Madeira VM (1994) Tamoxifen and hydroxytamoxifen as intramembraneous inhibitors of lipid peroxidation. Evidence for peroxyl radical scavenging activity. *Biochem Pharmacol* **47:**1989–1998.

Custodio JBA, Moreno AJM and Wallace KB (1998) Tamoxifen inhibits induction of the mitochondrial permeability transition by Ca^{2+} and inorganic phosphate. *Toxicol Appl Pharmacol* **152:**10–17.

Dawson TM, Steiner JP, Dawson VL, Dinerman JL, Uhl GR and Snyder SH (1993) Immunosuppressant FK506 enhances phosphorylation of nitric oxide synthase and protects against glutamate neurotoxicity. *Proc Natl Acad Sci USA* **90:**9808–9812.

Duchen MR, Leyssens A and Crompton M (1998) Transient mitochondrial depolarizations reflect focal sarcoplasmic reticular calcium release in single rat cardiomyocytes. *J Cell Biol* **142:**975–988.

Dugan LL, Sensi SL, Canzoniero LM, Handran SD, Rothman SM, Lin TS, Goldberg MP and Choi DW (1995) Mitochondrial production of reactive oxygen species in cortical neurons following exposure to *N*-methyl-D-aspartate. *J Neurosci* **15:**6377–6388.

Ellerby HM, Martin SJ, Ellerby LM, Naiem SS, Rabizadeh S, Salvesen GS, Casiano CA, Cashman NR, Green DR and Bredesen DE (1997) Establishment of a cell-free system of neuronal apoptosis: Comparison of premitochondrial, mitochondrial, and postmitochondrial phases. *J Neurosci* **17:**6165–6178.

Greene JG and Greenamyre JT (1995) Characterization of the excitotoxic potential of the reversible succinate dehydrogenase inhibitor malonate. *J Neurochem* **64:**430–436.

Gundimeda U, Chen ZH and Gopalakrishna R (1996) Tamoxifen modulates protein kinase C via oxidative stress in estrogen receptor-negative breast cancer cells. *J Biol Chem* **271:**13504–13514.

Hartnett KA, Stout AK, Rajdev S, Rosenberg PA, Reynolds IJ and Aizenman E (1997) NMDA receptor-mediated neurotoxicity: A paradoxical requirement for extracellular Mg^{2+} in Na^+/Ca^{2+}-free solutions in rat cortical neurons in vitro. *J Neurochem* **68:**1836–1845.

Hashimoto M, Inoue S, Muramatsu M and Masliah E (1997) Estrogens stimulate tamoxifen-induced neuronal cell apoptosis in vitro: A possible nongenomic action. *Biochem Biophys Res Commun* **240:**464–470.

Hoyt KR and Reynolds IJ (1998) Alkalinization prolongs recovery from glutamate-induced increases in intracellular Ca^{2+} concentration by enhancing Ca^{2+} efflux through the mitochondrial Na^+/Ca^{2+} exchanger in cultured rat forebrain neurons. *J Neurochem* **71:**1051–1058.

Hoyt KR, Sharma TA and Reynolds IJ (1997) Trifluoperazine and dibucaine-induced inhibition of glutamate-induced mitochondrial depolarization in rat cultured forebrain neurones. *Br J Pharmacol* **122:**803–808.

Hoyt KR, Stout AK, Cardman JM and Reynolds IJ (1998) The role of intracellular Na^+ and mitochondria in buffering of kainate-induced intracellular free Ca^{2+} changes in rat forebrain neurones. *J Physiol (Lond)* **509:**103–116.

Kroemer G, Dallaporta B and Resche-Rigon M (1998) The mitochondrial death/life regulator in apoptosis and necrosis. *Annu Rev Physiol* **60:**619–642.

Lemasters JJ, Nieminen AL, Qian T, Trost LC and Herman B (1997) The mitochondrial permeability transition in toxic, hypoxic and reperfusion injury. *Mol Cell Biochem* **174:**159–165.

Levin RM and Weiss B (1979) Selective binding of antipsychotics and other psychoactive agents to the calcium-dependent activator of cyclic nucleotide phosphodiesterase. *J Pharmacol Exp Ther* **208:**454–459.

Liu J, Farmer JD Jr, Lane WS, Friedman J, Weissman I and Schreiber SL (1991) Calcineurin is a common target of cyclophilin-cyclosporin A and FKBP-FK506 complexes. *Cell* **66:**807–815.

Mayer ML and Westbrook GL (1987) The physiology of excitatory amino acids in the vertebrate central nervous system. *Prog Neurobiol* **28:**197–276.

McLaughlin BA, Nelson D, Erecinska M and Chesselet MF (1998) Toxicity of dopamine to striatal neurons in vitro and potentiation of cell death by a mitochondrial inhibitor. *J Neurochem* **70:**2406–2415.

Nicholls D and Akerman K (1982) Mitochondrial calcium transport. *Biochim Biophys Acta* **683:**57–88.

Nieminen AL, Petrie TG, Lemasters JJ and Selman WR (1996) Cyclosporin A delays mitochondrial depolarization induced by *N*-methyl-D-aspartate in cortical neurons—Evidence of the mitochondrial permeability transition. *Neuroscience* **75:**993–997.

Physicians' Desk Reference (1997) Medical Economics Company, Montvale, NJ.

Reers M, Smith TW and Chen LB (1991) J-aggregate formation of a carbocyanine as a quantitative fluorescent indicator of membrane potential. *Biochemistry* **30:**4480–4486.

Reynolds IJ and Hastings TG (1995) Glutamate induces the production of reactive oxygen species in cultured forebrain neurons following NMDA receptor activation. *J Neurosci* **15:**3318–3327.

Rowlands MG, Budworth J, Jarman M, Hardcastle IR, McCague R and Gescher A (1995) Comparison between inhibition of protein kinase C and antagonism of calmodulin by tamoxifen analogues. *Biochem Pharmacol* **50:**723–726.

Savage MK and Reed DJ (1994) Release of mitochondrial glutathione and calcium by a cyclosporin A-sensitive mechanism occurs without large amplitude swelling. *Arch Biochem Biophys* **315:**142–152.

Scanlon JM and Reynolds IJ (1998) Effects of oxidants and glutamate receptor activation on mitochondrial membrane potential in rat forebrain neurons. *J Neurochem* **71:**2392–2400.

Schinder AF, Olson EC, Spitzer NC and Montal M (1996) Mitochondrial dysfunction is a primary event in glutamate neurotoxicity. *J Neurosci* **16:**6125–6133.

Schulz JB, Matthews RT, Henshaw DR and Beal MF (1996) Neuroprotective strategies for treatment of lesions produced by mitochondrial toxins: Implications for neurodegenerative diseases. *Neuroscience* **71:**1043–1048.

Stout AK, Raphael HM, Kanterewicz BI, Klann E and Reynolds IJ (1998) Glutamate-induced neuron death requires mitochondrial calcium uptake. *Nat Neurosci* **1:**366–373.

White RJ and Reynolds IJ (1995) Mitochondria and Na^+/Ca^{2+} exchange buffer glutamate-induced calcium loads in cultured cortical neurons. *J Neurosci* **15:**1318–1328.

White RJ and Reynolds IJ (1996) Mitochondrial depolarization in glutamate-stimulated neurons—An early signal specific to excitotoxin exposure. *J Neurosci* **16:**5688–5697.

White RJ and Reynolds IJ (1997) Mitochondria accumulate Ca^{2+} following intense glutamate stimulation of cultured rat forebrain neurons. *J Physiol (Lond)* **498.1:**31–47.

Zoratti M and Szabo I (1995) The mitochondrial permeability transition. *Biochim Biophys Acta* **1241:**139–176.

Send reprint requests to: Ian J. Reynolds, Ph.D., Department of Pharmacology, University of Pittsburgh School of Medicine, E1354 Biomedical Science Tower, Pittsburgh, PA 15261. E-mail: ianmda@pop.pitt.edu

Cellular/Molecular

Glutamate Decreases Mitochondrial Size and Movement in Primary Forebrain Neurons

Gordon L. Rintoul, Anthony J. Filiano, Jacques B. Brocard, Geraldine J. Kress, and Ian J. Reynolds
Department of Pharmacology, University of Pittsburgh, Pittsburgh, Pennsylvania 15261

Mitochondria are essential to maintain neuronal viability. In addition to the generation of ATP and maintenance of calcium homeostasis, the effective delivery of mitochondria to the appropriate location within neurons is also likely to influence their function. In this study we examined mitochondrial movement and morphology in primary cultures of rat forebrain using a mitochondrially targeted enhanced yellow fluorescent protein (mt-eYFP). Mt-eYFP-labeled mitochondria display a characteristic elongated phenotype and also move extensively. Application of glutamate to cultures results in a rapid diminution of movement and also an alteration from elongated to rounded morphology. This effect required the entry of calcium and was mediated by activation of the NMDA subtype of glutamate receptor. Treatment of cultures with an uncoupler or blocking ATP synthesis with oligomycin also stopped movement but did not alter morphology. Interestingly, application of glutamate together with the uncoupler did not prevent the changes in movement or shape but facilitated recovery after washout of the stimuli. This suggests that the critical target for calcium in this paradigm is cytosolic. These studies demonstrate that in addition to altering the bioenergetic properties of mitochondria, neurotoxins can also alter mitochondrial movement and morphology. We speculate that neurotoxin-mediated impairment of mitochondrial delivery may contribute to the injurious effects of neurotoxins.

Key words: green fluorescent protein; cytoskeleton; NMDA receptor; intracellular calcium; excitotoxicity; organelle transport

Introduction

It is widely appreciated that mitochondria in neurons are the target of a number of neurotoxins. These include agents such as rotenone, 1-methyl-4-phenyl-1,2,3,6-tetrahydropyridine (MPTP), and 3-nitroproprionic acid, and perhaps zinc, that impair mitochondrial electron transport and probably kill neurons by a combination of ATP depletion and excessive generation of reactive oxygen species (ROS) (Heales et al., 1999; Schapira, 1999; Beal, 2000; Weiss et al., 2000). Mitochondria also represent an important target in NMDA receptor-mediated excitotoxic neuronal injury. In this case, excessive calcium entry results in substantial mitochondrial calcium accumulation, mitochondrial depolarization, ROS generation, and, ultimately, cell death (Dugan et al., 1995; Reynolds and Hastings, 1995; White and Reynolds, 1995, 1996; Schinder et al., 1996; Nicholls and Budd, 2000). The neurotoxic effects of NMDA receptor activation can be occluded by prevention of mitochondrial calcium accumulation, suggesting that mitochondria are one of the critical targets of cellular calcium overload (Budd and Nicholls, 1996; Stout et al., 1998).

Studies on the role of mitochondria in neuronal injury have generally focused on the bioenergetic consequences of mitochondrial impairment; however, there are several important dynamics to consider that extend beyond the capacity of mitochondria to generate ATP and ROS. Mitochondria are semi-autonomous organelles that are capable of replicating their own genome, synthesizing proteins, and undergoing fission and fusion, and presumably degradation too (for review, see Scheffler, 1999). It is widely believed (although not necessarily proven) that new mitochondria are generated near the nucleus (Davis and Clayton, 1996), where they can import the large cohort of nuclear-encoded, mitochondrially targeted proteins (Scheffler, 1999). Mitochondria are then transported to appropriate cellular locations (Morris and Hollenbeck, 1993; Ligon and Steward, 2000a) that, in the case of neurons, may be a substantial distance from the presumed site of biogenesis at the cell soma. Alterations in mitochondrial distribution and morphology have been associated with various disease states. Ebneth and colleagues (1998) reported that overexpression of tau results in the failure of the cell to transport mitochondria to peripheral cell compartments, which may be of relevance to Alzheimer's disease. Alterations in mitochondrial transport and morphology have also been associated with cancer (Djaldetti, 1982), liver disease (Tandler and Hoppel, 1986), and muscular dystrophy (Nishino et al., 1998).

It is becoming clear that mitochondrial morphology is a dynamic that can be altered by a number of factors, including the induction of cell injury. Mitochondrial fragmentation has been reported in cells stimulated to undergo apoptosis, and prevention of fragmentation may be cytoprotective (Jouaville et al., 1999; Frank et al., 2001). Previous studies have also suggested calcium-mediated alterations in mitochondrial morphology in neurons and astrocytes (Kristal and Dubinsky, 1997; Dubinsky and Levi,

Received Feb. 24, 2003; revised June 23, 2003; accepted July 2, 2003.

These studies were supported by U.S. Army Medical Research and Materiel Command Neurotoxin Research Initiative Grant DAMD 17–98-1–8269 (I.J.R.) and Human Frontiers Science Program Grant LT0500/1999/B (J.B.B.). We thank Dr. Roger Y. Tsien for providing the mt-eYFP construct.

Correspondence should be addressed to Ian J. Reynolds, Department of Pharmacology, University of Pittsburgh, W1351 Biomedical Science Tower, Pittsburgh PA 15261. E-mail: iannmda@pitt.edu.

J. B. Brocard's present address: Département de Réponse et de Dynamique Cellulaires, laboratoire Canaux Ioniques et Signalisation, 38054 Grenoble Cedex, France.

 0270-6474/03/237881-08$15.00/0

Table 1. Summary of effects of various treatments on mitochondrial morphology and movement

	Reduction in movement	Change in morphology
0 Ca^{2+}	No	No
Glutamate	Yes	Yes
Glutamate 0 Ca^{2+}	No	No
750 nm FCCP	Yes	No
10 μM Oligomycin	Yes	No
Glutamate + FCCP	Yes	Yes
5 μM 4-Br-A23187	Yes	Yes
100 μM NMDA	Yes	Yes
Glutamate + 5 μM MK801	No	No
100 μM Kainate	No	No

1998). In the present study we have investigated characteristics of mitochondrial movement and morphology in primary cultures of forebrain neurons transfected with mitochondrially targeted fluorescent proteins. We have found that mitochondrial depolarization inhibits movement of mitochondria in processes; however, glutamate both inhibits movement and causes a profound remodeling of mitochondria as the result of an action of calcium in the cytosol of neurons. The rate of recovery of mitochondria from this insult is promoted when mitochondrial calcium loading is prevented. These studies reveal a novel aspect of glutamate-mediated injury to neurons and raise the possibility that altered mitochondrial morphology or trafficking might contribute to neuronal injury.

Some of these results have been published previously in abstract form (Rintoul et al., 2002).

Materials and Methods

DNA constructs. The mitochondrially targeted eYFP construct (generously provided by Dr. Roger Y. Tsien, University of California, San Diego) consists of the gene for eYFP, inserted into the mammalian expression vector pCDNA3 (Invitrogen). The recombinant protein is targeted to the mitochondrial matrix using the targeting sequence from subunit IV of cytochrome *c* oxidase (Llopis et al., 1998). All other fluorescent protein expression vectors were purchased from Clontech. The cytosolic eCFP vector was constructed by excising the enhanced cyan fluorescent protein (eCFP) gene from peCFP-mito with *Bam*HI and *Not*I. This fragment was then inserted into the *Bam*HI and *Not*I restriction sites of the pHcRed1-N1 expression vector (replacing the HcRed gene). All plasmids were amplified using Qiagen Maxi- and Mega-prep kits according to the manufacturer's instructions.

Transfection of cortical cultures. Experiments were performed on dissociated primary cortical cultures, used between 12 and 19 d *in vitro*. Details of the culturing technique have been described previously (Kress et al., 2002). At this age in culture they are synaptically connected and vulnerable to excitotoxic cell death. Neurons were transfected using a modified calcium phosphate transfection technique (Xia et al., 1996). This typically results in transfection efficiencies of 1–2%. Neurons were imaged 2–3 d after transfection.

Analysis of mitochondrial movement. Data were acquired using an acquisition system described previously (Buckman and Reynolds, 2001). Simple PCI software (Compix, Inc., Cranberry PA) was used for data acquisition. In all experiments we used a HEPES-buffered salt solution (HBSS) of the following composition (in mM): 137 NaCl, 5 KCl, 10 $NaHCO_3$, 20 HEPES, 5.5 glucose, 0.6 KH_2PO_4, 0.6. Na_2HPO_4, 1.4 $CaCl_2$, and 0.9 $MgSO_4$, adjusted to pH 7.4 with NaOH. In Ca^{2+}-free experiments, Ca^{2+} was omitted and the buffer was supplemented with 20 μM EGTA. All drugs used were purchased from Sigma (St. Louis, MO). Working solutions were prepared in HBSS from the following stock solutions: 10 mM glutamate in water, 10 mM glycine in water, 750 μM carbonylcyanide-p-(trifluoromethoxy)-phenylhydrazone (FCCP) in methanol, 10 mM kainate in water, and 10 mM NMDA in water. Cells were perfused with 5 ml/min HBSS for the duration of each experiment, and the chamber temperature was maintained at 37°C by heating the buffer.

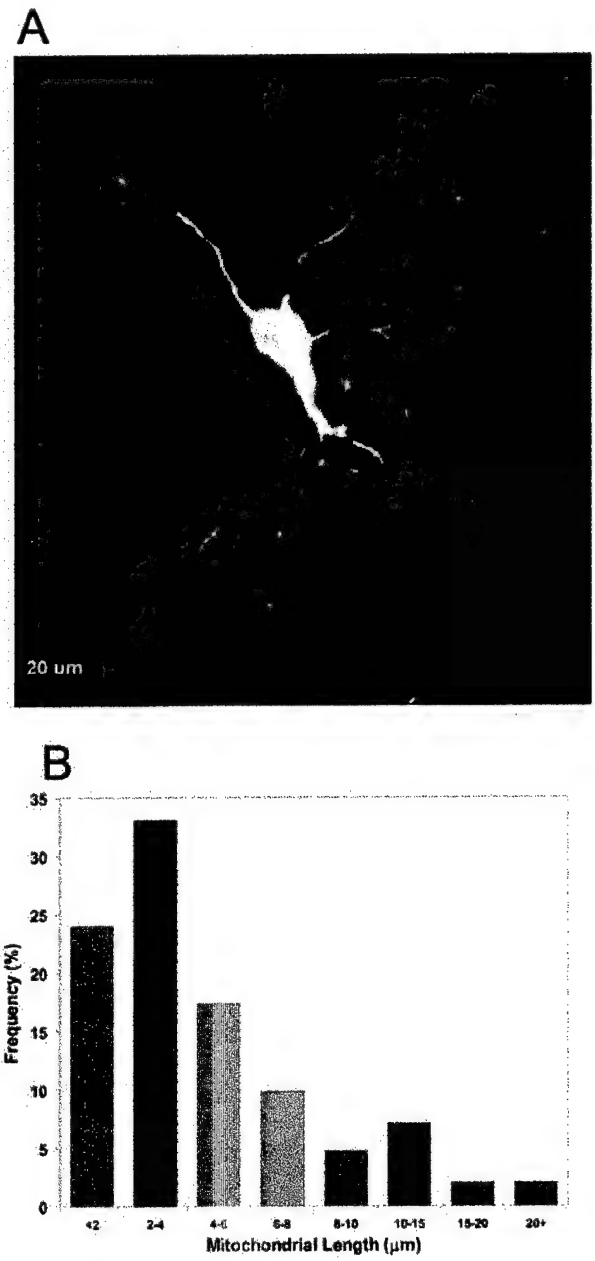

Figure 1. Identification and measurement of mitochondrial length. *A*, A fluorescence micrograph of a single cortical neuron transfected with mitochondrially targeted eYFP (grayscale image). Selected groups of mitochondria have been color coded to correspond to selected bins in the frequency histogram below. *B*, Frequency distribution of mitochondrial lengths. A representative frequency distribution derived from the above micrograph. This figure is representative of 10 additional fields in which mitochondrial length was determined.

Mitochondrial movement was detected by monitoring the fluorescence intensity of individual pixels in digitized images of fields containing a single transfected neuron. Twenty fluorescence digital images of a field were collected over 2 min. A 255 × 255 pixel subfield containing neuronal processes was selected for analysis of mitochondrial movement. Pixel intensities in successive images were subtracted. A "movement event" for each pixel was registered if the change in pixel fluorescence between successive fields exceeded 20 fluorescence units; i.e., movement was detected as an increase or decrease in individual pixel intensity over time. The threshold value of 20 fluorescence units was determined em-

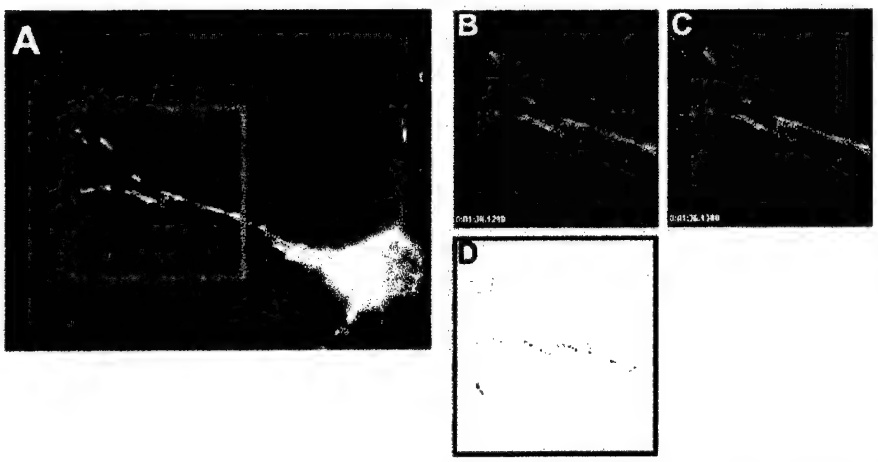

Figure 2. Measuring mitochondrial movement between two frames (see Materials and Methods). *A*, Collected image field. A 255 × 255 pixel subregion is selected for analysis. Individual pixel fluorescence values from successive images (*B*, *C*) are subtracted. *D*, Threshold difference image. Dark pixels indicate "events" where change in pixel fluorescence exceeds a threshold value (20 fluorescence units). Pixel events for 20 successive images (2 min) were summated in each experiment.

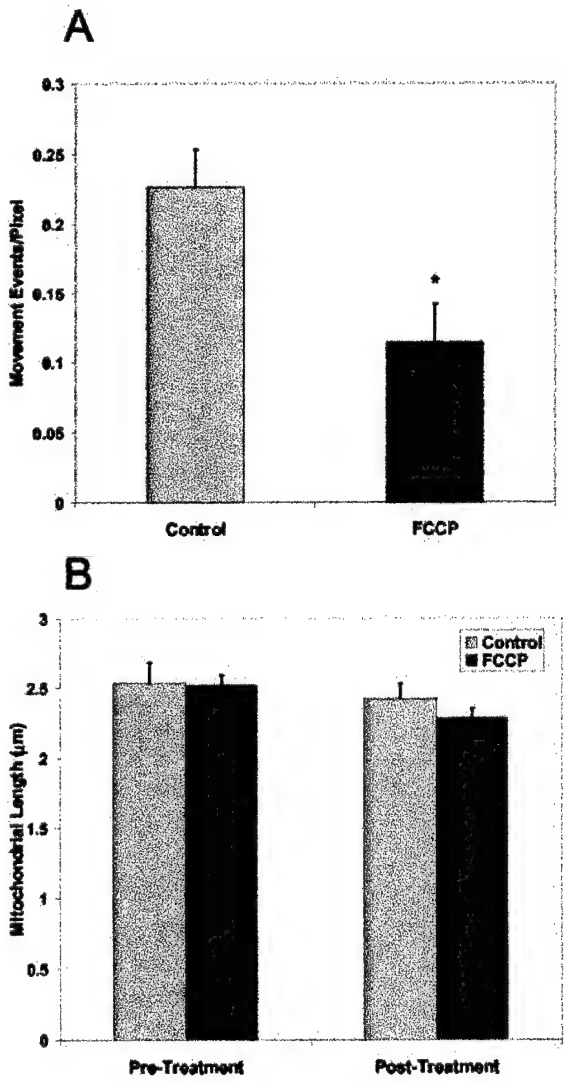

Figure 3. Effect of FCCP on mitochondrial movement and morphology. *A*, Mean movement events per pixel measured after treatment with 750 nM FCCP. *B*, Mean mitochondrial length after treatment of transfected cells with 750 nM FCCP. *Significantly different from control ($p < 0.05$; *t* test; control, $n = 10$; FCCP, $n = 7$).

pirically; using a masking function in the SimplePCI software, mitochondria were found to be well defined by pixels 20 U above background fluorescence. A quantitative measure of mitochondrial movement was obtained by summating movement events in a field over 2 min. Events were normalized by dividing the pixel events per field by the total number of pixels occupied by mitochondria. The analysis of mitochondrial movement described above was performed using custom Visual Basic macros. Determination of mitochondrial length and roundness was performed with a masking function in the SimplePCI software. The degree of mitochondrial roundness was calculated using the measured area and perimeter of identified objects and the following equation: roundness = $4\pi\text{Area}/\sqrt{\text{perimeter}}$. Statistical comparisons between treatment groups were performed using Student's unpaired *t* tests.

Results

Mitochondrial size and movement

In this study we have made use of mt-eYFP to label neuronal mitochondria. Using calcium phosphate we routinely obtained 1–2% transfection efficiency. With this efficiency the density of transfected cells was such that typically a single labeled cell was present per field, although sometimes additional labeled processes traversed the field. The imaging conditions were optimized to record individual mitochondria in processes, with the result that cell bodies were usually overexposed. The limited extent of labeling provided relatively simple images that were amenable to semi-automated image analysis. Thus, we were able to determine the characteristics of mitochondrial length quite readily (Fig. 1). Size varied considerably, but the numerical majority of objects was relatively small. This probably reflects the presence of bright, small mitochondria as well as marginally labeled organelles with fluorescence intensity that did not exceed threshold for the entire length of the organelle. The preponderance of small objects in these images diminishes the impact of the modest number of long mitochondria on the mean length, although the latter objects tend to stand out on visual examination of the images.

We also used semi-automated approaches to estimate movement (Fig. 2). To determine the overall movement in a field, we used an approach that involves subtraction of adjacent images of movies and then counted events that were defined as bright-to-dark or dark-to-bright transitions of individual pixels that exceeded an arbitrarily defined threshold. These events were summed over 2 min of data acquisition (20 frames). Typically, this approach identified 5,000–20,000 events per 2 min period. In cells that had been fixed in paraformaldehyde before imaging, the number of events detected in the same time frame was typically <20, indicating that the noise associated with the recording system did not make a meaningful contribution to this signal. This method detects both directed movement of objects as well as lateral movement of otherwise stationary objects ("wiggling"), although the latter type of movement was quite limited in mitochondria constrained within processes. We also tracked individual objects using the object tracking module of Simple PCI to determine the velocity of the most rapidly moving objects within fields. We visually identified individual objects from eight different fields of cells on the basis of their rapid movement and estimated a mean velocity of 0.63 ± 0.09 m/sec. These rapidly moving mitochondria were inevitably small in length.

Stimulus-induced alterations in size and movement

We next examined the effects of the mitochondrial uncoupler FCCP, which rapidly dissipates the mitochondrial membrane potential. This can deplete cellular ATP both by preventing its synthesis and also by consumption of ATP by the F_1F_O ATPase. A 5 min application of FCCP promptly decreased the movement of mitochondria without altering mitochondrial size (Fig. 3). This suggests that movement requires an adequate ATP supply, an intact mitochondrial membrane potential, or possibly both; however, treatment with 10 μM oligomycin produced a similar attenuation of mitochondrial movement (Fig. 4*C*). This suggests that local depletion of ATP and not changes in membrane potential may impede the movement of mitochondria.

Exposure of neurons to 30 μM glutamate with 1 μM glycine produced a somewhat different response. Although the mitochondria clearly stopped moving within 2–4 min of glutamate application, we also noted a profound alteration in mitochondrial morphology over the same time frame (Fig. 4). Thus, mitochondria that were initially thread-like in structure became notably rounded. It is also possible that there was fragmentation, such that individual thread-like objects became more than one rounded object; however, it is difficult to conclusively establish that fragmentation explicitly occurs rather than there being adjacent or overlapping objects that become distinguishable when rounded. Although fragmentation may occur, it is not clear that it would account for the majority of the morphological changes evident in these images. Quantitation of the alteration in both movement and length revealed that glutamate effectively decreased mitochondrial movement and also produced a significant decrease in mitochondrial length (Fig. 4). Sequential analysis of length and object roundness during glutamate exposure indicated that the decrease in length was associated with a simultaneous increase in roundness.

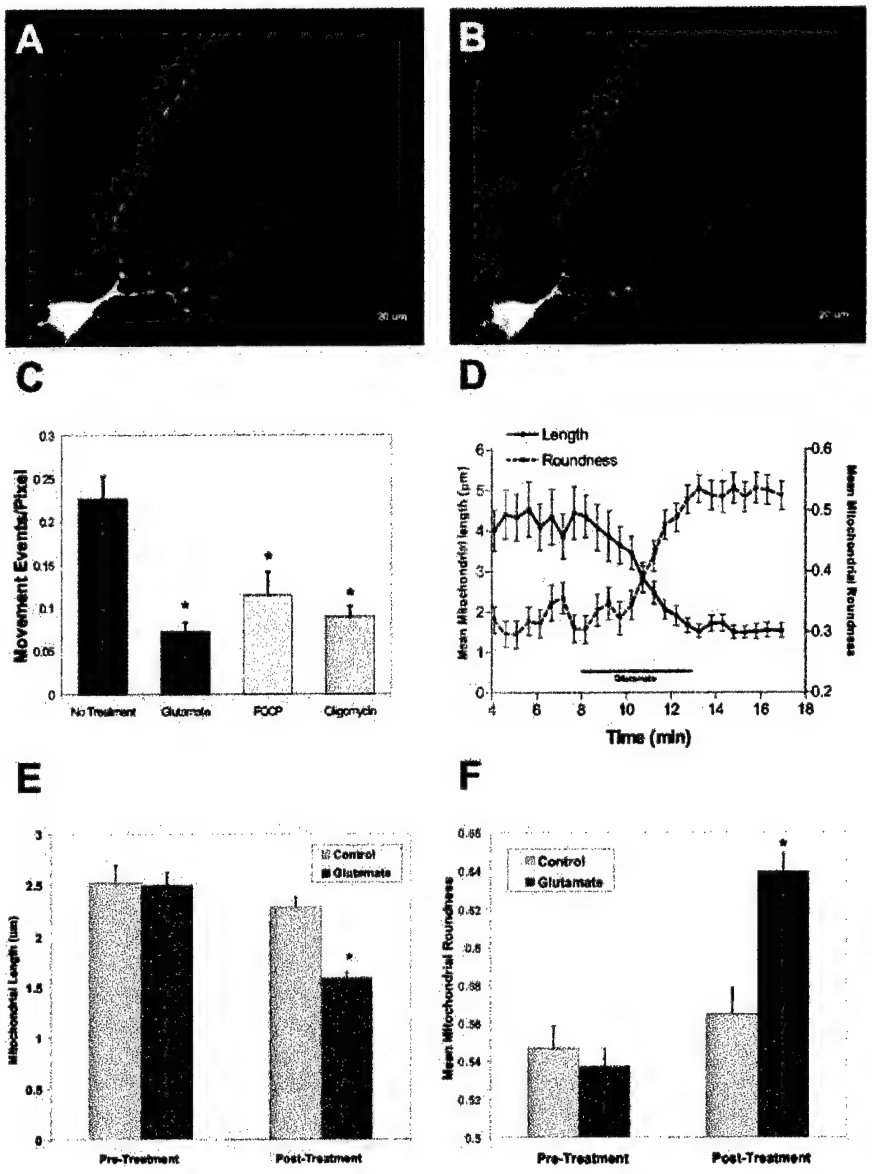

Figure 4. Glutamate induction of mitochondrial remodeling in cortical cultures. Shown are representative micrographs of cortical neurons transfected with mt-eYFP, before (*A*) and after (*B*) a 5 min treatment with 30 μM glutamate/1 μM glycine. *C*, Mean measured mitochondrial movement after treatment of transfected neurons with 30 μM glutamate/1 μM glycine. Reductions in movement after FCCP and oligomycin treatments are show for comparison. *Significantly different from control ($p < 0.05$; *t* test; No Treatment, $n = 7$; Glutamate, $n = 5$; FCCP, $n = 7$; Oligomycin, $n = 7$). *D*, Representative traces of mean mitochondrial length and roundness after treatment with glutamate/glycine, derived from the image sequence shown in *A* and *B*. Similar results were obtained in five additional fields of cells. *E*, Pooled data of mitochondrial length measured after treatment with glutamate/glycine. *Significantly different from control ($p < 0.05$; *t* test; Control, $n = 7$; Glutamate, $n = 10$). *F*, Mean mitochondrial roundness after glutamate/glycine treatment. *Significantly different from control ($p < 0.05$; *t* test; Control, $n = 7$; Glutamate, $n = 10$).

Mechanisms underlying glutamate-induced morphological alteration

An evaluation of the mechanisms underlying this effect of glutamate suggested a critical contribution of NMDA receptors. Applying glutamate in the presence of MK801 (5 μM) completely blocked the effects of the agonist, whereas the application of NMDA (100 μM with 1 μM glycine) also decreased mitochondrial length and diminished movement. Interestingly, kainate (100 μM) did not mimic the effects of glutamate. Given that kainate effectively depolarizes the plasma membrane but results in a much smaller calcium load (Stout and Reynolds, 1999), this observation suggested a key role for a substantial intracellular calcium accumulation. Supporting this hypothesis, treatment of cultures with the calcium ionophore 4-Br-A23187 (5 μM) produced the same effects as glutamate on mitochondrial motility and morphology. Applying glutamate in a calcium-free buffer also completely blocked the effect, indicating that the remodeling was the consequence of NMDA receptor-mediated calcium entry and presumably independent of either plasma membrane depolarization or intracellular sodium accumulation.

We have shown previously that FCCP can protect neurons from glutamate excitotoxicity, ostensibly as the result of preventing mitochondrial calcium accumulation. Interestingly, applying

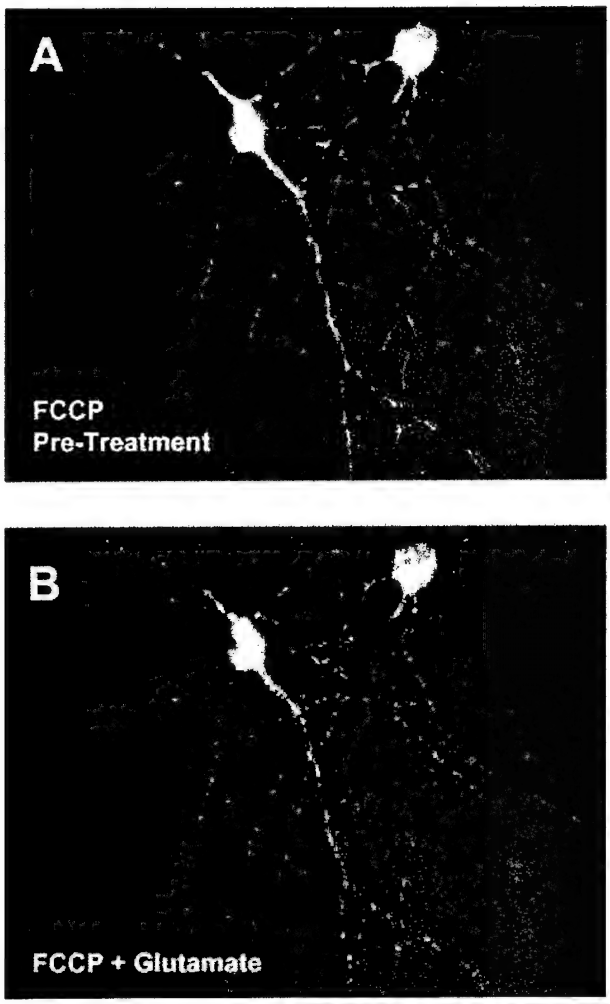

Figure 5. Glutamate-induced mitochondrial remodeling does not require mitochondrial calcium uptake. Shown are representative micrographs of a neuron pretreated (*A*) for 3 min with 750 nM FCCP and then superfused (*B*) with 30 μM glutamate/1 μM glycine in the continued presence of 750 nM FCCP.

glutamate in the presence of FCCP had no impact on the calcium-dependent remodeling of mitochondrial shape (Fig. 5). Under these conditions there is unlikely to be a substantial accumulation of calcium in the mitochondrial matrix, so this finding indicates that the probable locus of action of calcium in this experiment is in the cytosol.

Is the mitochondrial remodeling a consequence of dendrite remodeling?

Previous studies have reported a prompt and reversible alteration in the structure of the processes of cultured neurons in response to NMDA receptor activation (Park et al., 1996) that shows a similar time course to the phenomenon observed here. To evaluate the structure of the dendrites in comparison with the mitochondria, we cotransfected cells with a cytosolic form of CFP along with mt-eYFP. A parallel analysis of the two markers revealed that the mitochondrial remodeling was accompanied by beading of dendrites, so that the structural remodeling appears to occur concomitantly (Fig. 6); however, mitochondria do not appear to be specifically associated with either the swollen varicosities or the narrowed parts of the process. This suggests that it is unlikely that the remodeling is the consequence of the mitochondria essentially being "pinched off" by the alteration in the structure of the dendrite. It is also apparent that although the morphology of the dendrites is clearly altered by glutamate treatment, they remain contiguous rather than fragmented. This indicates that the rounded mitochondria do not simply represent cellular debris at the end of a gross injury process. This conclusion is reinforced by the studies on the recovery of normal morphology described in the next section.

Mitochondrial shape recovers after glutamate exposure

We next sought to determine whether mitochondrial shape recovered after glutamate exposure. We assessed mitochondrial size 1 and 2 hr after glutamate treatment. By 1 hr into the recovery period, the glutamate-treated neurons were still clearly different from controls in that movement was limited and the rounded mitochondria presented as the dominant phenotype. Interestingly, however, neurons exposed to glutamate in the presence of FCCP showed a much greater degree of recovery of morphology at this time point (Fig. 7) and were indistinguishable from controls. At longer time points (2 hr) but before frank injury was apparent, both populations of treated cells had recovered to control values. These data suggest that the FCCP co-treatment facilitated what might be considered a normal recovery process.

Discussion

The main findings of this study are that glutamate, as a consequence of NMDA receptor activation, produces a rapid and substantial remodeling of mitochondrial morphology and also causes a cessation of mitochondrial movement. These previously unappreciated aspects of the action of glutamate at concentrations just sufficient to cause excitotoxic injury suggest that there may be effects of glutamate on mitochondria that extend beyond the bioenergetic and ROS generation effects that we and other laboratories have documented previously. In particular, these findings suggest that neuronal injury might alter the trafficking of mitochondria to cellular destinations where ATP synthesis is required and thus impair cellular function.

There is an emerging appreciation that mitochondrial morphology is a dynamic parameter that may be associated with cell injury. In several different models of apoptosis it has been reported that the normal mitochondrial reticulum becomes fragmented after the application of apoptotic stimuli (Desagher and Martinou, 2000; Frank et al., 2001). Fragmentation of mitochondria may be a consequence of the association of proteins such as dynamin-related protein 1 (DRP1) with mitochondria. Overexpression of this protein causes fragmentation (Frank et al., 2001; Filiano et al., 2002), whereas a dominant-negative form of DRP1 decreases sensitivity to mitochondrially mediated apoptosis (Frank et al., 2001). It is not clear whether such mechanisms are activated by calcium, or even whether DRP1 is normally present in neurons. A different family of proteins appears to mediate fusion of mitochondria (Santel and Fuller, 2001). It is also possible that an inhibition of an ongoing fusion reaction could result in an apparent fragmentation or rounding, although there is no precedent for this kind of effect as far as we are aware.

Alterations in mitochondrial morphology in both neurons and astrocytes in response to calcium loading has also been reported by Dubinsky and colleagues (Kristal and Dubinsky, 1997; Dubinsky and Levi, 1998), who also found that mitochondria changed from a rod-like to spherical morphology when challenged. In these studies the authors concluded that the shape change was caused by mitochondrial permeability transition. Our preliminary experiments indicated that the classic transition

inhibitor cyclosporin A was ineffective in preventing these morphological changes (data not shown). There is also the ambiguity in these studies that the shape change was detected with a membrane potential-sensitive dye under conditions in which the membrane potential is clearly a variable (Schinder et al., 1996; White and Reynolds, 1996; Duchen et al., 1998). Nevertheless, our findings clearly support the morphological conclusions in these earlier reports. The consequence of the alteration in morphology for mitochondrial function is much less clear. It has been proposed that the elongated or reticulated form of mitochondria is beneficial on the basis of studies in cardiac myocytes (Amchenkova et al., 1988). Thus, because of the cable properties of mitochondria, the proton motive force generated by the electron transport chain can be effectively distributed across the reticulum and thus facilitate ATP synthesis. This advantage is hypothetical at this point, however, because it remains unclear whether the ability of mitochondria to generate a proton motive force is spatially limited. Because both FCCP or an excessive calcium load result in mitochondrial depolarization in our experiments, it is difficult to assess mitochondrial function in mitochondria after rounding, so we cannot readily establish whether function is modified as a direct consequence of the shape change.

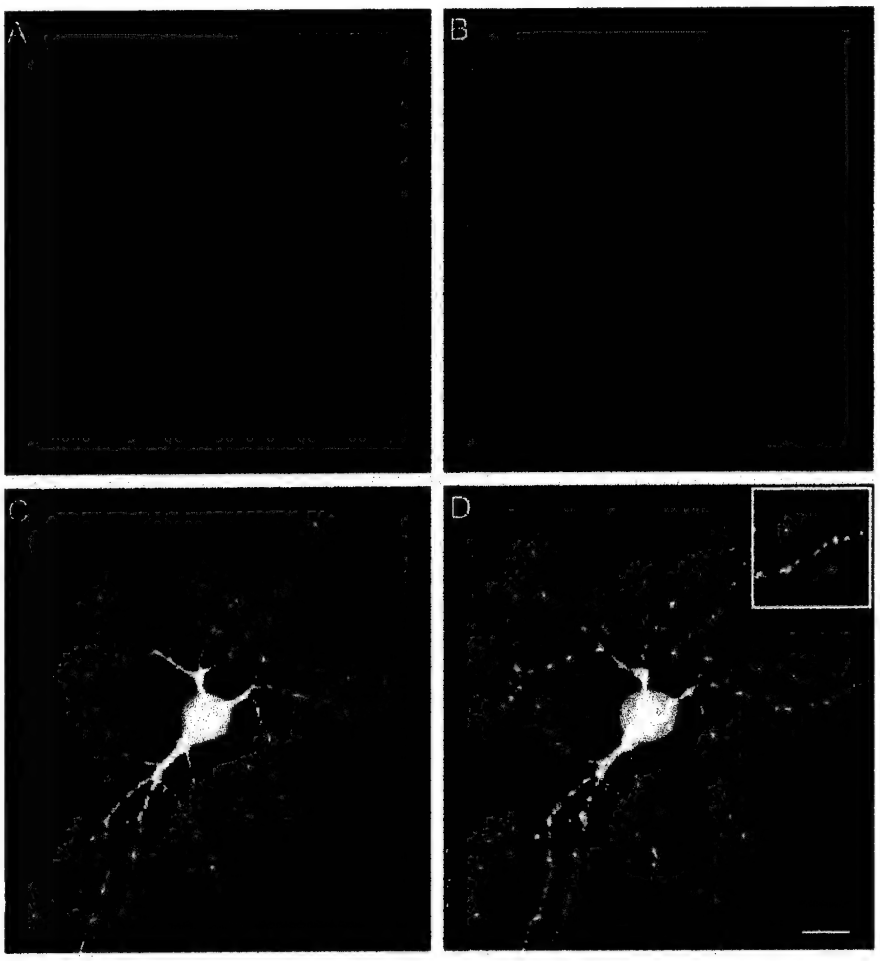

Figure 6. Comparison of mitochondrial and dendrite remodeling. *A*, Single cortical neuron transfected with cytosolic eCFP. *B*, Effect of perfusion on dendrite morphology after 5 min perfusion with 30 μM glutamate/1 μM glycine. *C*, Overlay of fluorescence images of mt-eYFP and cytosolic ECFP before glutamate exposure. *D*, Overlay image after superfusion with 30 μM glutamate/1 μM glycine. Inset, Magnified region. These data are representative of four additional fields.

A second dramatic consequence of the action of glutamate is the cessation of mitochondrial movement. The directional movement of mitochondria in neurons is accomplished using the microtubule network and can be inhibited by stabilizing microtubules with drugs like nocodazole (Morris and Hollenbeck, 1995; Overly et al., 1996; Ligon and Steward, 2000b). Movement on the actin cytoskeleton has also been reported (Morris and Hollenbeck, 1995). Movement is presumably driven by motor proteins such as kinesin and dynein (Goldstein, 2001) as well as myosin (Morris and Hollenbeck, 1995), although the specific interactions governing this mechanism in the context of neuronal mitochondria have not been clearly established. The cytoskeleton is clearly subject to profound alterations in the face of a robust calcium load. The actin cytoskeleton can be modified by calcium-mediated activation of gelsolin, whereas calcineurin activation results in dephosphorylation of microtubule-associated proteins (van Rossum and Hanisch, 1999). Fodrin is a substrate for calpains, which may also be activated under these circumstances (van Rossum and Hanisch, 1999), although we have found that calpain inhibitors do not prevent this effect of glutamate (data not shown). Thus, there are many factors that could alter the substrates on which mitochondria move. Movement is also an ATP-dependent process, and the depolarization of mitochondria combined with the potential impairment of function associated with the calcium load could deplete local ATP concentrations quite rapidly. Thus, a number of different mechanisms could contribute to the cessation of movement. The mechanisms responsible for the alteration in movement may also underlie

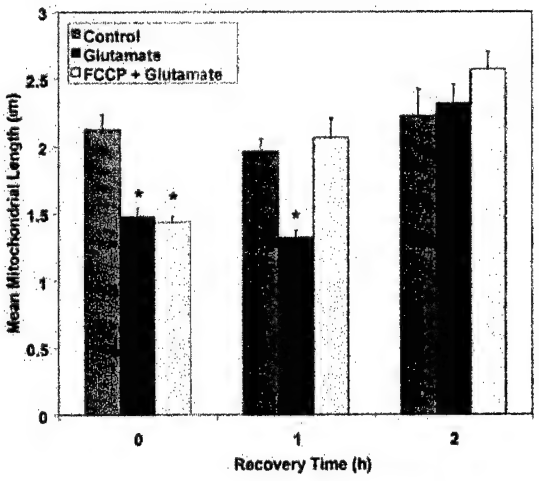

Figure 7. Recovery of mitochondria after glutamate and combined FCCP + glutamate treatments. Mitochondrial length was measured immediately after treatment of transfected cells with 30 μM glutamate/1 μM glycine and subsequently measured 1 and 2 hr after treatment. *Significantly different from control ($p < 0.05$; *t* test; *n* ranges between 7 and 15 for each bar).

the shape change. If the rod-like structure associated with normal mitochondria is essentially a function of the organelle being stretched out on a cytoskeletal structure, the dissolution of that structure could result in the rounding that we observe.

It is interesting to consider the role that these glutamate-mediated effects on mitochondria might have in the expression of excitotoxic injury. The effects are clearly produced by concentrations and exposure times of glutamate that are around the threshold for neuronal injury; however, the changes in shape and movement that we observe are the same in the presence and absence of FCCP. This is notable, because we have demonstrated previously that the combined application of FCCP with glutamate protects neurons from excitotoxic injury, ostensibly as the result of preventing mitochondrial calcium accumulation (Stout et al., 1998). Because both rounding and movement cessation occur in the presence of FCCP with glutamate, one can conclude that rounding of mitochondria or their temporary immobilization does not inevitably lead to injury; however, it is interesting to note that the presence of FCCP during glutamate exposure clearly facilitates the recovery of the normal morphological phenotype. This suggests that the protection of mitochondrial function (by preventing calcium overload) aids in the restoration of mitochondria to their normal state. Thus, in this experimental paradigm, the alteration of mitochondrial morphology would be considered a symptom rather than a cause of cell injury. Indeed, this raises the possibility that either the shape or movement change could be an attempt to protect the cell from injury, although what exactly is accomplished by this maneuver remains to be established.

More broadly, these experiments clearly establish an unappreciated dynamic that exists between the distribution of mitochondria within cells and their bioenergetic status. Under conditions of less acute injury mechanisms, one might anticipate that impaired mitochondrial function would alter the ability of mitochondria to move and thereby prevent the normal distribution of mitochondria within neurons. Under conditions of chronic stress, this could stop new mitochondria from being delivered to distal parts of the neuron or possibly even prevent the retrieval of dysfunctional mitochondria to the cell body for degradation, either of which may result in cell damage. When one considers the number of endogenous toxins (such as zinc, nitric oxide, and oxidative stress) as well as xenobiotics (such as MPTP, rotenone, 3-nitroproprionic acid), that impair mitochondrial function and dissipate the mitochondrial membrane potential, it seems likely that the alteration of the trafficking and morphology of mitochondria is likely to be a broadly important phenomenon associated with neuronal injury.

References

Amchenkova AA, Bakeeva LE, Chentsov YS, Skulachev VP, Zorov DB (1988) Coupling membranes as energy-transmitting cables. I. Filamentous mitochondria in fibroblasts and mitochondrial clusters in cardiomyocytes. J Cell Biol 107:481–492.

Beal MF (2000) Energetics in the pathogenesis of neurodegenerative diseases. Trends Neurosci 23:298–304.

Buckman JF, Reynolds IJ (2001) Spontaneous changes in mitochondrial membrane potential in cultured neurons. J Neurosci 21:5054–5065.

Budd SL, Nicholls DG (1996) Mitochondria, calcium regulation and acute glutamate excitotoxicity in cultured cerebellar granule cells. J Neurochem 67:2282–2291.

Davis AF, Clayton DA (1996) In situ localization of mitochondrial DNA replication in intact mammalian cells. J Cell Biol 135:883–893.

Desagher S, Martinou JC (2000) Mitochondria as the central control point of apoptosis. Trends Cell Biol 10:369–377.

Djaldetti M (1982) Mitochondrial abnormalities in the cells of myeloma patients. Acta Haematologica 68:241–248.

Dubinsky JM, Levi Y (1998) Calcium induced activation of the mitochondrial permeability transition in hippocampal neurons. J Neurosci Res 53:728–741.

Duchen MR, Leyssens A, Crompton M (1998) Transient mitochondrial depolarizations reflect focal sarcoplasmic reticular calcium release in single rat cardiomyocytes. J Cell Biol 142:975–988.

Dugan LL, Sensi SL, Canzoniero LMT, Handran SD, Rothman SM, Lin T-S, Goldberg MP, Choi DW (1995) Mitochondrial production of reactive oxygen species in cortical neurons after exposure to NMDA. J Neurosci 15:6377–6388.

Ebneth A, Godemann R, Stamer K, Illenberger S, Trinczek B, Mandelkow E (1998) Overexpression of tau protein inhibits kinesin-dependent trafficking of vesicles, mitochondria, and endoplasmic reticulum: implications for Alzheimer's disease. J Cell Biol 143:777–794.

Filiano AJ, Rintoul GL, Brocard JB, Votyakova TV, Reynolds IJ (2002) Mitochondrial homeostasis and neuronal injury in primary cortical cultures. Soc Neurosci Abstr 32:297.2.

Frank S, Gaume B, Bergmann-Leitner ES, Leitner WW, Robert EG, Catez F, Smith CL, Youle RJ (2001) The role of dynamin-related protein 1, a mediator of mitochondrial fission, in apoptosis. Dev Cell 1:515–525.

Goldstein LS (2001) Molecular motors: from one motor many tails to one motor many tales. Trends Cell Biol 11:477–482.

Heales SJ, Bolaños JP, Stewart VC, Brookes PS, Land JM, Clark JB (1999) Nitric oxide, mitochondria and neurological disease. Biochim Biophys Acta 1410:215–228.

Jouaville LS, Pinton P, Bastianutto C, Rutter GA, Rizzuto R (1999) Regulation of mitochondrial ATP synthesis by calcium: evidence for long term metabolic priming. Proc Natl Acad Sci USA 96:13807–13812.

Kress GJ, Dineley KE, Reynolds IJ (2002) The relationship between intracellular free iron and cell injury in cultured neurons, astrocytes, and oligodendrocytes. J Neurosci 22:5848–5855.

Kristal BS, Dubinsky JM (1997) Mitochondrial permeability transition in the central nervous system: induction by calcium cycling-dependent and independent pathways. J Neurochem 69:524–538.

Ligon LA, Steward O (2000a) Movement of mitochondria in the axons and dendrites of cultured hippocampal neurons. J Comp Neurol 347:340–350.

Ligon LA, Steward O (2000b) Role of microtubules and actin filaments in the movement of mitochondria in the axons and dendrites of cultured hippocampal neurons. J Comp Neurol 427:351–361.

Llopis J, McCaffery JM, Miyawaki A, Farquhar MG, Tsien RY (1998) Measurement of cytosolic, mitochondrial and Golgi pH in single living cells with green fluorescent proteins. Proc Natl Acad Sci USA 95:6803–6808.

Morris RL, Hollenbeck PJ (1993) The regulation of bidirectional mitochondrial transport is coordinated with axonal outgrowth. J Cell Sci 104:917–927.

Morris RL, Hollenbeck PJ (1995) Axonal transport of mitochondria along microtubules and F-actin in living vertebrate neurons. J Cell Biol 131:1315–1326.

Nicholls DG, Budd SL (2000) Mitochondria and neuronal survival. Physiol Rev 80:315–360.

Nishino I, Kobayashi O, Goto Y, Kurihara M, Kumagai K, Fujita T, Hashimoto K, Horai S, Nonaka I (1998) A new congenital muscular dystrophy with mitochondrial structural abnormalities. Muscle Nerve 21:40–47.

Overly CC, Rieff HI, Hollenbeck PJ (1996) Organelle motility and metabolism in axons vs dendrites of cultured hippocampal neurons. J Cell Sci 109:971–980.

Park JS, Bateman MC, Goldberg MP (1996) Rapid alterations in dendrite morphology during sublethal hypoxia or glutamate receptor activation. Neurobiol Dis 3:215–227.

Reynolds IJ, Hastings TG (1995) Glutamate induces the production of reactive oxygen species in cultured forebrain neurons following NMDA receptor activation. J Neurosci 15:3318–3327.

Rintoul GL, Filiano AJ, Brocard JB, Werner D, Reynolds IJ (2002) Mitochondrial remodeling in response to excitotoxic glutamate treatment of primary cortical cultures. Soc Neurosci Abstr 32:297.1.

Santel A, Fuller MT (2001) Control of mitochondrial morphology by a human mitofusin. J Cell Sci 114:867–874.

Schapira AH (1999) Mitochondrial involvement in Parkinson's disease,

Huntington's disease, hereditary spastic paraplegia and Friedreich's ataxia. Biochim Biophys Acta 1410:159–170.

Scheffler IE (1999) Mitochondria. New York: Wiley.

Schinder AF, Olson EC, Spitzer NC, Montal M (1996) Mitochondrial dysfunction is a primary event in glutamate neurotoxicity. J Neurosci 16:6125–6133.

Stout AK, Reynolds IJ (1999) High-affinity calcium indicators underestimate increases in intracellular calcium concentrations associated with excitotoxic glutamate stimulations. Neuroscience 89:91–100.

Stout AK, Raphael HM, Kanterewicz BI, Klann E, Reynolds IJ (1998) Glutamate-induced neuron death requires mitochondrial calcium uptake. Nat Neurosci 1:366–373.

Tandler B, Hoppel CL (1986) Studies on giant mitochondria. Ann NY Acad Sci 488:65–81.

van Rossum D, Hanisch UK (1999) Cytoskeletal dynamics in dendritic spines: direct modulation by glutamate receptors? Trends Neurosci 22:290–295.

Weiss JH, Sensi SL, Koh JY (2000) Zn(2+): a novel ionic mediator of neural injury in brain disease. Trends Pharmacol Sci 21:395–401.

White RJ, Reynolds IJ (1995) Mitochondria and Na^+/Ca^{2+} exchange buffer glutamate-induced calcium loads in cultured cortical neurons. J Neurosci 15:1318–1328.

White RJ, Reynolds IJ (1996) Mitochondrial depolarization in glutamate-stimulated neurons: an early signal specific to excitotoxin exposure. J Neurosci 16:5688–5697.

Xia Z, Dudek H, Miranti CK, Greenberg ME (1996) Calcium influx via the NMDA receptor induces immediate early gene transcription by a MAP kinase/ERK-dependent mechanism. J Neurosci 16:5425–5436.

Research

Cell Calcium (2000) **28**(5/6), 317–327

doi: 10.1054/ceca.2000.0171, available online at http://www.idealibrary.com on IDEAL®

Pharmacological investigation of mitochondrial Ca^{2+} transport in central neurons: studies with CGP-37157, an inhibitor of the mitochondrial Na^{+}–Ca^{2+} exchanger

J. M. Scanlon, J. B. Brocard, A. K. Stout, I. J. Reynolds

University of Pittsburgh, School of Medicine, Department of Pharmacology, Pittsburgh, USA

Summary Mitochondria buffer large changes in $[Ca^{2+}]_i$ following an excitotoxic glutamate stimulus. Mitochondrial sequestration of $[Ca^{2+}]_i$ can beneficially stimulate oxidative metabolism and ATP production. However, Ca^{2+} overload may have deleterious effects on mitochondrial function and cell survival, particularly Ca^{2+}–dependent production of reactive oxygen species (ROS) by the mitochondria. We recently demonstrated that the mitochondrial Na^{+}–Ca^{2+} exchanger in neurons is selectively inhibited by CGP-37157, a benzothiazepine analogue of diltiazem. In the present series of experiments we investigated the effects of CGP-37157 on mitochondrial functions regulated by Ca^{2+}. Our data showed that 25 μM CGP-37157 quenches DCF fluorescence similar to 100 μM glutamate and this effect was enhanced when the two stimuli were applied together. CGP-37157 did not increase ROS generation and did not alter glutamate or 3 mM hydrogen-peroxide-induced increases in ROS as measured by DHE fluorescence. CGP-37157 induces a slight decrease in intracellular pH, much less than that of glutamate. In addition, CGP-37157 does not enhance intracellular acidification induced by glutamate. Although it is possible that CGP-37157 can enhance mitochondrial respiration both by blocking Ca^{2+} cycling and by elevating intramitochondrial Ca^{2+}, we did not observe any changes in ATP levels or toxicity either in the presence or absence of glutamate. Finally, mitochondrial Ca^{2+} uptake during an excitotoxic glutamate stimulus was only slightly enhanced by inhibition of mitochondrial Ca^{2+} efflux. Thus, although CGP-37157 alters mitochondrial Ca^{2+} efflux in neurons, the inhibition of Na^{+}–Ca^{2+} exchange does not profoundly alter glutamate-mediated changes in mitochondrial function or mitochondrial Ca^{2+} content.

INTRODUCTION

Of the many ways in which neurons can die perhaps the most extensively studied are the processes collectively referred to as 'excitotoxicity' [1,2]. This phenomenon is associated with the release of glutamate from neuronal and non-neuronal stores and subsequently the excessive activation of ionotropic glutamate receptors. Excitotoxic glutamate injury probably reflects a collection of neurotoxic mechanisms depending on the duration and intensity of the glutamate exposure and the type of receptors activated. This is most readily appreciated, and well studied, in primary cell culture. In cortical neurons, for example, a brief exposure (approximately 5 min) to a high concentration of glutamate results in activation of the N-methyl-D-aspartate (NMDA) subtype of glutamate receptor, allows massive Ca^{2+} entry and results in predominantly necrotic cell injury [3,4]. Lower concentrations of glutamate can also be toxic via the activation of NMDA receptors, but it has been suggested that this results in apoptotic injury [5]. If non-NMDA glutamate receptors are activated a form of injury is triggered that depends less on extracellular calcium, and requires

Received 27 September 2000
Accepted 10 October 2000

Correspondence to: Dr Ian J. Reynolds, Department of Pharmacology, W1351 Biomedical Science Tower, University of Pittsburgh, School of Medicine, Pittsburgh, PA 15261, USA. Tel.: +1 412 648 2134; fax: +1 412 624 0794; e-mail: iannmda@pitt.edu

several hours of stimulation to commit neurons to die, but is expressed as necrotic cell death [6]. Evidence for all of these forms of injury have been found in vivo [2,7,8]. Thus, excitotoxicity should not be considered as a single homogenous phenomenon.

In this laboratory we have focused on the acute, necrotic injury that results from NMDA receptor activation and depends on Ca^{2+} entry [4]. This form of injury is likely to be a consequence of the particular effectiveness with which NMDA receptors permit neuronal Ca^{2+} accumulation, because they form a Ca^{2+}-permeable channel that only partially inactivates during prolonged exposure to agonists (unlike, for example, voltage-gated Ca^{2+} channels). Thus, excitotoxic NMDA receptor activation results in very high cytoplasmic free Ca^{2+} concentrations [9,10] in addition to potentially allowing Ca^{2+} entry into specific sites in neurons poised to cause injury [11]. As has been reported in several types of excitable cells [12–14], neuronal mitochondria buffer these glutamate-induced large Ca^{2+} loads particularly well [15–24]. However, it appears that the consequence of this mitochondrial Ca^{2+} buffering is lethal. Thus, if mitochondrial Ca^{2+} accumulation is prevented by eliminating the mitochondrial membrane potential (and thus abrogating the driving force for mitochondrial Ca^{2+} uptake) neurons are protected from NMDA receptor-mediated injury [25,26].

It remains unclear what links mitochondrial Ca^{2+} accumulation to injury. Studies in isolated mitochondria and intact neurons have suggested that glutamate-stimulated mitochondrial Ca^{2+} accumulation results in the production of reactive oxygen species (ROS) that may originate from mitochondria [27–31]. The activation of the permeability transition pore has also been suggested [32–34], although evidence supporting this mechanism is incomplete.

The finding that excitotoxicity requires mitochondrial Ca^{2+} accumulation is an exciting development because it suggests novel targets at which to aim neuroprotective drug strategies. However, at this stage the pharmacology of mitochondrial transport is rather poorly developed. The major Ca^{2+} uptake pathway is likely to be the Ca^{2+} uniporter [12], which may be complemented by a rapid uptake mode of the kind described in liver mitochondria [35,36]. There are several inhibitors of the Ca^{2+} uniporter, including ruthenium red and the related Ru360 [37], as well as some cobaltammine agents [38]. However, most of these agents penetrate cells very poorly, as exemplified by the 10 000-fold decrease in potency of Ru360 in intact cardiac myocytes compared to cardiac mitochondria [37]. Indeed, even applying relatively high concentrations of Ru360 (~10 μM) for several tens of minutes to intact neurons has very little effect on glutamate-induced cytosolic Ca^{2+} transients (JBB and IJR, unpublished observations). It was also recently suggested that mitochondrial Ca^{2+} accumulation can occur if the mitochondrial Na^+–Ca^{2+} exchanger reverses [39], although it is not known if this occurs in neurons.

An alternative approach to modifying mitochondrial Ca^{2+} loading is to manipulate the primary efflux pathways. In excitable cells mitochondrial Ca^{2+} efflux may be mediated by several different pathways. Under normal circumstances the mitochondrial Na^+–Ca^{2+} exchanger may be the primary mechanism for efflux [40]. In principle, it is also possible that the uniporter could reverse if the mitochondrial membrane potential is lost [41], and activation of permeability transition should also result in massive Ca^{2+} release [42]. Both of these latter situations would be associated with catastrophic alterations in mitochondrial membrane potential that might occur in relation to pathophysiological states, and we have seen little evidence for either process in intact neurons even following prolonged exposure to glutamate. However, using pharmacological approaches we have been able to demonstrate the presence of the mitochondrial Na^+–Ca^{2+} exchanger and the impact of mitochondrial Ca^{2+} release on cytosolic Ca^{2+} concentrations [43,44]. For example, when mitochondria are loaded with Ca^{2+} following the exposure of neurons to a relatively high glutamate concentration the resulting recovery of $[Ca^{2+}]_i$ to baseline levels is rather slow. This slow recovery is evidently due to the persistent efflux of mitochondrial Ca^{2+} stores through the Na^+–Ca^{2+} exchanger, because inhibiting this process with the diltiazem analogue CGP-37157 rapidly restores $[Ca^{2+}]_i$ to basal values, while removing the inhibitor is associated with a resumption of mitochondrial Ca^{2+} release. Similar effects are also observed in peripheral neurons that show a particularly prominent mitochondrial Ca^{2+} release component following the activation of voltage-gated Ca^{2+} channels [45]. Although CGP-37157 does have other pharmacological effects, such as the inhibition of voltage-gated Ca^{2+} channels [45], it rapidly and reversibly inhibits mitochondrial Ca^{2+} efflux in intact neurons and, as such, appears to be one of the more useful agents currently available to manipulate mitochondrial Ca^{2+} signalling.

In the experiments reported here we investigated the notion that by blocking what may be the major mitochondrial Ca^{2+} efflux pathway we could potentiate glutamate-stimulated, Ca^{2+}-mediated alterations in mitochondrial function. We examined the effects of CGP-37157 on several different aspects of mitochondrial physiology, including ROS generation, intracellular acidification, and excitotoxic neuronal injury, anticipating that CGP-37157 would increase mitochondrial Ca^{2+} accumulation and thereby potentiate glutamate-induced neuronal death.

MATERIALS AND METHODS

Cell culture

Primary neuronal cultures were obtained from the forebrains of embryonic day 17 Sprague-Dawley rats and dissociated as previously described [46]. Animals were handled in accordance with the National Institutes of Health Guide for the Care and Use of Laboratory Animals and with the Institutional Animal Care and Use Committee of the University of Pittsburgh. Briefly, the cortical lobes were incubated in 0.005–0.01% trypsin in Ca^{2+}-free, Mg^{2+}-free media (in mM: 116 NaCl, 5.4 KCl, 26.2 $NaHCO_3$, 11.7 NaH_2PO_4, 5 glucose, 0.001% Phenol Red, and minimum essential media amino acids; pH adjusted to 7.4 with NaOH) for 30 min at 37°C. Viability determinations were made with the trypan blue (0.08%) exclusion method. The plating suspension was diluted to 300 000 cells/ml using plating medium (v/v solution of 90% Dulbecco's modified Eagle's medium, 10% heat-inactivated fetal bovine serum, 24 U/ml penicillin, 24 μg/ml streptomycin; final glutamine concentration 3.1 mM). Cells were plated onto poly-L-lysine-coated (40 μg/ml) 31 mm glass coverslips that were inverted 1 day later in a maintenance medium (horse serum substituted for fetal calf serum, all other constituents identical). Inversion of the coverslips prevents glial proliferation. Cells were maintained under 95% air, 5% CO_2 until use 2 weeks later. Only those coverslips containing healthy neurons (rounded-oval, smooth, and bright cell bodies when viewed using phase-contrast optics) were used. On the day of experimentation, culture medium was removed and replaced with HEPES-buffered salt solution (HBSS) of the following composition (mM): 137 NaCl, 5 KCl, 0.9 $MgSO_4$, 1.4 $CaCl_2$, 3 $NaHCO_3$, 0.6 Na_2HPO_4, 0.4 KH_2PO_4, 5.6 glucose, and 20 HEPES; adjusted to pH 7.4 with NaOH.

Intracellular ROS production

ROS production was measured by fluorescence microscopy using the oxidation sensitive dyes, 2,7-dichlorodihydrofluorescein ($DCFH_2$) or dihydroethidium (DHE) [29,31] as previously described [47]. Fluorescence was recorded using a Meridian ACAS 570c laser scanning confocal imaging system. A 488 nm excitation line from an argon laser was used in conjunction with a 510 nm dichroic mirror and focused through a 225 m pinhole and a 40× phase-contrast objective to yield an optical slice of about 2.5 m through the middle of the neurons (0.20 m in diameter).

Forebrain neurons that were 2 weeks in culture were loaded with 10 M $DCFH_2$ or 2 M DHE for 15 min at 37°C in HBSS supplemented with 5 mg/ml bovine serum albumin; 4 mM stocks of $DCFH_2$ or DHE were made in methanol or anhydrous DMSO respectively. $DCFH_2$ was removed just prior to imaging whereas DHE was maintained in solution throughout the experiment. Fluorescence was recorded at room temperature from a single field of cells (180 × 180 μm) per coverslip typically containing 5–15 neurons. Cells were imaged over a period of 15 min at 1 scan per min. After obtaining 2 min of basal fluorescence, cells were exposed to various treatments for a period of 10–15 min Fluorescence was normalized to the intensity measured in the first scan to account for problems in equal dye loading. Data were presented for each test condition as the change in normalized fluorescence (mean ± SEM) over time (min). All experiments were performed on at least two coverslips from no less than two different culture dates. Cells displaying localized increases in DCF fluorescence were determined visually by an observer blinded to the treatment.

Measurement of intracellular pH

Fluorescence imaging, as previously described [26], was performed on a Nikon Diaphot 300 microscope fitted with a 40× quartz objective, a Dage-MTI cooled-CCD camera with 640 × 480-pixel resolution in combination with a Dage-MTI Gen II Sys image intensifier and a 75 watt Xenon lamp-based monochromator light source. Attenuation of incident light was achieved with a 0.1% neutral density filter and passed through a 515 nm dichroic mirror. Emitted fluorescence was measured with a 535 ± 12.5 nm band-pass filter after alternate excitation at 498 nm and 450 nm. Data acquisition analysis was controlled using Simple PCI software (Compix, Cranberry, PA). Forebrain neurons (2 weeks in culture) were incubated for 15 min at 37°C with 2′,7′-bis-(2-carboxyethyl)-5(and 6)-carboxyfluorescein (BCECF) (5 μM) in HBSS supplemented with 5 mg/ml BSA. After loading, coverslips were rinsed with HBSS, mounted in a recording chamber and perfused with HBSS at a rate of 20 ml/min. Cells were exposed to various treatments for a period of 5 min. After approximately 10 min of recovery in normal HBSS, cells were exposed to 25 mM NH_4Cl for 1 min as a positive control. Fluorescence was recorded at room temperature and background fluorescence values (determined from cell-free regions of each coverslip) were subtracted from all signals.

Toxicity assay

Forebrain neurons (2 weeks in culture) were rinsed twice with HBSS, and coverslips were inverted to orient the cultured neurons face-up. Neurons were exposed to various treatments for a period of 5 min and then rinsed with HBSS. Cells were placed in Minimum Essential

Medium containing penicillin (24 U/ml) and streptomycin (24 μg/ml) and allowed to incubate for 20–24 h at 37°C. Neuronal viability was then assessed with a trypan blue (0.4%) exclusion method as previously described [26]. Data are presented as the mean number of live cells from three experiments in which three fields, from each of three coverslips, were counted by an observer blinded to the treatment condition.

Determination of intracellular ATP

Forebrain neurons (2 weeks in culture) were rinsed twice with HBSS and coverslips were inverted to orient the cultured neurons face-up. Neurons were exposed to various treatments for a period of 10 min and then rinsed with ice-cold PBS. Cellular ATP was extracted from three coverslips per condition in 400 μL of 0.5% TCA/125 M EDTA using a disposable cell scraper. Extracts were centrifuged at 13 800 g for 5 min at 37°C. For each condition, 300 μL of supernatant was added to 120 μL of 0.1 M Tris and kept on ice throughout the experiment. ATP content was measured using a Luciferin-Luciferase Assay (Molecular Probes, Eugene, Oregon) with a scintillation counter (Beckman LS 1801) to detect luminescence. Sample [ATP] was determined using nonlinear regression analysis of the ATP Standard Curve. Data are presented as the percent of controls (mean ± SEM) from three separate experiments using two different cell culture dates.

Measurement of $[Ca^{2+}]_i$

The acetoxy methyl ester form of MagFura-2 (Molecular Probes, Oregon, USA) was diluted to 1 mM in anhydrous DMSO. Coverslips were incubated in HBSS containing 5 μM of MagFura-2, 0.5% of DMSO and 5 mg/ml of bovine serum albumin for 20 min at 37°C. Cells were then rinsed with HBSS, mounted on a record chamber and perfused with HBSS at a rate of 20 ml/min. All recordings were made at room temperature.

The imaging system consisted of a Nikon Diaphot 300 inverted microscope fitted with a 40× objective, a digital Orca camera (Hamamatsu Corporation, New Jersey) and a 75 Watt Xenon lamp-based monochromator light source as previously described [10]. Cells were alternately illuminated with 335 and 375 nm beams. Incident light was attenuated with neutral density filters (typically by about 90%; Omega Optical, Vermont) and emitted fluorescence passed through a 515 nm dichroic mirror and a 535 ± 12.5 nm band-pass filter (Omega Optical, Vermont). Background fluorescence, determined from three cell-free regions of the coverslips, was subtracted from all the signals prior to calculating the ratios as described.

Materials

CGP-37157 (7-chloro-3,5-dihydro-5-phenyl-1H-4,1-benzothiazepine-2-on) was a generous gift from Ciba-Geigy Pharmaceuticals (Basel, Switzerland) and was also purchased from Tocris Cookson Inc. (Missouri). Stock solutions of CGP-37157 were prepared using anhydrous dimethyl sulfoxide and further diluted in HBSS. All fluorescent indicators were purchased from Molecular Probes (Eugene, Oregon).

Statistical analysis

Statistical significance between groups of three or more experimental conditions was determined by one-way analysis of variance (ANOVA) followed with a Bonferroni post-hoc analysis using Prism v3.0 (GraphPad Software, San Diego, CA). Statistical significance between two groups was determined using a two-tailed, unpaired student's *t*-test.

RESULTS

Effects of CGP-37157 on production of ROS

Several studies have demonstrated a Ca^{2+}-dependent production of ROS via the mitochondria following a glutamate stimulus [29–31]. If one can speculate that blocking Ca^{2+} entry into the mitochondria may potentially inhibit glutamate-induced ROS production, then along the same line of reasoning blocking Ca^{2+} efflux may enhance mitochondrial ROS generation. Thus, we studied the impact of the Na^{+}–Ca^{2+} exchange inhibitor on the fluorescence of two oxidation sensitive indicators in the presence or absence of glutamate or an exogenous oxidant.

In this model system glutamate induced a three-fold increase in DHE fluorescence (Fig. 1A). Interestingly, hydrogen peroxide produced a somewhat smaller oxidation of DHE compared to glutamate (Fig. 1B). DHE fluorescence after exposure to CGP-37157 was similar to controls (Figs 1A & B). In addition, CGP-37157 did not alter glutamate or hydrogen-peroxide-induced increases in DHE fluorescence (Figs 1A & B).

Both CGP-37157 and glutamate decreased DCF fluorescence to a similar extent (Fig. 1C). This effect was enhanced when the two stimuli were applied together (Fig. 1C). Glutamate but not CGP-37157 produces localized increases in intracellular DCF fluorescence (Fig. 2). We used a cell counting method to assess DCF oxidation responses, as we have previously described [29]. The number of cells displaying glutamate-induced increases in localized fluorescence was reduced by 73% when CGP-37157 is applied with glutamate ($t = 5.23$; $P < 0.0008$; Fig. 2). In these experiments we used hydrogen peroxide

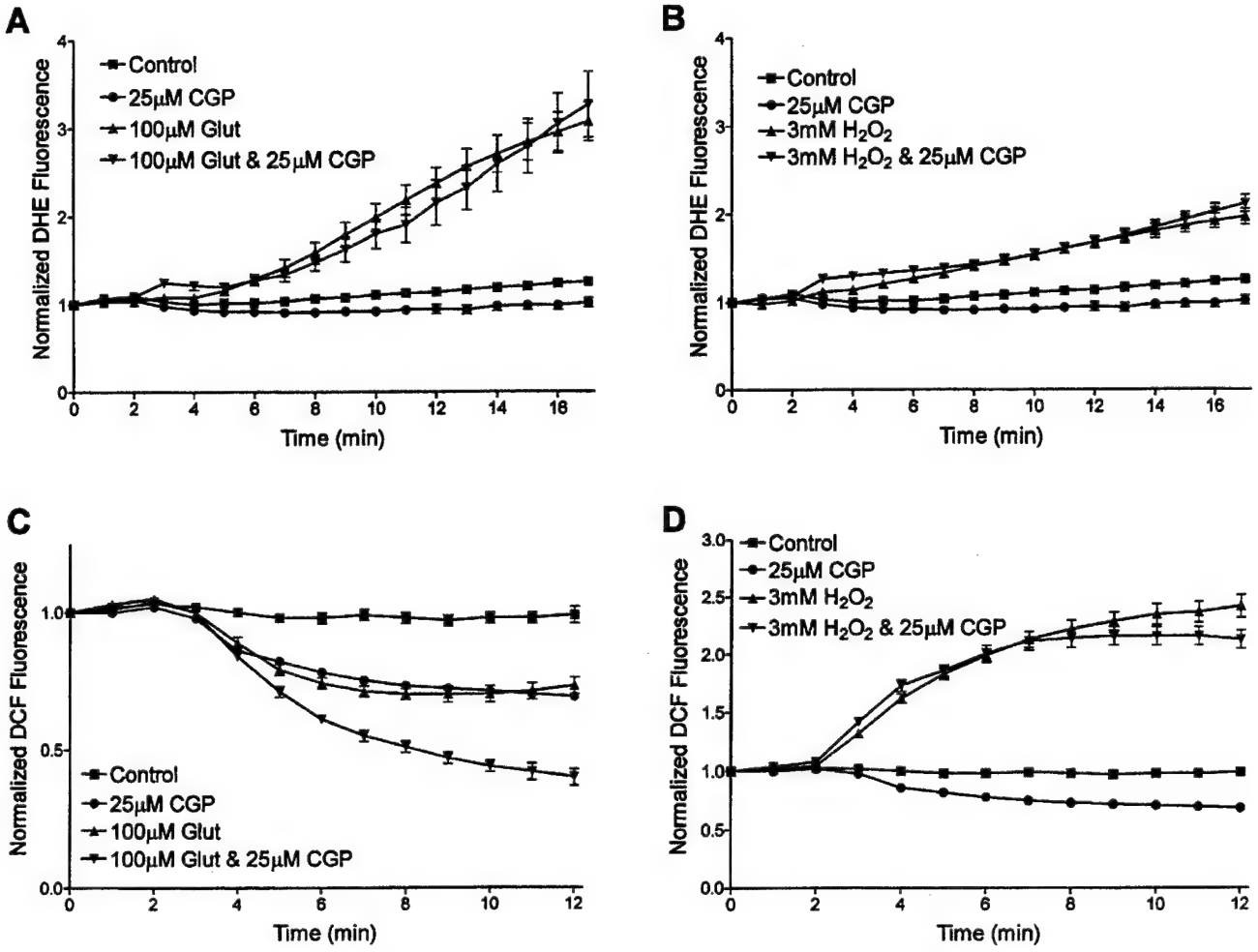

Fig. 1 CGP-37157 does not stimulate intracellular ROS generation. Neurons were loaded with 2 μM DHE (A, B) or 10 μM DCF (C, D) for 15 min at 37°C. After obtaining 2 min of basal fluorescence, neurons were exposed to various treatments for a period of 10–15 min (A, C). Data shows the effects of HBSS, 25 μM CGP-37157, 100 μM glutamate with 1 μM glycine, or both. (B, D) Data shows the effects of HBSS, 25 μM CGP-37157, 3 mM hydrogen peroxide, or both. Points represent the mean ± SEM from 20 to 100 neurons obtained from 2–6 coverslips from no less than 2 culture dates.

(3 mM) as a positive control, and this stimulus induced a 2–2.5-fold increase in DCF fluorescence which was not affected by the addition of CGP-37157 (Fig. 1D).

CGP-37157 produces decreases in intracellular pH

Glutamate will quench DCF fluorescence due to intracellular acidification [29]. Thus, we wanted to determine if CGP-37157 decreases DCF fluorescence due to a similar mechanism using the pH-sensitive indicator BCECF, which is not sensitive to ROS. CGP-37157 produces a slight and reversible decrease in intracellular pH (Fig. 3). The intracellular acidification induced by glutamate is much greater than the effect of CGP-37157. However, the intracellular acidification produced by glutamate is not altered by the addition of CGP-37157 (Fig. 3).

Blocking mitochondrial Na^+–Ca^{2+} exchange does not affect cellular ATP content

Ca^{2+} may act as a second messenger to stimulate ATP production. Mitochondrial Ca^{2+} can stimulate several key enzymes involved in cellular respiration [48]. Previous studies have shown that CGP-37157 will increase the P_m possibly as a result of enhanced mitochondrial activity [32]. Mitochondrial Ca^{2+} cycling following glutamate exposure uncouples oxidative respiration from ATP production. Thus, inhibition of mitochondrial Ca^{2+} cycling and enhancement of the mitochondrial Ca^{2+} load with CGP-37157 may enhance ATP production or inhibit decreases due to glutamate. A 5-min exposure to 100 μM glutamate and 1 μM glycine did not significantly decrease the ATP levels compared to controls (Fig. 4)

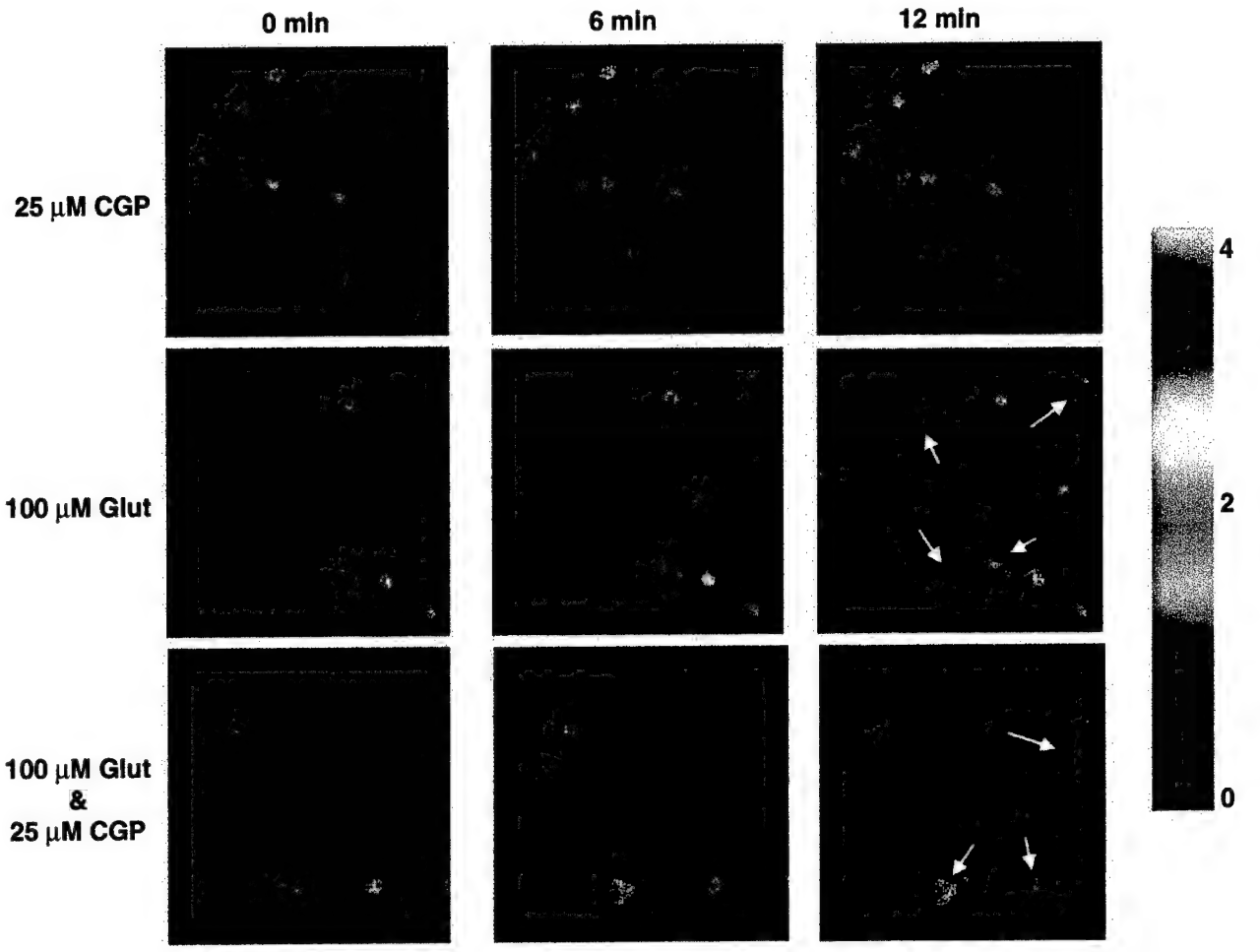

Fig. 2 CGP-37157 inhibits localized ROS production by glutamate. Representative images display the effects of 25 μM CGP-37157, 100 μM glutamate with 1 μM glycine, or both on intracellular DCF fluorescence. For each condition neurons are shown at the start of the experiment (3 min prior to exposure), 6 min (3 min after exposure), or 12 min (9 min after exposure). The colour scale represents arbitrary fluorescent units. Experiments were repeated on five different coverslips from four different culture dates typically yielding 50–100 cells ($n=5$). Glutamate produced localized increases in DCF fluorescence in 70.8% of the cells, whereas CGP-37157 plus glutamate only displayed localized increases in fluorescence in 18.8% of the cells. Examples of cells that would be scored as positive by the counting approach are identified by white arrows in the panels on the right. These effects were significantly different ($t=5.23$; $P<0.0008$, two-tailed, unpaired Student's *t*-test).

similar to a 5 min exposure to 750 nM FCCP (Fig. 4). CGP-37157 in the presence or absence of glutamate did not alter cellular ATP content (Fig. 4).

Effects of CGP-37157 on glutamate-induced neuronal viability

Excessive mitochondrial Ca^{2+} cycling following glutamate exposure can lead to mitochondrial depolarization and bioenergetic failure and may contribute to neuronal death. As a result of inhibiting Ca^{2+} cycling CGP-37157 may be neuroprotective following an excitotoxic glutamate stimulus. However, recent studies have demonstrated that inhibition of mitochondrial Ca^{2+} uptake is neuroprotective against glutamate excitotoxicity [25,26]. Also, mitochondrial Ca^{2+} can stimulate opening of the PTP. It is possible that enhancing mitochondrial Ca^{2+} loads with CGP-37157 could increase toxicity following a glutamate stimulus. Thus, we examined the effects of the Na^{+}–Ca^{2+} exchange inhibitor on glutamate-induced neurotoxicity. Our results show that a 5-min exposure to 100 μM glutamate/1 μM glycine typically produces a 40% loss in viable neurons as compared to cells exposed to buffer changes alone (Fig. 5). CGP-37157 does not alter neuronal viability. Glutamate and the combination of glutamate and CGP-37157 significantly decrease cell viability compared to controls ($P<0.01$). However, these two conditions are not significantly different from each other.

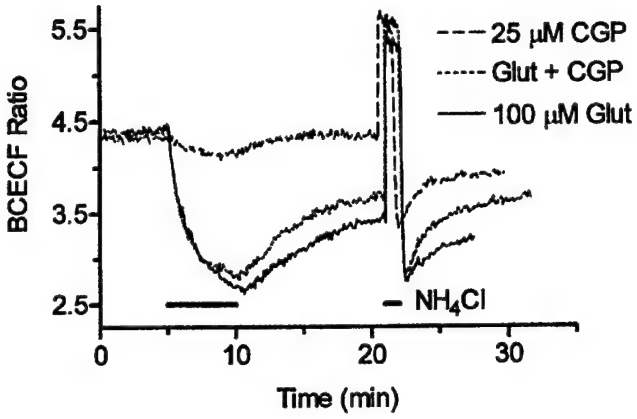

Fig. 3 Effects of CGP-37157 and glutamate on intracellular pH. Neurons were stimulated with 25 μM CGP-37157, 100 μM glutamate with 10 μM glycine, or both for 5 min (indicated by the bar). After approximately 10 min of recovery in normal HBSS, neurons were exposed to 25 mM NH_4Cl for 1 min as a positive control to display the dynamic range of dye response. A decrease in the BCECF ratio indicates a decrease in intracellular pH. Traces represent the mean data from separate coverslips containing 17–25 neurons. Similar results were obtained in cells from two additional culture dates.

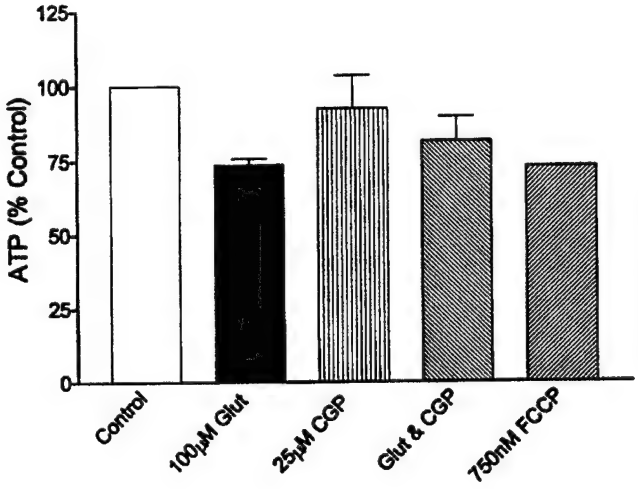

Fig. 4 Effects of CGP-37157 and glutamate on cellular ATP levels. Neuronal ATP levels are presented as the percent ATP of control values. Neurons were exposed to either HBSS, 750 nM FCCP, 25 μM CGP-37157, 100 μM glutamate with 1 μM glycine, or both CGP-37157 and glutamate for 10 min prior to extraction of cell lysate. Cell extracts were harvested from three coverslips per condition. ATP levels were determined by a luciferase assay system. Data are presented as the percent of control (mean ± SEM) of three separate experiments from two different culture dates. None of the conditions were significantly different from control as determined by ANOVA followed by a Bonferroni post-hoc analysis.

Effects of CGP-37157 on glutamate-induced changes in $[Ca^{2+}]_i$ and mitochondrial Ca^{2+}

The relative lack of effect of CGP-37157 on mitochondrial function and glutamate-induced changes in

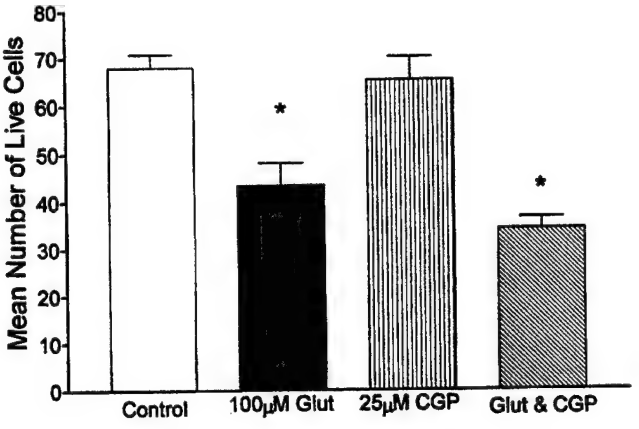

Fig. 5 CGP-37157 does not alter neuronal death. Bars represent the mean results from three experiments in which three fields from each of three coverslips were counted for each treatment condition in a blinded manner. On each experimental day coverslips were exposed (in triplicate) for 5 min to the following conditions: HBSS, 25 μM CGP-37157, 100 μM glutamate plus 1 μM glycine, or glutamate and CGP-37157. Cells excluding trypan blue were counted. Statistical significance was determined using a one-way ANOVA test followed by Bonferroni post-hoc analysis. *Significantly different ($P < 0.01$) compared to control.

mitochondrial function led us to examine the effects of Na^+–Ca^{2+}-exchange inhibition on glutamate-induced changes in $[Ca^{2+}]_i$ and mitochondrial Ca^{2+} loads. We have recently demonstrated the feasibility of estimating matrix Ca^{2+} by using FCCP to release mitochondrial Ca^{2+} and MagFura-2 to measure the $[Ca^{2+}]_i$ after this procedure (Fig. 6A, [49]).

A 5-min exposure to 100 μM glutamate and 1 μM glycine increases $[Ca^{2+}]_i$ as measured with MagFura-2 (Fig. 6D grey bar; glutamate). However, this may not indicate the full extent of Ca^{2+} influx following glutamate-receptor activation as the mitochondria are simultaneously buffering $[Ca^{2+}]_i$ (Fig. 6A). Thus, we used 750 nM FCCP to release accumulated mitochondrial Ca^{2+} following glutamate stimulation (Fig. 6D grey bar; FCCP). FCCP is applied in Ca^{2+}-free HBSS to ensure that Ca^{2+} entry is not occurring via voltage-sensitive Ca^{2+} channels as a result of FCCP-induced depolarization of the plasma membrane. The application of CGP-37157 during the 5-min glutamate stimulus had no significant effect on measurable $[Ca^{2+}]_i$ levels (Fig. 6D black bar; glutamate). Surprisingly, inhibition of the Na^+–Ca^{2+} exchanger only produced a slight enhancement of accumulated mitochondrial Ca^{2+} (Fig. 6D black bar; FCCP). Although the use of the low-affinity Ca^{2+} indicator MagFura-2 in these experiments makes it unlikely that dye saturation occurred during these experiments, this is a possible explanation for the failure of CGP-37157 to enhance glutamate-induced mitochondrial Ca^{2+} accumulation. To exclude this possibility we also monitored the effects of CGP-37157 using the same paradigm but

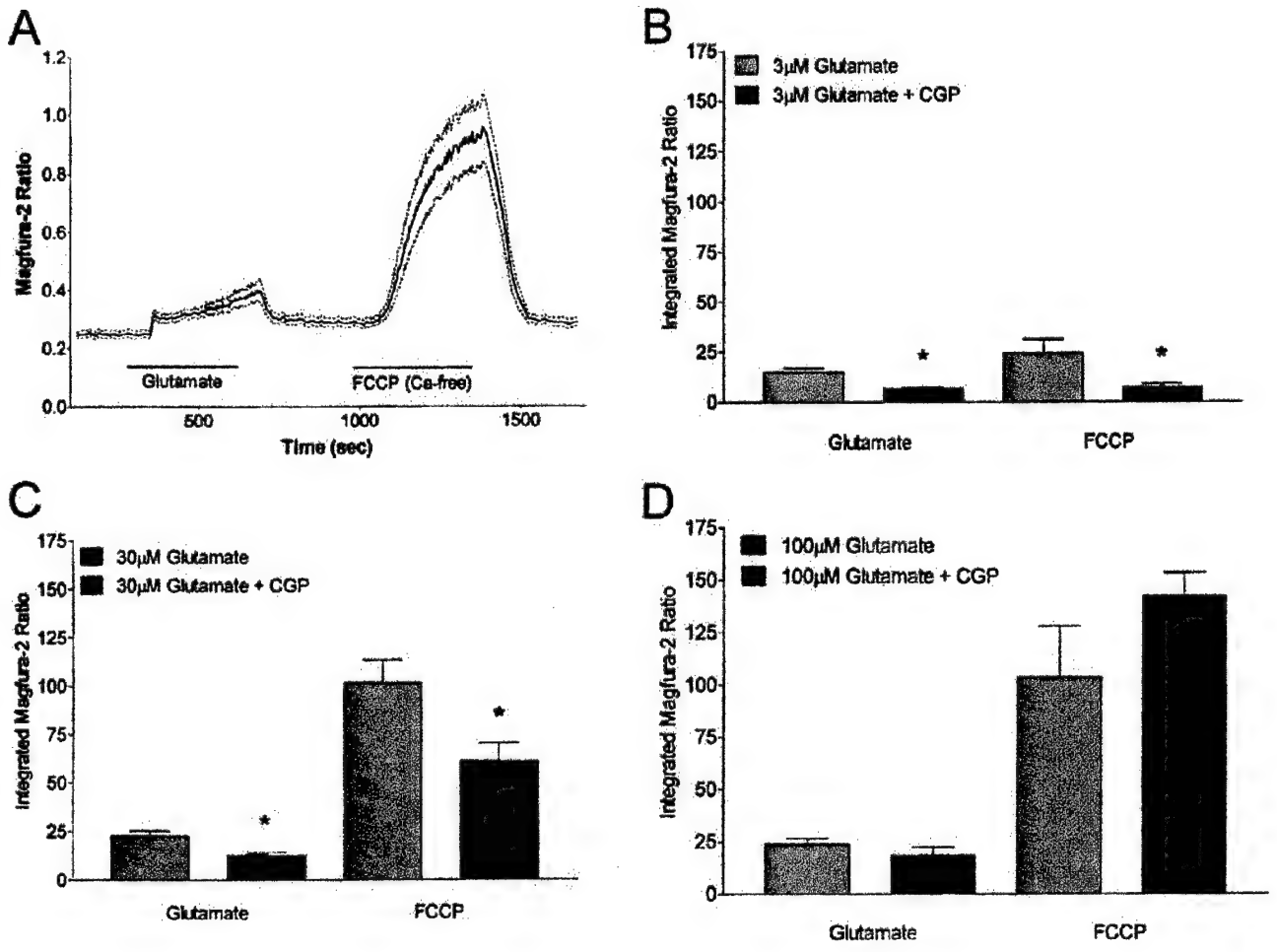

Fig. 6 Effects of CGP-37157 on glutamate-induced mitochondrial Ca^{2+} loading. (A) A representative trace is included to display the experimental paradigm. After 4 min of baseline monitoring of MagFura-2-loaded cells, glutamate (30 μM) and glycine (1 μM), were applied for 5 min. Cells were then rinsed with HBSS for 5 min and perfused with FCCP (750 nM) for a further 5 min. The baseline was taken as the ratio preceding the introduction of glutamate in the buffer. The solid line represents the mean of 15 neurons from a single cover slip, while the broken line shows the SEM for these cells. (B–D) Mean data obtained using this paradigm while varying the concentration of glutamate between three and 100 μM as indicated. Note that the experiments depicted in B and C were performed with 10 μM CGP-37157 while the experiment in D used 25 μM. Data represent the integrated area under the curve of baseline-subtracted values obtained during exposure to glutamate or to FCCP. Bars represent the mean results from 5–7 coverslips over two or more culture dates. CGP-37157 significantly *decreased* the glutamate-induced cytosolic and mitochondrial Ca^{2+} changes determined using ANOVA (*indicates significantly different from control, $P<0.05$).

with lower glutamate concentrations which result in reduced cytoplasmic and mitochondrial Ca^{2+} accumulation (Figs 6B & C). However, although an increase in mitochondrial Ca^{2+} might be expected in the presence of CGP-37157 we actually observed a decrease in cytosolic and mitochondrial Ca^{2+} under these conditions.

DISCUSSION

In this study we have explored the effect of the mitochondrial Na^+–Ca^{2+}-exchange inhibitor CGP-37157 on glutamate-stimulated, NMDA receptor-mediated changes in mitochondrial function in central neurons. Our anticipation in approaching these experiments was that CGP-37157 would increase matrix Ca^{2+} concentrations and thereby potentiate the glutamate stimulated changes in function. What is quite obvious from the present experiments is that this is not at all the case.

The oxidation sensitive dyes DCF and DHE are able to report several phenomena associated with glutamate receptor activation. DHE is preferentially oxidized by superoxide [31], but may also report alterations in mitochondrial membrane potential ($\Delta\Psi_m$) [50]. However, CGP-37157 did not potentiate the DHE signal. That it did not alter the effects of peroxide on DHE fluorescence argues that the apparent lack of effect is not due to some non-specific effect on the dye or that it has antioxidant properties (Fig. 1B). DCF is sensitive to the formation of

ROS and is also quenched by intracellular acidification [29]. The CGP-37157-induced decrease in DCF may be con-sistent with intracellular acidification, as is the potentiation of the effects of glutamate (although see below). Detecting an increase in oxidation of DCF can be somewhat problematic with the marked decrease in signal that occurs with acidification. However, counting the cells that show the characteristic localized increases in fluorescence circumvents this problem [29]. Once again, these results are not consistent with enhancement of the accumulation of matrix calcium.

Increases in matrix Ca^{2+} stimulates Ca^{2+}-sensitive, rate-limiting dehydrogenases involved in metabolism, and thus couples increased energy demand signalled by an elevation in $[Ca^{2+}]_i$ to the aerobic production of ATP [48]. This should have several consequences for the neurons stimulated by glutamate. Enhanced metabolic activation has been proposed to account for the well-documented intracellular acidification associated with NMDA receptor activation and Ca^{2+} influx [51–53], and this would be consistent with the increased quenching of DCF shown in Figure 1B. However, an authentic pH indicator, BCECF, showed relatively little effect either of CGP-37157 alone or in combination with glutamate (Fig. 3). In addition, mitochondrial Na^+–Ca^{2+} exchange occurs at the expense of ATP generation [40,53], so that inhibition of this process should at least prevent ATP loss. However, increases in the $\Delta\Psi_m$ can also result from ATP hydrolysis in an effort to maintain or restore $\Delta\Psi_m$ [19,54] and may alternatively explain the hyperpolarization induced by CGP-37157 over neuronal cultures. Surprisingly, CGP-37157 had no effect on cellular ATP levels, compared to controls, in the presence or absence of glutamate (Fig. 4). One could speculate that the lack of change in cellular ATP levels in our culture system is because of a greater dependence on glycolytic ATP production than on oxidative phosphorylation as seen in cultured cerebellar granule cells [19,25], but again it is difficult to relate these observations simply to enhanced matrix Ca^{2+} accumulation. The ultimate question with respect to glutamate-induced alterations in mitochondrial function is the impact of CGP-37157 on neuronal viability, and CGP-37157 evidently has no beneficial or detrimental effect on the viability of neurons in the absence or presence of glutamate (Fig. 5). Thus, although mitochondrial uptake of Ca^{2+} during excitotoxicity is clearly detrimental to cell viability [25,26], CGP-37157 clearly does not have a substantial impact on this process.

This raises the question of whether CGP-37157 has any effect on matrix Ca^{2+} content at all. This has been a difficult question to address experimentally for a variety of reasons. In the kinds of experimental approach used here, several laboratories have used the Ca^{2+} indicator rhod-2 to estimate matrix Ca^{2+} changes [55–60]. This is clearly an effective approach provided that the dye can be localized to the mitochondrial matrix rather than any other cellular compartment, and also provided that the matrix Ca^{2+} concentrations do not exceed the dynamic range of the dye. Indeed, some of the other reports in this volume elegantly demonstrate the use of this approach. However, under conditions of excitotoxicity it is likely that matrix Ca^{2+} greatly exceeds the limit of sensitivity of this dye (~5 μM, based on an affinity of about 500 nM). Thus, although it is possible to load the dye into mitochondria in neurons and to monitor changes in matrix Ca^{2+} [59–61] it is not clear that the dye faithfully reports the full extent of the Ca^{2+} change.

We recently developed an alternative approach to determining mitochondrial Ca^{2+} content following glutamate exposure [49]. This approach takes advantage of the reversibility of the Ca^{2+} uniporter [13]. Thus, following exposure of neurons to glutamate the cells are exposed to FCCP which collapses the mitochondrial membrane potential and releases Ca^{2+} into the matrix, presumably by the reversal of the uniporter. A low-affinity Ca^{2+} indicator (MagFura-2 in this case) can then be used to report the Ca^{2+} changes, and provide a semiquantitative insight into the Ca^{2+} contents of the mitochondria.

Using this approach we were thus able to monitor the Ca^{2+} loading of mitochondria following glutamate exposure in the absence or presence of CGP-37157 (Fig. 6). Rather surprisingly, CGP-37157 had little effect on the matrix Ca^{2+} content under the conditions employed for most of the studies reported here (i.e. 100 μM glutamate for 5 min). To ensure that the failure to observe an effect of CGP-37157 was not due to dye saturation, or to the possibility that mitochondria are overwhelmed with the Ca^{2+} load caused by this toxic stimulus, we also tried lower glutamate concentration, but also failed to see an effect of CGP-37157 beyond a small inhibition of the glutamate triggered Ca^{2+} entry, which may be a consequence of the Ca^{2+} channel inhibition produced by this drug.

It is not at all clear how to account for the lack of effect of a drug that, under some circumstances at least, has a substantial effect on the egress of Ca^{2+} from neuronal mitochondria [43,45,62]. Although the failure to increase matrix Ca^{2+} accounts for the lack of effect of CGP-37157 on ROS generation, ATP depletion or synthesis and neuronal viability, it is not obvious why Ca^{2+} was not increased. Perhaps the most obvious suggestion is that the major Ca^{2+} efflux pathway in effect during glutamate exposure is not, in fact, the Na^+–Ca^{2+} exchanger. Based on the observations of the effects of FCCP it is clear that a loss of $\Delta\Psi_m$ can result in release of Ca^{2+} from mitochondria, presumably via reversal of the uniporter. We know that at least some of the neurons will exhibit mitochondrial depolarization during glutamate exposure [32] which might result in Ca^{2+} release.

Activation of the permeability transition pore would also result in Ca^{2+} release that is insensitive to CGP-37157, although evidence for the activation of this process during glutamate stimulation is less than robust. Most tissues also have a Na^+-independent mitochondrial Ca^{2+} efflux pathway [40]. Although the Na^+–Ca^{2+} exchanger is considered to be the dominant mechanism in brain, it is perhaps possible that the Na^+-independent pathway is more active in our neurons under the circumstances of Na^+–Ca^{2+} exchanger inhibition. A more trivial explanation of such observations would be that CGP-37157 blocks NMDA receptors at the concentrations used. We have no evidence for such an effect at this point (and this would certainly not account for its ability to alter mitochondrial Ca^{2+} efflux previously reported) but this remains an issue with all pharmacological approaches to studying physiological function.

More broadly, the difficulties in interpreting what should be a straightforward set of results illustrate the problems encountered with the pharmacological manipulation of mitochondrial Ca^{2+} transport. The drugs that inhibit the main mitochondrial influx pathways do not penetrate cells well (Ru360), are not very specific for the uniporter (ruthenium red) and do not very clearly distinguish between the different modes of Ca^{2+} uptake [36]. Assuming that the Na^+–Ca^{2+} exchanger is the main efflux pathway, an apparently specific and effective inhibitor does not at all have the anticipated effect, as reported here. This leaves one with the option of manipulating these processes indirectly, such as by the use of FCCP or by inhibition of electron transport to manipulate membrane potential. However, these approaches cannot be considered specific either, and the other actions of FCCP, for example, are well recognized [63]. Thus, investigating mitochondrial Ca^{2+} transport in intact cells using pharmacological approaches remains quite problematic.

ACKNOWLEDGMENTS

These studies were supported by USAMRMC grant DAMD17-98-1-8627 and by NIH grant NS 34138 (IJR). JBB was supported by a Long-Term Fellowship from the Human Frontiers Science Program (LT0500/1999B).

REFERENCES

1. Mayer ML, Westbrook GL. Cellular mechanisms underlying excitotoxicity. *Trends Neurosci* 1987; **10**: 59–61.
2. Choi DW. Glutamate neurotoxicity and diseases of the nervous system. *Neuron* 1988; **1**: 623–634.
3. Choi DW, Maulucci-Gedde M, Kriegstein AR. Glutamate neurotoxicity in cortical cell culture. *J Neurosci* 1987; **7**: 357–368.
4. Choi DW. Ionic dependence of glutamate neurotoxicity. *J Neurosci* 1987; **7**: 369–379.
5. Ankarcrona M, Dypbukt JM, Bonfoco E et al. Glutamate-induced neuronal death: a succession of necrosis or apoptosis depending on mitochondrial function. *Neuron* 1995; **15**: 961–973.
6. Koh JY, Goldberg MP, Hartley DM, Choi DW. Non-NMDA receptor mediated neurotoxicity in cortical culture. *J Neurosci* 1990; **10**: 693–705.
7. Kristián T, Ouyang Y, Siesjö BK. Calcium-induced neuronal cell death in vivo and in vitro: are the pathophysiologic mechanisms different? *Adv Neurol* 1996; **71**: 107–118.
8. Doble A. The role of excitotoxicity in neurodegenerative disease: implications for therapy. *Pharmacol Ther* 1999; **81**: 163–221.
9. Hyrc K, Handran SD, Rothman SM, Goldberg MP. Ionized intracellular calcium concentration predicts excitotoxic neuronal death: observations with low affinity fluorescent calcium indicators. *J Neurosci* 1997; **17**: 6669–6677.
10. Stout AK, Reynolds IJ. High-affinity calcium indicators underestimate increases in intracellular calcium concentrations associated with excitotoxic glutamate stimulations. *Neuroscience* 1999; **89**: 91–100.
11. Sattler R, Xiong Z, Lu WY, Hafner M, MacDonald JF, Tymianski M. Specific coupling of NMDA receptor activation to nitric oxide neurotoxicity by PSD-95 protein. *Science* 1999; **284**: 1845–1848.
12. Nicholls DG, Akerman KEO. Mitochondrial calcium transport. *Biochim Biophys Acta* 1982; **683**: 57–88.
13. Gunter TE, Pfeiffer DR. Mechanisms by which mitochondria transport calcium. *Am J Physiol Cell Physiol* 1990; **258**: C755–C786.
14. Babcock DF, Hille B. Mitochondrial oversight of cellular Ca^{2+} signalling. *Curr Opin Neurobiol* 1998; **8**: 398–404.
15. Duchen MR. Ca^{2+}-dependent changes in the mitochondrial energetics in single dissociated mouse sensory neurons. *Biochem J* 1992; **283**: 41–50.
16. Friel DD, Tsien RW. An FCCP-sensitive Ca^{2+} store in bullfrog sympathetic neurons and its participation in stimulus-evoked changes in $[Ca^{2+}]_i$. *J Neurosci* 1994; **14**: 4007–4024.
17. Werth JL, Thayer SA. Mitochondria buffer physiological calcium loads in cultured rat dorsal root ganglion neurons. *J Neurosci* 1994; **14**: 348–356.
18. Kiedrowski L, Costa E. Glutamate-induced destabilization of intracellular calcium concentration homeostasis in cultured cerebellar granule cells: role of mitochondria in calcium buffering. *Mol Pharmacol* 1995; **47**: 140–147.
19. Budd SL, Nicholls DG. A reevaluation of the role of mitochondria in neuronal Ca^{2+} homeostasis. *J Neurochem* 1996; **66**: 403–411.
20. Khodorov B, Pinelis V, Storozhevykh T, Vergun O, Vinskaya N. Dominant role of mitochondria in protection against a delayed neuronal Ca^{2+} overload induced by endogenous excitatory amino acids following a glutamate pulse. *FEBS Lett* 1996; **393**: 135–138.
21. Wang GJ, Thayer SA. Sequestration of glutamate-induced Ca^{2+} loads by mitochondria in cultured rat hippocampal neurons. *J Neurophysiol* 1996; **76**: 1611–1621.
22. Brorson JR, Sulit RA, Zhang H. Nitric oxide disrupts Ca^{2+} homeostasis in hippocampal neurons. *J Neurochem* 1997; **68**: 95–105.
23. Murchison D, Griffith WH. Age-related alterations in caffeine-sensitive calcium stores and mitochondrial buffering in rat basal forebrain. *Cell Calcium* 1999; **25**: 439–452.
24. Pivovarova NB, Hongpaisan J, Andrews SB, Friel DD. Depolarization-induced mitochondrial Ca accumulation in sympathetic neurons: spatial and temporal characteristics. *J Neurosci* 1999; **19**: 6372–6384.

25. Budd SL, Nicholls DG. Mitochondria, calcium regulation and acute glutamate excitotoxicity in cultured cerebellar granule cells. *J Neurochem* 1996; **67**: 2282–2291.
26. Stout AK, Raphael HM, Kanterewicz BI, Klann E, Reynolds IJ. Glutamate-induced neuron death requires mitochondrial calcium uptake. *Nature Neurosci* 1998; **1**: 366–373.
27. Lafon-Cazal M, Pietri S, Culcasi M, Bockaert J. NMDA-dependent superoxide production and neurotoxicity. *Nature* 1993; **364**: 535–537.
28. Dykens JA. Isolated cerebral and cerebellar mitochondria produce free radicals when exposed to elevated Ca^{2+} and Na^{+}: implications for neurodegeneration. *J Neurochem* 1994; **63**: 584–591.
29. Reynolds IJ, Hastings TG. Glutamate induces the production of reactive oxygen species in cultured forebrain neurons following NMDA receptor activation. *J Neurosci* 1995; **15**: 3318–3327.
30. Dugan LL, Sensi SL, Canzoniero LMT et al. Mitochondrial production of reactive oxygen species in cortical neurons following exposure to N-methyl-D-aspartate. *J Neurosci* 1995; **15**: 6377–6388.
31. Bindokas VP, Jordan J, Lee CC, Miller RJ. Superoxide production in rat hippocampal neurons: selective imaging with hydroethidine. *J Neurosci* 1996; **16**: 1324–1336.
32. White RJ, Reynolds IJ. Mitochondrial depolarization in glutamate-stimulated neurons: An early signal specific to excitotoxin exposure. *J Neurosci* 1996; **16**: 5688–5697.
33. Schinder AF, Olson EC, Spitzer NC, Montal M. Mitochondrial dysfunction is a primary event in glutamate neurotoxicity. *J Neurosci* 1996; **16**: 6125–6133.
34. Nieminen A-L, Petrie TG, Lemasters JJ, Selman WR. Cyclosporin A delays mitochondrial depolarization induced by N-methyl-D-aspartate in cortical neurons: evidence of the mitochodrial permeability transition. *Neuroscience* 1996; **75**: 993–997.
35. Sparagna GC, Gunter KK, Sheu S-S, Gunter TE. Mitochondrial calcium uptake from physiological-type pulses of calcium. A description of the rapid uptake mode. *J Biol Chem* 1996; **270**: 27510–27515.
36. Gunter TE, Buntinas L, Sparagna GC, Gunter KK. The Ca^{2+} transport mechanisms of mitochondria and Ca^{2+} uptake from physiological type calcium transients. *Biochim Biophys Acta* 1998; **1366**: 5–15.
37. Matlib MA, Zhou Z, Knight S et al. Oxygen-bridged dinuclear ruthenium amine complex specifically inhibits Ca^{2+} uptake into mitochondria in vitro and in situ in single cardiac myocytes. *J Biol Chem* 1998; **273**: 10223–10231.
38. Crompton M, Andreeva L. On the interactions of Ca^{2+} and cyclosporin A with a mitochondrial inner membrane pore: a study using cobaltammine complex inhibitors of the Ca^{2+} uniporter. *Biochem J* 1994; **302**: 181–185.
39. Griffiths EJ. Reversal of mitochondrial NaCa exchange during metabolic inhibition in rat cardiomyocytes. *FEBS Lett* 1999; **453**: 400–404.
40. Gunter TE, Gunter KK, Sheu S-S, Gavin CE. Mitochondrial calcium transport: physiological and pathological relevance. *Am J Physiol Cell Physiol* 1994; **267**: C313–C339.
41. Fiskum G, Cockrell RS. Uncoupler-stimulated release of Ca^{2+} from Ehrlich ascites tumor cell mitochondria. *Arch Biochem Biophys* 1985; **240**: 723–733.
42. Zoratti M, Szabo I. The mitochondrial permeability transition. *Biochim Biophys Acta* 1995; **1241**: 139–176.
43. White RJ, Reynolds IJ. Mitochondria accumulate Ca^{2+} following intense glutamate stimulation of cultured rat forebrain neurones. *J Physiol (Lond)* 1997; **498**: 31–47.
44. Hoyt KR, Stout AK, Cardman JM, Reynolds IJ. An evaluation of intracellular sodium and mitochondria in the buffering of kainate-induced intracellular free calcium changes in rat forebrain neurons. *J Physiol (Lond)* 1998; **509**: 103–116.
45. Baron KT, Thayer SA. CGP 37157 modulates mitochondrial Ca^{2+} homeostasis in cultured rat dorsal root ganglion neurons. *Eur J Pharmacol* 1997; **340**: 295–300.
46. White RJ, Reynolds IJ. Mitochondria and Na^{+}/Ca^{2+} exchange buffer glutamate-induced calcium loads in cultured cortical neurons. *J Neurosci* 1995; **15**: 1318–1328.
47. Scanlon JM, Reynolds IJ. Effects of oxidants and glutamate receptor activation on mitochondrial membrane potential in rat forebrain neurons. *J Neurochem* 1998; **71**: 2392–2401.
48. McCormack JG, Halestrap AP, Denton RM. Role of calcium ions in regulation of mammalian intramitochondrial metabolism. *Physiol Rev* 1990; **70**: 391–425.
49. Brocard JB, Tassetto M, Reynolds IJ. Quantitative evaluation of mitochondrial calcium content following glutamate receptor stimulation in rat cortical neurones. *J Physiol (Lond)* 2000; (in press).
50. Budd SL, Castilho RF, Nicholls DG. Mitochondrial membrane potential and hydroethidine-monitored superoxide generation in cultured cerebellar granule cells. *FEBS Lett* 1997; **415**: 21–24.
51. Hartley Z, Dubinsky JM. Changes in intracellular pH associated with glutamate excitotoxicity. *J Neurosci* 1993; **13**: 4690–4699.
52. Irwin RP, Lin S-Z, Long RT, Paul SM. N-methyl-D-aspartate induces a rapid, reversible and calcium dependent intracellular acidosis in cultured fetal rat hippocampal neurons. *J Neurosci* 1994; **14**: 1352-1357.
53. Wang GJ, Randall RD, Thayer SA. Glutamate-induced intracellular acidification of cultured hippocampal neurons demonstrates altered energy metabolism resulting from Ca^{2+} loads. *J Neurophysiol* 1994; **72**: 2563–2569.
54. Di Lisa F, Blank PS, Colonna R et al. Mitochondrial membrane potential in single living adult rat cardiac myocytes exposed to anoxia or metabolic inhibition. *J Physiol (Lond)* 1995; **486**: 1–13.
55. Burnier M, Centeno G, Burki E, Brunner HR. Confocal microscopy to analyze cytosolic and nuclear calcium in cultured vascular cells. *Am J Physiol* 1994; **266**: C1118–C1127.
56. Simpson PB, Russell JT. Mitochondria support inositol 1,4,5-trisphosphate-mediated Ca^{2+} waves in cultured oligodendrocytes. *J Biol Chem* 1996; **271**: 33493–33501.
57. Babcock DF, Herrington J, Goodwin PC, Park YB, Hille B. Mitochondrial participation in the intracellular Ca^{2+} network. *J Cell Biol* 1997; **136**: 833–844.
58. Trollinger DR, Cascio WE, Lemasters JJ. Selective loading of Rhod 2 into mitochondria shows mitochondrial Ca^{2+} transients during the contractile cycle in adult rabbit cardiac myocytes. *Biochem Biophys Res Commun* 1997; **236**: 738–742.
59. David G, Barrett JN, Barrett EF. Evidence that mitochondria buffer physiological Ca^{2+} loads in lizard motor nerve terminals. *J Physiol (Lond)* 1998; **509**: 59–65.
60. Peng TI, Jou MJ, Sheu S-S, Greenamyre JT. Vizualization of NMDA receptor-induced mitochondrial calcium accumulation in striatal neurons. *Exp Neurol* 1998; **149**: 1–12.
61. Peng TI, Greenamyre JT. Privileged access to mitochondria of calcium influx through N-methyl-D-aspartate receptors. *Mol Pharmacol* 1998; **53**: 974–980.
62. Zhang YL, Lipton P. Cytosolic Ca^{2+} changes during in vitro ischemia in rat hippocampal slices: major roles for glutamate and Na^{+}-dependent Ca^{2+} release from mitochondria. *J Neurosci* 1999; **19**: 3307–3315.
63. Tretter L, Chinopoulos C, Adam-Vizi V. Plasma membrane depolarization and disturbed Na^{+} homeostasis induced by the protonophore carbonyl cyanide-p-trifluoromethoxyphenyl-hydrazone in isolated nerve terminals. *Mol Pharmacol* 1998; **53**: 734–741.

Biophysical Journal Volume 85 November 2003 3358–3366

Spontaneous Changes in Mitochondrial Membrane Potential in Single Isolated Brain Mitochondria

Olga Vergun, Tatyana V. Votyakova, and Ian J. Reynolds
Department of Pharmacology, University of Pittsburgh, Pittsburgh, Pennsylvania 15261 USA

ABSTRACT In this study we measured $\Delta\Psi$m in single isolated brain mitochondria using rhodamine 123. Mitochondria were attached to coverslips and superfused with K^+-based HEPES-buffer medium supplemented with malate and glutamate. In ~70% of energized mitochondria we observed large amplitude spontaneous fluctuations in $\Delta\Psi$m with a time course comparable to that observed previously in mitochondria of intact cells. The other 30% of mitochondria maintained a stable $\Delta\Psi$m. Some of the "stable" mitochondria began to fluctuate spontaneously during the recording period. However, none of the initially fluctuating mitochondria became stable. Upon the removal of substrates from the medium or application of small amounts of Ca^{2+}, rhodamine 123 fluorescence rapidly dropped to background values in fluctuating mitochondria, while nonfluctuating mitochondria depolarized with a delay and often began to fluctuate before complete depolarization. The changes in $\Delta\Psi$m were not connected to oxidant production since reducing illumination or the addition of antioxidants had no effect on $\Delta\Psi$m. Fluctuating mitochondria did not lose calcein, nor was there any effect of cyclosporin A on $\Delta\Psi$m, which ruled out a contribution of permeability transition. We conclude that the fluctuations in $\Delta\Psi$m reflect an intermediate, unstable state of mitochondria that may lead to or reflect mitochondrial dysfunction.

INTRODUCTION

Mitochondria serve many functions in eukaryotic cells. Perhaps the most important is the generation of adenosine 5′-triphosphate (ATP) by oxidative phosphorylation. This, along with many mitochondrial carrier-mediated processes, requires an electrochemical potential generated by the electron transport chain (for review see Bernardi, 1999). Thus, normally functioning mitochondria establish a mitochondrial membrane potential ($\Delta\Psi$m) and a pH gradient (ΔpH) which together comprise Δp, the proton motive force that drives ATP synthesis. Processes that dissipate Δp are usually considered harmful to cells, although it can be argued that regulated uncoupling of Δp from ATP synthesis has some beneficial effects (Nicholls, 2001; Skulachev, 1998).

The $\Delta\Psi$m is typically the more dynamic parameter in the proton motive force. $\Delta\Psi$m is typically maintained at −150-200 mV in respiring mitochondria and may be dissipated by ATP synthesis, Ca^{2+} transport, or the activity of other carrier proteins. Perhaps surprisingly, a number of laboratories have recently reported spontaneous changes in $\Delta\Psi$m in experimental conditions where $\Delta\Psi$m was monitored in individual mitochondria using fluorescent potential-sensitive dyes. Alterations in $\Delta\Psi$m detected as transient decreases in dye signals have been reported in neuroblastoma cells (Loew et al., 1993; Fall and Bennett, 1999), astrocytes (Belousov et al., 2001; Buckman and Reynolds, 2001b), cardiomyocytes (Duchen et al., 1998), vascular endothelial cells (Huser and Blatter, 1999), and pancreatic B-cells (Krippeit-Drews et al., 2000). We have also reported a slightly different phenomenon of transient *increases* in the signal of potential-sensitive dyes in primary cultures of forebrain neurons (Buckman and Reynolds, 2001a). Thus, spontaneous changes in mitochondrial function that are reported by these potential-sensitive dyes appear to be a common property of mitochondria in cells. The fundamental nature of the phenomenon and the mechanisms responsible for changing $\Delta\Psi$m remain unclear in these cell-based studies, although several laboratories have concluded that mitochondrial permeability transition (MPT) is an important contributor to the depolarizations (De Giorgi et al., 2000; Ichas et al., 1997; Huser et al., 1998).

Isolated mitochondria preparations offer a number of advantages over intact cells, particularly in the ability to manipulate access to substrates, to alter the local environment, and to deliver drugs. Typically these preparations are studied in a cuvette, which is an inherently unsuitable approach to study stochastic phenomena in individual organelles. However, several recent studies have demonstrated the feasibility of immobilizing individual mitochondria to permit imaging studies utilizing isolated mitochondria (Ichas et al., 1997; Huser et al., 1998; Huser and Blatter, 1999; Nakayama et al., 2002). Interestingly, immobilized mitochondria also exhibit spontaneous changes in $\Delta\Psi$m, suggesting that the mechanism producing this phenomenon can exist in a cell-free environment.

In the present study, we have applied this approach to the study of isolated rat forebrain mitochondria. We provide a quantitative demonstration of a number of different characteristics of this preparation, including the sensitivity to substrate removal, the effects of calcium loading, and the impact of oxidative stress. Interestingly, however, we find no evidence to support the suggestion that spontaneous depolarization of brain mitochondria is mediated by MPT.

Submitted March 25, 2003, and accepted for publication July 7, 2003.

Address reprint requests to Ian J. Reynolds, Dept. of Pharmacology, University of Pittsburgh, W1351 Biomedical Science Tower, Pittsburgh, PA 15261 USA. Tel.: 412-648-2134; Fax: 412-624-0794; E-mail: iannmda@pitt.edu.

0006-3495/03/11/3358/09 $2.00

MATERIALS AND METHODS

Materials

All materials and reagents were purchased through Sigma (St. Louis, MO), unless otherwise specified.

Isolation of mitochondria

All procedures using animals were in accordance with the National Institutes of Health Guide for the Care and Use of Laboratory Animals and were approved by the University of Pittsburgh's Institutional Animal Care and Use Committee. Rat brain mitochondria were isolated from the cortex of male Sprague-Dawley rats using a Percoll gradient method described by Sims (Sims, 1991) with minor modifications. Isolation buffer contained (in mM): mannitol 225, sucrose 75, EDTA 0.5, HEPES 5, 1 mg/mL fatty acid free BSA, pH adjusted to 7.3 with KOH. Brain tissue was homogenized using a glass/glass homogenizer in isolation buffer containing 12% Percoll and carefully layered on the top of a 12%/24%/42% discontinuous gradient of Percoll. After 11 min of centrifugation at 31,000 × *g*, the mitochondrial fraction was collected from the top of the 42% Percoll layer of the gradient and then washed twice. For the final wash we used isolation buffer where BSA was omitted, and concentration of EDTA was reduced to 0.1 mM. All isolation procedures were carried out at 0–2°C. During experimentation mitochondria were stored on ice at a final concentration of 15–20 mg protein/ml in isolation medium until use. The protein concentration in each preparation was determined by the Biuret method using a plate reader.

Experimental solutions and fluorescence measurements

All imaging experiments were performed at room temperature in KCl-based buffer containing (in mM): KCl 125, K_2HPO_4 2, HEPES 5, $MgCl_2$ 5, EDTA 0.02, malate 5, glutamate 5, pH 7.0. Mitochondria were added to this buffer at final concentration of 0.75–1 mg protein/ml immediately before each experiment. Thirty-one mm glass coverslips were washed with 70% alcohol, then with H_2O and dried before use. A small drop (20 μl) of mitochondrial suspension was placed in the middle of the coverslip for 5–7 min. The coverslips with the mitochondrial suspension were carefully placed into a 700 μl perfusion chamber that was then mounted onto a microscope fitted for fluorescence imaging as described below. The mitochondria were perfused at 7 ml/min with KCl buffer; after 1 min of perfusion, mitochondria which had not attached to the coverslip were effectively washed out of the recording chamber. Typically, the density of attached mitochondria was 400,000–500,000 mitochondria per square millimeter. Thus, in a field observed with a 100× objective ~2000 mitochondria were present.

For $\Delta\Psi$m measurements, we used the potentiometric probes rhodamine 123 and tetramethylrhodamine methyl ester (Rh123 and TMRM, Molecular Probes, Eugene, OR) at nonquenching concentrations. Rh123 (200 nM) or TMRM (40 nM) were added to the perfusion buffer 2–3 min before the start of the recording and were present in the perfusion medium during the experiment. No preloading was necessary. To monitor calcein (Molecular Probes) fluorescence within the mitochondria, the mitochondria were loaded with 8 μM calcein AM for 30 min at room temperature, and then placed onto the coverslip as described above. For the fluorescence recording, we used a BX50WI Olympus Optical (Tokyo, Japan) microscope fitted with an Olympus Optical LUM PlanFI 100× water immersion quartz objective. The fluorescence was monitored using excitation light provided by a 75 W xenon lamp-based monochromator (T.I.L.L. Photonics GmbH, Martinsried, Germany), and emitted light was detected using a CCD camera (Orca; Hamamatsu, Shizouka, Japan). For Rh123 or calcein, mitochondria were illuminated with 490 nm, and emitted fluorescence was passed through a 500-nm long-pass dichroic mirror and a 535/25 nm band-pass filter (Omega Optical, Brattleboro, VT). TMRM was excited with a 550-nm light, the signal was passed through a 570-nm long-pass dichroic mirror and collected using a 605/55-nm filter. An excitation exposure time and neutral density filters were chosen to avoid detector saturation during recording and to minimize light exposure. Mitochondria were exposed to light only during image acquisition (<0.5 s per image). Rh123 and TMRM images were acquired every 10 s, whereas calcein images were acquired every 20 s. Fluorescence data were acquired and analyzed using Simple PCI software (Compix, Cranberry, PA). Fluorescence was measured in 100–150 individual mitochondria for each coverslip. Objects smaller then 0.3 μm were not analyzed. Background fluorescence, determined from three or four mitochondrion-free regions of the coverslip, was subtracted from all the signals. All experiments were repeated 4–6 times using mitochondria from different animals.

Statistics

Statistical analysis was performed using Prism 3.0 (Graph Pad Software, San Diego, CA). All the data are presented as mean ± SE. Comparisons were made using Student's *t*-test, with *P* values of less than 0.05 taken as significant.

RESULTS

Fig. 1 shows a typical recording of Rh123 fluorescence obtained from individual mitochondria. Comparing phase contrast (DIC) and fluorescence images, we observed fluorescence in ~70% of mitochondria attached to the coverslip (Fig. 1 *A*). Nonfluorescent mitochondria were presumably already depolarized. Since a small nonquenching Rh123 concentration (200 nM) was used, the increase in fluorescence intensity reflected an increase in $\Delta\Psi$m (Nicholls and Ward, 2000). In response to mitochondrial depolarization caused by either application of mitochondrial uncoupler carbonyl cyanide *p*-trifluoro-methoxyphenyl hydrazone (FCCP, 250 nM) or by removal of respiratory substrates from the perfusion medium, the fluorescence of Rh123 dropped to background levels without an initial increase, confirming that Rh123 was not quenched (see Fig. 2 *A*). Fig. 1 *B* shows examples of the different patterns of changes in $\Delta\Psi$m observed in individual mitochondria. About 30% of the energized mitochondria maintained a stable $\Delta\Psi$m, which was rapidly dissipated after addition of FCCP (Fig. 2 *A*) or spontaneously during experiment (Fig.1 *B*, *trace* 1). The remaining 70% of mitochondria showed large amplitude spontaneous fluctuations in $\Delta\Psi$m, with maximal fluorescence comparable with that in "stable" mitochondria and minima near background levels (Fig.1 *B*, *traces* 3–5). Some nonfluctuating mitochondria began to fluctuate spontaneously during the recording period. However, none of the initially fluctuating mitochondria became stable. Fig. 1 *B* shows that the mean fluorescence of Rh123 gradually decreased during the time of recording.

To characterize the dynamics of $\Delta\Psi$m, three parameters were analyzed: a mean Rh123 fluorescence, a percentage of fluctuating mitochondria, and a frequency of fluctuations. All of those parameters were measured in the beginning (first

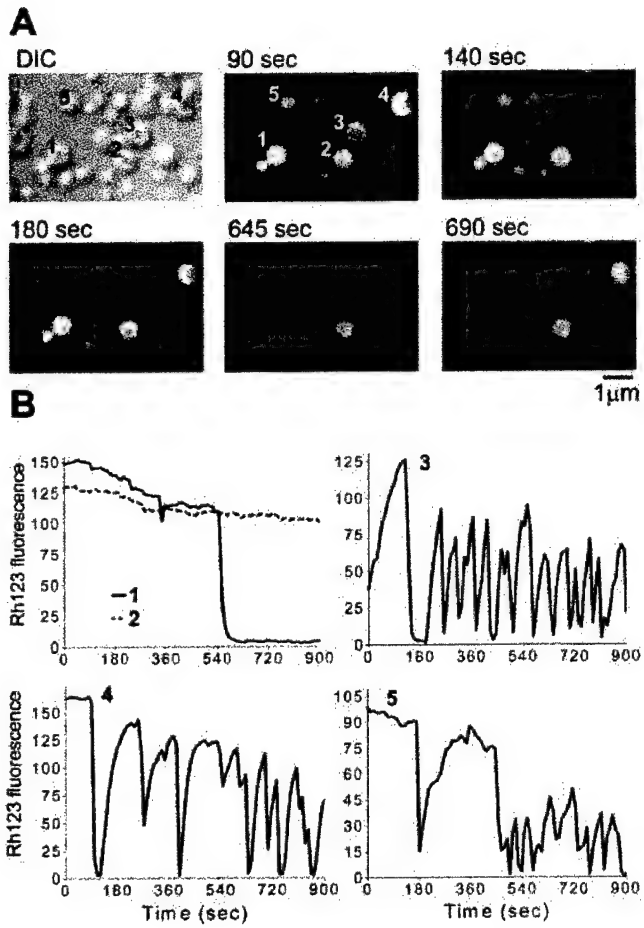

FIGURE 1 Examples of characteristic changes in Rh123 fluorescence in single mitochondria. (*A*) Representative DIC image and fluorescent images taken at different time points illustrating spontaneous $\Delta\Psi$m fluctuations. (*B*) The plots show different patterns of spontaneous changes in Rh123 fluorescence in five individual mitochondria from panel *A*. Mitochondria 1 and 2 would be considered nonfluctuating, whereas 3–5 show various characteristics of individual mitochondria with fluctuating $\Delta\Psi$m.

1–3 min) and at the end (12–15 min) of each experiment. We calculated the number of fluctuations using a custom macro written in Visual Basic for Microsoft Excel. Rapid decreases or increases in fluorescence with a minimal amplitude of 10 fluorescence units were counted as a single event. Thus, the mitochondrion presented in Fig. 1 *B*, *trace* 4, had two fluctuations during the first 180 s and four fluctuations between 720 and 900 s of the recording. Loss of fluorescence without recovery (as shown on Fig.1 *B*, *trace* 1) was not considered as an event. We noted that Rh123 fluorescence intensity varied between preparations (compare Fig. 1 to Fig. 2, for example). Collectively, there was an overall decrease in mean Rh123 fluorescence over the course of the recording, and an increase in the frequency of fluctuations. The characteristics of the spontaneous fluctuations in $\Delta\Psi$m were similar when using TMRM to report membane potential to those seen with Rh123 (data not shown).

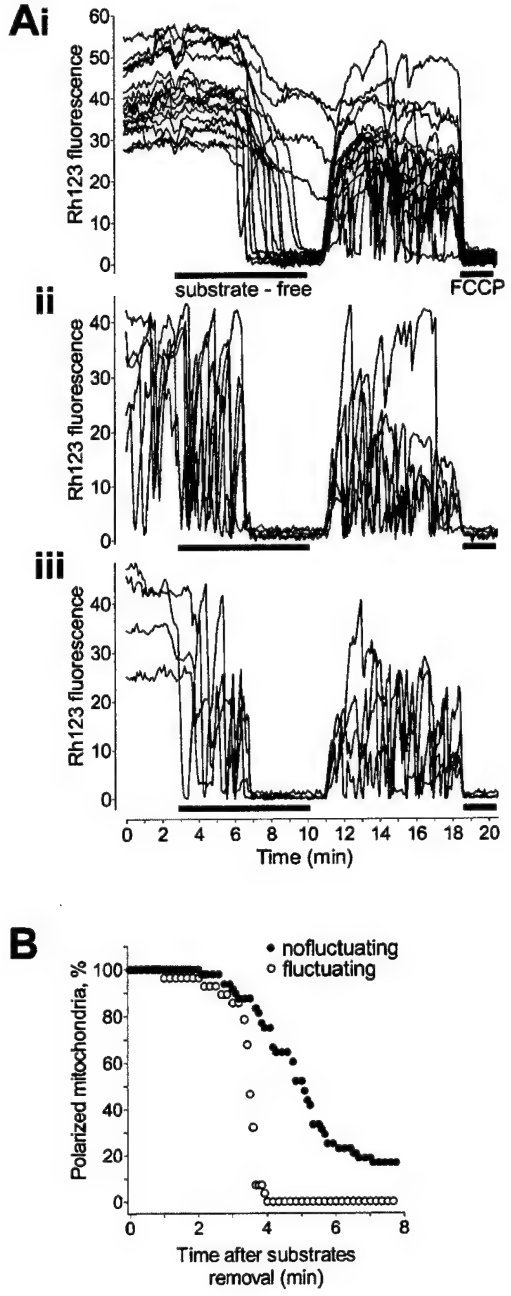

FIGURE 2 Time course of the mitochondrial depolarization in the response to removal of substrates and addition of Ca^{2+}. (*A*) Changes in Rh123 fluorescence in nonfluctuating (*i*), fluctuating (*ii*), and initially nonfluctuating (*iii*) individual mitochondria. (*B*) Summarized data of the single experiment presented in *A*, showing the rate of depolarization in fluctuating compared to nonfluctuating mitochondria. The time of the beginning of the application of substrate-free medium was defined as 0. The percentage of polarized mitochondria was calculated from 150 individual mitochondria; mitochondria that had an Rh123 fluorescence level less than four units were determined as depolarized. These results are representative of four additional experiments.

Characteristics of $\Delta\Psi$m fluctuations

In the next series of experiments, mitochondria were deenergized by deprivation of substrates. After the removal

of substrates, mitochondria maintained $\Delta\Psi$m for 1.5–3 min, and then depolarized. As illustrated in Fig. 2 *A*, where the nonfluctuating (*panel Ai*) and fluctuating (*panel Aii*) mitochondria are shown separately, stable mitochondria depolarized with a characteristic delay compared with fluctuating mitochondria. Indeed, some nonfluctuating mitochondria did not completely depolarize even after 10 min of substrate deprivation. Interestingly, most of the nonfluctuating and all of the fluctuating mitochondria lost $\Delta\Psi$m abruptly in substrate-free buffer, although the delay before loss of $\Delta\Psi$m was variable. This would be consistent with the loss of $\Delta\Psi$m requiring the activation of an explicit conductance, rather than as a slow leak of protons in the absence of ongoing proton extrusion. The results of this experiment are summarized on Fig. 2 *B*, which shows the percentage of mitochondria remaining polarized after substrate removal as a function of time. After 3 min of substrate-free medium, more then 80% of mitochondria in both groups remained polarized. However, by 4 min all fluctuating mitochondria had lost $\Delta\Psi$m, whereas 75% of nonfluctuating mitochondria still remained polarized. Qualitatively similar results were obtained in four other experiments.

Similar patterns of changes in $\Delta\Psi$m were observed in the next experiment, when mitochondria were exposed to Ca^{2+}. In these experiments 35 μM of Ca^{2+} was added to the buffer containing 20 μM EDTA, which should result in a free Ca^{2+} concentration of ~15μM. Fig. 3 *B* presents the data of one experiment, in which 150 individual mitochondria were analyzed. By the time all of the fluctuating mitochondria lost $\Delta\Psi$m, only 50% of the nonfluctuating mitochondria were fully depolarized. We also observed a subpopulation of initially nonfluctuating mitochondria which began to fluctuate in response to Ca^{2+} or substrate removal before they depolarized completely (Figs. 2 *Aiii* and 3 *Aiii*). The overall pattern of $\Delta\Psi$m behavior, after segregation into fluctuating and nonfluctuating populations, is illustrated in Fig. 3 *A*.

These data show that mitochondria which did not initially show spontaneous changes in $\Delta\Psi$m were more resistant to challenges like substrate deprivation or Ca^{2+} loading. This suggests that the fluctuation in $\Delta\Psi$m may be an intermediate state between stable, fully coupled mitochondria and damaged organelles that are fully depolarized.

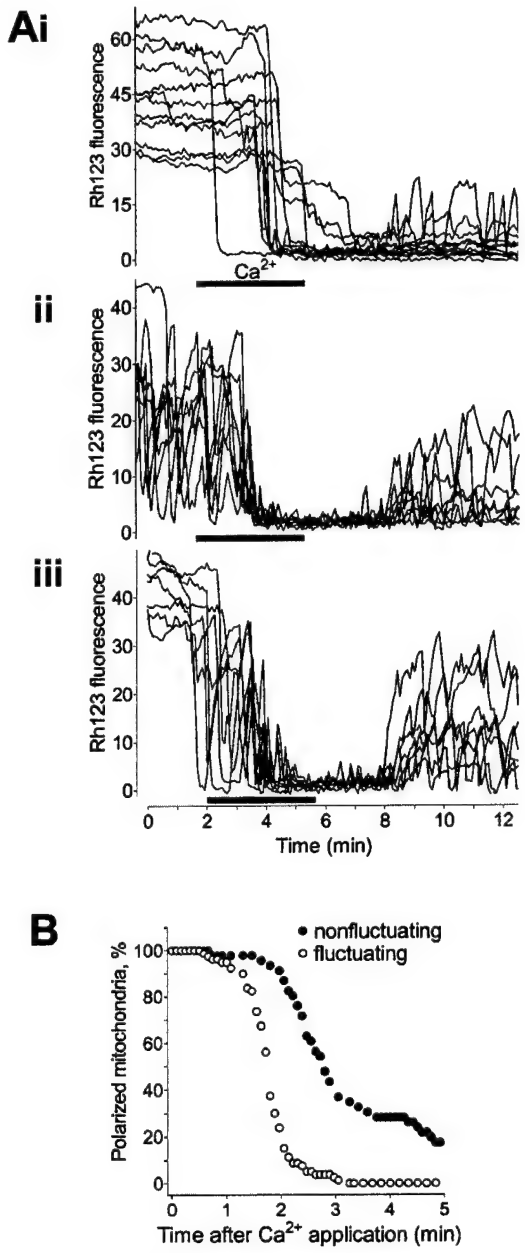

FIGURE 3 The effects of Ca^{2+} on $\Delta\Psi$m in individual mitochondria. A total of 35 μM Ca^{2+} was added to the normal 20 μM EDTA-containing superfusate, yielding a free calcium concentration of ~15μM. (*A*) Each panel shows separately nonfluctuating (*i*), fluctuating (*ii*), and initially nonfluctuating (*iii*) individual mitochondria. (*B*) Percentage of mitochondria remaining polarized shown as a function of time after Ca^{2+} application. Traces from individual mitochondria were segregated into fluctuating and nonfluctuating based on the Rh123 signal before calcium application. The time of the beginning of the application of substrate-free medium was defined as 0. These curves represent the mean of 200 individual mitochondria from the same field, and are representative of five additional experiments.

The effects of oxidative stress

Several rhodamine-based $\Delta\Psi$m probes produce singlet oxygen upon illumination (Bunting, 1992). It is well established that oxidative stress can compromise mitochondrial functions (Zhang et al., 1990). In addition, oxidation of mitochondrial thiol groups together with Ca^{2+} exposure may trigger MPT activation in isolated mitochondria (Chernyak and Bernardi, 1996), which could plausibly explain the spontaneous depolarizations. We first investigated whether the loss of Rh123 signal or the increase in fluctuation frequency was a consequence of illumination (and presumably the generation of singlet oxygen). Mitochondria were attached to the coverslip in two different regions located as far as possible from each other. Then we recorded the Rh123 fluorescence only from one field, which was

selectively illuminated, while the other remained in the dark. Fig. 4 *A* shows Rh123 fluorescence in the mitochondria illuminated normally (field *a*) at the beginning and at the end of a 14-min recording period, and a second field from the same coverslip that was not illuminated until the very end of the experiment (field *b*). This experiment clearly demonstrates that the intensity of the fluorescence and frequency of fluctuations in mitochondria at the end of the recording period was the same in both fields regardless of light exposure (Fig. 4 *B*). Data from several experiments of this nature are provided in Fig. 4, *C* and *D*.

We also examined the effect of ROS scavengers on the changes in mitochondrial $\Delta\Psi$m. Fig. 5 illustrates that neither the singlet oxygen scavenger histidine nor glutathione (GSH) significantly altered any of the $\Delta\Psi$m parameters. These results argue that the gradual depolarization of mitochondria and the enhancement of spontaneous fluctuations of $\Delta\Psi$m during the recording period were not the immediate consequence of oxidative damage.

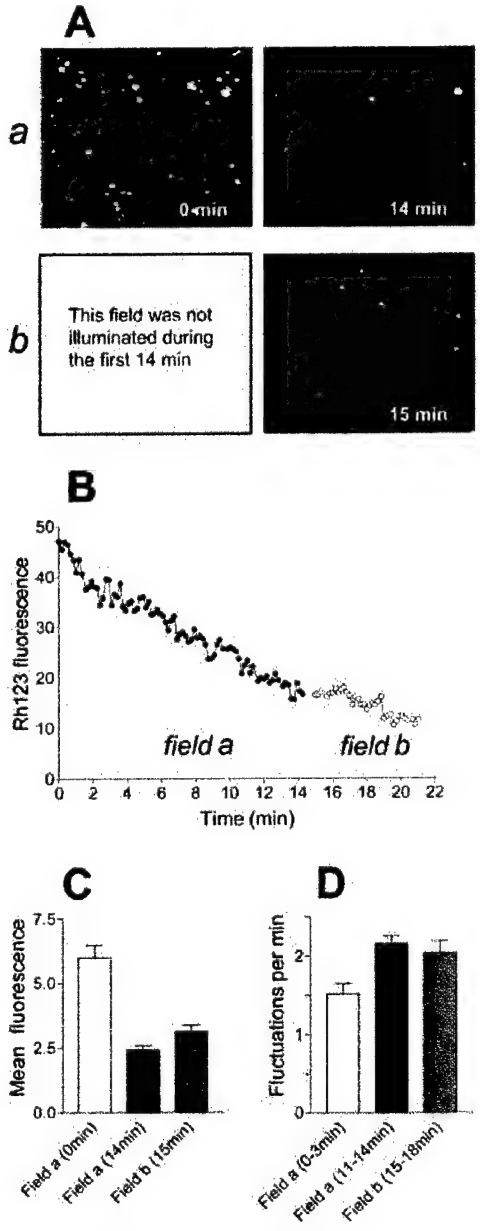

FIGURE 4 Effect of illumination on $\Delta\Psi$m in single isolated mitochondria. (*A*) Images of Rh123 fluorescence in the two different fields of the coverslip with the attached mitochondria. The mitochondria in panels *a* were subjected to the normal illumination, whereas the mitochondria in panel *b* were illuminated only at the end of the experiment. (*B*) The average Rh123 fluorescence of 150 individual mitochondria from each field shown in the previous panel. Panels *A* and *B* are from a single experiment that was repeated four additional times with similar results. (*C* and *D*) Mean Rh123 fluorescence and the frequency of the fluctuations, respectively, were not significantly different in the mitochondria from field *a* and *b* when they were measured at the closed time points. The data in *C* and *D* represent the mean ± SE of five experiments.

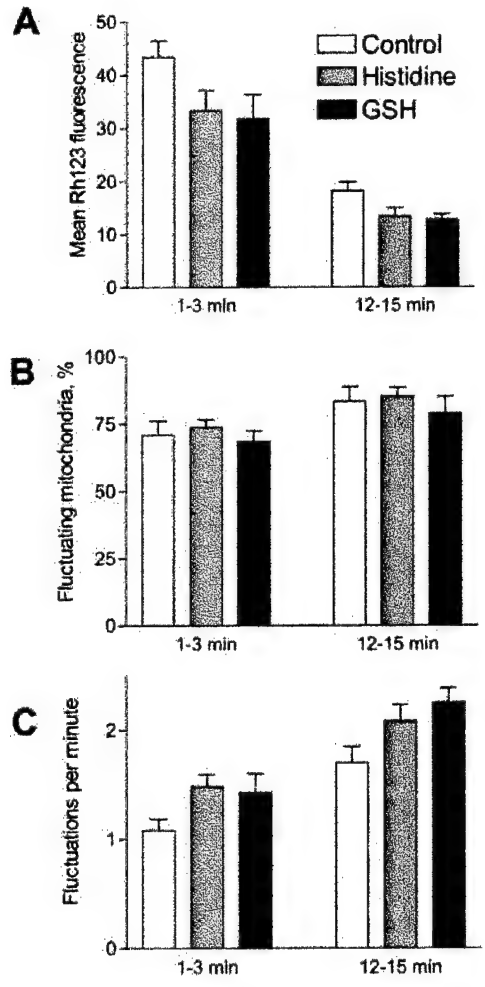

FIGURE 5 Effect of antioxidants on $\Delta\Psi$m. A scavenger of singlet oxygen histidine (300 μM) or glutathione (GSH, 5 mM) did not have any effect on $\Delta\Psi$m. All parameters (mean Rh123 fluorescence, percentage of blinking mitochondria, and frequency of fluctuations) were measured at the beginning (1–3 min) and at the end (12–15 min) of the experiment. The antioxidants were added to the perfusion medium for 2 min before the start of the recording and were present for the entire experiment. The data represent the mean ± SE of five experiments.

A role for mitochondrial permeability transition

Most studies of spontaneous changes in $\Delta\Psi$m have concluded that the MPT plays a critical role (Ichas et al., 1997; Fall and Bennett, 1999; Huser et al., 1998; Huser and Blatter, 1999; Nakayama et al., 2002). We therefore performed experiments to determine whether the spontaneous changes in $\Delta\Psi$m could be attributed to a change in the permeability of the inner mitochondrial membrane associated with MPT. Activation of MPT renders the inner mitochondrial membrane permeable to hydrophilic molecules up to 1500 Da (Zoratti and Szabo, 1995). Calcein (~620 Da when deesterified) has been used to identify opening of PTP in both cells (Petronilli et al., 1999) and in isolated mitochondria (Huser et al., 1998). We loaded mitochondria with the ester form of calcein, which is hydrolyzed and entrapped in the mitochondrial matrix. To record the calcein fluorescence and $\Delta\Psi$m in the same mitochondria, calcein-loaded mitochondria were perfused with TMRM (which avoids the problem of overlap of excitation and emission wavelengths). Because we were not able to monitor the fluorescence of calcein and TMRM with the same optics, we measured calcein fluorescence first, then changed the dichroic mirror for TMRM wavelength, monitored $\Delta\Psi$m for a few minutes in the same field, and then switched the optics back for calcein measurements. Fig. 6 shows the fluorescence images of calcein (*green*) and TMRM (*red*) and the plots obtained from three individual mitochondria. As can be seen, despite continuous fluctuations in $\Delta\Psi$m reported by TMRM fluorescence, mitochondria did not demonstrate equivalent, stochastic loss of the calcein signal that should accompany an increase in permeability of the inner membrane. The minor decrease in the average calcein fluorescence was presumably due to photobleaching because we did not observe a decrease in calcein fluorescence in cells that were not illuminated during the recording. To provide a positive control for calcein release from mitochondria when the permeability of mitochondrial membrane is increased, we used the pore-forming antibiotic alamethicin (Fox and Richards, 1982; Marsh, 1996). Fig. 6 shows that application of alamethicin induces a quick loss of fluorescence in calcein-loaded mitochondria (Fig. 6 *B*) and a complete mitochondrial depolarization (Fig. 6 *C*). The loss of calcein signal was not the consequence of mitochondrial depolarization, because deenergization of mitochondria induced by the removal of the substrates did not change calcein fluorescence (data not shown). We did not observe an interference of the calcein and TMRM signals as has been reported by Huser et al. (1998). This may be because we used a smaller concentration of TMRM (40 nM) instead of 200–400 nM, which was used in the experiments of Huser et al. (1998).

We also checked the effect of the MPT blocker cyclosporin A (CsA) on $\Delta\Psi$m. CsA (1 μM) was added into the perfusion medium for the duration of the $\Delta\Psi$m recording. Fig. 7 shows that the treatment of mitochondria with CsA did not change any of the parameters of the fluctuations in $\Delta\Psi$m. The lack of calcein movement across the mitochondrial membrane and the absence of effect of CsA is inconsistent with a role for MPT in the spontaneous changes in $\Delta\Psi$m.

DISCUSSION

In this study we have provided the first demonstration of spontaneous fluctuations in $\Delta\Psi$m in isolated rat brain mitochondria. These mitochondria develop a $\Delta\Psi$m when provided with glutamate and malate as substrates, and then a substantial fraction of the mitochondria display stochastic, large amplitude decreases in fluorescence consistent with transient depolarization of $\Delta\Psi$m. These changes become more substantial with increased duration of experimental recordings or exposure to calcium but do not appear to be a consequence of fluorescence illumination. Moreover, the fluctuations do not appear to be the result of activation of MPT.

As noted above, spontaneous changes in the signals of fluorescence indicators of and exposure to calcium have previously been reported in both cultured cells and isolated mitochondria, although not in isolated brain mitochondria. In general, these studies have reported rather similar basic phenomena to the findings reported here. Thus, mitochondria loaded with $\Delta\Psi$m-sensitive dyes show a progressively enhanced frequency of spontaneous, large amplitude changes in fluorescence that is typically attributed to mitochondrial depolarization (Ichas et al., 1997; Fall and Bennett, 1999; Huser et al., 1998; Huser and Blatter, 1999; Duchen et al., 1998; Belousov et al., 2001). We have additionally observed transient increases in dye signals that appear to be the only form of spontaneous activity exhibited by neurons (Buckman and Reynolds, 2001a) and are distinct from the spontaneous depolarizations seen in cultured astrocytes (Buckman and Reynolds, 2001b). It is thus evident that spontaneous changes in mitochondrial membrane potential are a common, if underappreciated, phenomenon. However, there does not appear to be a clear consensus regarding the mechanism that is responsible for this effect.

A number of studies have identified MPT in mitochondria of brain origin. Exposing neurons to elevated intracellular Ca^{2+} after *N*–methyl-D-aspartate (NMDA) receptor activation produces a mitochondrial depolarization that has been attributed to MPT (White and Reynolds, 1996; Schinder et al., 1996; Nieminen et al., 1996). Inhibitors of MPT have also been reported to protect neurons from hypoglycemic and ischemic injury (Friberg et al., 1998), although this effect has previously been attributed to calcineurin inhibition (Dawson et al., 1993). Expression of MPT also appears to vary according to the region of the brain used as a source of mitochondria (Friberg et al., 1999). However, there are also differences between MPT in brain mitochondria compared to liver mitochondria. For example, the amplitude of swelling

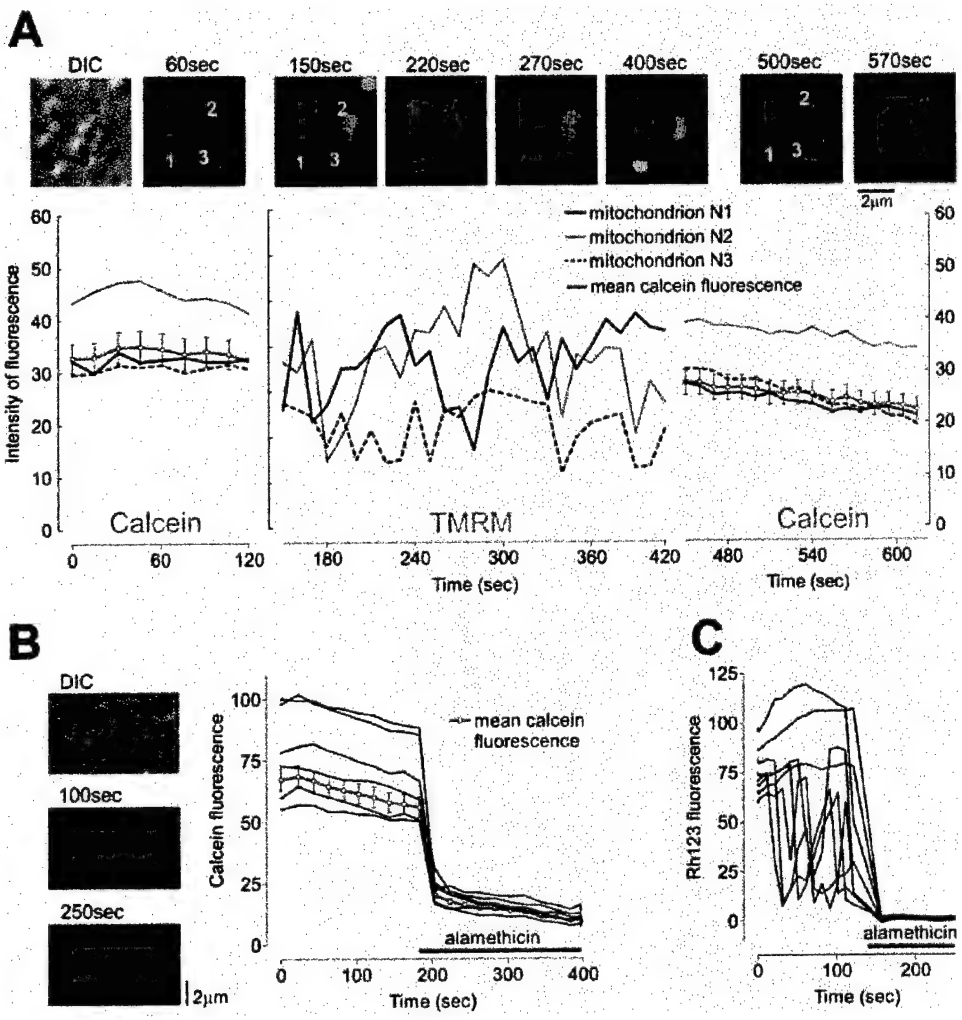

FIGURE 6 The measurement of calcein fluorescence in single mitochondria. (*A*) The calcein fluorescence and $\Delta\Psi$m (TMRM) were measured in the same mitochondria (see explanation in the text). The series of images at the top represent DIC and fluorescent images taken at the different time points indicated. The images show the fluorescence of calcein (*green images*) and TMRM (*red images*). The traces illustrate individual mitochondria and mean calcein signal ($\pm$ SE, $n = 100$ mitochondria). These data are representative of five additional experiments. (*B*) Left panel, DIC image and fluorescence images showing the loss of calcein fluorescence in the presence of 40 μg/ml alamethicin; right panel, the traces obtained from individual mitochondria and mean calcein signal ($\pm$ SE, $n = 50$ mitochondria). The data are representative of three additional experiments. (*C*) Alamethicin-induced depolarization of $\Delta\Psi$m measured by Rh123. The concentration of alamethicin was 40 μg/ml. Each trace corresponds to an individual mitochondrion.

induced by MPT in isolated brain mitochondria is clearly much smaller than in liver mitochondria (Berman et al., 2000; Andreyev and Fiskum, 1999; Brustovetsky and Dubinsky, 2000). It is also evident that NMDA receptor-mediated mitochondrial depolarization can occur independently of MPT activation, and it is difficult to unequivocally attribute alterations in mitochondrial function in intact neural cells to MPT (Reynolds and Hastings, 2001). Nevertheless, under appropriate conditions, MPT can clearly be expressed by brain mitochondria (Berman et al., 2000; Andreyev et al., 1998; Brustovetsky and Dubinsky, 2000).

Given the regularity with which previous studies have attributed spontaneous depolarizations in isolated mitochondria to MPT, it is perhaps surprising that MPT does not appear to be the source of this phenomena in our experiments. CsA is the prototypical MPT inhibitor and can inhibit MPT-like events in our brain mitochondria preparation. However, our observations of CsA sensitivity (of mitochondrial Ca^{2+} handling) were seen only in mitochondria suspended in a sucrose/mannitol buffer, and the CsA sensitivity was lost in a potassium-based buffer of the kind used in this study (T.V.V. and I.J.R., unpublished observations). The actions of CsA can be overcome by the addition of excess Ca^{2+}, but that is unlikely to be occurring in our experiments under basal conditions because of the presence of EDTA in the normal superfusion buffer. We would also expect altered permeability of the inner membrane to be associated with the loss of calcein, which should be small enough to permeate the pore (Zoratti and Szabo, 1995). Calcein quenching has previously been used to detect MPT activation (Petronilli et al., 1999), although in that case calcein was used in conjunction with cobalt which quenches calcein fluorescence. It was not clear whether calcein leaves mitochondria or whether cobalt enters through the pore in these studies. Huser and colleagues (1998) have demonstrated, however, that calcein leaves rat ventricular mitochondria under similar conditions, supporting the contention that it would report permeability changes if these were to occur. Thus, we conclude that the changes in $\Delta\Psi$m are not due to MPT activation in this mitochondrial preparation. This

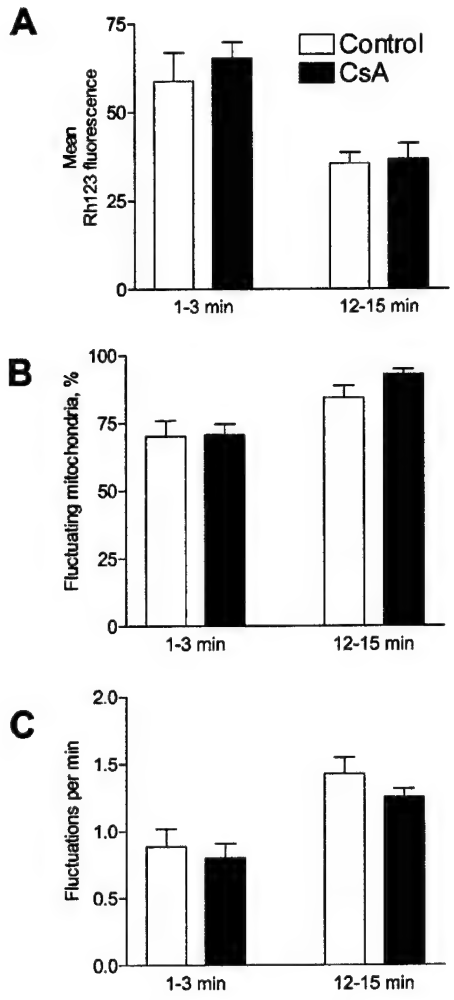

FIGURE 7 Effect of cyclosporin A (CsA) on $\Delta\Psi$m. The histograms show a mean Rh123 fluorescence (*A*), percentage of fluctuating mitochondria (*B*), and frequency of fluctuations (*C*) in single mitochondria in control and 1 μM CsA-containing medium. Each histogram represents the mean ($\pm$ SE) of five experiments, and 150 mitochondria were analyzed in each experiment. None of the relevant differences reached statistical significance ($P > 0.05$).

leaves open the question of the conductance that is activated in our experiments. There are many potential candidates, including ATP-sensitive and Ca^{2+}-activated potassium currents (Grover and Garlid, 2000; Xu et al., 2002), a variety of putative uncoupling proteins (Skulachev, 1998; Ricquier and Bouillaud, 2000), and perhaps even the Ca^{2+} uniporter, not to mention proteins like the adenine nucleotide translocator that can evidently operate as either a carrier or as an ion channel under different circumstances (Connern and Halestrap, 1994). The identity of the conductance in brain mitochondria awaits further experimentation.

The physiological relevance of spontaneous depolarizations has yet to be demonstrated, too. It has been suggested that the entire phenomenon is a consequence of the oxidative stress associated with light exposure and the subsequent generation of oxidants like singlet oxygen (Belousov et al., 2001). If this were the case, one could still credibly claim that the phenomenon was relevant to pathophysiological conditions that are associated with oxidative stress. Our studies presented here and others (Huser et al., 1998) clearly demonstrate that the spontaneous changes are a progressive phenomenon, so that the mean fluorescence signal decreases as the experiment progresses, and also demonstrate that the frequency of the spontaneous changes increases. This has also been reported in intact astrocytes (Belousov et al., 2001). Although we initially assumed that this was likely to be due to oxidative stress triggered by light exposure, this does not appear to be the case. The finding that mitochondria also lose Rh123 fluorescence even without light exposure argues against light and oxidative stress as a cause of the loss of signal (Fig. 4), as does the failure of histidine or GSH to protect mitochondria (Fig. 5). Similar concentrations of GSH were previously found to delay the onset of MPT (Huser et al., 1998), and this might provide an additional argument against the expression of MPT in our mitochondria. The cause of the time-dependent loss of dye signal and increase in frequency of fluctuations remains unclear, but might be attributable to the washout of some key extra-mitochondrial factor during superfusion.

One of the more striking features of the recording of responses from individual organelles is the heterogeneity in the responses. Even when presented simultaneously with the depletion of substrates or Ca^{2+}, there was a remarkable difference in the time between the earliest and latest response within a given field. The basis of this heterogeneity is not clear. Although the mitochondria preparation is enriched in nonsynaptosomal, and presumably thus astrocyte, mitochondria (Sims, 1991), we lack definitive markers to differentiate the organelles at this level. It is also possible that the difference in the responses reflects varying degrees of damage of the organelles during preparation. In this way one might consider the spontaneous changes as a marker of injured mitochondria, and the increase in fluctuations would therefore reflect additional "injury" during the course of the experiment. This interpretation would be consistent with a more marked response to the introduction of Ca^{2+} in mitochondria that are already fluctuating. Identifying the mechanism responsible for the spontaneous changes would be of great value to resolve this issue. Even so, it seems likely that this preparation may offer some useful and novel insights into physiological or pathophysiological properties of brain mitochondria.

We thank Ms. Nicole Zeak for the preparation of mitochondria and Dr. Gordon Rintoul for the help with data analysis.

This work was supported by National Institutes of Health grants AG 20899 and NS 41299.

REFERENCES

Andreyev, A. Y., B. Fahy, and G. Fiskum. 1998. Cyctochrome c release from brain mitochondria is independent of the mitochondrial permeability transition. *FEBS Lett.* 439:373–376.

Andreyev, A., and G. Fiskum. 1999. Calcium induced release of mitochondrial cytochrome c by different mechanisms selective for brain versus liver. *Cell Death Differ.* 6:825–832.

Belousov, V. V., L. L. Bambrick, A. A. Starkov, D. B. Zorov, V. P. Skulachev, and G. Fiskum. 2001. Oscillations in mitochondrial membrane potential in rat astrocytes in vitro. *Abstr. Soc. Neurosci.* 27:205–218.

Berman, S. B., S. C. Watkins, and T. G. Hastings. 2000. Quantitative biochemical and ultrastructural comparison of mitochondrial permeability transition in isolated brain and liver mitochondria: evidence for relative insensitivity of brain mitochondria. *Exp. Neurol.* 164:415–425.

Bernardi, P. 1999. Mitochondrial transport of cations: channels, exchangers, and permeability transition. *Physiol. Rev.* 79:1127–1155.

Brustovetsky, N., and J. M. Dubinsky. 2000. Dual responses of CNS mitochondria to elevated calcium. *J. Neurosci.* 20:103–113.

Buckman, J. F., and I. J. Reynolds. 2001a. Spontaneous changes in mitochondrial membrane potential in cultured neurons. *J. Neurosci.* 21:5054–5065.

Buckman, J. F., and I. J. Reynolds. 2001b. Spontaneous mitochondrial activities in astrocytes. *Abstr. Soc. Neurosci.* 27:96–99.

Bunting, J. R. 1992. A test of the singlet oxygen mechanism of cationic dye photosensitization of mitochondrial damage. *Photochem. Photobiol.* 55:81–87.

Chernyak, B. V., and P. Bernardi. 1996. The mitochondrial permeability transition pore is modulated by oxidative agents through both pyridine nucleotides and glutathione at two separate sites. *Eur. J. Biochem.* 238:623–630.

Connern, C. P., and A. P. Halestrap. 1994. Recruitment of mitochondrial cyclophilin to the mitochondrial inner membrane under conditions of oxidative stress that enhance opening of a calcium-sensitive non-specific channel. *Biochem. J.* 302:321–324.

Dawson, T. M., J. P. Steiner, V. L. Dawson, J. L. Dinerman, G. R. Uhl, and S. H. Snyder. 1993. Immunosuppressant FK506 enhances phosphorylation of nitric oxide synthase and protects against glutamate neurotoxicity. *Proc. Natl. Acad. Sci. USA.* 90:9808–9812.

De Giorgi, F., L. Lartigue, and F. Ichas. 2000. Electrical coupling and the plasticity of the mitochondrial network. *Cell Calcium.* 28:365–370.

Duchen, M. R., A. Leyssens, and M. Crompton. 1998. Transient mitochondrial depolarizations reflect focal sarcoplasmic reticular calcium release in single rat cardiomyocytes. *J. Cell Biol.* 142:975–988.

Fall, C. P., and J. P. Bennett, Jr. 1999. Visualization of cyclosporin A and Ca^{2+}-sensitive cyclical mitochondrial depolarizations in cell culture. *Biochem. Biophys. Res. Commun.* 1410:77–84.

Fox, R. O., and F. M. Richards. 1982. A voltage-gated ion channel model inferred from the crystal structure of alamethicin at 1.5-A resolution. *Nature.* 300:325–330.

Friberg, H., C. P. Connern, A. P. Halestrap, and T. Wieloch. 1999. Differences in the activation of the mitochondrial permeability transition among brain regions correlates with selective vulnerability. *J. Neurochem.* 72:2488–2497.

Friberg, H., M. Ferrand-Drake, F. Bengtsson, A. P. Halestrap, and T. Wieloch. 1998. Cyclosporin A, but not FK 506, protects mitochondria and neurons against hypoglycemic damage and implicates the mitochondrial permeability transition in cell death. *J. Neurosci.* 18:5151–5159.

Grover, G. J., and K. D. Garlid. 2000. ATP-sensitive potassium channels: a review of their cardioprotective pharmacology. *J. Mol. Cell. Cardiol.* 32:677–695.

Huser, J., and L. A. Blatter. 1999. Fluctuations in mitochondrial membrane potential caused by repetitive gating of the permeability transition pore. *Biochem. J.* 343:311–317.

Huser, J., C. E. Rechenmacher, and L. A. Blatter. 1998. Imaging the permeability pore transition in single mitochondria. *Biophys. J.* 74:2129–2137.

Ichas, F., L. S. Jouaville, and J. P. Mazat. 1997. Mitochondria are excitable organelles capable of generating and conveying electrical and calcium signals. *Cell.* 89:1145–1153.

Krippeit-Drews, P., M. Dufer, and G. Drews. 2000. Parallel oscillations of intracellular calcium activity and mitochondrial membrane potential in mouse pancreatic B-cells. *Biochem. Biophys. Res. Commun.* 267:179–183.

Loew, L. M., R. A. Tuft, W. Carrington, and F. S. Fay. 1993. Imaging in five dimensions: time-dependent membrane potentials in individual mitochondria. *Biophys. J.* 65:2396–2407.

Marsh, D. 1996. Peptide models for membrane channels. *Biochem. J.* 315:345–361.

Nakayama, S., T. Sakuyama, S. Mitaku, and Y. Ohta. 2002. Fluorescence imaging of metabolic responses in single mitochondria. *Biochem. Biophys. Res. Commun.* 290:23–28.

Nicholls, D. G. 2001. A history of UCP1. *Biochem. Soc. Trans.* 29:751–755.

Nicholls, D. G., and M. W. Ward. 2000. Mitochondrial membrane potential and neuronal glutamate excitotoxicity: mortality and millivolts. *Trends Neurosci.* 23:166–174.

Nieminen, A.-L., T. G. Petrie, J. J. Lemasters, and W. R. Selman. 1996. Cyclosporin A delays mitochondrial depolarization induced by *N*-methyl-D-aspartate in cortical neurons: evidence of the mitochondrial permeability transition. *Neuroscience.* 75:993–997.

Petronilli, V., G. Miotto, M. Canton, M. Brini, R. Lonna, P. Bernardi, and F. Di Lisa. 1999. Transient and long-lasting openings of the mitochondrial permeability transition pore can be monitored directly in intact cells by changes in mitochondrial calcein fluorescence. *Biophys. J.* 76:725–734.

Reynolds, I. J., and T. G. Hastings. 2001. Role of the permeability transition in glutamate mediated neuronal injury. *In* Mitochondria in Pathogenesis. J. J. Lemasters and A.-L. Nieminen, editors. Kluwer Academic/Plenum Publishers, New York. 301–16.

Ricquier, D., and F. Bouillaud. 2000. The uncoupling protein homologues: UCP1, UCP2, UCP3, StUCP and AtUCP. *Biochem. J.* 345:161–179.

Schinder, A. F., E. C. Olson, N. C. Spitzer, and M. Montal. 1996. Mitochondrial dysfunction is a primary event in glutamate neurotoxicity. *J. Neurosci.* 16:6125–6133.

Sims, N. R. 1991. Selective impairment of respiration in mitochondria isolated from brain subregions following transient forebrain ischemia in the rat. *J. Neurochem.* 56:1836–1844.

Skulachev, V. P. 1998. Uncoupling: new approaches to an old problem of bioenergetics. *Biochim. Biophys. Acta.* 1363:100–124.

White, R. J., and I. J. Reynolds. 1996. Mitochondrial depolarization in glutamate-stimulated neurons: an early signal specific to excitotoxin exposure. *J. Neurosci.* 16:5688–5697.

Xu, W. H., Y. G. Liu, S. Wang, T. McDonald, J. E. Van Eyk, A. Sidor, and B. O'Rourke. 2002. Cytoprotective role of Ca2+-activated K+ channels in the cardiac inner mitochondrial membrane. *Science.* 298:1029–1033.

Zhang, Y., O. Marcillat, C. Guilivi, L. Ernster, and K. J. A. Davies. 1990. The oxidative inactivation of mitochondrial electron transport chain components and ATPase. *J. Biol. Chem.* 265:16330–16336.

Zoratti, M., and I. Szabo. 1995. The mitochondrial permeability transition. *Biochim. Biophys. Acta.* 1241:139–176.

ACADEMIC PRESS

Available online at www.sciencedirect.com

SCIENCE DIRECT®

Experimental Neurology 183 (2003) 682–694

Experimental Neurology

www.elsevier.com/locate/yexnr

Glucose deprivation produces a prolonged increase in sensitivity to glutamate in cultured rat cortical neurons

Olga Vergun,[a] Yong Y. Han,[b] and Ian J. Reynolds[a,*]

[a] *Department of Pharmacology, University of Pittsburgh, Pittsburgh, PA 15261, USA*
[b] *Department of Critical Care Medicine, University of Pittsburgh, Pittsburgh, PA 15261, USA*

Received 22 January 2003; revised 9 April 2003; accepted 15 April 2003

Abstract

In this study we investigated whether the link between mitochondrial dysfunction and deregulation of Ca^{2+} homeostasis preceding excitotoxic cell death is mediated by cellular deenergization. Glycolytic and/or mitochondrial ATP synthesis was inhibited with 2-deoxy-D-glucose (2DG) and oligomycin, respectively. Changes in cytoplasmic Ca^{2+} concentration ($[Ca^{2+}]_c$) and mitochondrial membrane potential were simultaneously measured in response to low (10 μM) glutamate concentrations, using the fluorescence dyes fura-2FF and rhodamine 123. 2DG, which blocks glycolysis and also inhibits mitochondrial respiration due to depletion of pyruvate, greatly increased and accelerated glutamate-induced elevation of $[Ca^{2+}]_c$ and mitochondrial depolarization. The 2DG-induced hypersensitivity to glutamate was observed even after 150-min washout of 2DG with glucose-containing medium, suggesting a permanent deterioration of mitochondrial function. Prior blockade of only glycolytic (2DG with pyruvate) or only mitochondrial (oligomycin) ATP synthesis did not affect neuronal sensitivity to glutamate. Collectively, these studies show that to maintain the sensitivity of neurons to glutamate at control levels at least one of the cellular sources of ATP production must be intact. Either glycolysis or oxidative phosphorylation can effectively support Ca^{2+} homeostasis in cultured forebrain neurons.

Keywords: Mitochondria; Excitotoxicity; Glutamate; Glycolysis; ATP; 2-Deoxy-D-glucose

Introduction

Pathologic elevation of extracellular glutamate concentration during hypoxic–ischemic brain injury induces overstimulation of NMDA receptors and leads to a sustained increase in cytoplasmic Ca^{2+} concentration ($[Ca^{2+}]_c$)[1] (Choi and Rothman, 1990). It is widely believed that a disturbance of Ca^{2+} homeostasis in neurons triggers a series of processes leading to delayed neuronal death (Schanne et al., 1979; Choi, 1988; Ogura et al., 1988; Manev et al., 1989; Choi and Rothman, 1990; Glaum et al., 1990; deErausquin et al., 1990; Limbrick et al., 1995). However, the exact mechanism of irreversible neuronal calcium overload induced by overstimulation of glutamate receptors remains under investigation. The possibilities include enhanced Ca^{2+} entry across the plasma membrane (Manev et al., 1989) and impairment of Ca^{2+} extrusion from the cytoplasm both out of the cell (Na^+/Ca^{2+} exchanger, Ca^{2+}-pump) and into mitochondria (for review see Khodorov, 2000). In neurons, cytosolic Ca^{2+} overload, correlating with glutamate excitotoxicity, is coupled with mitochondrial Ca^{2+} uptake and mitochondrial depolarization (Ankarcrona et al., 1995; Budd and Nicholls, 1996a; Isaev et al., 1996; Khodorov et al., 1996; Schinder et al., 1996; White and Reynolds, 1996; Scanlon and Reynolds, 1998; Stout et al., 1998; Kiedrowski, 1998; Vergun et al., 1999; Ward et al., 2000). Profound mitochondrial depolarization reverses the

* Corresponding author. Department of Pharmacology, University of Pittsburgh, W1351 Biomedical Science Tower, Pittsburgh, PA 15261, USA Fax: +1-412-624-0794.

E-mail address: iannmda@pitt.edu (I.J. Reynolds).

[1] Abbreviations used: $\Delta\psi_m$, mitochondrial membrane potential; $[Ca^{2+}]_c$, cytosolic Ca^{2+} concentration; $[Na^+]_c$, cytosolic Na^+ concentration; Rh123, rhodamine 123; 2DG, 2-deoxy-D-glucose; FCCP, carbonyl cyanide *p*-trifluoromethoxyphenyl hydrazone; HBSS, Hepes-buffered salt solution; TTX, tetrodotoxin.

0014-4886/03/$ – see front matter © 2003 Elsevier Science (USA). All rights reserved.
doi:10.1016/S0014-4886(03)00243-7

mitochondrial ATP synthase, which both suppresses mitochondrial ATP production and promotes ATP hydrolysis (Nicholls, 1986; Leyssens et al., 1996; Duchen, 1999). Prolonged exposure of neuronal cultures to glutamate reduces the intracellular ATP content (Tsuji et al., 1994; Marcaida et al., 1995; Budd and Nicholls, 1996a). Because the major neuronal Ca^{2+}-extrusion systems, the plasma membrane Ca^{2+} pump, and the Na^+/Ca^{2+} exchanger require ATP (DiPolo and Beauge, 1988; Carafoli, 1991; Sheu and Blaustein, 1992), cytoplasmic ATP depletion could be associated with a failure of Ca^{2+} extrusion. This concept was supported by Budd and Nicholls (1996a, 1996b) who showed that a decrease in ATP/ADP ratio causes a deregulation of $[Ca^{2+}]_c$ in cerebellar granule cells in response to glutamate or KCl. A correlation between the glutamate-induced decrease in ATP content and neuronal degeneration in cultured spinal neurons has also been reported (Tsuji et al., 1994).

On other hand, there is evidence that the depletion of cytoplasmic ATP mediated by activation of kainate and NMDA receptors does not directly correlate with neuronal death (Marcaida et al., 1995). Moreover, growth factors can protect against excitotoxic/ischemic damage without prevention of ATP depletion (Mattson et al., 1993, Mattson and Cheng, 1993), and increased [ATP] by antagonism of glutamate receptors is not associated with neuroprotection (Riepe et al., 1994).

In order to investigate the role of cellular energy production in neuronal Ca^{2+} overload and mitochondrial dysfunction, we examined how inhibition of mitochondrial and/or glycolytic ATP synthesis affects neuronal responses to relatively low, subtoxic concentrations of glutamate. Our results show that blockade of only glycolytic ATP synthesis or only mitochondrial ATP synthesis does not increase neuronal responses to glutamate. A suppression of both glycolytic and mitochondrial ATP synthesis produced a sustained increase in sensitivity of the neurons to glutamate. These data show that either glycolysis or oxidative phosphorylation can effectively support Ca^{2+} homeostasis in forebrain neurons.

Materials and methods

General materials

All raw materials and reagents were purchased through Sigma (St. Louis, MO), unless otherwise specified.

Cell culture

All procedures using animals were in accordance with the National Institutes of Health Guide for the Care and Use of Laboratory Animals and were approved by the University of Pittsburgh's Institutional Animal Care and Use Committee. Cultures of forebrain neurons were prepared as described previously (Brocard et al., 2001). In brief, forebrains from embryonic day 17 Sprague–Dawley rats were removed and dissociated with trypsin. Cells were plated on poly-D-lysine-coated 31-mm glass coverslips and inverted after 24 h to decrease glial growth. Neurons were cultured in Dulbecco's modified Eagle's medium, containing 10% fetal bovine serum, 24 U/ml penicillin, 24 μg/ml streptomycin; final glutamine concentration, 3.9 mM. Experiments were performed on cells at 12–14 days in culture.

Experimental paradigm

Unless otherwise specified, all experiments were performed using Hepes-buffered salt solution (standard HBSS) of the following composition (in mM): NaCl 137, KCl 5, $NaHCO_3$ 10, KH_2PO_4 0.6, Na_2HPO_4 0.6, $MgSO_4$ 0.9, $CaCl_2$ 1.4, Hepes 20, and glucose 5.5 (pH adjusted to 7.4 with NaOH). For experimental conditions requiring glucose deprivation, the HBSS solution was devoid of glucose (glucose-free HBSS). Coverslips containing neuronal cells were preincubated for 60 min at 37°C (concurrent to fluorescent dye loading; see below) in HBSS containing various inhibitors of glycolytic and/or mitochondrial ATP synthesis. The cells were then washed for 20 to 25 min at room temperature (~25°C) in standard HBSS (containing glucose). The coverslips were placed into a perfusion chamber that was then mounted onto a microscope fitted for fluorescence imaging. Fluorescence measurements were performed at room temperature while the cells were perfused at 10 ml/min with HBSS and were then exposed to glutamate for 10 min. All experiments were repeated three to seven times using cells from different culture preparations. Controls for each experiment were performed on sister cultures.

Fluorescence measurements of $[Ca^{2+}]_c$ and $\Delta\psi_m$

For $[Ca^{2+}]_c$ measurements, cells were incubated for 60 min at 37°C with 5 μM fura-2FF/AM (Teflabs, Austin, TX) and 5 μg/ml bovine serum albumin in HBSS. For simultaneous measurements of $[Ca^{2+}]_c$ and $\Delta\psi_m$, 5 μM rhodamine 123 (Rh123, Molecular Probes, Eugene, OR) was added to the medium during the last 15 min of the fura-2FF/AM incubation period. The cells were then washed with standard HBSS and placed onto a perfusion chamber on a BX50WI Olympus Optical (Tokyo, Japan) microscope fitted with an Olympus Optical LUM PlanFI 40X water immersion quartz objective. $[Ca^{2+}]_c$ and $\Delta\psi_m$ were monitored in single cells using excitation light provided by a 75-W xenon lamp-based monochromator (T.I.L.L. Photonics GmbH, Martinsried, Germany). Light was detected using a CCD camera (Orca; Hamamatsu, Shizouka, Japan). Cells were alternatively illuminated with 340- and 380-nm light for fura-2FF and 490-nm light for Rh123. Emitted fluorescence was passed through a 500-nm longpass dichromatic mirror and a 535 ± 40-nm bandpass filter (Omega Optical). Fluorescence data were acquired and analyzed using Simple PCI

software (Compix, Inc., Cranberry, PA). Fluorescence was measured in 15–25 individual neurons for each coverslip. Background fluorescence, determined from three or four cell-free regions of the coverslips, was subtracted from all signals prior to calculating the ratios. The fura-2FF data were not calibrated in terms of $[Ca^{2+}]_c$ because it was shown recently (Dineley et al., 2002) that the calibration of fura-2-related dyes cannot be appropriately performed without measurement of intracellular dye concentration. Accumulation of Rh123 in polarized mitochondria quenches the fluorescence signal; in response to mitochondrial depolarization the dye redistributes throughout the cell and fluorescence is dequenched. An increase in Rh123 signal therefore indicates mitochondrial depolarization (Duchen and Biscoe, 1992). Because Rh123 is a single wavelength dye the fluorescence signal varies between the cells. The Rh123 data therefore are presented as normalized values between zero representing the baseline fluorescence and unity representing the maximal increase in fluorescence observed during the experiment. In cells where glutamate did not depolarize mitochondria completely, the maximum Rh123 signal was obtained following complete dissipation of $\Delta\psi_m$ with FCCP (750 nM) at the end of the experiment. An excitation light exposure time and a neutral density filter were chosen to avoid saturation of the fluorescence signal. One should note, however, that this method is sensitive to synchronous changes in $\Delta\psi_m$ in a high percentage of the organelles but quite insensitive to changes in the temporal pattern of individual and/or nonsynchronous depolarizations (Zhang et al., 2001).

Statistics

Statistical analysis was performed using Prism 3.0 (Graph Pad Software, San Diego, CA). All data are presented as means ± SE. Comparisons were made using Student's *t* test, with *P* values of less than 0.05 taken as significant.

Results

Glutamate-induced increase in $[Ca^{2+}]_c$ and mitochondrial membrane depolarization

Incubation of cortical neurons with glutamate (in the presence of glycine) induced an increase in $[Ca^{2+}]_c$ and a concurrent depolarization of mitochondrial membrane. As shown in Fig. 1A and B, application of glutamate produced a small first phase of response followed by a secondary large rise in $[Ca^{2+}]_c$ and mitochondrial depolarization to a plateau. The secondary mitochondrial depolarization coincided in time with the secondary $[Ca^{2+}]_c$ rise. The time from the onset of the glutamate stimulus to the secondary large rise in $[Ca^{2+}]_c$ and mitochondrial depolarization varied considerably between individual neurons from seconds to minutes, but usually did not exceed 10 min. In these and following experiments we analyzed (1) the percentage of cells with only a first phase — small and reversible mitochondrial depolarization and $[Ca^{2+}]_c$ rise; (2) the percentage of the cells which developed the second large phase; (3) the time from the beginning of glutamate application to maximum of glutamate-induced mitochondrial depolarization. The last parameter was calculated only in the neurons with a large biphasic response. The scheme in Fig. 1C illustrates how the time to maximum was calculated.

Application of high (100 μM) glutamate concentrations induced an initial peak followed by a secondary increase in $[Ca^{2+}]_c$ and mitochondrial depolarization that were essentially irreversible and did not return to the preglutamate levels during a 15- to 20-minutes glutamate washout period (Fig. 1A). Similar relationships between $[Ca^{2+}]_c$ and $\Delta\psi_m$ were described before in hippocampal cultured neurons (Vergun et al., 1999, 2001; Keelan et al., 1999).

Application of a lower (10 μM) glutamate concentration produced a smaller increase in $[Ca^{2+}]_c$ and a more modest mitochondrial depolarization. With these lower glutamate concentration the large, secondary change was observed in 38% of cells (Fig. 1B), and the second phase developed with a longer delay compared with 100 μM glutamate. In the remaining 62% of the neurons we did not observe the secondary change during the 10 min of glutamate exposure. Fig. 1D presents the summarized data of these experiments.

A loss of $[Ca^{2+}]_c$ homeostasis after overstimulation of glutamate receptors and excessive Ca^{2+} influx into the cytosol is correlated with glutamate-induced neurotoxicity (see Choi and Rothman, 1990) and is believed to be central to the process of excitotoxicity. One of the possible mechanisms responsible for the deregulation of Ca^{2+} homeostasis is a decrease in intracellular [ATP]. In order to investigate this hypothesis we suppressed cellular ATP production by blockade of glycolytic and/or mitochondrial ATP synthesis.

Glucose-deprivation-induced hypersensitivity to glutamate

Substitution of glucose in HBSS with 10 mM 2-deoxy-D-glucose (2DG), a glucose analog that is phosphorylated but not further metabolized, induced a small mitochondrial depolarization (Fig. 2A) with no increase in baseline $[Ca^{2+}]_c$ (measured with Fura-2FF). However, 40–60 min of glucose deprivation (with addition of 2DG) greatly enhanced the neuronal responses to subsequent prolonged (10 min) application of glutamate. Fig. 2A shows the changes in $[Ca^{2+}]_c$ and $\Delta\psi_m$ induced by 10 μM glutamate in 2DG-treated cells, while Fig. 2B shows controls from sister cultures. In control cells glutamate failed to induce the second phase of Ca^{2+} and mitochondrial responses in 38% ($n = 3$ experiments); the development of the second phase in the remaining 62% occurred with a delay of about 500 s. However, in 2DG-treated cells the response to glutamate was large and rapid. After glucose deprivation the number of the

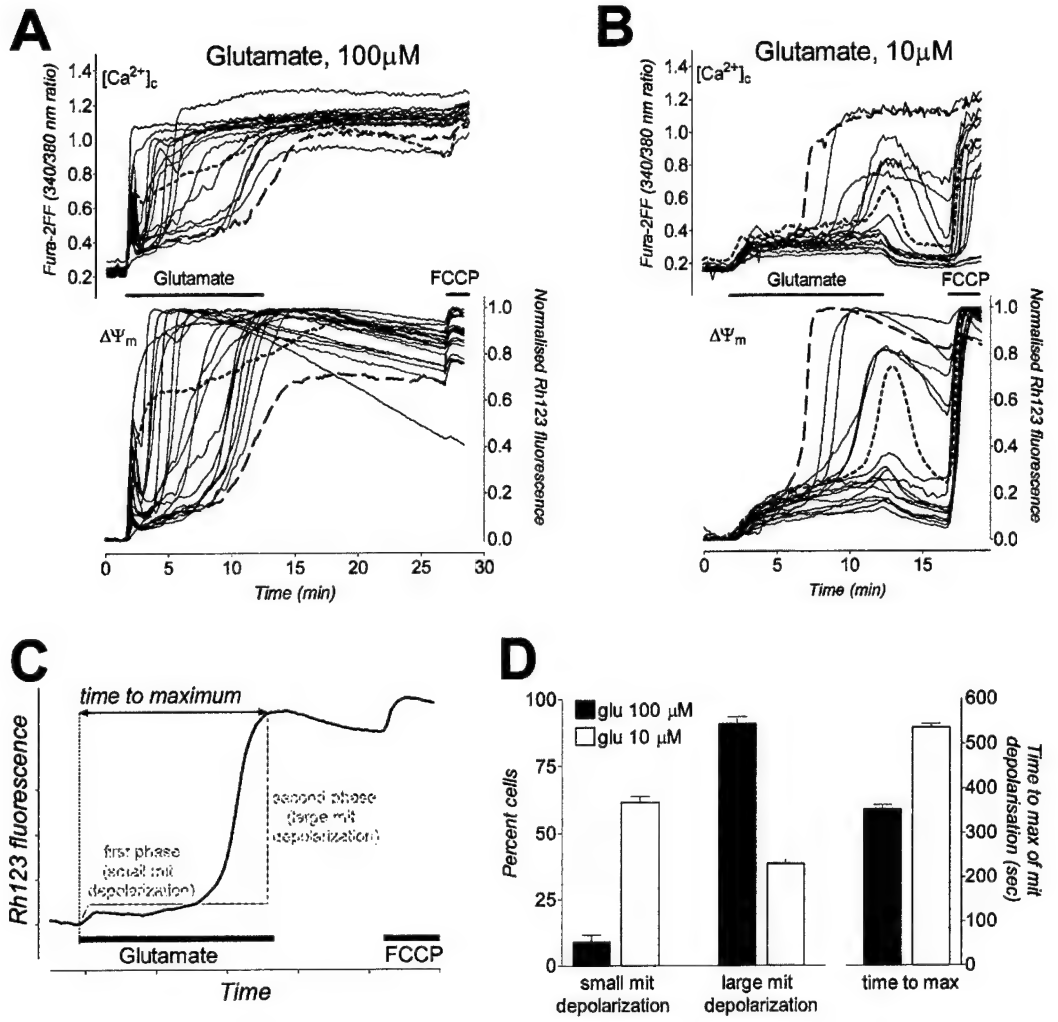

Fig. 1. Changes in $[Ca^{2+}]_c$ and $\Delta\psi_m$ in response of different glutamate concentrations. A, B: Simultaneous measurements of $[Ca^{2+}]_c$ and $\Delta\psi_m$ in individual cultured cortical neurons were made using fura-2FF and Rh123. Neurons were stimulated with 100 μM (A) and 10 μM (B) glutamate in the presence of 2 μM glycine. The mitochondrial uncoupler FCCP (750 nM) was added at the end of the experiments to produce a full depolarization of mitochondria. The dotted lines show $[Ca^{2+}]_c$ and $\Delta\psi_m$ in the same cells. C: The delay interval between the beginning of glutamate application and the maximum of the secondary mitochondrial depolarization that was compared among control and 2DG-treated cells. D: Percentage of the cells with mono- (small mitochondrial depolarization) and biphasic (large mitochondrial depolarization) responses to 10-min glutamate application and time of delay in the development of the secondary phase (time to maximum). Each bar and associated error bar represent the mean ± SE (n = 6 experiments).

neurons with a large response to glutamate was increased and the time to maximal glutamate-induced mitochondrial depolarization was much shorter than in the control. The differences in response of magnitude and delay are summarized in Fig. 2C. Note that in some neurons with a very quick glutamate-induced collapse of $\Delta\psi_m$ a slow decrease in Rh123 fluorescence after initial peak was observed (Fig. 2A, bottom). This decrease in Rh123 fluorescence was due to leakage of the dye from the cell; the distribution of the Rh123 in the cell under similar conditions has been analyzed in detail by Nicholls and Ward (2000).

The response to glutamate remained enhanced after a 10- to 150-min washout of 2DG. Thus, in subsequent experiments we incubated neurons in 2DG-containing glucose-free buffer for 1 h at 37°C during the dye loading period and then returned the cells to glucose-containing HBSS for 20–25 min at room temperature prior to imaging. Using this approach, the small 2DG-induced mitochondrial depolarizations recovered to baseline prior to the start of the recording. Glutamate was then applied for 10 min. Fig. 3A and B shows an example illustrating these experiments; the summarized data are presented in Fig. 3D. (The data presented in Fig. 3C will be discussed below). Clearly, preincubation with 2DG produced a profound increase in the sensitivity to glutamate in these neurons. Fig. 4 shows a similar increase in $[Ca^{2+}]_c$ responses of the neurons following 2DG exposure, but this time using repeated brief exposures to glutamate. Fig. 4A illustrates the changes in $[Ca^{2+}]_c$ in the response to 1.5-min stimulus of 10 μM glutamate in control cells. After the cells were deprived of glucose (with addition

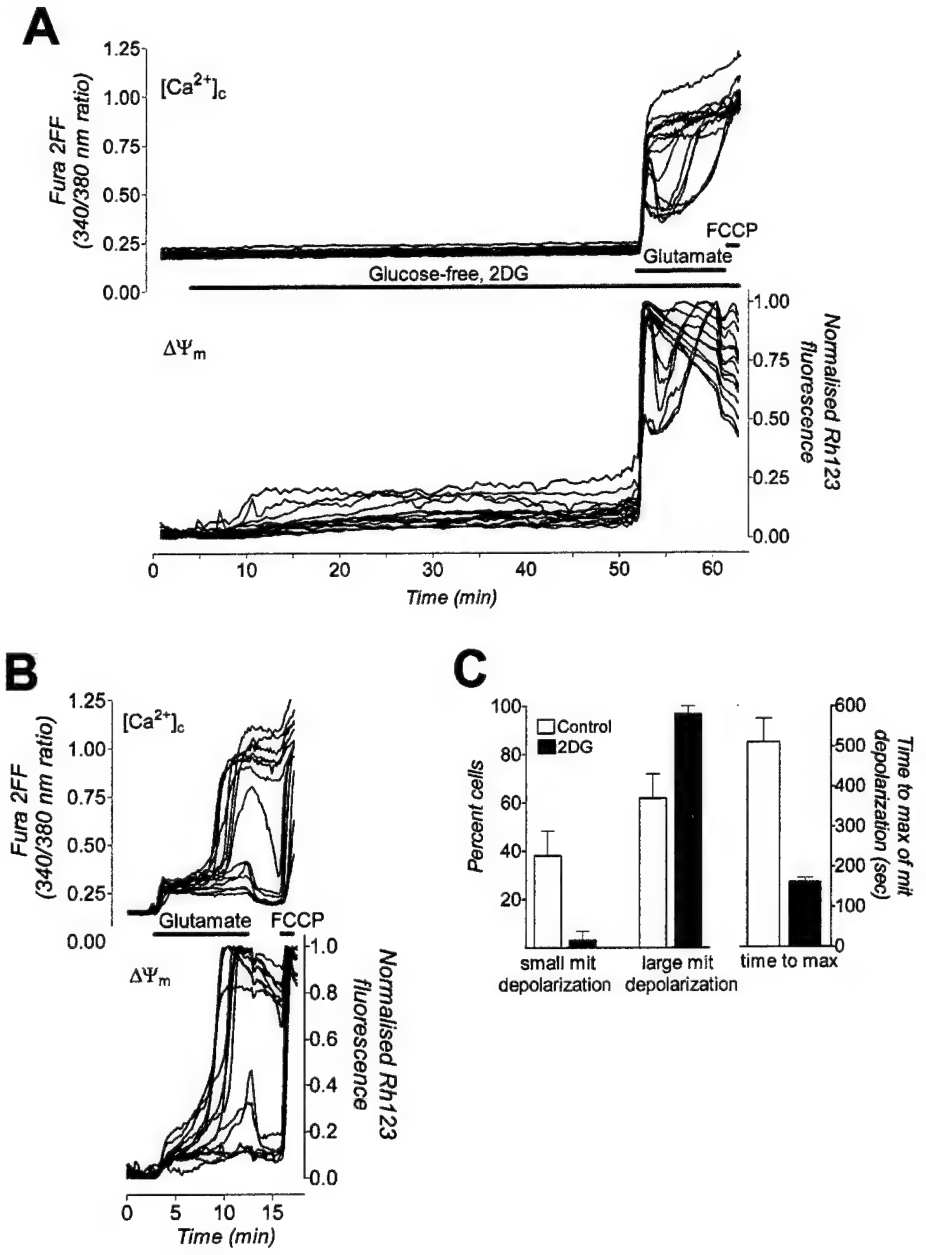

Fig. 2. 2DG-induced hypersensitivity of neurons to glutamate. A: Effect of substitution of glucose in the perfusion medium to 10 mM 2DG on changes in basal $[Ca^{2+}]_c$ and $\Delta\psi_m$ and on response to 10 μM glutamate. B: Glutamate-induced changes in $[Ca^{2+}]_c$ and $\Delta\psi_m$ in control neurons. FCCP (750 μM) was added at the end of each experiment to fully depolarize mitochondria. C: Summarized data show the percentage of the cells with mono- (small mitochondrial depolarization) and biphasic (large mitochondrial depolarization) responses to 10-min glutamate application and time of delay in the development of the secondary phase (time to maximum). The time to maximum was calculated as shown in Fig. 1. Each bar and associated error bar represent the mean ± SE (n = 3 experiments).

of 10 mM 2DG) for 60 min followed by 25 min washout with normal HBSS, $[Ca^{2+}]_c$ responses were greatly enhanced (Fig. 4B). In some cells after the second and third stimulus $[Ca^{2+}]_c$ reached a plateau level and did not recover, while in other cases the recovery was greatly delayed. Note that the baseline ratio of fura-2FF in the cells that were deprived of glucose had not changed from the control level, showing that basal Ca^{2+} homeostasis remained intact in this paradigm.

It is possible that the effects of 2DG could be mediated by an acute modulation of glutamate receptors. To test this possibility we applied 20 mM 2DG against a background of a small concentration of glutamate (Fig. 5). 2DG did not further increase $[Ca^{2+}]_c$, suggesting that this compound has

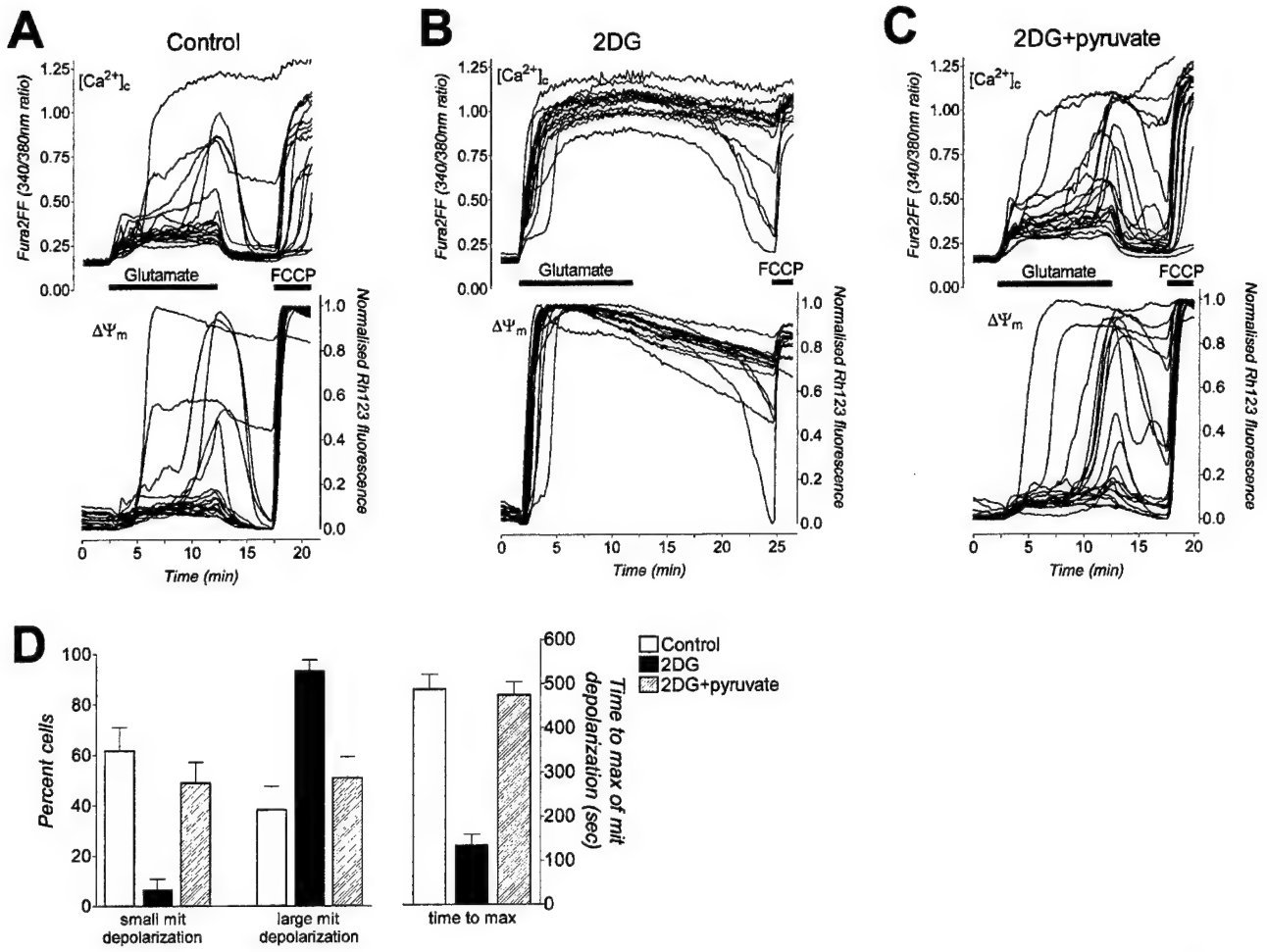

Fig. 3. Prolonged 2DG-induced hypersensitivity of neurons to glutamate and protective effect of pyruvate. A: Simultaneous measurements of $[Ca^{2+}]_c$ and $\Delta\psi_m$ in control neurons treated with 10 μM glutamate for 10 min. B, C: Cells were incubated in glucose-free 10 mM 2DG or 2DG with 10 mM pyruvate -containing solution for 1 h at 37°C and then washed with standard HBSS for 25 min at room temperature. After that the recording was performed at room temperature with a perfusion of standard HBSS. D: Summarized data show the proportion of the neurons with small and large responses to glutamate and the time to maximum of mitochondrial depolarization in the cells with biphasic responses; the time to maximum was calculated as shown in Fig. 1. Each column and associated error bar represent the mean ± SE (n = 8 experiments).

no direct action on glutamate receptors and that the effect of 2DG is not associated with an enhanced Ca^{2+} influx into the cytosol.

To show that 2DG-induced hypersensitivity of neurons to glutamate is not associated with nonspecific effect of 2DG, we also incubated the cells in glucose-free medium without 2DG for 5 h. We found that after 5 h of glucose deprivation the response to glutamate was much larger than in control cells incubated in standard HBSS. The difference was similar to that in 2DG-treated compared to control cells (data not shown). This is consistent with the notion that the primary effect of 2DG is a consequence of the inhibition of glycolysis.

It has been shown that preventing mitochondrial Ca^{2+} uptake during stimulation of NMDA receptors significantly enhanced increases in $[Ca^{2+}]_c$ and significantly reduced glutamate-stimulated neuronal cell death (Stout et al., 1998). It is possible that mitochondria accumulated Ca^{2+} during glucose deprivation so that hypersensitivity of the neurons to glutamate is due to mitochondrial Ca^{2+} overload. Depolarization of mitochondria with an uncoupler (FCCP) can be used as a method of estimating the accumulation of Ca^{2+} in the mitochondria of neurons (Brocard et al., 2001). In Figs. 1B and 3A it is clearly seen that application of 750 nM FCCP at the end of the experiments induced release of mitochondrial calcium. However, application of FCCP to cells prior to glutamate exposure induced only a small increase in $[Ca^{2+}]_c$ (Fig. 6A). Glucose deprivation did not enhance the FCCP-induced increase in $[Ca^{2+}]_c$ (Fig. 6B), indicating that mitochondria did not take up Ca^{2+} during incubation of the cells in 2DG medium. These experiments do not support the hypothesis that 2DG-induced hyposensitivity to glutamate is induced by mitochondrial Ca^{2+} overload.

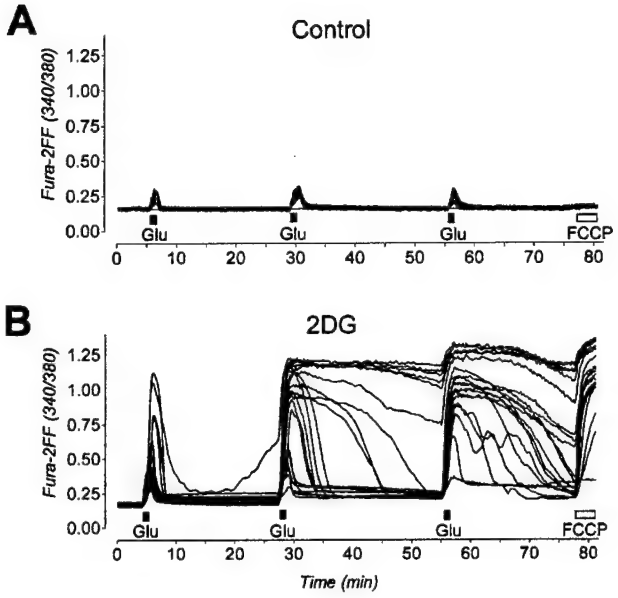

Fig. 4. 2DG increases of neuronal $[Ca^{2+}]_c$ response to a short glutamate stimulus. A: Increase in $[Ca^{2+}]_c$ in response to repetitive 1.5-min glutamate (10 μM, glycine, 2 μM) stimulus in control neurons. B: The cells were preincubated for 1 h in glucose-free 2DG (10 mM) -containing medium at 37°C and then washed with standard HBSS for 25 min at room temperature. The records were made at room temperature in the presence of glucose.

It has been shown by others (Drejer et al., 1985; Longuemare et al., 1994; Silver et al., 1997; Tekkok et al., 1999) that hypoxia or hypoglycemia may induce the release of endogenous excitatory amino acids. In our experiments blockade of NMDA receptors by the reversible antagonist memantine (100 μM) did not prevent 2DG-induced hypersensitivity to glutamate (Data not shown). There is also evidence that a blocker of Na^+ channels, tetrodotoxin (TTX), had a protective effect against ischemia (Zeevalk and Nicklas, 1991; Vornov et al., 1994; Lynch et al., 1995). However, addition of 1 μM TTX during 2DG treatment did not alter the 2DG-induced hypersensitivity (data not shown).

Selective inhibition of glycolytic ATP synthesis

Suppression of glycolysis by removal of glucose (or substitution of glucose by 2DG) leads not only to reduced glycolytic energy production, but also to decreased respiration due to depletion of pyruvate. To determine the specific contribution of glycolytic ATP synthesis 10 mM of pyruvate (with or without 10 mM lactate) was added to the glucose-free 2DG-containing solution. Addition of the substrates fully prevented the 2DG-induced hypersensitivity to glutamate (Fig. 3C and D). This indicates that mitocondrial ATP synthesis can support calcium homeostasis when glycolysis is inhibited. This observation is consistent with the findings of Castilho et al. (1998) in cerebellar granule cells.

If the effects of pyruvate result from supporting respiration, then the blockade of the ATP-synthase by oligomycin should prevent the actions of pyruvate. Fig. 7 shows that an addition of 10 μM oligomycin into the glucose-free medium containing pyruvate and lactate fully abolished the protective action of substrates. Because the combination of hypoglycemic medium with an ATP-synthase inhibitor induced a release of endogenous excitatory amino acids and cell swelling (not shown), in these experiments a reversible inhibitor of NMDA receptors memantine (100 μM) was added into hypoglycemic medium. When NMDA receptors were inhibited during the treatment of cells with hypoglycemic medium, addition of oligomycin did not affect $\Delta\psi_m$ or $[Ca^{2+}]_c$ (data not shown).

Interestingly, adding pyruvate to cells during 2DG exposure was notably more protective than adding pyruvate after 2DG treatment. In this paradigm, neurons were incubated with 2DG for 1 h and then washed with HBSS containing 5 mM pyruvate for 25 min and finally exposed to glutamate in the presence of pyruvate. The addition of substrate *after* 2DG treatment slightly decreased effect of 2DG, but to a smaller extent than pyruvate application *during* 2DG. The summarized data are presented in Fig. 8.

Selective inhibition of mitochondrial ATP synthesis

We next investigated the consequences of inhibiting mitochondrial ATP synthesis while glycolytic ATP production remained intact. We blocked mitochondrial ATP-synthase using the specific inhibitor oligomycin. Cells were incubated with oligomycin for 1 h and then washed with HBSS for 20–25 min, after which simultaneous measurements of $[Ca^{2+}]_c$ and $\Delta\psi_m$ were made. Summary data from these experiments are presented in Fig. 9. 2DG treatment was performed in parallel experiments to provide controls within batches of cells. The inhibition of mitochondrial ATP synthesis did not result in the hypersensitivity of neurons to glutamate. The difference is not likely to be attributable to the duration of drug action, because oligomycin is usually

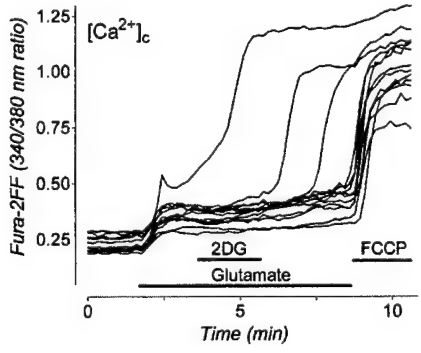

Fig. 5. 2DG does not enhance the glutamate-induced increase in $[Ca^{2+}]_c$ 2DG (20 mM) and 10 μM glutamate (in the presence of 2 μM glycine) were used.

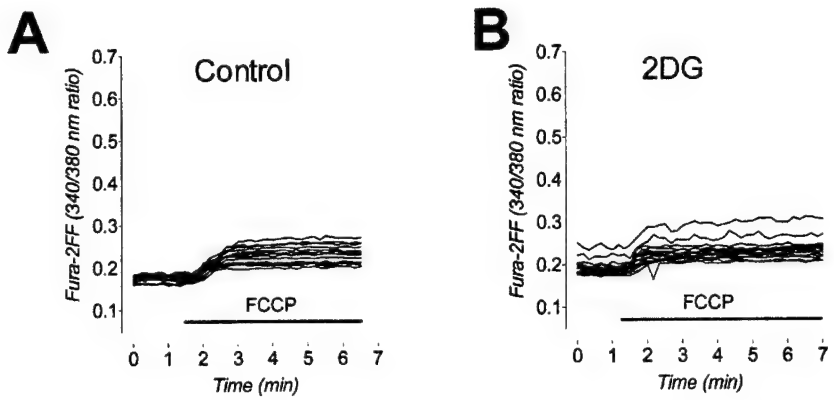

Fig. 6. In resting cells the mitochondrial Ca^{2+} content remains unchanged after a prolonged 2DG application. FCCP (750 nM) was applied to the control neurons (A) and to the cells pretreated with 10 mM 2DG for 1 h with a following 20-min washout with normal HBSS (B).

considered irreversible. The data shown in Fig. 9 indicate that under conditions when glycolysis remained intact, inhibition of mitochondrial ATP synthesis does not increase the sensitivity of neurons to glutamate. This result agrees with that of Budd and Nicholls (1996a), who showed that blockade of mitochondrial ATP synthesis by oligomycin had no effect on the delayed calcium deregulation in the cultured cerebellar granule cells.

Discussion

In this study we investigated the impact of glycolytic and/or mitochondrial ATP synthesis inhibition on the sensitivity of neurons to glutamate. Our studies show that an upstream inhibitor of glycolysis profoundly enhances the sensitivity of neurons to glutamate, as measured by the impairment of neuronal Ca^{2+} homeostasis and loss of $\Delta\psi_m$. However, our studies also show that supporting either glycolysis or respiration alone is sufficient to maintain neurons at their normal level of sensitivity to glutamate. This suggests that in primary culture glycolysis may be sufficient to maintain normal neuronal Ca^{2+} homeostasis functions, which is different from neurons in the intact brain where 95% of total energy is provided by oxidative phosphorylation (Erecinska and Silver, 1994).

Glutamate-induced neuronal Ca^{2+} overload leads to neurodegeneration, and a number of studies have concluded that neuronal Ca^{2+} overload and excitotoxicity correlate with mitochondrial dysfunction. Collapse of $\Delta\psi_m$ depletes cellular ATP via inhibition of mitochondrial ATP synthesis and rapid hydrolysis of cytoplasmic ATP (Budd and Nicholls, 1996a). In this work we have preincubated the cells with the agents that inhibit glycolytic and/or mitochondrial ATP synthesis and then examined the response to a glutamate concentration that normally does not cause $[Ca^{2+}]_c$ dysregulation in the majority of neurons. We established that 2DG greatly enhances the sensitivity of neurons to glutamate. The concentrations of glutamate, which normally induced only small and reversible changes in $[Ca^{2+}]_c$ and $\Delta\psi_m$, after 2DG treatment collapsed $\Delta\psi_m$ immediately and increased $[Ca^{2+}]_c$ irreversibly. Of special interest is that this effect of 2DG is very stable; the cells did not restore their normal susceptibility to glutamate even after 150 min of washout with glucose-containing medium. This is presumably because 2DG is phosphorylated and then trapped in neurons (Chi et al., 1987). Blockade of glycolysis not only leads to reduction of ATP synthesis through the glycolytic pathway, but also decreases the supply of energy substrates to mitochondria. To separate the two effects, 2DG was used in combination with pyruvate. It has been demonstrated by others that pyruvate protects neurons against glucose-deprivation-induced toxicity by rescuing the cellular energy charge (Cox et al., 1989; Izumi et al., 1994; Matsumoto et al., 1994; Eimerl and Schramm, 1995; Ruiz et al., 1998; Maus et al., 1999; Lee et al., 2001). We have found that pyruvate prevented the 2DG-induced hyprsensitivity of neurons to glutamate, indicating that under conditions of intact respiration, blockade of glycolytic ATP synthesis is not enough to increase neuronal sensitivity to glutamate. Like selective inhibition of glycolytic ATP synthesis by a combined application of 2DG and pyruvate, the oligomycin-induced blockade of mitochondrial ATP synthesis failed to enhance the sensitivity to glutamate. In contrast, an addition of oligomycin to the 2DG plus pyruvate solution abolished the protective effect of pyruvate (see Fig. 7). This strongly supports our conclusion that pyruvate protects neurons from a deterioration of Ca^{2+} homeostasis due to maintaining mitochondrial ATP synthesis but not simply due to restoration of respiration required for generation of mitochondrial potential. These data show that both glycolysis and oxidative phosphorylation have the capacity to support normal cell function.

Numerous studies have reported that neurotoxicity induced by hypoxia, hypoglycemia, or oxygen–glucose deprivation is mediated by activation of NMDA receptors through the action of endogenously released glutamate (Novelli et al., 1988; Facci et al., 1990; Goldberg and Choi,

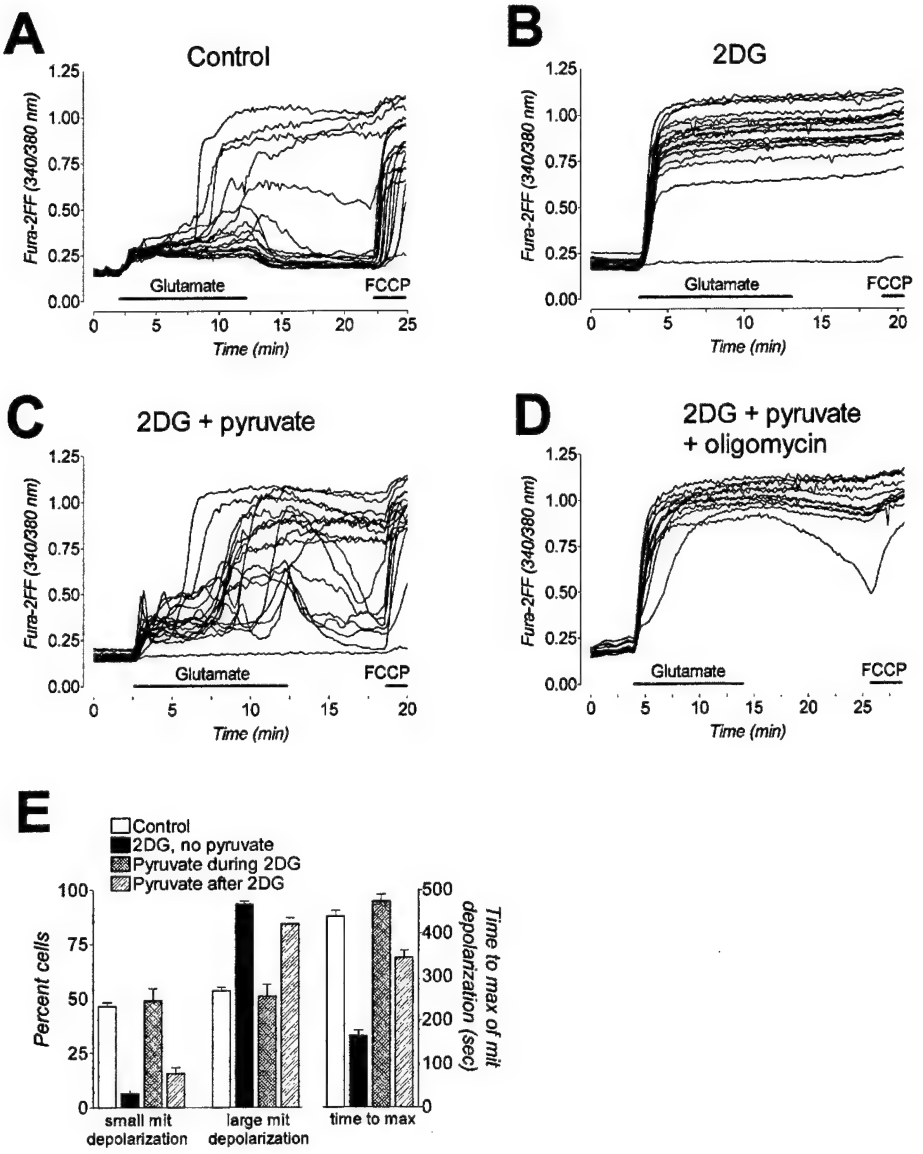

Fig. 7. Effects of the blockade of glycolytic or both glycolytic and mitochondrial ATP synthesis on neuronal response to glutamate. Before the records were made, cultured cortical neurons were treated for 1 h with 10 mM 2DG (B); 10 mM 2DG with 10 mM pyruvate (C); or a mixture of 2DG, pyruvate, 10 μM oligomycin, and 100 μM memantine (D) (see explanation in the text) and then washed with standard HBSS for 20–25 min at room temperature.

1993; Mattson et al., 1993a; Cheng et al., 1993; Maus et al., 1999). This raises the possibility that the 2DG effect is the result of activation of glutamate receptors during the period of hypoglycemia. However, in our experiments addition of an NMDA receptor blocker to the 2DG-containing medium did not have a protective effect, suggesting that mechanisms other than stimulation of NMDA receptors contribute to sensitization of the glutamate response. It is possible that the contribution of released glutamate to the sensitization was minimized by the paucity of astrocytes in our culture preparation. We did not find an additional increase in $[Ca^{2+}]_c$ when 2DG was applied against a background of a low glutamate concentration (see Fig. 5), which provides indirect evidence that 2DG does not exert a nonspecific effect on glutamate-receptor-gated channels. However, we cannot exclude the possibility that the changes in ion influx could occur through the steps downstream of glycolysis blockade. Thus, previous electrophysiological study has demonstrated that hypoglycemia reversibly potentiates glutamate responses of dopaminergic neurons (Marinelli et al., 2001). However, other reports have shown that anoxia either suppresses the NMDA-induced current (Krnjevic et al., 1989) or does not affect the postsynaptic responses to AMPA and NMDA (Khazipov et al., 1995) in hippocampal neurons.

We also checked the possibility that hypersensitivity to glutamate could be related to an increase in mitochondrial Ca^{2+} uptake during 2DG treatment. The results presented in Fig. 6 show that FCCP-induced release of Ca^{2+} from mi-

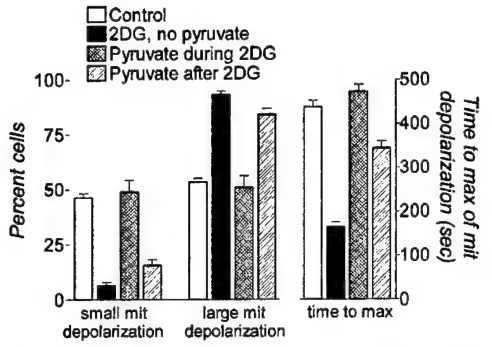

Fig. 8. Washout of cells after 2DG treatment with pyruvate had a less protective effect than the presence of pyruvate during 2DG treatment. Summarized data show the proportion of the neurons with small and large responses to glutamate and the time to maximum of mitochondrial depolarization in the cells with biphasic responses; the time to maximum was calculated as shown in Fig. 1. Each column and associated error bar represent the mean ± SE (n = 5 experiments).

tochondria was the same in control and 2DG-treated cells. This does not support the hypothesis that the effect of 2DG is due to mitochondrial Ca^{2+} overload. However, this cannot fully exclude the possibility that intramitochondrial Ca^{2+} in its nonreleasable form can play a role in the mechanism of enhanced glutamate toxicity. The results of Fig. 6 also emphasize the notion that mitochondria in resting cells do not store large quantities of calcium (White and Reynolds, 1997).

There are several reports of 2DG-induced increase in sensitivity to glutamate-mediated neuronal injury (Lysko et al., 1989; Cox et al., 1989; Rego et al., 1999). Cox et al., (1989) showed that lower concentrations of glutamate become toxic in cerebellar cultured neurons deprived of glucose. The authors proposed that glucose deprivation leads to depolarization of neurons, relieving Mg^{2+} -block of the NMDA channels, which promotes ion influx and glutamate toxicity. However, the direct measurement of membrane potential of CA1 hippocampal neurons showed that 15- to 20-min application of glucose-free 2DG (10 mM) -containing medium produced hyperpolarization of neuronal membrane (Zhao et al., 1997). These data are at variance with the hypothesis that 2DG-induced increase in sensitivity of neurons to glutamate is due to relief of Mg^{2+} -block of the NMDA channels and the concomitant increase of Ca^{2+} influx into the cytosol.

There are also several reports suggesting that ATP generated from different sources can be preferentially used by the different cellular structures. Thus, it has been reported

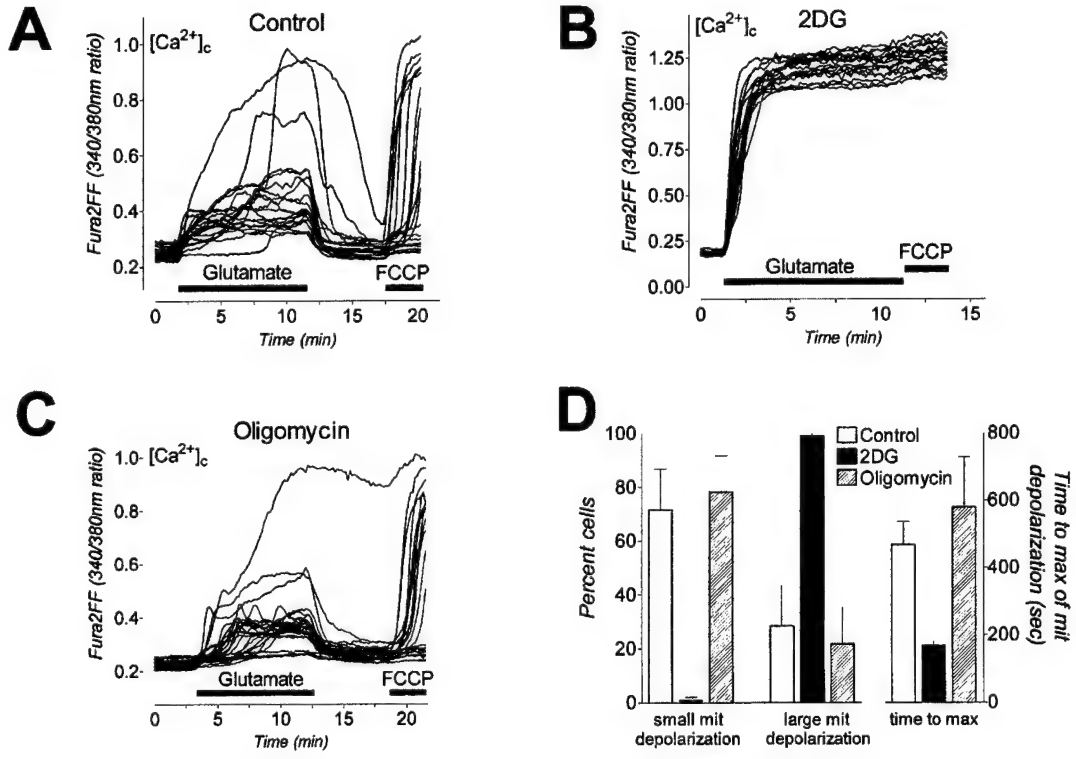

Fig. 9. Effect of blockade of mitochondrial ATP synthesis on neuronal response to glutamate. For all records, glutamate concentration is 10 μM; FCCP, 750 nM. The records in B and C were made after 1-h incubation of the cells with 10 mM DOG (B) or 10 μM oligomycin (C) following 25-min washout with standard HBSS. The records of simultaneous measurement of $\Delta\psi_m$ are not shown. Summarized data presented in the histograms (D) were calculated as shown in Fig. 1. Each bar and associated error bar represent the mean ± SE (n = 4 experiments); Oligomycin and control were not significantly different, $P > 0.05$.

that the Na^+–K^+ -pump may be fueled preferentially by glycolytically generated ATP (Campbell and Paul, 1992; Raffin et al., 1992). Silver et al. (1997) suggested that this preference is due to a specific requirement for ATP by the ATPase imposed by local conditions, which is fulfilled better by glycolysis. Association of some glycolytic pathway enzymes with the plasma membrane and its proteins (Knull, 1978) could provide a structural basis for such a "compartmentalization." Our experiments did not explicitly demonstrate that one of the cellular sources of ATP production is more important than another to maintain Ca^{2+} homeostasis.

The correlation between neuronal degeneration and cellular ATP content is controversial. On one hand, there are data showing that irreversible Ca^{2+} overload and excitotoxicity are accompanied by neuronal ATP depletion (Tsuji et al., 1994; Budd and Nicholls, 1996a, 1996b). However, there is also some evidence that ATP depletion does not necessarily correlate with neuronal death, because neurons can survive while experiencing low levels of ATP (Mattson et al., 1993, Mattson and Cheng, 1993; Riepe et al., 1994; Marcaida et al., 1995). Perhaps these differences can be reconciling by data showing that changes in total cellular [ATP] do not necessarily reflect the changes in the free [ATP] in cellular microdomains (Kennedy et al., 1999). Thus, in MIN6 cells changes in [ATP] in cytosol and beneath the plasma membrane after exposure to high $[K^+]$ could be detected, even in the absence of significant changes in the total ATP content. The same study showed that changes in [ATP] in response to the elevation in extracellular glucose concentration are not the same in the different cellular subdomains (i.e., the cytosol, mitochondrial matrix, and under the plasma membrane). It is reasonable to expect that the changes in [ATP] in the neuronal microdomains are also different from those in the bulk of the cell [ATP]; perhaps even a moderate decrease in the rate of mitochondrial ATP production, under condition when glycolytic ATP synthesis is inhibited, can greatly reduce [ATP] under the plasma membrane because of the high ATP consumption by the plasma membrane Na^+–K^+ and Ca^{2+}–ATPases. However, measurements of [ATP] in neuronal microdomains have not been performed. Measurement of total neuronal [ATP] in mixed (neurons and glia) culture may not be accurate because glial ATP might mask changes in neuronal [ATP]. Taking into account these technical difficulties, we did not measure total neuronal [ATP].

Other factors responsible for the 2DG-induced hypersensitivity of neurons to glutamate may include increased free radical production, increased cytosolic $[Na^+]$ ($[Na^+]_c$), or intracellular acidification. It is possible that oxygen–glucose deprivation induces an increase in free radical production (Almeida et al., 2002), which could contribute to the increase in sensitivity. In fact, Delgado-Esteban et al. (2000) showed that D-glucose abolished glutamate-mediated glutathione oxidation and NADH depletion, which protect the neurons against glutamate toxicity. An increase in $[Na^+]_c$ when the cellular energy production was limited has been demonstrated (Silver et al., 1997). TTX reduced glucose- and oxygen–glucose deprivation -induced neuronal injury (Lynch et al., 1995; Nijjar and Belgrave, 1997) and substitution of extracellular Na^+ with Li^+ prevented NMDA-induced excitotoxicity in glucose-deprived neurons (Czyz et al., 2002). In our experiments TTX had no effect, suggesting that Na^+ influx via Na^+ channels was not involved. However, we did not investigate whether Na^+ entering through NMDA channels was increased in 2DG-treated cells.

In conclusion, we have shown here that a suppression of both glycolytic and mitochondrial ATP synthesis produced a sustained increase in sensitivity of cultured neurons to glutamate. To maintain the sensitivity of cultured neurons to glutamate at the control level, at least one of these sources of ATP must be intact.

Acknowledgments

We thank Geraldine Kress for preparation of the cell cultures and Prof. Boris Khodorov, Dr. Alexandr Surin, Dr. Kirk E. Dineley, and Latha Malaiyandi for helpful discussion and comments. This work was supported by U.S. Army Neurotoxin Initiative Grant DAMD 17-98-1-8627 (IJR) and NICHD Grant T32-HD40686 (YYH).

References

Almeida, A., Delgado-Esteban, M., Bolanos, J.P., Medina, J.M., 2002. Oxygen and glucose deprivation induces mitochondrial dysfunction and oxidative stress in neurones but not in astrocytes in primary culture. J. Neurochem. 81, 207–217.

Ankarcrona, M., Dypbukt, J.M., Bonfoco, E., Zhivotovsky, B., Orreniusm, S., Lipton, S.A., Nicotera, P., 1995. Glutamate-induced neuronal death: a succession of necrosis or apoptosis depending on mitochondrial function. Neuron 15, 961–973.

Brocard, J.B., Tassetto, M., Reynolds, I.J., 2001. Quantitative evaluation of mitochondrial calcium content in rat cortical neurones following a glutamate stimulus. J. Physiol. 531, 793–805.

Budd, S.L., Nicolls, D.G., 1996a. Mitochondria, calcium regulation, and acute glutamate excitotoxicity in cultured cerebellar granule cells. J. Neurochem. 67, 2282–2291.

Budd, S.L., Nicolls, D.G., 1996b. A reevaluation of the role of mitochondria in neuronal Ca^{2+} homeostasis. J. Neurochem. 66, 403–411.

Campbell, J.D., Paul, R.J., 1992. The nature of fuel provision for the Na^+, K^+-ATPase in porcine vascular smooth muscle. J. Physiol. 447, 67–82.

Carafoli, E., 1991. Calcium pump of the plasma membrane. Physiol. Rev. 71, 129–153.

Castilho, R.F., Hansson, O., Ward, M.W., Budd, S.L., Nicholls, D.G., 1998. Mitochondrial control of acute glutamate excitotoxicity in cultured cerebellar granule cells. J. Neurosci. 18, 10277–10286.

Chi, M.M., Pusateri, M.E., Carter, J.G., Norris, B.J., McDougal, D.B., Lowry, O.H., 1987. Enzymatic assays for 2-deoxyglucose and 2-deoxyglucose 6-phosphate. Anal. Biochem. 161, 508–513.

Cheng, B., McMahon, D.G., Mattson, M.P., 1993. Modulation of calcium current, intracellular calcium levels and cell survival by glucose deprivation and growth factors in hippocampal neurons. Brain Res. 607, 275–285.

Choi, D.W., 1988. Calcium-mediated neurotoxicity: relationship to specific channel types and role in ischemic damage. Trends Neurosci. 11, 465–469.

Choi, D.W., Rothman, S.M., 1990. The role of glutamate neurotoxicity in hypoxic–ischemic neuronal death. Ann. Rev. Neurosci. 13, 171–182.

Cox, J.A., Lysko, P.G., Henneberry, R.C., 1989. Excitatory amino acid neurotoxicity at the *N*-methyl-D-aspartate receptor in cultured neurons: role of the voltage-dependent magnesium block. Brain Res. 499, 267–272.

Czyz, A., Baranauskas, G., Kiedrowski, L., 2002. Instrumental role of Na^+ in NMDA excitotoxicity in glucose-deprived and depolarized cerebellar granule cells. J. Neurochem. 81, 379–389.

deErausquin, G.A., Manev, H., Guidotti, A., Costa, E., Brooker, G., 1990. Gangliosides normalize distorted single-cell intracellular free Ca^{2+} dynamics after toxic doses of glutamate in cerebellar granule cells. Proc. Natl Acad. Sci. USA 87, 8017–8021.

Delgado-Esteban, M., Almeida, A., Bolanos, J.P., 2000. D-Glucose prevents glutathione oxidation and mitochondrial damage after glutamate receptor stimulation in rat cortical primary neurons. J. Neurochem. 75, 1618–1624.

Dineley, K.E., Malaiyandi, L.M., Reynolds, I.J., 2002. A reevaluation of neuronal zinc measurements: artifacts associated with high intracellular dye concentration. Mol. Pharmacol. 62, 618–627.

DiPolo, R., Beauge, L., 1988. Ca^{2+} transport in nerve fibers. Biochim. Biophys. Acta 947, 549–569.

Drejer, J., Benveniste, H., Diemer, N.H., Schousboe, A., 1985. Cellular origin of ischemia-induced glutamate release from brain tissue in vivo and in vitro. J. Neurochem. 45, 145–151.

Duchen, M.R., 1999. Contributions of mitochondria to animal physiology: from homeostatic sensor to calcium signalling and cell death. J. Physiol. 516, 1–17.

Duchen, M.R., Biscoe, T.J., 1992. Relative mitochondrial membrane potential and $[Ca^{2+}]_i$ in type I cells isolated from the rabbit carotid body. J. Physiol. 450, 33–61.

Eimerl, S., Schramm, M., 1995. Resuscitation of brain neurons in the presence of Ca^{2+} after toxic NMDA-receptor activity. J. Neurochem. 65, 739–743.

Erecinska, M., Silver, I.A., 1994. Ions and energy in mammalian brain. Prog. Neurobiol. 43, 37–71.

Facci, L., Leon, A., Skaper, S.D., 1990. Excitatory amino acid neurotoxicity in cultured retinal neurons: involvement of *N*-methyl-D-aspartate (NMDA) and non-NMDA receptors and effect of ganglioside GM1. Neuroscience 37, 709–716.

Glaum, S.R., Scholz, W.K., Miller, R.J., 1990. Acute- and long-term glutamate-mediated regulation of $[Ca^{2+}]_i$ in rat hippocampal pyramidal neurons in vitro. J Pharmacol. Exp. Ther. 253, 1293–1302.

Goldberg, M.P., Choi, D.W., 1993. Combined oxygen and glucose deprivation in cortical cell culture: calcium-dependent and calcium-independent mechanisms of neuronal injury. J. Neurosci. 13, 3510–3524.

Isaev, N.K., Zorov, D.B., Stelmashook, E.V., Uzbekov, R.E., Kozhemyakin, M.B., Victorov, I.V., 1996. Neurotoxic glutamate treatment of cultured cerebellar granule cells induces Ca^{2+} -dependent collapse of mitochondrial membrane potential and ultrastructural alterations of mitochondria. FEBS Lett. 392, 143–147.

Izumi, Y., Benz, A.M., Zorumski, C.F., Olney, J.W., 1994. Effects of lactate and pyruvate on glucose deprivation in rat hippocampal slices. Neuroreport 5, 617–620.

Keelan, J., Vergun, O., Duchen, M.R., 1999. Excitotoxic mitochondrial depolarisation requires both calcium and nitric oxide in rat hippocampal neurons. J. Physiol. 520, 797–813.

Kennedy, H.J., Pouli, A.E., Ainscow, E.K., Jouaville, L.S., Rizzuto, R., Rutter, G.A., 1999. Glucose generates sub-plasma membrane ATP microdomains in single islet beta-cells. Potential role for strategically located mitochondria. J. Biol. Chem. 274, 13281–13291.

Khazipov, R., Congar, P., Ben-Ari, Y., 1995. Hippocampal CA1 lacunosum-moleculare interneurons: comparison of effects of anoxia on excitatory and inhibitory postsynaptic currents. J. Neurophysiol. 74, 2138–2149.

Khodorov, B.I., 2000. Mechanisms of destabilization of Ca^{2+}-homeostasis of brain neurons caused by toxic glutamate challenge. Membr. Cell. Biol. 14, 149–162.

Khodorov, B., Pinelis, V., Vergun, O., Storozhevykh, T., Vinskaya, N., 1996. Mitochondrial deenergization underlies neuronal calcium overload following a prolonged glutamate challenge. FEBS Lett. 397, 230–234.

Kiedrowski, L., 1998. The difference between mechanisms of kainite and glutamate excitotoxicity in vitro: osmotic lesion versus mitochondrial depoilarization. Restor. Neurol. Neurosci. 12, 71–79.

Knull, H.R., 1978. Association of glycolytic enzymes with particulate fractions from nerve endings. Biochim. Biophys. Acta 522, 1–9.

Krnjevic, K., Cherubini, E., Ben-Ari, Y., 1989. Anoxia on slow inward currents of immature hippocampal neurons. J. Neurophysiol. 62, 896–906.

Lee, J-Y., Kim, Y-H., Koh, J-Y., 2001. Protection by pyruvate against transient forebrain ischemia in rats. J. Neurosci. 21, 1–6 RC171.

Leyssens, A., Nowicky, A.V., Patterson, L., Crompton, M., Duchen, M.R., 1996. The relationship between mitochondrial state, ATP hydrolysis, $[Mg^{2+}]_i$ and $[Ca^{2+}]_i$ studied in isolated rat cardiomyocytes. J. Physiol. 496, 111–128.

Limbrick Jr., D.D., Churn, S.B., Sombati, S., DeLorenzo, R.J., 1995. Inability to restore resting intracellular calcium levels as an early indicator of delayed neuronal cell death. Brain Res. 690, 145–156.

Longuemare, M.C., Hill, M.P., Swanson, R.A., 1994. Glycolysis can prevent non-synaptic excitatory amino acid release during hypoxia. Neuroreport 5, 1789–1792.

Lynch, J.J., Yu, S.P., Canzoniero, L.M., Sensi, S.L., Choi, D.W., 1995. Sodium channel blockers reduce oxygen–glucose deprivation-induced cortical neuronal injury when combined with glutamate receptor antagonists. J. Pharmacol. Exp. Ther. 273, 554–560.

Lysko, P.G., Cox, J.A., Vigano, M.A., Henneberry, R.C., 1989. Excitatory amino acid neurotoxicity at the *N*-methyl-D-aspartate receptor in cultured neurons: pharmacological characterization. Brain Res. 499, 258–266.

Manev, H., Favaron, M., Guidotti, A., Costa, E., 1989. Delayed increase of Ca^{2+} influx elicited by glutamate: role in neuronal death. Mol. Pharmacol. 36, 106–112.

Marcaida, G., Minana, M.D., Grisolia, S., Felipo, V., 1995. Lack of correlation between glutamate-induced depletion of ATP and neuronal death in primary cultures of cerebellum. Brain Res. 695, 146–150.

Marinelli, S., Federici, M., Giacomini, P., Bernardi, G., Mercuri, N.B., 2001. Hypoglycemia enhances ionotropic but reduces metabotropic glutamate responses in substantia nigra dopaminergic neurons. J. Neurophysiol. 85, 1159–1166.

Matsumoto, K., Yamada, K., Kohmura, E., Kinoshita, A., Hayakawa, T., 1994. Role of pyruvate in ischaemia-like conditions on cultured neurons. Neurol. Res. 16, 460–464.

Mattson, M.P., Zhang, Y., Bose, S., 1993. Growth factors prevent mitochondrial dysfunction, loss of calcium homeostasis, and cell injury, but not ATP depletion in hippocampal neurons deprived of glucose. Exp. Neurol. 121, 1–13.

Mattson, M.P., Cheng, B., 1993. Growth factors protect neurons against excitotoxic/ischemic damage by stabilizing calcium homeostasis. Stroke 24, I136–I140.

Maus, M., Marin, P., Israel, M., Glowinski, J., Premont, J., 1999. Pyruvate and lactate protect striatal neurons against *N*-methyl-D-aspartate-induced neurotoxicity. Eur. J. Neurosci. 11, 3215–3224.

Nicholls, D.G., 1986. Intracellular calcium homeostasis. Br. Med. Bull. 42, 353–358.

Nicholls, D.G., Ward, M.W., 2000. Mitochondrial membrane potential and neuronal glutamate excitotoxicity: mortality and millivolts. Trends Neurosci. 23, 166–174.

Nijjar, M., Belgrave, R.L., 1997. Regulation of Ca^{2+} homeostasis by glucose metabolism in rat brain. Mol. Cell. Biochem. 176, 317–326.

Novelli, A., Reilly, J.A., Lysko, P.G., Henneberry, R.C., 1988. Glutamate becomes neurotoxic via the *N*-methyl-D-aspartate receptor when intracellular energy levels are reduced. Brain Res. 451, 205–212.

Ogura, A., Miyamoto, M., Kudo, Y., 1988. Neuronal death in vitro: parallelism between survivability of hippocampal neurones and sus-

tained elevation of cytosolic Ca^{2+} after exposure to glutamate receptor agonist. Exp. Brain. Res. 73, 447–458.

Raffin, C.N., Rosenthal, M., Busto, R., Sick, T.J., 1992. Glycolysis, oxidative metabolism, and brain potassium ion clearance. J. Cereb. Blood Flow Metab. 12, 34–42.

Rego, A.C., Areias, F.M., Santos, M.S., Oliveira, C.R., 1999. Distinct glycolysis inhibitors determine retinal cell sensitivity to glutamate-mediated injury. Neurochem. Res. 24, 351–358.

Riepe, M., Ludolph, A., Seelig, M., Spencer, P.S., Ludolph, A.C., 1994. Increase of ATP levels by glutamate antagonists is unrelated to neuroprotection. Neuroreport 5, 2130–2132.

Ruiz, F., Alvarez, G., Pereira, R., Hernandez, M., Villalba, M., Cruz, F., Cerdan, S., Bogonez, E., Satrustegui, J., 1998. Protection by pyruvate and malate against glutamate-mediated neurotoxicity. Neuroreport 9, 1277–1282.

Scanlon, J.M., Reynolds, I.J., 1998. Effects of oxidants and glutamate receptor activation on mitochondrial membrane potential in rat forebrain neurons. J. Neurochem. 71, 2392–2400.

Schanne, F.A., Kane, A.B., Young, E.E., Farber, J.L., 1979. Calcium dependence of toxic cell death: a final common pathway. Science 206, 700–702.

Schinder, A.F., Olson, E.C., Spitzer, N.C., Montal, M., 1996. Mitochondrial dysfunction is a primary event in glutamate neurotoxicity. J. Neurosci. 16, 6125–6133.

Sheu, S.-S., Blaustein, M.P., 1992. Sodium/calcium exchange and control of cell calcium and contractility in cardiac and vascular smooth muscles, in: Fozzard, H.A., Haber, E., Jennings, R.B., Katz, A.M., Morgan, H.E. (Eds.), The Heart and Cardiovascular System. Raven, New York, pp. 509–537.

Silver, I.A., Deas, J., Erecińska, M., 1997. Ion homeostasis in brain cells: differences in intracellular ion responses to energy limitation between cultured neurons and glial cells. Neuroscience 78, 589–601.

Stout, A.K., Raphael, H.M., Kanterewicz, B.I., Klann, E., Reynolds, I.J., 1998. Glutamate-induced neuron death requires mitochondrial calcium uptake. Nature (Neurosci.) 1, 366–373.

Tekkok, S., Medina, I., Krnjevic, K., 1999. Intraneuronal $[Ca^{2+}]$ changes induced by 2-deoxy-D-glucose in rat hippocampal slices. J. Neurophysiol. 81, 174–183.

Tsuji, K., Nakamura, Y., Ogata, T., Shibata, T., Kataoka, K., 1994. Rapid decrease in ATP content without recovery phase during glutamate-induced cell death in cultured spinal neurons. Brain Res. 662, 289–292.

Vergun, O., Keelan, J., Khodorov, B.I., Duchen, M.R., 1999. Glutamate-induced mitochondrial depolarisation and perturbation of calcium homeostasis in cultured rat hippocampal neurones. J. Physiol. 519, 451–466.

Vergun, O., Sobolevsky, A.I., Yelshansky, M.V., Keelan, J., Khodorov, B.I., Duchen, M.R., 2001. Exploration of the role of reactive oxygen species in glutamate neurotoxicity in rat hippocampal neurones in culture. J. Physiol. 531, 147–163.

Vornov, J.J., Tasker, R.C., Coyle, J.T., 1994. Delayed protection by MK-801 and tetrodotoxin in a rat organotypic hippocampal culture model of ischemia. Stroke 25, 457–464.

Ward, M.W., Rego, A.C., Frenguelli, B.G., Nicholls, D.G., 2000. Mitochondrial membrane potential and glutamate excitotoxicity in cultured cerebellar granule cells. J. Neurosci. 20, 7208–7219.

White, R.J., Reynolds, I.J., 1996. Mitochondrial depolarization in glutamate-stimulated neurons: an early signal specific to excitotoxin exposure. J. Neurosci. 16, 5688–5697.

White, R.J., Reynolds, I.J., 1997. Mitochondria accumulate Ca^{2+} following intense glutamate stimulation of cultured rat forebrain neurones. J. Physiol. 498, 31–47.

Zeevalk, G.D., Nicklas, W.J., 1991. Mechanisms underlying initiation of excitotoxicity associated with metabolic inhibition. J. Pharmacol. Exp. Ther. 257, 870–878.

Zhang, H., Huang, H.M., Carson, R.C., Mahmood, J., Thomas, H.M., Gibson, G.E., 2001. Assessment of membrane potentials of mitochondrial populations in living cells. Anal. Biochem. 298, 170–180.

Zhao, Y.T., Tekkok, S., Krnjevic, K., 1997. 2-Deoxy-D-glucose-induced changes in membrane potential, input resistance, and excitatory postsynaptic potentials of CA1 hippocampal neurons. Can. J. Physiol. Pharmacol. 75, 368–374.

Journal of Neurochemistry, 2001, **79**, 266–277

$\Delta\Psi_m$-Dependent and -independent production of reactive oxygen species by rat brain mitochondria

Tatyana V. Votyakova and Ian J. Reynolds

Department of Pharmacology, University of Pittsburgh, Pittsburgh, Pennsylvania, USA

Abstract

Mitochondria are widely believed to be the source of reactive oxygen species (ROS) in a number of neurodegenerative disease states. However, conditions associated with neuronal injury are accompanied by other alterations in mitochondrial physiology, including profound changes in the mitochondrial membrane potential $\Delta\Psi_m$. In this study we have investigated the effects of $\Delta\Psi_m$ on ROS production by rat brain mitochondria using the fluorescent peroxidase substrates scopoletin and Amplex red. The highest rates of mitochondrial ROS generation were observed while mitochondria were respiring on the complex II substrate succinate. Under this condition, the majority of the ROS signal was derived from reverse electron transport to complex I, because it was inhibited by rotenone. This mode of ROS generation is very sensitive to depolarization of $\Delta\Psi_m$, and even the depolarization associated with ATP generation was sufficient to inhibit ROS production. Mitochondria respiring on the complex I substrates, glutamate and malate, produce very little ROS until complex I is inhibited with rotenone, which is also consistent with complex I being the major site of ROS generation. This mode of oxidant production is insensitive to changes in $\Delta\Psi_m$. With both substrates, ubiquinone-derived ROS can be detected, but they represent a more minor component of the overall oxidant signal. These studies demonstrate that rat brain mitochondria can be effective producers of ROS. However, the optimal conditions for ROS generation require either a hyperpolarized membrane potential or a substantial level of complex I inhibition.

Keywords: Amplex red, free radicals, mitochondrial membrane potential, rotenone, scopoletin.

J. Neurochem. (2001) **79**, 266–277.

In addition to their critical role in ATP synthesis, mitochondria are also the major source of reactive oxygen species (ROS) in most cell types. Generated by the incomplete reduction of molecular oxygen during the process of oxidative phosphorylation, superoxide is the main form of ROS produced by mitochondria (Sorgato *et al.* 1974; Boveris and Cadenas 1975). It has been suggested that 2% of the oxygen consumed by mitochondria is converted to superoxide (Boveris and Chance 1973). In turn, superoxide is converted by manganese superoxide dismutase to H_2O_2, which is more stable and more lipid soluble, and thus can be more readily released by mitochondria. Although it is possible that mitochondrially derived ROS serve a signaling function in cells, it is more widely believed that ROS are harmful as the result of the oxidative modification of proteins, nucleic acids and lipid membranes.

The mechanisms responsible for the generation of ROS by the electron transport chain have been extensively investigated, primarily in mitochondria derived from heart muscle (Loschen *et al.* 1971; Boveris and Chance 1973; Cadenas and Boveris 1980; Turrens *et al.* 1985; Korshunov *et al.* 1997). The principal source appears to be the redox cycling ubiquinone in complex III (Boveris *et al.* 1976; Cadenas *et al.* 1977). An additional source of superoxide is complex I, which is also endowed with a number of redox centers (Cadenas *et al.* 1977; Takeshige and Minakami 1979; Turrens and Boveris 1980). In isolated mitochondrial preparations it is possible to demonstrate ROS generation from these two major sites when mitochondria respire on substrates that drive either complex I (glutamate and malate) or complex II (succinate). It is interesting to note that the relative magnitude of the ROS signal deriving from either substrate varies quite considerably between tissues. For example, in heart mitochondria complex I substrates

Received June 7, 2001; revised manuscript received July 19, 2001; accepted July 19, 2001.

Address correspondence and reprint requests to Ian J. Reynolds, Department of Pharmacology, University of Pittsburgh, W1351 Biomedical Science Tower, Pittsburgh PA 15261, USA.
E-mail: iannmda@pitt.edu

Abbreviations used: $\Delta\Psi_m$, mitochondrial transmembrane potential; 2,4-DNP, 2,4-dinitrophenol; FCCP, carbonyl cyanide *p*-(trifluoromethoxy) phenyl hydrazone; HRP, horseradish peroxidase; ROS, reactive oxygen species.

generate the largest ROS signal (in the presence of appropriate inhibitors) (Boveris and Chance 1973), while in brain mitochondria complex II substrates appear to be quantitatively more important (Cino and Del Maestro 1989). However, the specific, endogenous mechanisms responsible for altering ROS production by mitochondria are poorly understood.

It is widely believed that ROS contribute to the pathogenesis of a number of neurodegenerative diseases (Halliwell 1992; Beal *et al.* 1997), and given the high rate of oxygen consumption by the brain, it may be reasonable to assume that mitochondria are responsible for the majority of the ROS burden under both normal and pathophysiological situations. However, the mechanisms by which brain mitochondria produce ROS have been investigated less than in other tissues. Indeed, the earliest investigation of this topic concluded that brain mitochondria do not produce ROS (Sorgato *et al.* 1974). More recent studies have conclude that peroxide production can be detected from brain mitochondria from several species, and that the ROS derive from both complex I and ubiquinone (Patole *et al.* 1986; Zoccarato *et al.* 1988; Cino and Del Maestro 1989). Several studies in intact neurons have used oxidation-sensitive fluorescent dyes to detect ROS generation following glutamate receptor activation, and have concluded that mitochondria are the likely source of the ROS signal (Reynolds and Hastings 1995; Dugan *et al.* 1995; Bindokas *et al.* 1996). This suggests that glutamate- and calcium-mediated alterations in mitochondrial function might contribute to the acute injury of neurons, as well as to chronic neurodegenerative states. However, there is a major gap in the understanding of the mechanisms that link glutamate receptor activation to the alteration of mitochondrial ROS production.

We undertook the present study to characterize the mechanisms responsible for ROS production by brain mitochondria using the peroxidase substrates scopoletin and Amplex red to detect peroxide production by mitochondria. In particular, we have investigated the influence of the mitochondrial membrane potential on ROS production because this has been reported to modify certain forms of ROS production by mitochondria in some tissues (Loschen *et al.* 1971; Korshunov *et al.* 1997), and may also be a key variable in the injury of neurons by glutamate (Nieminen *et al.* 1996; Schinder *et al.* 1996; White and Reynolds 1996; Vergun *et al.* 1999). We report here that there are mitochondrial membrane potential dependent and independent mechanisms for the generation of ROS by isolated rat brain mitochondria.

Materials and methods

Isolation of rat brain mitochondria

All procedures using rats were approved by the Institutional Animal Care and Use Committee of the University of Pittsburgh, and are consistent with guidelines provided by the National Institutes of Health. Rat brain mitochondria were isolated from the cortex of adult Sprague–Dawley strain rats by conventional differential centrifugation as described by Rosenthal *et al.* (1987) with minor modifications. After removal, brains were placed in isolation media which contained: 225 mM mannitol, 75 mM sucrose, 5 mM HEPES buffer (pH adjusted to 7.3 with KOH), 1 mg/mL BSA and 0.5 mM tetrapotassium EDTA. After centrifugation at 10 500 *g*, the first mitochondrial pellet was treated with digitonin (40 : 1 of 10% w/v digitonin solution per brain) with a final concentration of 0.013%. Mitochondria were then resuspended and centrifuged in isolation medium without digitonin. All the isolation procedures were carried out at 0 ± 2°C. Prior to experimentation, mitochondria were stored on ice at final concentration of 20–30 mg protein/mL in isolation medium. The protein concentration was determined by the Bradford method (Bradford 1976). Mitochondria prepared in this way were active for 5–6 h, as determined by their ability to maintain a transmembrane potential in the presence of oxidizable substrates.

Fluorescence measurements of H_2O_2 production and mitochondrial transmembrane potential $\Delta\Psi_m$

Fluorescence measurements were performed in a Shimadzu RF5301 spectrofluorimeter in a stirred cuvette maintained at 37°C. Mitochondria were added to a standard incubation buffer that contained: 125 mM KCl; 2 mM K_2HPO_4; 5 mM $MgCl_2$; 10 mM HEPES (pH adjusted to 7.0 with KOH); 10:M EGTA; and 0.2 mg/mL mitochondrial protein. Substrates (5 mM of succinate or 5 mM of glutamate plus 5 mM malate) and adenine nucleotides were added separately as indicated on figures. Hydrogen peroxide was measured using either scopoletin or Amplex red in the presence of 1 U/mL of horseradish peroxidase (HRP). The concentration of both dyes was 2 μM. Measurements were carried out at excitation/emission wavelengths of 365 nm (slit 3 nm)/460 nm (slit 5 nm) for scopoletin and 560 (slit 1.5 nm)/590 (slit 3 nm) for Amplex red, respectively. Since hydrogen peroxide was measured by a decrease of fluorescence in the case of scopoletin, this method is less sensitive to low concentrations of H_2O_2 and may underestimate slow rates of release by mitochondria. On the other hand, the advantage of this method is the opportunity to follow long-lasting reactions by addition of a second aliquot of dye upon the complete oxidation of the initial dye addition. In the case of Amplex red, fluorescence is increased with the generation of H_2O_2. This method is more sensitive to low concentrations of H_2O_2 (Mohanty *et al.* 1997; Zhou and Panchuk-Voloshina 1997). We tested both Amplex red and its oxidation product, resorufin, on mitochondrial function using polarography and found that neither agent at 4 μM had any effect on the respiratory control ratio with either glutamate and malate or succinate as substrate. Note also that the addition of superoxide dismutase to the assay medium did not further increase the signal with either scopoletin or Amplex red (data not shown) suggesting that the endogenous dismutase capacity was sufficient to metabolize all of the superoxide produced in this system. The signals detected by both scopoletin and Amplex red were decreased by 85% by the inclusion of 800 U/mL catalase in the reaction mixture. $\Delta\Psi_m$ was estimated using fluorescence quenching of the cationic dye safranine O which is accumulated and quenched inside energized mitochondria (Akerman and Wikstrom 1976). The excitation wavelength was 495 nm (slit

3 nm) and emission 586 nm (slit 5 nm), and the dye concentration used was 2.5 μM. We attempted to calibrate the safranine O signal using media with different KCl concentrations and valinomycin. Using rat liver mitochondria we obtained a good linear correlation between values calculated from the Nernst equation and measured changes in dye fluorescence within the range of 48–150 mV (data not shown). However, using similar conditions with rat brain mitochondria we were not able to record significant changes in safranine O fluorescence in the calibration buffer because the mitochondria appeared to spontaneously depolarize. This could be due to depletion of potassium from the matrix during the tissue isolation process (in potassium free buffer), or it is also possible that brain mitochondria could be more sensitive to valinomycin-induced swelling. However, this limitation prevented precise calibration of the safranine O signal, and instead the results for this dye are reported in fluorescence units or as a percent of maximal values.

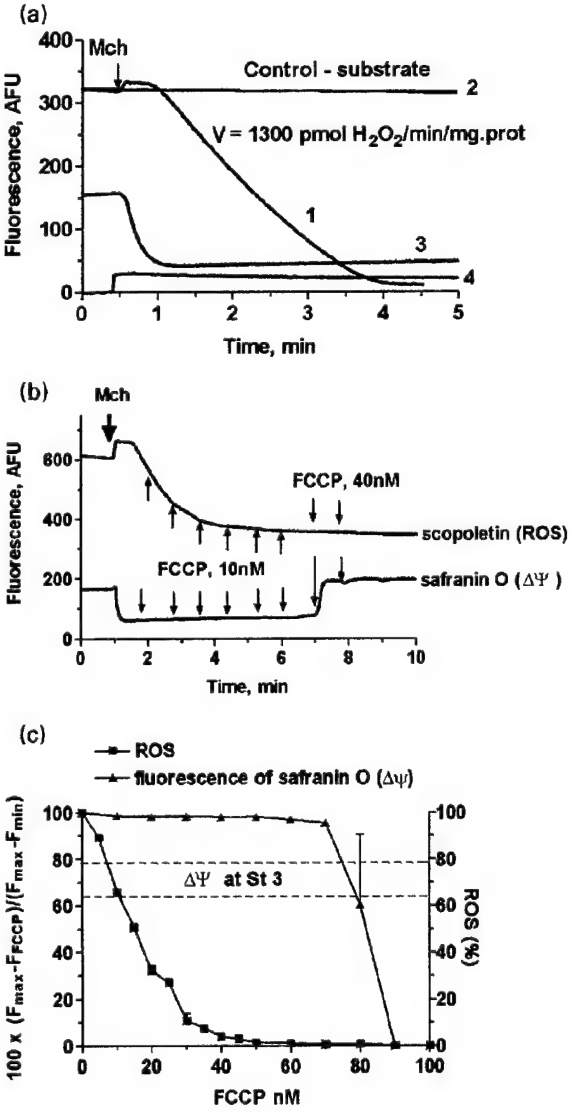

Fig. 1 Hydrogen peroxide production by rat brain mitochondria respiring in the presence of succinate. Hydrogen peroxide release was measured by the scopoletin method. The traces represent independent measurements of the different parameters that were then aligned by the start positions. (a) Typical traces of hydrogen peroxide release (traces 1 and 2), membrane potential (trace 3) and NADH fluorescence (trace 4). Substrate was absent in trace 2. (b) The effect of uncoupler FCCP on hydrogen peroxide release and membrane $\Delta\Psi_m$. FCCP was added to increment the final concentration by 10 or 40 nM with each addition as indicated. (c) The dependence of the rate of hydrogen peroxide release and membrane potential value on FCCP concentration. The plot presents calculations of the data similar to that from panel (b) with the following designations: F_{max}, fluorescence with saturated concentration of uncoupler; F_{min}, fluorescence at maximal energized state; F_{FCCP}, fluorescence with a given concentration of FCCP. The values of rate of ROS production are the means of three or four experiments. The interval in between two dotted lines indicates margins of mitochondrial membrane potential in state 3 respiration.

Data analysis

H_2O_2 generation was calibrated by constructing standard curves using known H_2O_2 concentrations in the presence of the standard incubation buffer, the appropriate dye and horseradish peroxidase but without mitochondria. In this study we show either traces reflecting the fluorescence values measured during the experiment or rates determined from the slope of the fluorescence change and converted to H_2O_2/min/mg protein. Statistical analysis was performed using PRISM (GraphPad Software, San Diego, CA, USA). Typically data were subjected to an ANOVA followed by an appropriate *post hoc* test. Differences were considered significant when $p < 0.05$.

Materials

Amplex red was obtained from Molecular Probes (Eugene, OR, USA). Scopoletin, safranine O, and HRP were obtained from Sigma (St Louis, MO, USA). Myxothiazol was purchased from Fluka (Buchs, Switzerland). All other reagents and inhibitors were purchased from Sigma.

Results

ROS production by mitochondria metabolizing succinate

We first investigated the characteristics of mitochondrial ROS production in rat brain mitochondria incubated with the complex II substrate succinate (Fig. 1). In the absence of succinate the rate of oxidation of scopoletin was very low. However, mitochondria aerobically incubated in media with succinate begin to release hydrogen peroxide after a short lag period of some 30 s. This lag period coincides with the time necessary for mitochondria to gain their maximal value of $\Delta\Psi_m$ (Fig. 1a). Interestingly, the ROS generation supported by succinate is highly sensitive to small changes in $\Delta\Psi_m$ (Fig. 1b). To determine the threshold of $\Delta\Psi_m$ loss necessary to block ROS production, mitochondria were titrated with uncoupler in small increments. Figure 1(b)

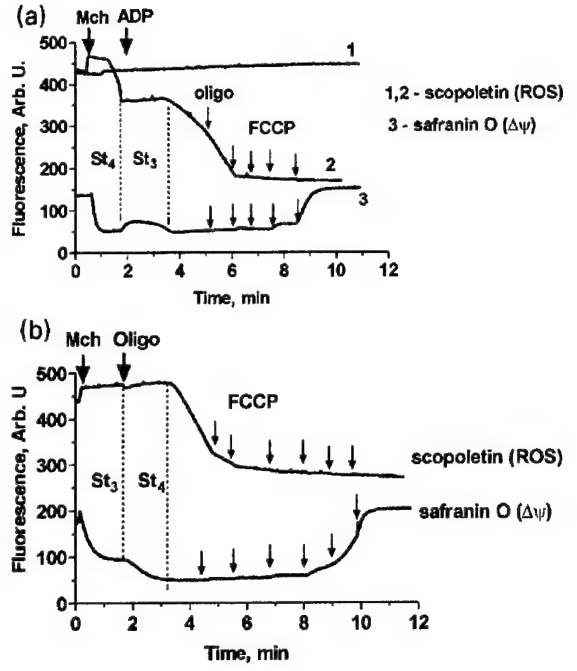

Fig. 2 Activation of ATP synthesis strongly inhibits generation of hydrogen peroxide. Hydrogen peroxide was measured with scopoletin in these experiments. (a) Rat brain mitochondria were incubated in standard media with succinate (traces 2 and 3) or in the same media supplemented with 3 mM ADP (trace 1). Additions: 40 μM ADP; 100 μM oligomycin; FCCP in 30 nM increments. (b) The mitochondria were incubated in standard media with succinate and 3 mM ADP. Additions: 100 nM oligomycin; FCCP in 20 nM increments. Dotted vertical lines on both graphs indicate time points when mitochondria switched phosphorylation on and off, as determined from the $\Delta\Psi_m$ recordings.

shows that 15 nM of carbonyl cyanide *p*-(trifluoromethoxy) phenyl hydrazone (FCCP) caused 50% inhibition of ROS production while producing very small changes in $\Delta\Psi_m$. The minimum concentration of uncoupler that fully blocks the ROS generation was found to be 40–50 nM, which caused decreased the safranine O signal by only 2–3%, while a complete depolarization was observed at 80–100 nM depending on mitochondrial preparation (Fig. 1c). A similar result was obtained with the uncoupler 2,4-dinitrophenol (2,4-DNP) which is known to have a different uncoupling mechanism (Skulachev 1998). The ROS generation was inhibited by 95% at 4 μM of 2,4-DNP while the corresponding decrease of $\Delta\Psi_m$ was as little as 5% (data not shown). It is important to note that the measurements of membrane potential with safranine O may underestimate hyperpolarized values of $\Delta\Psi_m$ which, in turn, might underestimate the magnitude of the depolarization in the presence of low uncoupler concentrations (Akerman and Wikstrom 1976). The concentration of uncoupler that abruptly and completely depolarizes mitochondria varies for different mitochondria preparations, and this is reflected at greater standard error at the end of the graph for membrane potential (Fig. 1c). Nevertheless, these data clearly indicate that succinate driven ROS production is very sensitive to changes in $\Delta\Psi_m$.

The physiological relevance of small depolarizations of $\Delta\Psi_m$ are illustrated in Fig. 2. Providing ADP together with succinate results in phosphorylating, or state 3 respiration. The synthesis of ATP depletes $\Delta\Psi_m$, and this depletion is sufficient to decrease $\Delta\Psi_m$ to the point that ROS generation is fully inhibited. The subsequent addition of oligomycin to prevent oxidative phosphorylation results in hyperpolarization of $\Delta\Psi_m$ and the resumption of ROS production. This principle can also be illustrated by the addition of a limited concentration of ADP (40 μM). This completely stopped ROS generation concurrently with a depolarization of mitochondria by some 30–40% of the safranine O signal (Fig. 2b). After the ADP was fully consumed and $\Delta\Psi_m$ recovered to a maximum value, the ROS production resumes. When ADP was present in excess and mitochondria are permanently in state 3, no ROS production was observed up to 30 min of incubation (Fig. 2a and data not shown). A low concentration of oligomycin (100 nM) inhibited the ATPase and restored $\Delta\Psi_m$ and then re-initiated ROS generation when the membrane potential reached its maximal value. These data show the reversibility of the process of free radical generation supported by succinate. It is worth noting that the changes of $\Delta\Psi_m$ at the transition from state 4 to state 3 (ATP synthesis switched off and switched on, respectively) measured by safranine O are greater than the depolarization necessary for complete inhibition of ROS production by an uncoupler. This suggests that brain mitochondria with an uninhibited respiratory chain engaged in ATP synthesis are protected from ROS generation mediated by complex II substrates.

Mechanism of ROS generation mediated by succinate

Previous studies have shown that in mitochondria derived mainly from tissues other than brain, ROS originate in two sites of the respiratory chain. Superoxide can be generated from complex I as a result of reverse electron transfer at high membrane potential values (Hinkle *et al.* 1967) (Croteau *et al.* 1997) (Korshunov *et al.* 1998), and also from the Q-cycle of complex III (see Turrens 1997). We used a series of selective inhibitors to evaluate the site(s) of the respiratory chain of rat brain mitochondria responsible for succinate supported ROS production.

Addition of the complex I inhibitor rotenone to mitochondria oxidizing succinate decreased ROS production (Fig. 3, Table 1). $\Delta\Psi_m$ remains high in this case, because proton pumping can still occur at complexes III and IV (data not shown). This suggests that the principle effect of rotenone is to block reverse electron transfer from complex II to complex I, and that this pathway is the major route of succinate-driven ROS generation. The complex III

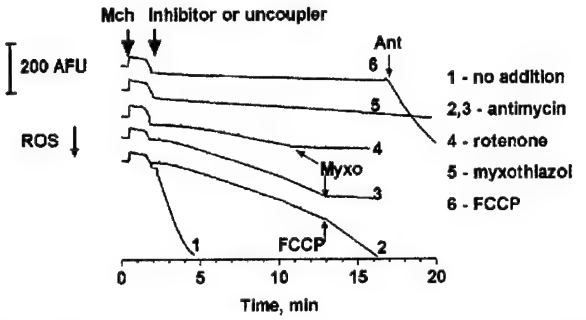

Fig. 3 The effect of respiratory chain inhibitors or uncoupler on hydrogen peroxide release by rat brain mitochondria oxidizing succinate. Hydrogen peroxide was measured with scopoletin in these experiments. Mitochondria were incubated in standard media. 1.5 min after addition of mitochondria to the incubation media an inhibitor or uncoupler was added. Additions: trace 2, 150 nM FCCP; traces 2,3, 1 μM myxothiazol; trace 6, 1 μM antimycin. These traces have been offset for clarity.

inhibitor antimycin also substantially inhibited ROS generation (Fig. 3), and also rapidly decreased $\Delta\Psi_m$. However, it is evident from Fig. 3 that there is a smaller and delayed oxidation of scopoletin that occurs following the addition of rotenone or antimycin. This remaining ROS production is likely to be due to free radical formation in the Q-cycle. Myxothiazol was reported to inhibit ROS generation in Q-cycle of bovine heart submitochondrial particles (Turrens *et al.* 1985). In our experiments, the addition of myxothiazol alone inhibited ROS generation by 97–98%. Application of myxothiazol after rotenone or antimycin results in the same rate of ROS generation, supporting, supporting the suggestion of Q-cycle as a source of the residual ROS signal when reverse electron transport to complex I is blocked.

Interestingly, when mitochondria are uncoupled with FCCP, antimycin stimulates Q-cycle ROS generation to an even greater extent. The rate of H_2O_2 generation is dependent on the ratio of [fumarate]/[succinate] in the mitochondrial matrix with maximum at 10 : 1 (Ksenzenko *et al.* 1984). Thus, building up fumarate as a result of succinate oxidation favors H_2O_2 production. For this reason, both the order and timing of additions of inhibitor and uncoupler is important. When inhibitor comes first the amount of fumarate accumulated is less compared to the case when mitochondria were first uncoupled. In our conditions, when succinate is present in excess, the later antimycin was added the higher rate of H_2O_2 was observed (not shown). This process was also substantially inhibited by myxothiazol (Fig. 3, Table 1).

ROS production supported by NADH-linked substrates

We next examined the characteristics of ROS generation by mitochondria utilizing glutamate and malate to drive NADH-linked respiration at complex I. The rate of endogenous hydrogen peroxide release was much lower when rat brain mitochondria oxidize NADH-linked substrates glutamate and malate and was undetectable using the scopoletin method (Fig. 4a, Table 1). However, the addition of rotenone, antimycin and even myxothiazol increased the rate of scopoletin oxidation (Fig. 4a, Fig. 5, Table 1).

The mechanism(s) of NADH-supported ROS generation

We further investigated the properties of ROS production triggered by the addition of inhibitors to mitochondria utilizing glutamate and malate. However, the short lag period observed between the addition of the inhibitor and the initiation of scopoletin oxidation added an ambiguity to these experiments, because this might reflect either a delay in ROS production or else a threshold below which scopoletin was unable to detect a ROS signal. To avoid this problem we detected ROS with the Amplex red method instead. We first investigated the concentration dependence of ROS generation triggered by rotenone. The aim of these experiments was to find out minimal degree of complex I inhibition which causes ROS generation in the respiratory chain and whether any correlation between ROS generation

Table 1 Effect of electron transport inhibitors and uncoupler on ROS generation by isolated mitochondria

	Rate of peroxide production (pmol/min/mg protein)	
	Succinate	Glutamate + malate
Control	1388 ± 59 (25)	Not detected
Antimycin	275 ± 18 (11)	228 ± 6 (20)
+ Myxothiazole	46 ± 2 (3)	59 ± 7 (4)
+ Rotenone	–	1266 ± 98 (3)
Rotenone	174 ± 18 (8)	434 ± 9 (19)
+ Myxothiazole	56 ± 18 (3)	–
Myxothiazole	40 ± 2 (6)	82 ± 11 (4)
+ Rotenone	–	450 ± 20 (5)
+ Antimycin	–	67 ± 7 (3)
FCCP then antimycin	1105 ± 130 (3)	254 ± 39 (3)
+ Myxothiazole	53 ± 12 (3)	85 ± 9 (3)
Antimycin then FCCP	463 ± 29 (6)	283 ± 8 (6)
+ Myxothiazole	–	79 ± 11 (3)
FCCP then rotenone	–	148 ± 7 (3)
Rotenone then FCCP	–	155 ± 15 (8)

Values are the mean ± SEM (*N* in parentheses) of determinations from different mitochondrial preparations. Peroxide production was determined using the scopoletin/horseradish peroxidase technique. Concentrations of drugs: antimycin 1 μM; rotenone 1 μM; myxothiazol 1 μM; FCCP 150 nM. Drugs were added together when indicated by +, and sequentially when indicated by 'then'. –, condition not tested.

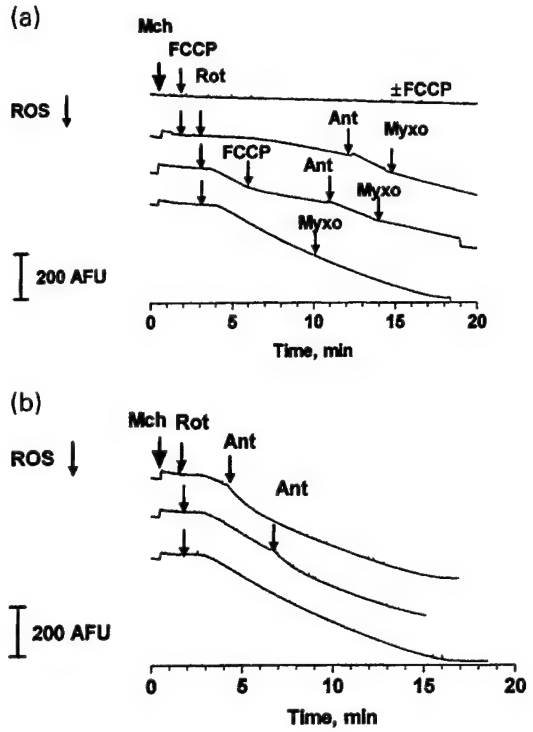

Fig. 4 The effect of respiratory chain inhibitors or uncoupler on the rotenone-induced hydrogen peroxide release by rat brain mitochondria oxidizing glutamate and malate as substrates. (a) Effect of uncoupler and myxothiazole. (b) Effect of antimycin. Mitochondria were incubated in standard media. Drugs were added in the following concentrations: 150 nM FCCP; 1 μM rotenone; 1 μM antimycin; 1 μM myxothiazol. Hydrogen peroxide was measured by the scopoletin method. These traces have been offset for clarity.

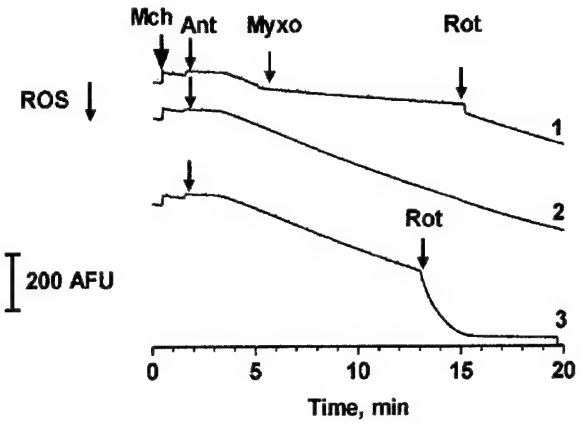

Fig. 5 The effect of respiratory chain inhibitors on antimycin-induced hydrogen peroxide release by rat brain mitochondria with glutamate and malate as substrates. Mitochondria were incubated in standard media. Drugs were added in the following concentrations: 1 μM antimycin; 1 μM rotenone; 1 μM myxothiazol. Hydrogen peroxide was measured by the scopoletin method.

and membrane potential value existed (Fig. 6). Treatment of mitochondria with increasing rotenone concentrations resulted in a gradual increase in the rate of ROS generation (Fig. 6a). The minimal rotenone concentration causing noticeable hydrogen peroxide release was 20 nM (equal to 100 pmol rotenone per mg mitochondrial protein). ROS generation by rotenone-inhibited mitochondria was not linear and typically increased during the experiment. The initial rate of ROS production (V_i) gradually rose with increasing inhibitor concentration and showed saturation at 500 nM, while the maximal rate (V_m) reached a plateau at a lower concentration (200 nM) (Figs 6a and c). Complex I contains several types of redox centers including eight or nine Fe–S clusters, flavin mononucleotide (FMN) and the tightly bound ubiquinone pool (Onishi 1998). The accelerated rate of peroxide production may be due to the progressive reduction of the upstream redox groups upon complete block of electron flow at rotenone binding site. Alternatively, increase in rate may reflect the point at which the endogenous antioxidant systems become depleted.

The kinetics of depolarization upon administration of different rotenone concentrations (Fig. 6b) are biphasic. These two components are likely to be attributable to a combination of the removal of the proton-motive force upon inhibition by rotenone, and the non-ohmic inherent proton leak of the inner membrane because the remaining respiratory chain activity is no longer able to compensate this passive leak. These experiments do not allow us to determine which component is attributable to which phase of the response. The apparent similarity between the kinetics of ROS production and loss of membrane potential can be explained by the fact that both processes are dependent on the degree of inhibition at complex I. However, in this case, membrane potential does not control the process of free radical production (see below).

To determine the extent of respiratory chain inhibition necessary to start free radical generation we performed polarographic measurements of oxygen consumption (Fig. 6c). There is an interesting discrepancy between the concentration dependence of the inhibition of respiration compared to ROS generation. Twenty nanomolar rotenone inhibits respiration by some 50%, while minimally altering H_2O_2 release. In the presence of 50 nM of rotenone 90% of respiration is inhibited, whereas V_m of ROS generation is only half maximal. Likewise, rotenone at 200 nM inhibited respiration by 98%, and V_m also reached a maximum, although the initial rate of ROS generation, V_i, is still submaximal at this concentration.

The addition of rotenone to mitochondria clearly decreases $\Delta\Psi_m$ in addition to increasing ROS generation. To determine whether ROS production was driven by the loss of $\Delta\Psi_m$ we performed experiments with FCCP. Depolarization of

mitochondria itself with FCCP does not cause ROS production (Fig. 4a, Table 1). Indeed, uncoupler FCCP partially inhibited ROS generation induced by rotenone. Similarly, addition of rotenone to mitochondria previously exposed to FCCP results in ROS generation at a rate comparable to the experiment with the reversed order of drug addition. These data show that dissipation of $\Delta\Psi_m$ alone is insufficient to trigger ROS production. Additionally, in rotenone-induced ROS production with glutamate and malate as substrate there is an uncoupler sensitive component. The latter is consistent with previous reports using mitochondria derived from tissues other than brain (Vinogradov *et al.* 1995).

To further probe the source of ROS in rotenone-inhibited mitochondria we tested the effects of antimycin and myxothiazol. Addition of antimycin to rotenone-poisoned mitochondria (Fig. 4b) accelerates H_2O_2 release. However, this enhancement is quite transient, because within 1–2 min the rate returns to the same level as observed with rotenone alone. In addition, myxothiazol has minimal effects on ROS generation in rotenone-inhibited mitochondria (Fig. 4a). The transient effect of antimycin may be due to small amounts of succinate present in the system from the transamination of glutamate and oxaloacetate, giving α-ketoglutarate. As this source of succinate donating electrons to Q-cycle is limited (analogous to the succinate experiments shown in Fig. 3) the addition of antimycin causes only transient acceleration of ROS production before the succinate is consumed. The limited effects of myxothiazol in this case indicates that upon glutamate-malate oxidation ROS generation does not involve the ubiquinone pool from complex III.

We also examined the effects of antimycin alone on ROS generation supported by glutamate and malate. For these studies we used Amplex red to ensure that we detected the full range of the ROS signal. Where rotenone provided a clear concentration dependence for ROS generation and mitochondrial depolarization, antimycin essentially produced an all-or-none effect with the critical concentration being between 40 and 50 nM (Fig. 7). Like rotenone, the effects of antimycin on both ROS production and $\Delta\Psi_m$ were only apparent when respiration had been almost completely inhibited (Fig. 7c). Increasing the antimycin concentration from 50 nM up to 1 μM did not further increases in the rate of ROS generation, though mitochondria lost membrane potential faster (Figs 7a and b). Similar data were obtained with scopoletin (not shown). The antimycin-induced ROS generation by mitochondria was almost completely inhibited by myxothiazol, and resumed after the subsequent addition

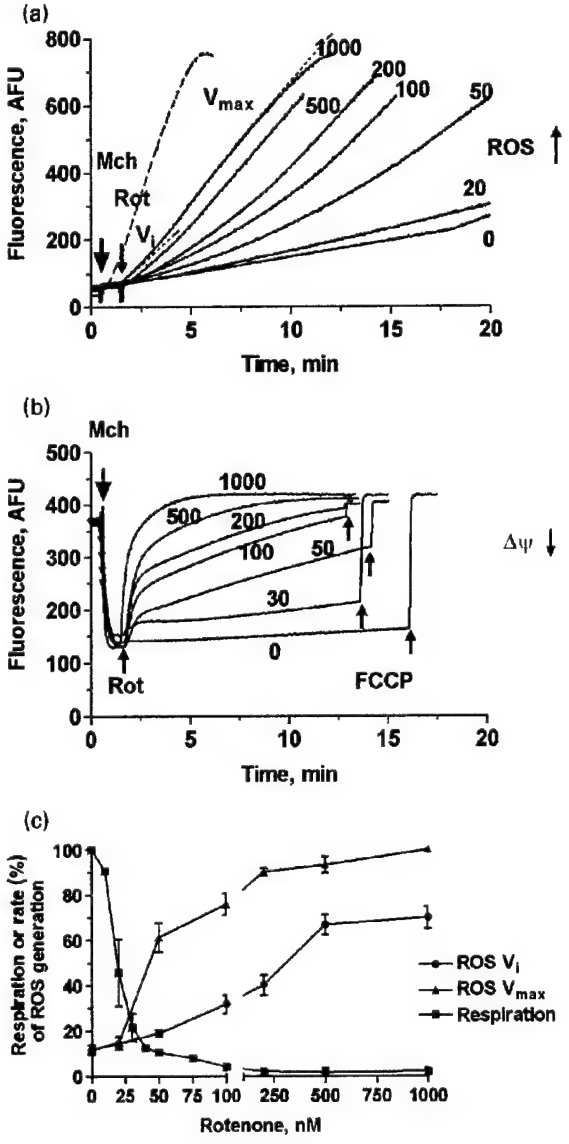

Fig. 6 Rotenone-induced hydrogen peroxide release (a and c), changes in membrane potential (b), and inhibition of respiration (c) of rat brain mitochondria oxidizing glutamate and malate. Hydrogen peroxide was measured with Amplex red in these experiments. (a and b) Various concentrations of rotenone were added to the mitochondria incubated in the standard media after maximal membrane potential had been established. Figures by each trace indicate rotenone concentration in nM. V_i and V_{max} indicate the initial and the maximal rate of H_2O_2 generation, respectively, as illustrated by the lines superimposed on the fluorescence traces. The dashed line shows succinate supported ROS generation for comparison. The concentration of FCCP in (b) was 150 nM. (c) The degree of inhibition of respiratory chain activity by different concentrations of rotenone was accessed in the media supplemented with 3 mM ATP and 1 μM oligomycin. The reaction was started by addition of 150 nM FCCP followed by addition of rotenone. A separate trace was made for each rotenone concentration. The ratio of the respiration rate in the presence of given rotenone concentration to uncoupled, maximal respiration in percent was plotted as curve 1. Calculation of the rates of hydrogen peroxide generation were normalized to the rate at 1000 nM rotenone.

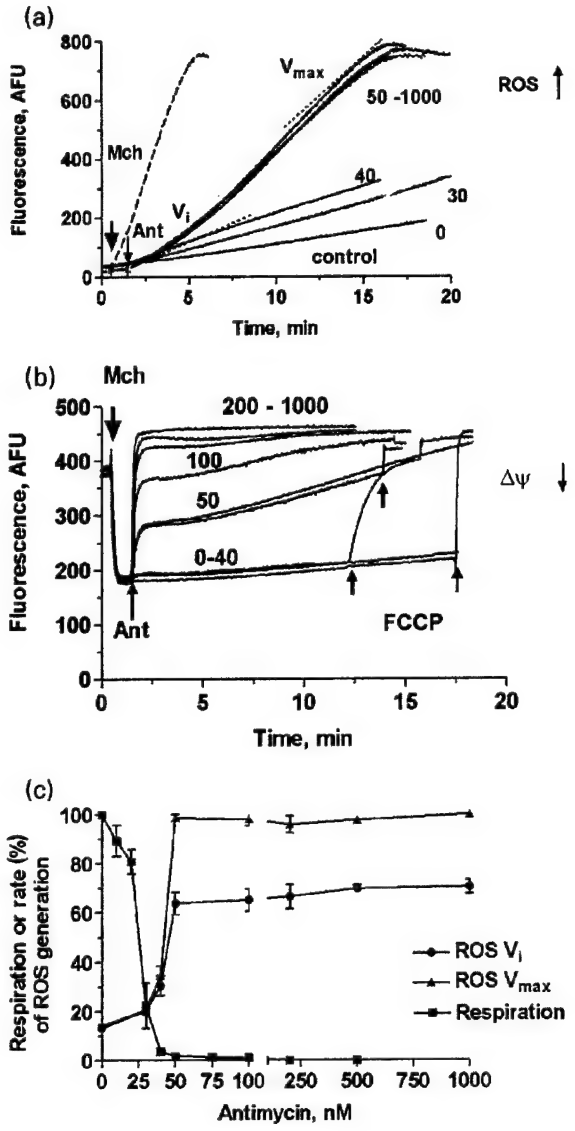

Fig. 7 The effect of antimycin on hydrogen peroxide release (a and c), membrane potential (b) and inhibition of respiration (c) of rat brain mitochondria oxidizing glutamate and malate. Conditions and experimental design are similar that of Fig. 6, except that antimycin was added as indicated when $\Delta\Psi_m$ was maximal. The dashed line on (a) shows succinate supported ROS generation for comparison.

of rotenone (Fig. 5, Table 1). The fact that myxothiazol suppressed the ROS production supported by glutamate and malate substrates in the presence of antimycin suggests that the hydrogen peroxide derives from Q-cycle under these conditions. However, in the presence of rotenone ROS production is likely to originate from complex I. Consistent with the involvement of the Q-cycle in antimycin-induced ROS production is the slight stimulatory effect of FCCP (Table 1).

Administration of myxothiazol to mitochondria oxidizing glutamate and malate caused a slow ROS production (Table 1). This is an interesting observation because myxothiazol is known to inhibit free radical production in Q-cycle (Turrens *et al.* 1985) and can be used to identify the Q-cycle as the source of ROS. A recent study also reported a slow ROS production in the presence of myxothiazol (Starkov and Fiskum 2001). Using another inhibitor of complex III, stigmatellin, the authors concluded that myxothiazol induces ROS in complex III, but at a site different from that of antimycin A action. In our experiments addition of rotenone to myxothiazol-poisoned mitochondria increased ROS production, though antimycin had no effect in this condition. The rates of ROS generation induced by rotenone alone and rotenone added to myxothiazol-poisoned mitochondria were the same indicating that myxothiazol block does not affect the ability of complex I to generate radicals.

Discussion

In this study we have investigated the regulation of mitochondrial ROS generation by $\Delta\Psi_m$ in a brain mitochondria preparation. There is clear evidence for ROS production originating from at least two different sites in the electron transport chain. In addition, mitochondria clearly produce ROS using both $\Delta\Psi_m$-dependent and -independent mechanisms.

Detailed information on the mechanism of ROS generation by respiratory chain in mitochondria and submitochondrial particles has been accumulated for tissues other than brain. In the majority of studies investigating intact mitochondria, it has been shown that oxidation of succinate gives the most effective production of ROS (Loschen *et al.* 1971; Boveris *et al.* 1972; Boveris and Chance 1973; Croteau *et al.* 1997; Korshunov *et al.* 1998; Kwong and Sohal 1998). Data on brain mitochondria are rather less, and have been summarized in Table 2. Our data along with data of Cino and Del Maestro (1989) and Kwong and Sohal (1998) clearly indicate succinate as the most effective ROS generating substrate for intact mitochondria, while others (Herero and Barja 1997; Barja and Herero 1998) failed to measure significant ROS production by rat mitochondria in the presence of this substrate. Arnaiz (Arnaiz *et al.* 1999) found that for mice brain mitochondria succinate was almost as effective as NADH-linked substrates. There are clearly several critical variables in these studies; the choice of incubation media is important, as well as the method of ROS detection. However, perhaps the most important factor is the ability of the mitochondria to maintain a sufficiently hyperpolarized membrane potential to support reversed electron transport. Some of the studies summarized in Table 2 used uncouplers or antimycin in their experiments,

Table 2 Prior studies on ROS generation by brain mitochondria

Study	Species	Incubation media	Detection method	Substrates tested	Key conclusions on source of ROS
Sorgato *et al.* (1974)	Rat	Sucrose	Scopoletin/HRP	Succinate	None
Patole *et al.* (1986)	Rat	KCl	Scopoletin/HRP	Succinate, _-glycerol phosphate, glutamate, malate, pyruvate	Q cycle > Complex I
Cino and Del Maestro (1989)	Rat	KCl	Compound II/HRP	Succinate, glutamate, malate	Complex I > Q cycle
Zoccarato *et al.* (1988)	Guinea pig	KCl	Cytochrome c/HRP	Succinate, α-glycerol phosphate, malate, pyruvate	Q cycle in uncoupled mitochondria
Dykens (1994)	Rat	KCl	Electron paramagnetic resonance	Succinate	Succinate signal stimulated by calcium
Herero and Barja (1997)	Rat, Pigeon	KCl	Homovanillic acid/HRP	Succinate, pyruvate, malate	No effect of $\Delta\Psi_m$ on Complex I
Barja and Herero (1998)	Rat, Pigeon	KCl	Homovanillic acid/HRP	Succinate, pyruvate, malate	Q cycle > complex I
Kwong and Sohal (1998)	Mouse	KCl	p-hydroxyphenylacetate /HRP	Succinate, α-glycerol phosphate, malate, pyruvate, β-hydroxybutyrate	Complex I > Q cycle
Arnaiz *et al.* (1999)	Mouse	Mannitol/ sucrose	Scopoletin/HRP	Succinate, glutamate, malate	Q cycle > complex I
Starkov and Fiskum (2001)	Rat	KCl	Scopoletin/HRP	Succinate, α-glycerol phosphate, malate	Myxothiazole induces Q cycle ROS signal

which would result in different results than those reported here.

The substantial succinate driven ROS production observed in previous studies and in our experiments is likely to be the result of reversed electron transport from complex II to complex I. Reversed electron transport has been shown to be very sensitive to $\Delta\Psi_m$ (Korshunov *et al.* 1998), and the present studies show that a very small degree of depolarization are sufficient to completely inhibit ROS generation by this pathway. Thus, low concentrations of the uncouplers FCCP and dinitrophenol, active oxidative phosphorylation, and the complex III inhibitors are each sufficient to depolarize $\Delta\Psi_m$ to the extent that ROS production is greatly reduced in succinate-oxidizing mitochondria. The finding that rotenone blocks this ROS signal, even though it does not depolarize $\Delta\Psi_m$ is also consistent with this conclusion, because it prevents electrons from reaching the redox centers associated with complex I responsible for superoxide generation. This means that the redox center(s) responsible for ROS production during reverse electron transport are located upstream of rotenone block. According to Hansford and colleagues (Croteau *et al.* 1997) all free radicals generated upon succinate oxidation originate in complex I.

Our data, along with experiments on rat heart mitochondria (Korshunov *et al.* 1998), clearly indicate that there is a secondary source of ROS in mitochondria respiring on succinate. This signal is likely to be derived from the ubiquinone cycle, because it is enhanced by antimycin and blocked by myxothiazol, and in the presence of antimycin is stimulated by the addition of uncouplers. This is consistent with the model of superoxide generation proposed in previous studies (Boveris *et al.* 1976; Cadenas *et al.* 1977; Cadenas and Boveris 1980; Turrens and Boveris 1980; Turrens *et al.* 1985). Notably, this pathway appears to be insensitive to changes in $\Delta\Psi_m$. Reverse electron transfer is a function that requires tightly coupled mitochondrial membranes capable of maintaining hyperpolarized potentials.

The contribution of complex III in overall ROS signal may depend on the concentration of CoQ in mitochondrial membrane, which is type and tissue specific. As Turrens has shown (Turrens *et al.* 1982), there is strong correlation between rates of H_2O_2 release and ubiquinone content in mitochondria of different sources. In addition, the impact of complex III and complex I in the overall ROS signal associated with succinate respiration depends on other factors, such as functional integrity of mitochondrial membrane and the potential, the redox state of the electron transport complexes under the appropriate experimental conditions, relative activity of the complexes themselves, and also the activity of ROS scavenging systems.

Rat brain mitochondria respiring on NADH-linked substrates produce a very small ROS signal in the absence of electron transport chain inhibitors. This is distinct from mitochondria derived from other species and tissues [mouse heart, kidney, brain (Kwong and Sohal 1998); pigeon heart (Boveris and Chance 1973); rat liver (Boveris *et al.* 1972);

porcine lung (Turrens *et al.* 1982); and mouse brain (Arnaiz *et al.* 1999)], where the uninhibited, complex I-derived signal is some 50–70% of that obtained with succinate. The basis for these intertissue differences remains unclear.

Significant ROS generation is triggered by the addition of rotenone which promotes superoxide generation by the redox center(s) of complex I. Our data are in agreement with those of Takeshige and Minakami (1979) who concluded that rotenone induces ROS only from complex I in NADH oxidizing bovine heart submitochondrial particles. It has subsequently been demonstrated that there are redox centers in complex I that are capable of generating superoxide though the precise location of the site(s) has not been identified (Kang *et al.* 1983; Krishnamoorthy and Hinkle 1988; Onishi 1998; Vinogradov 1998). These centers are apparently upstream of the site of rotenone blockade, and ROS production at this site(s) would account for the lack of sensitivity of this signal to myxothiazol or antimycin beyond that which can be accounted for by succinate generation (Fig. 3).

When either antimycin or rotenone were present with complex I substrates, the ROS production appears to be largely independent of $\Delta\Psi_m$. Although the addition of these inhibitors substantially alters $\Delta\Psi_m$, the changes in membrane potential occur independently of ROS generation, as indicated by the failure of FCCP to trigger a ROS signal in mitochondria respiring on glutamate and malate (Fig. 6). Interestingly, in the presence of rotenone and FCCP, antimycin does have a more substantial accelerating effect on ROS generation (Fig. 6a) than the transient effect of antimycin in the presence of rotenone alone (Fig. 6b), although the mechanism underlying this effect is not clear. Free radical production supported by succinate in the presence of antimycin block has previously been shown to be dependent on the redox potential of the fumarate/succinate pair (Loschen *et al.* 1973; Ksenzenko *et al.* 1984). The dependence had a bell shape with maximum at about 40 mV which is close to E_m of ubiquinones. These experiments were carried out on submitochondrial particles since fumarate poorly penetrates into mitochondria. Similar results were obtained for brain mitochondria, where dependence of ROS production in the presence of antimycin on the concentration of succinate had the same bell-shaped form (Patole *et al.* 1986; Zoccarato *et al.* 1988). Another confirmation of this notion was recently reported, where the problem of poor delivery of fumarate was overcome by using alamethicin-permeabilized mitochondria (Starkov and Fiskum 2001).

It is important to notice that both types of substrates we used in this work, succinate and glutamate with malate, cannot be considered 'pure' substrates of a particular complex. The oxidation of succinate in the Krebs cycle results in the production of fumarate and then malate, which can fuel complex I. In turn, some quantity of succinate is built up in the process of malate oxidation as well as from the transamination of glutamate. The transient effect of antimycin on rotenone treated mitochondria may be due to the to oxidation of succinate formed in this way.

It is widely believed that oxidative stress contributes to the demise of neurons in a number of neurodegenerative diseases, and it is likely that mitochondria are quantitatively the most important source of ROS in the brain. There have been numerous reports of impairment of the function of electron transport complexes in association with disorders like Parkinson's disease and Alzheimer's disease, conditions that are also associated with increases in markers of oxidative stress (Halliwell 1992; Beal *et al.* 1997). It is tempting to speculate that the partial inhibition of the electron transport chain reported in these diseases results in a feed forward effect, such that mitochondrial ROS generation is enhanced by the mechanisms evident when mitochondria respire on glutamate and malate. There are several potential limitations to this speculation, including the finding that very substantial inhibition of respiration is required prior to observing increased ROS generation, in other words the mitochondrial machinery may have a broad margin of safety. There is little evidence that the inhibition of respiration reaches this extent in any chronic neurological disorder. Perhaps a more reasonable speculation is that there may be conditions whereby mitochondria are excessively hyperpolarized under certain conditions, so that succinate-driven ROS generation occurs. This would not require extensive impairment of electron transport, but would imply that endogenous mechanisms that limit membrane potential [such as uncoupling proteins or endogeneous fatty acids, for example, Korshunov *et al.* (1998); Ricquier and Bouillaud (2000)] are dysfunctional. It is also possible that inhibition of ATP synthesis could generate a sufficiently hyperpolarized state to support succinate-driven ROS generation in intact tissues. Given the magnitude of the ROS signal from this mechanism and the liability this oxidant burden would impose on neurons, these are clearly issues which require further investigation.

One circumstance of mitochondrial involvement in neuronal injury that has received particular attention is excitotoxicity, where neurons die as the result of excessive activation of NMDA receptors and substantial cellular calcium accumulation. This process is associated with mitochondrial depolarization (Nieminen *et al.* 1996; Schinder *et al.* 1996; White and Reynolds 1996; Vergun *et al.* 1999), mitochondrial calcium accumulation (Kiedrowski and Costa 1995; White and Reynolds 1995; White and Reynolds 1997) and ROS generation (Lafon-Cazal *et al.* 1993; Dugan *et al.* 1995; Reynolds and Hastings 1995; Bindokas *et al.* 1996). Moreover, preventing mitochondrial calcium accumulation protects neurons from injury (Budd and Nicholls 1996; Stout *et al.* 1998). The mechanisms linking glutamate-induced mitochondria calcium accumulation to neuronal death

remain unclear. One candidate mechanism is the generation of ROS. Previously, it has been suggested that mitochondrial calcium and sodium accumulation could promote ROS generation by isolated mitochondria (Dykens 1994). However, this paper reported a lack of ROS production in mitochondria respiring on succinate, and an increase in ROS generation under conditions where mitochondria would be depolarized following the addition of calcium. These claims are in direct contrast to the present findings, as well as those of Cino and Del Maestro (1989). The basis for this substantial discrepancy remains unclear. Indeed, it is not easy to account for the effects of glutamate or calcium on the basis of the results presented here. The depolarization of $\Delta\Psi_m$ that is associated with mitochondria calcium cycling (Nicholls and Akerman 1982) is sufficient to completely inhibit succinate-driven ROS generation. In addition, the experiments reporting glutamate-induced ROS generation in intact neurons is obviously performed without the addition of complex I or complex III inhibitors. In fact, Dugan *et al.* (1995) reported that glutamate-induced oxidation of dihydrorhodamine was prevented by rotenone. There are rather few reports of mitochondrial ROS generation in intact neurons that can be compared to the present study, although Budd *et al.* (1997) did find that antimycin increased the oxidation of dihydroethidium in cerebellar granule cells. Perhaps the most reasonable way to account for the consequences of NMDA receptor activation in intact neurons is to propose a calcium-mediated inhibition of complex I or complex III. This might be accomplished by the production of nitric oxide, which is an effective inhibitor of complex III (Brown 1999; Stewart *et al.* 2000), although NOS inhibitors did not prevent the oxidation of either dichlorofluorescin or dihydroethidium (Reynolds and Hastings 1995; Bindokas *et al.* 1996). The actual mechanism of calcium-mediated mitochondrial ROS generation in neurons awaits further investigation.

Acknowledgements

This work was supported by USAMRMC Neurotoxin Initiative (grant number DAMD17–98–1-8627). We would like to thank Lauren Richards for help in some experiments, Dr Teresa Hastings for access to an oxygen electrode, Kirk Dineley for reading the manuscript and Dr Alexei Permin for helpful discussion of these findings.

References

Akerman K. E. O. and Wikstrom M. K. F. (1976) Safranine as a probe of the mitochondrial membrane potential. *FEBS Lett.* **68**, 191–197.

Arnaiz S. L., Coronel M. F. and Boveris A. (1999) Nitric Oxide, superoxide, and hydrogen peroxide production in brain mitochondria after haloperidol treatment. *Nitric Oxide: Biol. Chem.* **3**, 235–243.

Barja G. and Herero A. (1998) Localization at complex I and mechanism of higher free radical production of brain nonsynaptic mitochondria in the short-lived rat than in the longevous pigeon. *J. Bioenerg. Biomemb.* **30**, 235–243.

Beal M. F., Howell N. and Bodis-Wollner I. (1997). *Mitochondria and Free Radicals in Neurodegenerative Disease.* Wiley-Liss, New York.

Bindokas V. P., Jordan J., Lee C. C. and Miller R. J. (1996) Superoxide production in rat hippocampal neurons: selective imaging with hydroethidine. *J. Neurosci* **16**, 1324–1336.

Boveris A. and Chance B. (1973) The mitochondrial generation of hydrogen peroxide: general properties and effect of hyperbaric oxygen. *Biochem. J.* **134**, 707–716.

Boveris A. and Cadenas E. (1975) Mitochondrial production of superoxide anions and its relationship to the antimycin insensitive respiration. *FEBS Lett.* **54**, 311–314.

Boveris A., Oshino N. and Chance B. (1972) The cellular production of hydrogen peroxide. *Biochem. J.* **128**, 617–630.

Boveris A., Cadenas E. and Stoppani A. O. M. (1976) Role of ubiquinone in the mitochondrial generation of hydrogen peroxide. *Biochem. J.* **156**, 435–444.

Bradford M. M. (1976) A rapid and sensitive method for the quantitation of microgram quantities of protein utlizing the principle of protein-dye binding. *Anal. Biochem.* **72**, 248–254.

Brown G. C. (1999) Nitric oxide and mitochondrial respiration. *Biochim. Biophys. Acta Bio-Energetics* **1411**, 351–369.

Budd S. L. and Nicholls D. G. (1996) Mitochondria, calcium regulation and acute glutamate excitotoxicity in cultured cerebellar granule cells. *J. Neurochem.* **67**, 2282–2291.

Budd S. L., Castilho R. F. and Nicholls D. G. (1997) Mitochondrial membrane potential and hydroethidine-monitored superoxide generation in cultured cerebellar granule cells. *FEBS Lett.* **415**, 21–24.

Cadenas E. and Boveris A. (1980) Enhancement of hydrogen peroxide formation by protonophores and ionophores in antimycin supplemented mitochondria. *Biochem. J.* **188**, 31–37.

Cadenas E., Boveris A., Ragan C. I. and Stoppani A. O. M. (1977) Production of superoxide radicals and hydrogen peroxide by NADH-ubiquinone reductase and ubiquinol-cytochrome c reductase from beef heart mitochondria. *Arch. Biochem. Biophys.* **180**, 248–257.

Cino M. and Del Maestro R. F. (1989) Generation of hydrogen peroxide by brain mitochondria: the effect of reoxygenation following postdecapitative ischemia. *Arch. Biochem. Biophys.* **269**, 623–638.

Croteau D. L., Ap R., Hudson E. K., Dianov G. L., Hansford R. G. and Bohr V. A. (1997) An oxidative damage-specific endonuclease from rat liver mitochondria. *J. Biol. Chem.* **272**, 27338–27344.

Dugan L. L., Sensi S. L., Canzoniero L. M. T., Handran S. D., Rothman S. M., Lin T.-S., Goldberg M. P. and Choi D. W. (1995) Mitochondrial production of reactive oxygen species in cortical neurons following exposure to N-methyl-D-aspartate. *J. Neurosci* **15**, 6377–6388.

Dykens J. A. (1994) Isolated cerebral and cerebellar mitochondria produce free radicals when exposed to elevated Ca^{2+} and Na^{+}: implications for neurodegeneration. *J. Neurochem.* **63**, 584–591.

Halliwell B. (1992) Reactive oxygen species in the central nervous system. *J. Neurochem.* **59**, 1609–1623.

Herero A. and Barja G. (1997) ADP-regulation of mitochondrial free radical production is different with complex I- or complex II-linked substrates: implications for the exercise paradox and brain hypermetabolism. *J. Bioenerg. Biomemb.* **29**, 241–249.

Hinkle P. C., Butow R. A. and Racker E. (1967) Partial resolution of the enzymes catalyzing oxidative phosphorylation. *J. Biol. Chem.* **242**, 5169–5173.

Kang D., Narabayashi H., Sata T. and Takeshige K. (1983) Kinetics of superoxide formation by respiratory chain NADH dehydrogenase of bovein heart mitochondria. *J. Biochem. (Tokyo)* **64**, 1301–1306.

Kiedrowski L. and Costa E. (1995) Glutamate-induced destabilization of intracellular calcium concentration homeostasis in cultured cerebellar granule cells: role of mitochondria in calcium buffering. *Mol. Pharmacol.* **47**, 140–147.

Korshunov S. S., Skulachev V. P. and Starkov A. A. (1997) High protonic potential actuates a mechanism of production of reactive oxygen species in mitochondria. *FEBS Lett.* **416**, 15–18.

Korshunov S. S., Korkina O. V., Ruuge E. K., Skulachev V. P. and Starkov A. A. (1998) Fatty acids as natural uncouplers preventing generation of O_2^- and H_2O_2 by mitochondria in the resting state. *FEBS Lett.* **435**, 215–218.

Krishnamoorthy G. and Hinkle P. C. (1988) Studies on the electron transfer pathway, topography of iron sulfur centers, and site of coupling in NADH-Q oxidoreductase. *J. Biol. Chem.* **263**, 17566–17575.

Ksenzenko M., Konstantinov A. A., Khomutov G. B., Tikhonov A. N. and Ruuge E. K. (1984) Relationships between the effects of redox potential, α-thenoyltrifluoroacetone and malonate on O_2^- and H_2O_2 generation by submitochondrial particles in the presence of succinate and antimycin. *FEBS Lett.* **175**, 105–108.

Kwong L. K. and Sohal R. S. (1998) Substrate and site specificity of hydrogen peroxide generation in mouse mitochondria. *Arch. Biochem. Biophys.* **350**, 118–126.

Lafon-Cazal M., Pietri S., Culcasi M. and Bockaert J. (1993) NMDA-dependent superoxide production and neurotoxicity. *Nature* **364**, 535–537.

Loschen G., Flohe L. and Chance B. (1971) Respiratory chain linked H_2O_2 production in pigeon heart mitochondria. *FEBS Lett.* **18**, 261–264.

Loschen G., Azzi A. and Flohe L. (1973) Mitochondrial H_2O_2 formation: relationship with energy conservation. *FEBS Lett.* **33**, 84–88.

Mohanty J. G., Jaffe J. S., Schulman E. S. and Raible D. G. (1997) A highly sensitive fluorescent micro-assay of H_2O_2 release from activated human leukocytes using a dihydroxyphenoxazine derivative. *J. Immunol. Methods* **202**, 133–141.

Nicholls D. G. and Akerman K. E. O. (1982) Mitochondrial calcium transport. *Biochim. Biophys. Acta* **683**, 57–88.

Nieminen A.-L., Petrie T. G., Lemasters J. J. and Selman W. R. (1996) Cyclosporin A delays mitochondrial depolarization induced by *N*-methyl-D-aspartate in cortical neurons: evidence of the mitochodrial permeability transition. *Neuroscience* **75**, 993–997.

Onishi T. (1998) Iron-sulfur clusters/semiquinones in complex I. *Biochim. Biophys. Acta* **1364**, 186–206.

Patole M. S., Swaroop A. and Ramarsarma T. (1986) Generation of H_2O_2 in brain mitochondria. *J. Neurochem.* **47**, 1–8.

Reynolds I. J. and Hastings T. G. (1995) Glutamate induces the production of reactive oxygen species in cultured forebrain neurons following NMDA receptor activation. *J. Neurosci.* **15**, 3318–3327.

Ricquier D. and Bouillaud F. (2000) The uncoupling protein homologues: UCP1, UCP2, UCP3, StUCP and AtUCP. *Biochem. J.* **345**, 161–179.

Rosenthal R. E., Hamud F., Fiskum G., Varghese P. J. and Sharpe S. (1987) Cerebral ischemia and reperfusion: prevention of brain mitochondrial injury by lidoflazine. *J. Cereb. Blood Flow Metab.* **7**, 752–758.

Schinder A. F., Olson E. C., Spitzer N. C. and Montal M. (1996) Mitochondrial dysfunction is a primary event in glutamate neurotoxicity. *J. Neurosci.* **16**, 6125–6133.

Skulachev V. P. (1998) Uncoupling: new approaches to an old problem of bioenergetics. *Biochim. Biophys. Acta* **1363**, 100–124.

Sorgato M. C., Sartorelli L., Loschen G. and Azzi A. (1974) Oxygen radicals and hydrogen peroxide in rat brain mitochondria. *FEBS Lett.* **45**, 92.

Starkov A. A. and Fiskum G. (2001) Myxothiazol induces H2O2 production from mitochondrial respiratory chain. *Biochem. Biophys. Res. Comm* **281**, 645–650.

Stewart V. C., Sharpe M. A., Clark J. B. and Heales S. J. (2000) Astrocyte derived nitric oxide causes both reversible and irreversible damage to the neuronal mitochondria respiratory chain. *J. Neurochem.* **75**, 649–700.

Stout A. K., Raphael H. M., Kanterewicz B. I., Klann E. and Reynolds I. J. (1998) Glutamate-induced neuron death requires mitochondrial calcium uptake. *Nat. Neurosci.* **1**, 366–373.

Takeshige K. and Minakami S. (1979) NADH- and NADPH-dependent formation of superoxide anions by bovine heart submitochondrial particles and NADH-ubiquinone reductase preparation. *Biochem. J.* **180**, 129–135.

Turrens J. F. (1997) Superoxide production by the mitochondrial respiratory chain. *Biosci. Rep.* **17**, 3–8.

Turrens J. F. and Boveris A. (1980) Generation of superoxide anion by the NADH dehydrogenase of bovine heart mitochondria. *Biochem. J.* **191**, 421–427.

Turrens J. F., Freeman B. A. and Crapo J. D. (1982) Hyperoxia increases H_2O_2 release by lung mitochondria and microsomes. *Arch. Biochem. Biophys.* **217**, 411–421.

Turrens J. F., Alexandre A. and Lehninger A. L. (1985) Ubisemiquinone is the electron donor for superoxide formation by complex III of heart mitochondria. *Arch. Biochem. Biophys.* **237**, 408–414.

Vergun O., Keelan J., Khodorov B. I. and Duchen M. R. (1999) Glutamate-induced mitochondrial depolarisation and pertubation of calcium homeostasis in cultured rat hippocampal neurons. *J. Physiol. (Lond.)* **519**, 451–466.

Vinogradov A. D. (1998) Catalytic properties of the mitochondrial NADH-ubiquinone oxidoreductase (complex I) and the pseudo-reversible active/inactive enzyme transition. *Biochim. Biophys. Acta* **1364**, 169–185.

Vinogradov A. D., Sled V. D., Burbaev D. S., Drivennikova V. G., Moroz I. A. and Onishi T. (1995) Energy-dependent complex I-associated ubisemiquinones in submitochondrial particles. *FEBS Lett.* **370**, 83–87.

White R. J. and Reynolds I. J. (1995) Mitochondria and Na^+/Ca^{2+} exchange buffer glutamate-induced calcium loads in cultured cortical neurons. *J. Neurosci.* **15**, 1318–1328.

White R. J. and Reynolds I. J. (1996) Mitochondrial depolarization in glutamate-stimulated neurons: an early signal specific to excitotoxin exposure. *J. Neurosci.* **16**, 5688–5697.

White R. J. and Reynolds I. J. (1997) Mitochondria accumulate Ca^{2+} following intense glutamate stimulation of cultured rat forebrain neurones. *J. Physiol. (Lond.)* **498**, 31–47.

Zhou M. and Panchuk-Voloshina N. (1997) A one-step fluorometric method for the continuous measurement of monoamine oxidize activity. *Anal. Biochem.* **253**, 169–174.

Zoccarato F., Cavallini L., Deana R. and Alexandre A. (1988) Pathways of hydrogen peroxide generation in guinea pig cerebral cortex mitochondria. *Biochem. Biophys. Res. Commun.* **154**, 727–734.